UNIVERSIDAD COMPLUTENSE DE MADRID

FACULTAD DE CIENCIAS BIOLÓGICAS

TESIS DOCTORAL

Role of the pulmonary surfactant protein SP-C
in alveolar homeostasis

Papel de la proteína del surfactante pulmonar SP-C
en la homeostasis alveolar

MEMORIA PARA OPTAR AL GRADO DE DOCTORA

PRESENTADA POR

Juranny Michelle Morán Lalangui

DIRIGIDA POR

María Begoña García Álvarez
Jesús Pérez Gil

UNIVERSIDAD COMPLUTENSE DE MADRID

FACULTAD DE CIENCIAS BIOLÓGICAS

Programa de Doctorado en Bioquímica, Biología Molecular y Biomedicina

TESIS DOCTORAL

ROLE OF THE PULMONARY SURFACTANT PROTEIN SP-C IN ALVEOLAR HOMEOSTASIS

PAPEL DE LA PROTEÍNA DEL SURFACTANTE PULMONAR SP-C EN LA HOMEOSTASIS ALVEOLAR

MEMORIA PARA OPTAR AL GRADO DE DOCTORA

PRESENTADA POR

Juranny Michelle Morán Lalangui

DIRECTORES

María Begoña García Álvarez
Jesús Pérez Gil

A mis madres

A mi familia

A mis amigas

AGRADECIMIENTOS

Gracias a todas las personas que, de alguna manera, me han apoyado y acompañado durante el desarrollo de esta Tesis. Cada consejo, abrazo y palabra de aliento ha sido esenciales para realización de este documento. Sois las mejores.

Gracias por estar ahí y por creer en mí.

The research project presented in this Thesis has been conducted in the Department of Biochemistry and Molecular Biology of the Faculty of Biology, of Complutense University of Madrid (Madrid, Spain), under the supervision of Prof. Begoña García Álvarez and Prof. Jesús Pérez-Gil. Part of the experimental work presented in the current Thesis was performed in collaboration with Prof. Manuel Prieto at iBB Institute for Bioengineering and Bioscience (IST, Universidade de Lisboa, Lisbon, Portugal).

The Funding for short-term stay was provided by the European Biophysical Societies' Association (EBSA), The financial support to develop this work was provided by the Spanish Ministry of Universities (FPI19/ 476421) and research grants from Spanish Ministry of Science, Innovation and Universities (RTI2018-094564-B-100), Spanish Ministry of Science and Innovation (PID2021-124932OB-I00) and the Regional Government of Madrid (S2013/MIT-2807, P2018/NMT-4389).

TABLE OF CONTENTS

TABLE OF CONTENTS

LIST OF ABBREVIATIONS

AECI: Type I Alveolar Epithelial Cells

AECII: Type II Alveolar Epithelial Cells

AMϕ: Alveolar macrophages

BALF: Bronchoalveolar lavage fluid

BiFC: Bimolecular fluorescence complementation

BrSP-C: BODIPY-labeled rSP-C

BSP-C: BODIPY-labeled SP-C

COPD: Chronic obstructive pulmonary disease

CRD: Carbohydrate recognition domain

DPPC: Dipalmitoylphosphatidylcholine

FRET: Förster Resonance Energy Transfer

GpA: Glycophorin A

GUVs: Giants unilamellar vesicles

LBP: Lamellar body-like particles

LBs: Lamellar bodies

L_c: Liquid-condensed phase

L_d: Liquid-disordered phase

L_e: Liquid-expanded phase

LM: Synthetic lipid model mixture

L_o: Liquid-ordered phase

LPS: lipopolysaccharide

LS: Lipid surfactant derived from lipid fraction of organic extract of native pulmonary surfactant

LUVs: Large unilamellar vesicles

L_α: Disordered liquid-crystalline phases

L_β: Ordered gel phases

mSP-C: Mature SP-C

ncLM: Non-charged synthetic lipid mixture

NTA: Nanoparticle tracking analysis

OE: Organic extract

PAMPs: Pathogen-associated molecular patterns

PC: Phosphatidylcholine

PCR: Polymerase chain reaction

PE: Phosphatidylethanolamine

PG: Phosphatidylglycerol

PI: Phosphatidylinositol

POPC: Palmitoyloleoylphosphatidylcholine

POPG: Palmitoyloleoylphosphatidylglycerol

PS: Phosphatidylserine

rSP-C: Recombinant version of SP-C

SP-A: Surfactant protein A

SP-B: Surfactant protein B

SP-C: Surfactant protein C

SP-D: Surfactant protein D

SQ: Self-quenching

sSP-C: Scrambled version of SP-C

SSSQ: Steady-state self-quenching

SUVs: Small unilamellar vesicles

T_m: Melting temperature

TRPS: Tunable resistive pulse sensing setup

TRSQ: Time-resolved self-quenching

VC: C-terminal segment of Venus fluorescent protein

VFP: Venus Fluorescent Protein

VN: N-terminal segment of Venus fluorescent protein

γ: Surface tension

1.

SUMMARY
RESUMEN

Pulmonary surfactant, a lipoprotein complex that covers the alveoli, prevents lung collapse by reducing surface tension at the air-liquid interface. It is composed of lipids (90% by mass), including dipalmitoylphosphatidylcholine (DPPC, 40%), unsaturated phospholipids (35%) and neutral lipids such as cholesterol (8-10%). Additionally, it contains specific proteins (8-10%) essential for its function. Pulmonary surfactant proteins A and D (SP-A and SP-D) are hydrophilic proteins belonging to the collectin family and are involved in the innate defense of the lung, while pulmonary surfactant proteins B and C (SP-B and SP-C) are very small, highly cationic, and extraordinarily hydrophobic proteins responsible for the biophysical function of surfactant, as they participate in the rearrangement of surfactant membranes required during breathing cycles.

Pulmonary surfactant acts as a barrier against microorganisms and harmful particles inhaled into the lungs, through a cross-talk with alveolar macrophages (AMϕ). In the alveolar spaces, surfactant is challenged by an oxidative environment that can affect its function. Therefore, in healthy lungs, a balance is maintained between its secretion by type II alveolar epithelial cells (AECII) and its recycling and clearance. Alveolar homeostasis depends on the interaction between AECII, AMϕ, and surfactant, ensuring pulmonary protection and performance.

SP-C, the smallest (4.2 kDa) and most hydrophobic protein of pulmonary surfactant, accounts for 1% of its mass. It is synthesized as a 197-amino acid preprotein (21 kDa) that, following processing alongside SP-B, is converted into a mature 35-amino acid form. The C-terminal moiety presents a transmembrane α-helix rich in valines, which confers significant rigidity. SP-C helix inserts into lipid bilayers with a tilting of approximately 25°. On the other hand, the N-terminal end of the protein, containing two palmitoylated cysteines flanked by proline residues (PCCP), is oriented outside from the membrane and has an undefined conformation.

Previous studies have shown that the presence of SP-C in vesicles could induce membrane curvature, leading to membrane fragmentation and the generation of small vesicles. Additionally, its capacity to interact with lipopolysaccharide (LPS) or CD-14 (an LPS coreceptor in AMϕ) has been characterized, promoting an anti-inflammatory response, as well as the activity of the protein to enhance the uptake of lipid vesicles and modulate cholesterol metabolism in AMϕ.

Taking account these evidences, the main objective of this Thesis is to explore the role of SP-C in the recycling and processing of pulmonary surfactant, processes that are crucial for alveolar homeostasis, as well as to investigate the molecular mechanisms behind these processes. In order to achieve this goal, the following specific objectives have been outlined:

1. Summary

1. To investigate the propensity of SP-C to form dimers and oligomers, assessing protein-protein interactions through Bimolecular Fluorescence Complementation (BiFC) assays and fluorescence spectroscopy. This will include an analysis of how factors such as lipid composition, specific structural motifs, and the palmitoylation status influence these interactions.

2. To study the ability of SP-C to induce membrane fragmentation using synthetic and native lipid systems. Techniques such as Nanoparticle Tracking Analysis (NTA), Tunable Resistive Pulse Sensing (TRPS), and the use of giant unilamellar vesicles (GUVs) will be employed to analyze SP-C distribution and effects in membranes and to assess overall membrane characteristics as promoted by SP-C.

3. To analyze the role of SP-C in surfactant homeostasis, exploring its contribution to the recycling, uptake, and intracellular processing of lipids and proteins by different alveolar cell types. This objective will involve the use of confocal microscopy to visualize the localization and dynamics of vesicles within cells, as well as cellular models to evaluate SP-C's capacity to promote vesicle uptake by alveolar epithelial type II cells and alveolar macrophages.

The study of the oligomerization state of SP-C conducted in this Thesis indicates that SP-C is primarily monomeric, as no self-quenching of BODIPY-labeled SP-C protein or Förster resonance energy transfer (FRET) between Marina Blue SP-C and BODIPY SP-C was observed at low concentrations in the different lipid systems. However, at high concentrations in the lipid system derived from the lipid fraction of pulmonary surfactant, the formation of a low concentration of dimer was observed. On the other hand, protein palmitoylation appears to interfere with SP-C dimerization, as the non-palmitoylated recombinant version (rSP-C) labeled with BODIPY exhibited self-quenching. This self-quenching was more pronounced in synthetic membranes with phase separation, indicating that dimer formation depends on the lipid environment and on the palmitoylation state of the protein.

It was determined that SP-C requires a minimum concentration of 7.5% to significantly reduce the concentration of vesicle particles detectable by TRPS, as a consequence of membrane fragmentation. Additionally, NTA assays showed that membrane fragmentation induced by SP-C is lipid-environment-dependent, which is consistent with the observations on SP-C dimerization. Absence of anionic lipids and/or, possibly, the presence of cholesterol, appear to be relevant. The non-palmitoylated version of SP-C also induces membrane fragmentation, albeit to a

lesser extent. In GUV micrographs, lipid refinement was lower in the presence of the non-palmitoylated version, and in some cases, vesicle adhesion was observed.

The relationship between dimerization and fragmentation was investigated using peptide analogs of the N-terminal and C-terminal regions of SP-C, which contain putative dimerization motifs. These peptides in combination with SP-C displayed synergistic effects increasing membrane fragmentation. Peptides of these SP-C segments with mutated dimerization motifs exhibited variable effects depending on the lipid system, requiring further experiments to reach a conclusion.

Finally, it was observed that SP-C facilitates vesicle internalization by both AECII and AMϕ. In MH-S cells (AMϕ-like), a correlation between fragmentation and uptake could be inferred, as lipid systems with higher fragmentation also showed increased cellular fluorescence and thus greater vesicle internalization. However, in A549 cells, vesicle uptake was independent of lipid composition and increased with higher SP-C concentrations. In both cell types, most of the protein was located in acidic organelles, such as lysosomes in AMϕ or lysosomes and lamellar bodies in AECII, indicating its involvement in surfactant processing and recycling.

In conclusion, the results of this Thesis highlight the multifaceted role of SP-C in pulmonary homeostasis considering its ability to induce membrane fragmentation, facilitate lipid recycling, and promote vesicle internalization.

El surfactante pulmonar, un complejo lipoproteico que recubre los alveolos, previene el colapso pulmonar al reducir la tensión superficial en la interfase aire-liquido. Está compuesto por lípidos (90%, en masa), como la dipalmitoilfosfatidilcolina (DPPC, 40%), fosfolípidos insaturados (35%) y lípidos neutros como el colesterol (8-10%), además de proteínas específicas (8-10%) esenciales para su función. Las proteínas del surfactante pulmonar A y D (SP-A y SP-D) son hidrofílicas, pertenecen a la familia de las colectinas y están implicadas en la defensa innata del pulmón, mientras que las proteínas del surfactante B y C (SP-B y SP-C) son proteínas catiónicas muy pequeñas y extraordinariamente hidrofóbicas, responsables de la función biofísica del surfactante al facilitar los reordenamientos de membranas del surfactante necesarios durante los ciclos respiratorios.

El surfactante pulmonar actúa como barrera frente a microorganismos y partículas nocivas inhaladas en colaboración con los macrófagos alveolares (AMϕ). En el espacio alveolar se enfrenta a un ambiente oxidativo que puede afectar su función, por lo que en pulmones sanos se mantiene un equilibrio entre su secreción por parte de las células alveolares epiteliales tipo II (AECII) y su procesamiento. La homeostasis alveolar depende de la interacción entre AECII, AMϕ y el surfactante.

SP-C, la proteína más pequeña e hidrofóbica del surfactante (4,2 kDa, 1% en masa), se sintetiza como una preproteína de 197 aminoácidos (21 kDa) que, tras un procesamiento conjunto con SP-B, se convierte en su forma madura de 35 aminoácidos. La secuencia C-terminal se organiza en forma de una hélice α transmembrana rica en valinas, lo que le confiere gran rigidez, insertándose en la bicapa lipídica con una inclinación de aproximadamente 25°. El extremo N-terminal, orientado hacia el exterior de la membrana, carece de una estructura definida y presenta dos cisteínas palmitoiladas flanqueadas por residuos de prolina (PCCP).

Estudios previos han demostrado que SP-C puede inducir curvatura de membranas en vesículas lipídicas, lo que provoca su fragmentación y la formación de vesículas pequeñas. Además, se ha caracterizado su capacidad para interactuar con lipopolisacáridos (LPS) o CD-14 (correceptor del LPS en AMϕ) promoviendo respuestas antiinflamatorias, así como la captación de vesículas lipídicas y la modulación del metabolismo del colesterol en AMϕ.

Considerando lo anterior, el objetivo principal de esta Tesis es explorar el papel de SP-C en el reciclaje y procesamiento del surfactante pulmonar, procesos cruciales para la homeostasis alveolar, así como investigar los mecanismos moleculares subyacentes a estos procesos. Para alcanzar este objetivo, se han llevado a cabo los siguientes objetivos específicos:

1. Investigar la propensión de SP-C para formar dímeros y/o oligómeros mediante ensayos de Complementación de Fluorescencia Bimolecular (BiFC) y espectroscopía de fluorescencia. El análisis abarcará cómo factores como la composición lipídica y el estado de palmitoilación afectan las interacciones proteína-proteína.
2. Estudiar la capacidad de SP-C para inducir la fragmentación de membranas utilizando sistemas lipídicos sintéticos y nativos. Se emplearán técnicas como el análisis de seguimiento de nanopartículas (NTA), detección de pulsos de resistividad modificables (TRPS) y el uso de vesículas unilamelares gigantes (GUVs) para evaluar la distribución de SP-C en las membranas, sus efectos, y las características generales de las membranas promovidas por esta proteína.
3. Analizar el papel de SP-C en la homeostasis del surfactante, explorando su contribución al reciclaje, la captación y el procesamiento intracelular de lípidos y proteínas en diferentes tipos de células alveolares. Este objetivo implicará el uso de microscopía confocal para visualizar la localización y dinámica de las vesículas dentro de las células, así como el uso de citometría de flujo para evaluar la capacidad de SP-C para promover la captación de vesículas por células epiteliales alveolares tipo II y macrófagos alveolares.

El estudio del estado de oligomerización de SP-C muestra que la proteína es mayoritariamente monomérica, evidenciado por la ausencia de autoapagamiento de la proteína marcada con BODIPY SP-C y la falta de transferencia de energía de resonancia de Förster entre Marina Blue SP-C y BODIPY SP-C a bajas concentraciones. Sin embargo, a altas concentraciones en sistemas lipídicos derivados del surfactante pulmonar, se observó la formación de dímeros. La palmitoilación de SP-C parece influir en su dimerización. La versión recombinante no palmitoilada (rSP-C), marcada con BODIPY, presenta autoapagamiento incluso en membranas de POPC, con un aumento significativo en membranas sintéticas con separación de fases. Esto sugiere que la formación de dímeros depende tanto del ambiente lipídico como del estado de palmitoilación de la proteína.

Se determinó que la proteína SP-C requiere una concentración mínima del 7,5% para reducir significativamente la concentración de partículas de vesículas detectables por TRPS, debido a la fragmentación de membranas. Los ensayos de NTA revelaron que esta fragmentación depende del ambiente lipídico, siendo clave la ausencia de lípidos aniónicos y, posiblemente, la presencia de colesterol. La falta de palmitoilación en la SP-C también promueve la fragmentación, aunque en menor medida. Además, las micrografías de GUVs mostraron menor refinamiento lipídico, causando ocasionalmente adhesión de vesículas. La

relación entre dimerización y fragmentación se evaluó con péptidos análogos a los extremos N-terminal y C-terminal de SP-C. Estos péptidos mostraron un efecto sinérgico con SP-C, aumentando la fragmentación. Los péptidos con motivos de dimerización mutados tuvieron efectos variables según el sistema lipídico, requiriendo experimentos adicionales para llegar a una conclusión.

Por último, se demostró que SP-C facilita la internalización de vesículas lipídicas tanto en AECII como en AMϕ. En células MH-S derivadas de AMϕ, parece que existe una correlación entre fragmentación y captación, ya que en los sistemas lipídicos con mayor fragmentación se observó una mayor fluorescencia celular y, por ende, mayor internalización. En células A549 derivadas de AECII, la captación es independiente de la composición lipídica y aumenta con la concentración de SP-C. En ambas células, SP-C se localiza principalmente en orgánulos ácidos como lisosomas en AMϕ o lisosomas y cuerpos lamelares en AECII, lo que indica su participación en el procesamiento y reciclaje celular.

En conclusión, los resultados de esta Tesis subrayan el papel multifacético de SP-C en la homeostasis pulmonar dada su capacidad para inducir fragmentación de membranas, facilitar el reciclaje de lípidos y promover la internalización de vesículas.

2.
INTRODUCTION

Respiratory System

The Evolution of Respiratory Systems: From Anoxic Origins to Terrestrial Adaptations

The transition of aquatic organisms to terrestrial environments marks one of the most significant milestones in the evolutionary history of animals. This process involved overcoming various ecological, anatomical, and physiological challenges which were addressed by only certain groups, such as decapod crustaceans and early terrestrial vertebrates, successfully addressed (Hsia *et al.*, 2013; Maina, 2002; Nolte, 1989).

Before the advent of respiration in aquatic environments, organisms lived under anoxic conditions, meaning the absence of molecular oxygen (O_2) in their surroundings. These primitive organisms relied exclusively on anaerobic processes, generating energy through metabolic pathways that did not require oxygen, such as fermentation. However, as O_2 levels increased in the atmosphere and oceans—driven by the photosynthetic activity of organisms like cyanobacteria approximately 3.5 billion years ago—life began to adapt to aerobic conditions. Aerobic respiration proved to be far more efficient for energy production, yielding up to 36 moles of ATP per molecule of glucose compared to just 2 moles from anaerobic processes (Kasting & Siefert, 2002).

In aquatic environments, respiration evolved to maximize the capture of oxygen dissolved in water, a limited resource influenced by factors such as temperature and partial oxygen pressure. Diffusion-based respiration across cellular membranes was predominant in simpler organisms. As complexity increased, specialized systems, such as gills, emerged to optimize oxygen extraction from water and facilitating the elimination of carbon dioxide (CO_2) (Maina, 2000; Nolte, 1989)

As organisms began to explore terrestrial habitats, they faced the need to adapt to a medium much richer in oxygen but one that also vale with challenges such as desiccation and mechanical support for respiratory tissues (Lovelock, 2003; Roux, 2002).

This shift led to the emergence of primitive lungs in lungfish and amphibians, facilitating a gradual transition from water to air. Amphibians combined pulmonary respiration with cutaneous respiration, while reptiles diversified this structure by developing more complex pulmonary compartments that also served as oxygen reservoirs for prolonged apneas (Maina, 2000; Roux, 2002). Birds, in their adaptation to flight and high altitudes, evolved a unidirectional airflow system that

maximizes gas exchange efficiency even in low-oxygen environments (Farmer, 2015).

In mammals, lungs have evolved into a bronchoalveolar system that optimizes gas exchange through an extensive diffusion surface and thin barrier. This design allows for a precise balance between efficient oxygenation and protection against oxidative damage in delicate pulmonary tissues, particularly under conditions of hypoxia or hypercapnia (Hsia *et al.*, 2013; Maloney *et al.*, 1989; West, 2003). Furthermore, the complete separation between pulmonary and systemic circulation in mammals has enabled better regulation of circulatory pressures, thereby enhancing the specialization of oxygen distribution (Hsia *et al.*, 2016; Hsia *et al.*, 2013; Roux, 2002). These adaptations have allowed mammals to diversify and thrive successfully across a wide variety of terrestrial ecosystems, from deserts to Arctic regions.

The Human Lung: Anatomy and Physiology

The human lung is a highly specialized organ, designed to facilitate gas exchange and ensure the delivery of oxygen to tissues while removing carbon dioxide. Its intricate anatomy and physiology reflect an evolutionary adaptation aimed at optimizing respiratory efficiency within the constraints of the thoracic cavity.

The human lung, situated within the thoracic cavity, is divided into two asymmetrical structures: the right lung, which is larger and comprises three lobes (superior, middle, and inferior), and the left lung, slightly smaller to accommodate the heart, with two lobes (superior and inferior). This external division reflects an intricate internal architecture, characterized by a highly branched system that maximizes surface area for gas exchange while maintaining compactness within the thoracic cavity (Hsia *et al.*, 2016; Roux, 2002). From a single-entry point, the trachea, the respiratory system progressively bifurcates into smaller passages, forming a network that can be divided into the conducting and respiratory zones. The conducting zone, encompassing the trachea, bronchi, bronchioles, and terminal bronchioles, serves as a conduct for air, ensuring its humidification, warming, and filtration. This zone undergoes 16 generations of branching before transitioning into the respiratory zone, where gas exchange takes place. This respiratory zone begins with the respiratory bronchioles, continues through alveolar ducts to culminate in alveolar sacs (**Figure 1**). These sacs contain approximately 480 million alveoli, the functional units of the lung. Together, they provide an extraordinary surface area of around 140 square meters, facilitating the efficient diffusion of oxygen into the bloodstream and the removal of carbon dioxide. Thus, the lung's structure is a remarkable balance of maximizing surface area while maintaining minimal thickness of the gas-exchange barrier, approximately 2 micrometers, to optimize diffusion (Knudsen & Ochs, 2018).

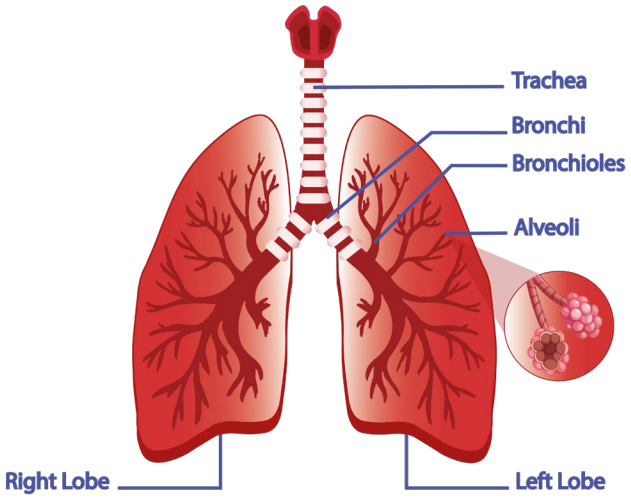

Figure 1: Schematic representation of the human lung anatomy. *This diagram illustrates the hierarchical organization of the respiratory system, from larger airways to the microscopic alveoli, where gas exchange occurs.*

Breathing relies on precise mechanical and physiological processes driven by pressure gradients within the thoracic cavity. The diaphragm and intercostal muscles play a central role by contracting during inspiration to increase thoracic volume, which decreases intrapulmonary pressure and draws air into the lungs. During expiration, these muscles relax, allowing the elastic recoil of the lungs to expel air. This dynamic process is supported by structural elements within the lung, including a network of elastic and collagen fibers in the interstitial matrix, which provide mechanical stability and prevent overdistension. Additionally, the alveolar epithelium produces pulmonary surfactant, a critical substance that reduces surface tension within the alveoli, preventing collapse and ensuring their uniform inflation during each respiratory cycle (Olmeda *et al.*, 2017; West, 2003).

The integration of ventilation and perfusion is crucial to the lung's function. Deoxygenated blood from the pulmonary arteries is delivered to the alveoli, where it comes into close proximity with atmospheric air across the thin alveolar-capillary barrier. Here, oxygen diffuses into the blood, binding to hemoglobin for transport to tissues, while carbon dioxide follows the reverse path to be expelled during exhalation. This efficient exchange is supported by the extensive vascular network surrounding the alveoli, ensuring that the lungs process approximately 12,000 liters of air and 6,000 liters of blood daily (Hsia *et al.*, 2016).

At the heart of this system lies the alveolus, a microscopic air sac that exemplifies the lung's functional elegance. Each alveolus is supported by a delicate matrix of capillaries, elastic fibers, and surfactant, working in unison to maintain structural integrity and optimize gas exchange. The detailed physiology of the alveolus, as the fundamental unit of respiration, will be explored further in subsequent sections, emphasizing its critical role in sustaining life (Knudsen & Ochs, 2018).

2. Introduction

The alveoli

Alveolus is essential for efficient gas exchange. These small, thin-walled sacs, averaging 200 µm in diameter, are located at the terminal ends of the respiratory tree and are surrounded by a dense network of capillaries. Gas exchange occurs through passive diffusion, facilitated by a thin air-capillary barrier of approximately 500 nm (Hogan *et al*., 1986; Ochs *et al*., 2004). This structure allows oxygen to diffuse into the blood and carbon dioxide to exit, thereby maintaining respiratory homeostasis.

The alveolar structure is supported by a mosaic of epithelial cells, connective tissue, and capillary endothelium (**Figure 2**). The epithelial lining of the alveolus consists of two main types of cells:

1. Type I Alveolar Epithelial Cells (AECI): These squamous epithelial cells cover approximately 95% of the alveolar surface area. Their thin, flat morphology (~0.1 µm) minimizes the diffusion distance and is critical for efficient gas exchange. AECI cells also play a role to maintain the structural integrity of the alveolar wall (Crapo *et al*., 1982; Mason, 2006).

2. Type II Alveolar Epithelial Cells (AECII): These cuboidal epithelial cells are responsible for producing and secreting pulmonary surfactant, a lipid-protein complex that reduces surface tension and prevents alveolar collapse during exhalation. AECII cells also play a vital role in alveolar repair and regeneration, by differentiating into AECI cells following injury. Additionally, they contribute to maintaining alveolar homeostasis by modulating the composition of the alveolar lining fluid (Fehrenbach, 2001; Guillot *et al*., 2013; Mason, 2006).

Other important cells within the alveolus include capillary endothelial cells, which form the blood-facing side of the air-capillary barrier. These cells facilities efficient gas exchange while regulating vascular tone and fluid balance (Maina & West, 2005). Fibroblasts are located in the interstitial space between epithelial and endothelial layers and produce collagen and elastin fibers, providing mechanical stability and elasticity to the alveoli during the breathing cycle (Knudsen & Ochs, 2018).

Alveolar macrophages (AMϕ), another critical cell type, reside on the alveolar surface and within the air-liquid interface. They are essential for maintaining alveolar sterility by phagocytosing pathogens, debris, and inhaled particles. These macrophages also regulate immune responses, balancing pro-inflammatory and anti-inflammatory activities to ensure lung homeostasis, and participate in the metabolism and recycling of surfactant (Hussell & Bell, 2014; Trapnell *et al*., 2003). However, excessive activation can lead to inflammatory damage, contributing to

conditions such as chronic obstructive pulmonary disease (COPD) (Knudsen & Ochs, 2018).

This intricate cellular network, supported by the alveolar structure, enables the lung efficient gas exchange while withstanding the mechanical stresses of respiratory cycles. The interaction between epithelial cells, connective tissue, and immune components underscores the complexity and adaptability of the alveolar microenvironment.

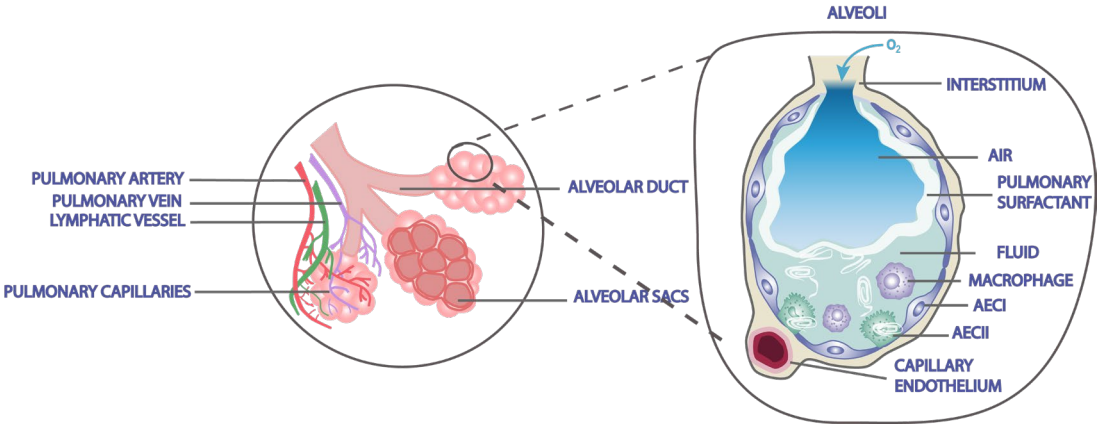

Figure 2: Schematic representation of the alveolar structure and its cellular composition. *The diagram illustrates the thin type I alveolar cells (AECI), the cuboidal alveolar type II cells (AECII) and the alveolar macrophages. The close association between epithelial cells, capillaries, and the interstitial matrix highlights the efficiency of the alveolar gas-exchange system. This figure was kindly provided by PhD student Paula Losada-Oliva.*

The alveolar surface is lined by a thin aqueous film, or hypophase, that forms an air-liquid interface essential for gas exchange. Within this interface, cohesive forces among water molecules generate surface tension (γ), defined as the energy required to increase the surface area of a liquid at constant temperature and pressure. Surface tension arises because molecules at the interface lack balanced interactions with air molecules, creating a net inward force that minimizes the exposed surface area (**Figure 3A**) (Soncini & Klein, 2023). For pure water at 37°C, the surface tension is approximately 72 mN/m, which, if unregulated, would significantly hinder alveolar function by promoting collapse during expiration (Hills, 1999). According to the Young-Laplace law, the pressure inside a spherical structure, the approximate shape of an alveolus, is directly proportional to the surface tension and inversely proportional to the radius:

$$\Delta P = \frac{2\gamma}{r}$$

This relationship implies that smaller alveoli experience higher internal pressures compared to larger ones, which would lead to a collapse of smaller alveoli into larger ones during exhalation, exacerbating respiratory inefficiency (**Figure 3B**). Such a scenario would result in progressive alveolar collapse and respiratory failure in the absence of compensatory mechanisms (Orgeig *et al.*, 2007).

Pulmonary surfactant, a complex mixture of lipids and proteins produced by AECII, is critical in counteracting these effects. Surfactant molecules, primarily composed of dipalmitoylphosphatidylcholine (DPPC), insert into the air-liquid interface, disrupting cohesive water interactions. This reduces the surface tension to a value below 1 mN/m during expiration when alveolar volume is smallest (Perez-Gil & Weaver, 2010; Schürch *et al.*, 1992). By reducing γ proportionally to alveolar area, surfactant stabilizes alveoli of varying sizes, preventing the smaller alveoli from collapsing into larger ones and ensuring uniform inflation during inspiration (Figura 3C) (Hills, 1999; Lopez-Rodriguez & Pérez-Gil, 2014).

The surfactant system adapts dynamically to the mechanical stresses of breathing. During compression (exhalation), surfactant molecules pack tightly, minimizing surface tension and avoiding alveolar collapse. During expansion (inhalation), the surfactant monolayer reorganizes to maintain a low surface tension while accommodating increased alveolar area. This ability to modulate surface tension across varying alveolar sizes is essential for maintaining respiratory homeostasis and minimizing the energy cost of breathing (Hills, 1999; Lopez-Rodriguez & Pérez-Gil, 2014).

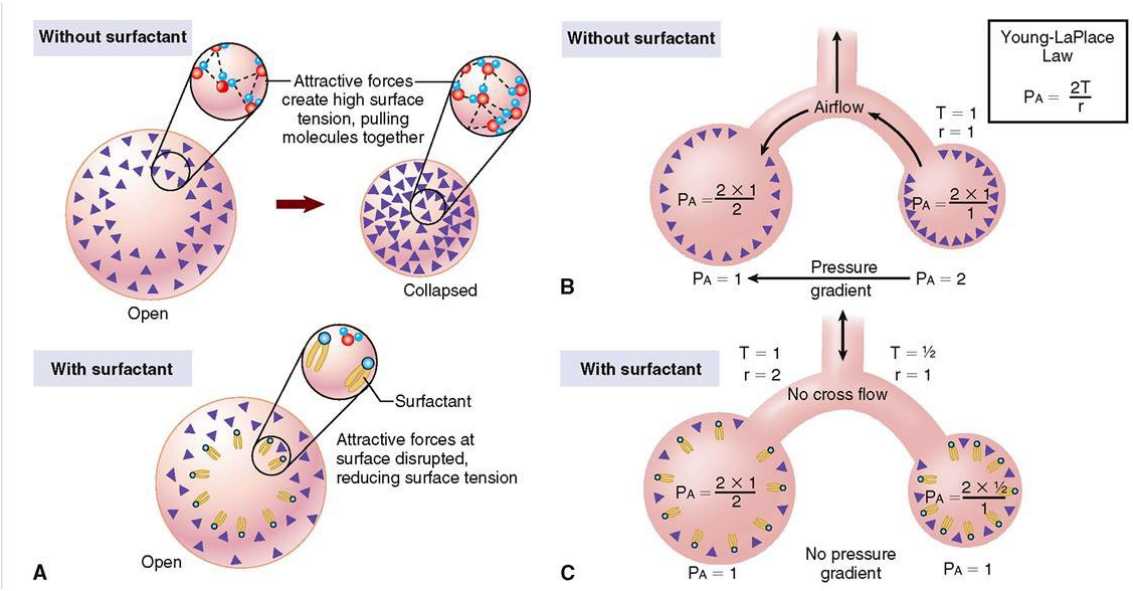

Figure 3: Role of surfactant. *A) Water lining the alveolar surface creates high surface tension, causing alveoli to contract and risk of collapse. Surfactant reduces surface tension by disrupting water molecule cohesion, preventing collapse. According to the Young-LaPlace law, alveolar pressure is proportional to surface tension and inversely proportional to radius. B) Without surfactant, smaller alveoli would collapse into larger ones due to pressure differences. (C) Whit surfactant, surface tension is reduced more effectively in smaller alveoli. This equalizes alveolar pressure, stabilizing alveoli of different sizes and ensuring uniform ventilation. Adapted from Basic Medical Key (2017).*

Pulmonary surfactant: Composition and Structure

As mentioned earlier, pulmonary surfactant is composed of approximately 90% (by mass) lipids and the remaining 10% proteins. Phospholipids predominate as the major component, playing a key role in reducing alveolar surface tension. The four

associated surfactant proteins (SP-A, SP-B, SP-C and SP-D) are essential for both the biophysical stability of the surfactant and the innate immune defense of the alveolus (Perez-Gil & Weaver, 2010).

Lipid fraction

Among the lipids in pulmonary surfactant, phosphatidylcholines (PCs) are the most prominent, accounting for 60-70% of the total lipid fraction mass. Of these, 40% correspond to dipalmitoylphosphatidylcholine (DPPC), the most abundant lipid species, while 25% are unsaturated phosphatidylcholines. The 8-15% by mass of the lipid fraction includes anionic lipids such as phosphatidylglycerol (PG) and phosphatidylinositol (PI), which could interact electrostatically with the cationic surfactant proteins SP-B and SP-C. Additionally, 8-10% of the lipids are neutral, primarily cholesterol, which plays a crucial role in modulating lipid packing and phase segregation within the surfactant film. The remaining percentage consists of minor lipid species, such as phosphatidylethanolamine (PE), phosphatidylserine (PS), and sphingomyelin, among others (**Figure 4**) (Bernhard, 2016; Goerke, 1998; Orgeig *et al*., 2003; Parra & Pérez-Gil, 2015).

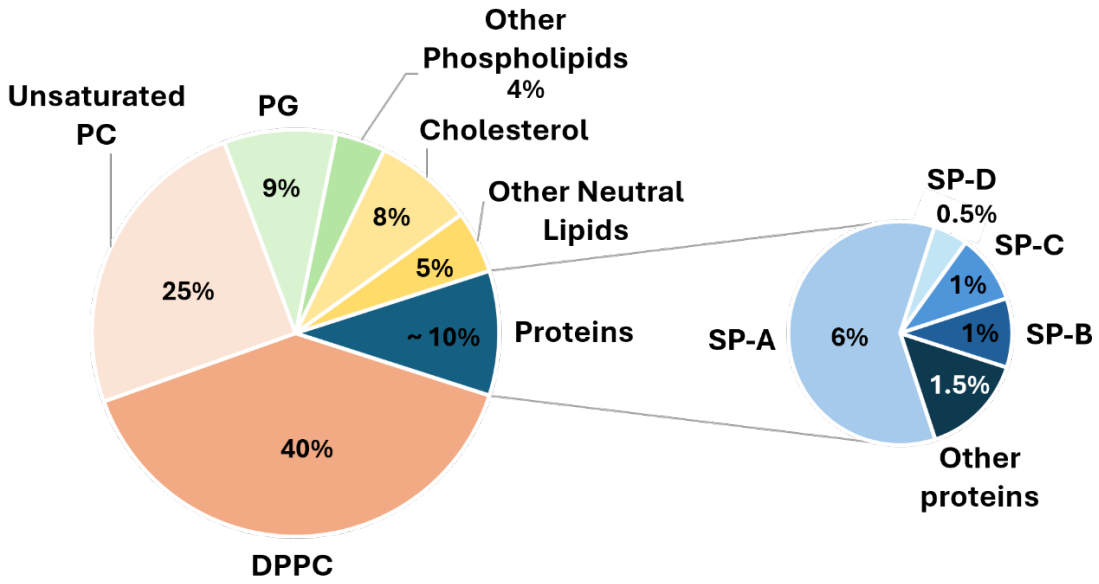

Figure 4: Composition of pulmonary surfactant by mass. *DPPC: dipalmitoylphosphatidylcholine; PC: Phosphatidylcholine; PG: Phosphatidylglycerol.*

Phospholipids are amphipathic molecules characterized by a polar headgroup and two hydrophobic hydrocarbon chains. In surfactant, they primarily include glycerophospholipids, which consist of a glycerol backbone esterified with two fatty acid chains and a phosphate group attached to a variable polar head (**Figure 5A**). The nature of these headgroups determines the charge of the phospholipid, classifying them as zwitterionic (null net charge), such as PC and PE or anionic

(negatively charged) including PG, PI, and phosphatidylserine (PS). Additionally, the chain length, saturation level, and position of unsaturation in the hydrocarbon chains influence the functionality and structural behavior of these molecules.

A critical feature of phospholipids is their ability to self-assemble into various supramolecular structures at the alveolar air-liquid interface, a process essential for surfactant functionality and the mechanics of respiration. This phenomenon, known as lipid polymorphism, involves the spontaneous organization of phospholipids into specific structures based on their molecular geometry and environmental conditions (Perkins *et al.*, 1996; Zuo *et al.*, 2008). Phospholipids exhibit three main structural behaviors (**Figure 5B**):

- Cylindrical Lipids: PCs are considered cylindrical because the cross-sectional areas of their headgroups and acyl chains are similar. This geometry promotes the spontaneous formation of flat bilayer structures, or lamellar phases, with negligible curvature.
- Inverted Conical Lipids: Molecules with cross-sectional areas of their headgroups larger than those of acyl chains, such as lysophospholipids, favor positive curvature, resulting in micelles or hexagonal type I phases.
- Conical Lipids: PEs, with smaller headgroups compared to their acyl chains, adopt a conical shape. These lipids induce negative curvature, leading to non-lamellar structures such as hexagonal type II phases or cubic phases.

The organization of these lipid structures is influenced by factors such as temperature, pH, lateral pressure, and hydration levels, as well as the presence of surfactant-associated proteins. This dynamic polymorphism is essential for surfactant adsorption, stability, and recycling during the respiratory cycle.

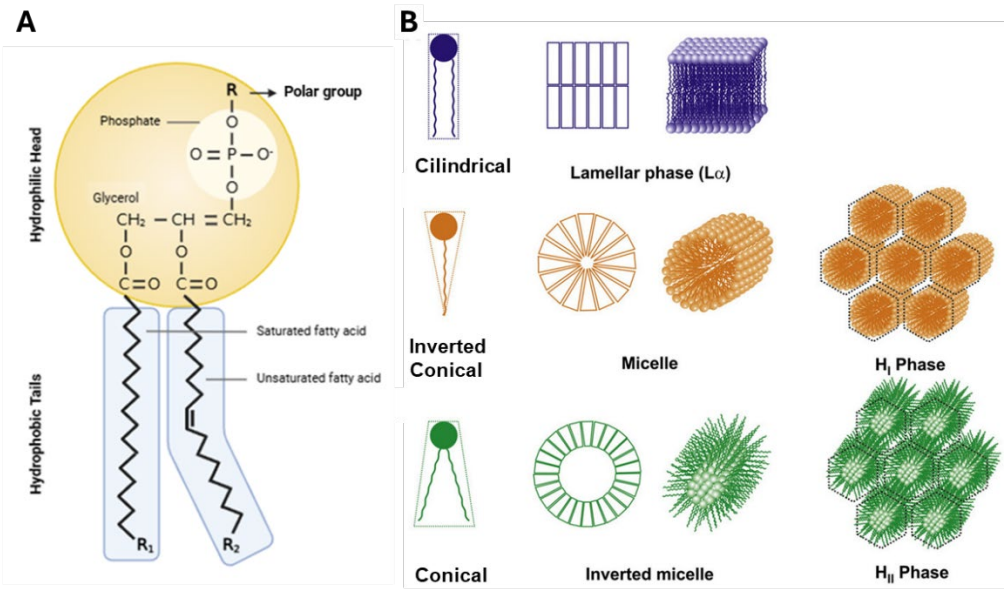

Figure 5: Glycerophospholipids structure and membrane lipid polimorphism. A) *Schematic representation of the molecular structure of a glycerophospholipid, highlighting its amphipathic nature. The hydrophilic head consists of a phosphate group, glycerol, and a variable polar group, while the hydrophobic region is composed of two hydrocarbon chains.* ***B)*** *Diagram illustrating the self-assembly of lipids into various supramolecular structures based on the ratio of the polar head to the lipid tail areas. When the head and tail areas are approximately equal as in PCs, cylindrical lipids form lamellar structures. If the areas differ, non-lamellar structures arise: larger head areas favor micelles and hexagonal type I phases (H_I phase), while smaller head areas as occurs with PE promote inverted micelles and hexagonal type II phases (H_{II} phase). Adapted from Escriba (2018).*

Phospholipids arranged in lamellar forms establish interactions that generate distinct thermodynamic phases. Within bilayers, phospholipids transition from ordered gel phases (L_β), characterized by tightly packed molecules with limited mobility, to disordered liquid-crystalline phases (L_α) as temperature increases (**Figure 6**). This transition occurs at the melting temperature (T_m), a threshold unique to each phospholipid species, influenced by factors such as chain saturation, chain length, and polar headgroup. Saturated lipids like DPPC have higher T_m values (41°C), while unsaturated species such as POPC or POPG exhibit lower T_m (-2°C). At T_m, the system reaches equilibrium, with L_β and L_α phases coexisting, allowing for adaptive lipid organization.

In pulmonary surfactant, lipid behavior is further modulated by the unique monolayer arrangement at the alveolar air-liquid interface, where temperature and lateral pressure drive phase transitions. During the respiratory cycle, compression reduces the area per lipid molecule, causing a shift from a liquid-expanded (L_e) phase, analogous to L_α, to a liquid-condensed (L_c) phase, similar to L_β (**Figure 6**) (Casals & Cañadas, 2012; Zuo *et al.*, 2008). At extreme compression, as seen at the end of expiration, the monolayer can approach a nearly solid state dominated by DPPC, competent to achieve surface tension values near 0 mN/m. This adaptation is critical for preventing alveolar collapse and highlights the

importance of the lipid composition in pulmonary surfactant performance (Possmayer *et al*., 2001).

Cholesterol plays a pivotal role in modulating lipid packing and phase behavior within surfactant membranes. This small amphipathic molecule integrates into bilayers and monolayers by positioning its hydroxyl group (OH) near the polar region of the membrane while its rigid steroid ring structure and isoprenoid tail extend into the hydrophobic core of the bilayer. Through this integration, cholesterol mediates phase coexistence, creating liquid-ordered (L_o) and liquid-disordered (L_d) domains (**Figure 6**) (Veatch & Keller, 2002; Zuo *et al*., 2008). In fluid membranes, cholesterol enhances order and restricts lipid mobility, whereas in ordered states, it disrupts molecular interactions, promoting fluidity (Bernardino de la Serna *et al*., 2004; Sankaram & Thompson, 1991). This dual functionality enables pulmonary surfactant to balance mechanical stability and dynamic adaptability during the breathing cycle.

The surfactant lipid-protein complex further refines these properties, with proteins such as SP-B and SP-C preferentially partitioning into disordered domains, enhancing dynamic responsiveness and stability (**Figure 6**) (Liekkinen *et al*., 2023; Nag *et al*., 1997). The coexistence of ordered (L_c) and disordered (L_e) phases at physiological temperatures (37°C) allows surfactant to function effectively under varying respiratory demands (Casals & Cañadas, 2012; Zuo *et al*., 2008). Additionally, factors like pH, hydration, ionic strength, and lateral pressure contribute to lipid phase behavior and domain morphology, further fine-tuning surfactant performance.

Overall, the intricate balance of lipid composition, cholesterol content, and protein interactions ensures that pulmonary surfactant can withstand the mechanical stresses of the respiratory cycle while maintaining its critical role in lowering surface tension and stabilizing the alveolar interface.

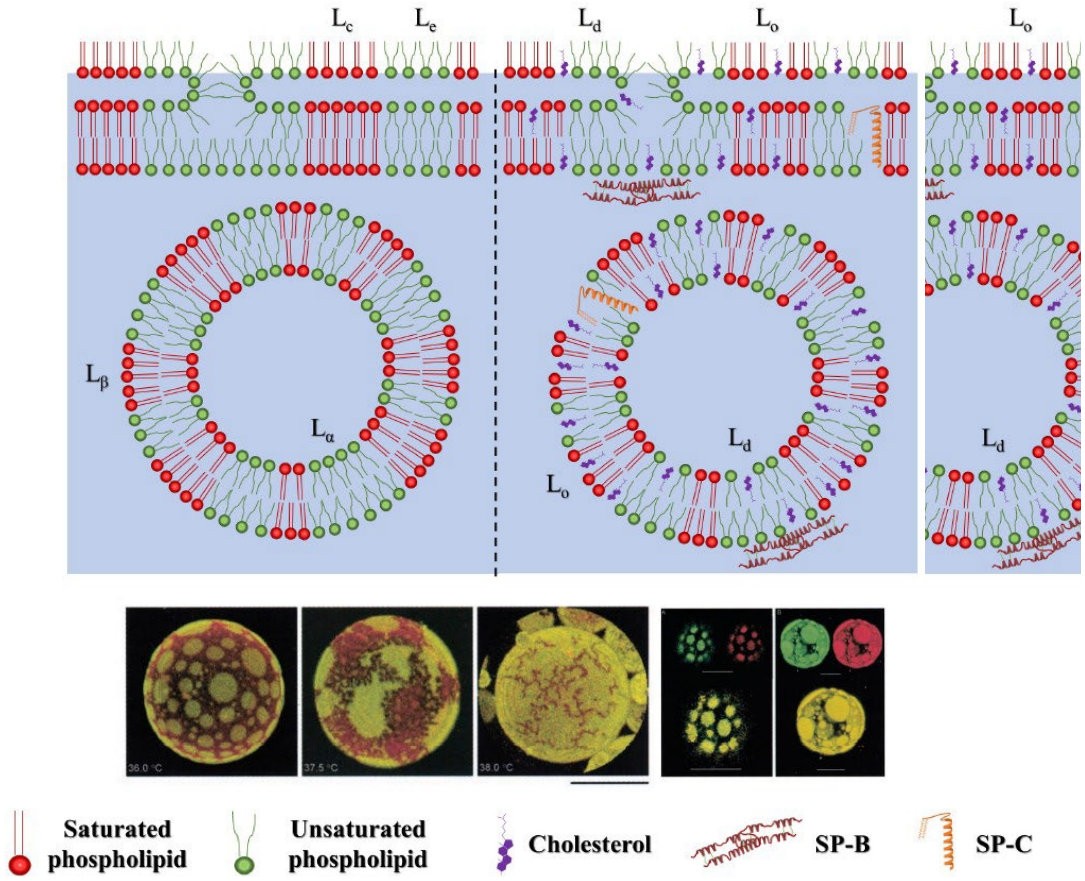

Figure 6: Lateral structure of surfactant membranes. *The lateral organization of surfactant membranes is characterized by the segregation of lipid phases based on their molecular properties. Left panel: Saturated phospholipids, such as DPPC, and unsaturated phospholipids, like POPC, tend to segregate within bilayers or monolayers, resulting in phase coexistence between ordered gel-like (L_β) and fluid liquid-crystalline (L_α) phases, or between liquid-condensed (L_c) and liquid-expanded (L_e) phases. Right panel: In pulmonary surfactant, cholesterol plays a crucial structural role, fluidizing gel phases and stiffening fluid phases to create a coexistence of liquid-ordered (L_o) and liquid-disordered (L_d) domains at physiological temperatures. Below: Fluorescently labeled Giant Unilamellar Vesicles (GUVs) composed of native pulmonary surfactant demonstrate temperature-dependent phase coexistence (left panel, green fluorescence from NBD-PC in disordered-like phases and red fluorescence from DiIC18 in ordered-like phases) and protein partitioning (right panel, SP-B labeled in red and SP-C in green). Adapted from Castillo-Sánchez (2021).*

Pulmonary Surfactant Proteins

Specific pulmonary surfactant proteins can be classified into two groups, the hydrophilic proteins, SP-A and SP-D, and the hydrophobic proteins, SP-B and SP-C. While hydrophilic proteins play key role in surfactant innate immune response, hydrophobic proteins have been classically linked to the biophysical action of PS, being key elements for improving surfactant adsorption into the interface, stabilizing the surface-active film and spreading surfactant during inspiration-exhalation cycles in alveoli (Lopez-Rodriguez & Pérez-Gil, 2014; Olmeda *et al.*, 2017; Pérez-Gil, 2008; Perez-Gil & Weaver, 2010).

Hydrophilic proteins: SP-A and SP-D

Surfactant proteins SP-A and SP-D are hydrophilic components of pulmonary surfactant that belong to the collectin family, a subgroup of calcium-dependent C-

type lectins. These proteins are essential for lung immunity and surfactant regulation, performing complementary roles in pathogen defense and surfactant homeostasis (García-Álvarez *et al.*, 2019; Hawgood & Poulain, 2001; Johansson, Curstedt, *et al.*, 1994; van Golde, 1995). Structurally, both proteins share a conserved organization consisting of a cysteine-rich N-terminal domain, a collagen-like triple helix, an α-helical neck region, and a carbohydrate recognition domain (CRD). The CRD enables specific binding to lipids such as DPPC and PI, as well as to pathogen-associated molecular patterns (PAMPs), including lipopolysaccharides (LPS) from Gram-negative bacteria, playing a pivotal role in their antimicrobial function (Carreto-Binaghi *et al.*, 2016; Kishore *et al.*, 2006; Kuroki & Akino, 1991; Ogasawara *et al.*, 1992).

SP-A, accounting for about 6% of the surfactant mass, predominantly exists in a bouquet-like structure composed of six trimeric units. Each trimer is formed by monomers of approximately 35 kDa, which are interconnected through disulfide bridges located at their N-terminal region (**Figure 7**) (Crouch & Wright, 2001). On the other hand, SP-D, accounting for 0.5%, assembles into cruciform-shaped dodecamers or higher-order oligomers named fuzzy-balls (**Figure 7**) (Arroyo *et al.*, 2020; Crouch *et al.*, 1994). These proteins are produced in AECII and club cells, with SP-A often integrated into lamellar bodies, whereas SP-D is predominantly released into the alveolar lining fluid (Lopez-Rodriguez & Pérez-Gil, 2014). Their synthesis involves folding and glycosylation processes that ensure functional assembly (Crouch, 1998; Voorhout *et al.*, 1992; Wang *et al.*, 1994).

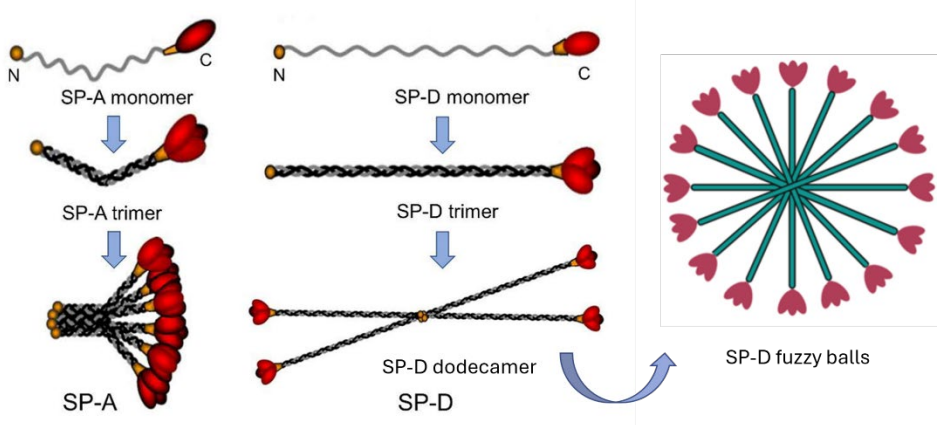

Figure 7: Structure of lung collectins: SP-A and SP-D. *Illustration adapted from (Possmayer et al., 2023) and Yasmin and Kishore (2021).*

In immune defense, SP-A and SP-D bind carbohydrate structures and LPS on the surface of pathogens, facilitating aggregation and opsonization, which enhances phagocytosis by immune cells such as macrophages and neutrophils. They also modulate inflammatory responses by interacting with immune receptors, promoting tissue protection during infections. These interactions contribute to a

balanced immune response while directly impairing pathogen viability (Kishore *et al.*, 2006; Minutti *et al.*, 2016; Wright, 2005).

In surfactant homeostasis, SP-A improves lipid adsorption at the air-liquid interface, stabilizing the surfactant film and supporting tubular myelin formation (Palaniyar *et al.*, 1999). SP-D, though less integrated within the surfactant structure, influences the organization of minor lipid components and regulates surfactant turnover (Ikegami, 2000; Ikegami *et al.*, 2009). Both proteins ensure the proper recycling and maintenance of surfactant, critical for efficient respiratory function (Lopez-Rodriguez & Pérez-Gil, 2014; Wright & Clements, 1987).

The deficit of both SP-A and SP-D does not affect the biophysical function of pulmonary surfactant but is linked to impaired innate immune defense, making the organism more susceptible to infections and exacerbating inflammation. The absence of SP-A prevents the formation of tubular myelin, while SP-D deficiency leads to lipid accumulation in airspaces, acute pulmonary alveolar proteinosis (PAP), foamy alveolar macrophages, and emphysema (Lopez-Rodriguez & Pérez-Gil, 2014).

Hydrophobic proteins: SP-B and SP-C

In contrast to hydrophilic proteins, SP-B and SP-C are small hydrophobic proteins critical for maintaining the biophysical properties required for efficient respiratory function (Johansson, Curstedt, *et al.*, 1994; Parra & Pérez-Gil, 2015; Perez-Gil & Weaver, 2010). SP-C will be discussed in detail separately, as it is the main focus of this Thesis.

SP-B is a small amphipathic protein of 8.7 kDa that primarily exists as a covalent homodimer of 17.4 kDa. It belongs to the saposin-like protein (SAPLIP) family, characterized by six highly conserved cysteine residues forming three intramolecular disulfide bonds and an additional cysteine (C48) that facilitates dimerization through an intermolecular disulfide bridge. The protein's sequence includes a significant proportion of hydrophobic residues and nine charged amino acids (eight cationic and one anionic), which confer its net positive charge and amphipathic nature. Spectroscopic analyses suggest that SP-B exhibits a high α-helical content (40-50%) (Andersson *et al.*, 1995; García-Álvarez *et al.*, 2019; Johansson *et al.*, 1991; Liekkinen *et al.*, 2023; Olmeda *et al.*, 2013; Serrano *et al.*, 2005). The protein orients itself superficially within lipid membranes, with its amphipathic helices interacting with the polar headgroups of phospholipids, particularly anionic species such as phosphatidylglycerol (PG), through electrostatic forces (Baatz *et al.*, 1990; Cabré *et al.*, 2012; Cruz *et al.*, 1998; Gordon *et al.*, 1996; Morrow, Perez-Gil, *et al.*, 1993; Pérez-Gil *et al.*, 1995; Vandenbussche, Clercx, Clercx, *et al.*, 1992). A notable structural feature of SP-B is the formation of two oligomeric rings, which are associated to create a channel

connecting membranes. This channel facilitates the rapid and efficient flow of lipids to the air-liquid interface, a critical mechanism for maintaining surfactant functionality, and facilitates oxygen diffusion across surfactant layers (Olmeda *et al.*, 2015; Olmeda *et al.*, 2010; Parra *et al.*, 2013; Parra *et al.*, 2011).

SP-B's function is multifaceted. It promotes the adsorption of surfactant lipids to the air-liquid interface and facilitates the re-spreading of lipid films during inhalation, ensuring effective surface activity (Krol *et al.*, 2000; Rodriguez-Capote *et al.*, 2001; Schürch *et al.*, 2010). It plays a significant role in reorganizing membranes by inducing vesicle aggregation and fusion, which results in substantial membrane curvature changes (Baoukina & Tieleman, 2010; Chang *et al.*, 1998; Ryan *et al.*, 2005). These effects enable the transfer of lipids from surfactant reservoirs to the interfacial film, a critical process during the breathing cycle (Chavarha *et al.*, 2010; Rugonyi *et al.*, 2008). Together with SP-A, SP-B organizes surfactant membranes into tubular myelin, a very unusual, ordered network of membranes, in a calcium-dependent manner (Poulain *et al.*, 1992; Suzuki *et al.*, 1989). Additionally, SP-B contributes to the formation and secretion of lamellar bodies and to stablish structural connections between membranes, which act as reservoirs of surfactant and ensure its availability at the alveolar surface (Clark *et al.*, 1995; Stahlman *et al.*, 2000).

These properties make SP-B indispensable for maintaining alveolar surface stability and respiratory efficiency. Deficiencies in SP-B lead to fatal respiratory failure and death, highlighting its essential role in pulmonary function and survival (Lopez-Rodriguez & Pérez-Gil, 2014; Weaver & Conkright, 2001).

SP-C

SP-C, the smallest and most hydrophobic of the pulmonary surfactant proteins, consists of 35 amino acids and has a molecular weight of 4.2 kDa. It accounts for approximately 1% of the total molecular mass of pulmonary surfactant but is nevertheless the most abundant in terms of molar concentration (García-Álvarez *et al.*, 2019; Johansson, 1998). Due to its exclusive expression in the lungs, SP-C is commonly used as a specific marker for alveolar type II cells (AECII) (Korfhagen *et al.*, 1990). In these cells, SP-C is initially synthesized as a 197 amino acids precursor of 21 kDa (proSP-C), with a N-terminal propeptide of 23 residues and a 139 amino acid C-terminal propeptide (processing will be discussed later) (Olmeda *et al.*, 2017).

The remarkable hydrophobicity of SP-C is attributed to its composition, characterized by 70% non-polar amino acids, including phenylalanine, leucine, valine, isoleucine, alanine, and methionine, as well as the double palmitoylation of cysteine residues at positions 5 and 6 (Johansson, 1998; ten Brinke *et al.*, 2001).

This structure and composition exhibit a high degree of evolutionary conservation across different species (**Figure 8**) (Potter *et al.*, 2007).

Figure 8: Amino acid alignment of SP-C protein from different mammal species. *In bold are proposed dimerization motifs.*

Structure

SP-C protein is embedded within the membranes of pulmonary surfactant, with its C-terminal domain adopting an alpha-helical structure that penetrates deeply into the lipid bilayer, while its N-terminal domain, whose structure remains undefined, has a more superficial character in the membrane (**Figure 9**). In monolayers, SP-C is oriented with its N-terminal domain exposed to the aqueous phase and its C-terminal alpha-helix inserted into the lipid layer, aligning with the hydrophobic core (Casals & Cañadas, 2012; García-Álvarez *et al.*, 2019).

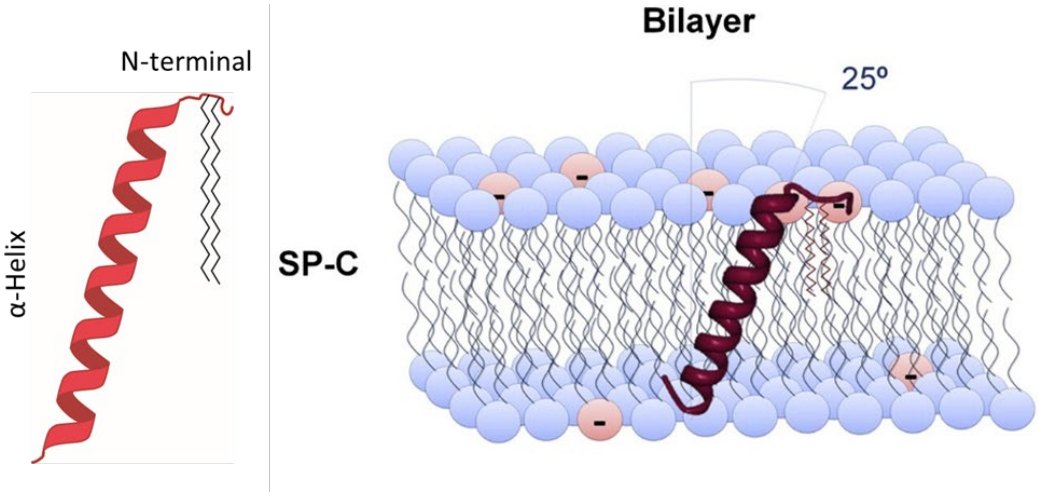

Figure 9: SP-C structure and insertion in membrane bilayers. *Adapted from Roldan et al. (2015).*

The C-terminal domain, comprising residues 13-25, is characterized by a high content of hydrophobic amino acids, which enables its effective anchoring within the lipid layers of pulmonary surfactant. Furthermore, studies on the incorporation

of proteins into membranes at different temperatures have shown that SP-C inserts into the lipid bilayer with an inclination of approximately 25° relative to the plane of the membrane at a physiological temperature of 37 °C (Roldan *et al.*, 2015).

Although the residues that predominantly compose the C-terminal domain, such as valine, leucine, and isoleucine, are typically associated with beta-sheet structures due to their branched side chains, this segment primarily maintains an alpha-helical conformation, as previously noted. However, SP-C has been observed in amyloid fibril form in bronchoalveolar lavage samples from patients suffering from interstitial lung diseases, such as alveolar proteinosis and pulmonary fibrosis. Additionally, it has been reported that SP-C can undergo a conformational transition into beta-sheet structures when the surrounding environment is insufficiently apolar (Cruz *et al.*, 1995). This structural change appears to be associated with a loss of protein function, suggesting that the transition to a beta-sheet conformation could contribute to the development of pathological processes in lung tissue. Some evidences have been found about a likely dimerization of SP-C through a specific motif in its C-terminal segment (Kairys *et al.*, 2004; Luy *et al.*, 2004).

The N-terminal domain (residues 1-12) is positively charged due to the presence of lysine and arginine at residues 11 and 12, respectively. This allows it to establish electrostatic interactions with negatively charged phospholipids, such as phosphatidylglycerol (PG), resulting in greater protein stability and imparting membrane-disruptive properties (Lopez-Rodriguez & Pérez-Gil, 2014; Pérez-Gil *et al.*, 1995; Plasencia *et al.*, 2004).

Additionally, this segment exhibits a hairpin-like structure due to the presence of two prolines flanking two cysteines (PCCP motif) (Johansson, 1998). Consequently, this segment can remain close to the membrane via the dual palmitoylation of the cysteine residues. These palmitic acid chains play a crucial role in anchoring the N-terminal segment. Notably, non-palmitoylated versions of the protein are more readily excluded from the interface than their palmitoylated counterparts (Bi *et al.*, 2002; Lukovic *et al.*, 2012).

Some studies have demonstrated that the N-terminal domain of SP-C is capable of interacting with membranes even in the absence of palmitoylation, suggesting that palmitoylation might serve additional roles beyond facilitating SP-C membrane anchoring. Palmitoylation could also stabilize the alpha-helical structure, preventing protein aggregation (Chevallet *et al.*, 2006; Dluhy *et al.*, 2003; Vandenbussche, Clercx, Curstedt, *et al.*, 1992; Wang *et al.*, 1996). Roldán and collaborators observed that palmitoylation induces changes in protein plane tilting, with the palmitoylated form being more tilted with respect to the

membrane. Furthermore, it induces alterations in the configuration of the headgroup region of phospholipid layers, potentially affecting membrane permeability (Roldan *et al*., 2015).

It is important to note that in surfactant samples from individuals with pulmonary alveolar proteinosis, a significant number of non-palmitoylated or mono-palmitoylated SP-C variants have been identified, underscoring the critical importance of protein acylation (Voss *et al*., 1992).

Function

Biophysical function

SP-B and SP-C are critical components of the lung surfactant system, enabling the membrane dynamics required for efficient respiratory mechanics. These hydrophobic proteins play complementary roles in ensuring that the surfactant film adapts to the constantly changing alveolar environment during the breathing cycle. By facilitating lipid reorganization and exchange, SP-B and SP-C are central to the squeeze-out model, a widely accepted explanation for surfactant function (Keating *et al*., 2012; Pastrana-Rios *et al*., 1994). This model describes how surfactant films adapt to compression during exhalation and expansion during inhalation. During alveolar compression, the surfactant film at the air-liquid interface becomes selectively enriched in DPPC, a lipid capable of forming a tightly packed monolayer that reduces surface tension to near-zero levels. Lipids that fluidize DPPC and facilitate its adsorption are excluded from the interface during this phase. SP-B and SP-C play a key role in ensuring that these excluded lipids form reservoirs in the subphase, composed of multilamellar or bilayer structures (**Figure 10**). These reservoirs serve as a source of lipids for re-spreading into the interface during expansion, allowing the surfactant film to dynamically regulate surface tension throughout the breathing cycle. Evidence from in vitro studies supports the existence of stacked multilayers as surfactant reservoirs, although their orientation (toward the air or the hypophase) and occurrence in vivo remain under investigation (Amrein *et al*., 1997; Keating *et al*., 2012; Sachan & Galla, 2013).

Given the surfactant's exposure to oxidative damage, pollutants, and other inactivating agents, periodic renewal is essential for maintaining its efficient performance. Deep inhalation recruits fresh surfactant from reservoirs or newly secreted lamellar bodies, incorporating DPPC and unsaturated lipids into the interface. During subsequent compression cycles, oxidized molecules and less packable unsaturated lipids are excluded via the squeeze-out mechanism, preserving the surfactant’s structural integrity and performance. SP-B and SP-C thus ensure the surfactant system's elasticity, stability, and adaptability, maintaining the delicate balance required for efficient respiratory mechanics.

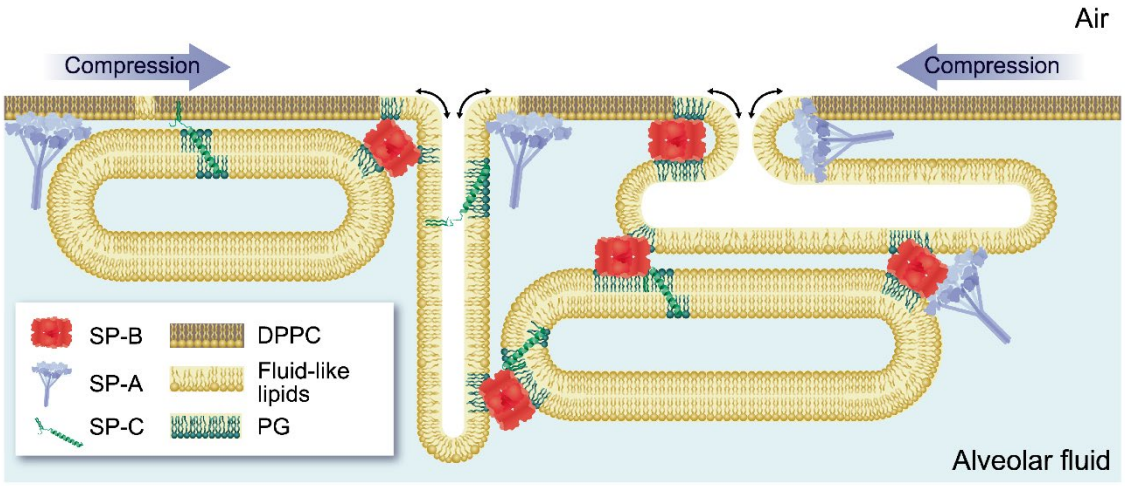

Figure 10: Schematic representation of the dynamic behavior of lung surfactant during the respiratory cycle. *During alveolar compression (exhalation), the surfactant monolayer becomes enriched in dipalmitoylphosphatidylcholine (DPPC), which forms a tightly packed structure capable of achieving near-zero surface tension. Non-DPPC lipids, which are necessary for fluidizing the monolayer and facilitating lipid adsorption, are excluded from the interface and temporarily stored in underlying multilayered reservoirs. These lipid reservoirs are stabilized and reorganized by the action of SP-B and SP-C, which mediate lipid exchange between the monolayer and multilayers, enabling re-spreading during alveolar expansion (inhalation). This continuous remodeling ensures surfactant performance and adaptability under dynamic compression and expansion conditions. Illustration from Cañadas et al. (2020).*

In particular, SP-C plays a variety of critical and complementary roles in the biophysical dynamics of lipid membranes and surfactant function. The protein is involved in the transfer of lipids between monolayers and multilayered structures, the adsorption of surface-active molecules into the air-liquid interface, and the preservation of the structural integrity of multilayered surfactant reservoirs (Plasencia *et al.*, 2008; Taneva & Keough, 1994). SP-C greatly alters lipid packing in membranes, influencing lipid motion and lateral distribution, which facilitates interfacial adsorption and lipid transfer among bilayers and between bilayers and monolayers (Dico *et al.*, 1997; Morrow, Taneva, *et al.*, 1993). This process is essential for the reversible formation of multilayered stacks connected to the interfacial monolayer, allowing the capture of surfactant material presumably squeezed out during exhalation and its re-spreading during inhalation

The functional activity of SP-C is largely dependent on its rigid transmembrane helix, which induces lipid alterations through hydrophobic interactions. Additionally, its N-terminal segment contributes to these effects by interacting with membranes, inducing packing defects that lead to vesicle aggregation and leakage in vitro (Plasencia *et al.*, 2005; Plasencia *et al.*, 2004). Electrostatic interactions between the cationic charges of the N-terminal segment and acidic phospholipids, such as phosphatidylglycerol, further highlight its role in modifying lipid organization (Takamoto *et al.*, 2001). Importantly, SP-C's palmitoylation is considered crucial for sustaining these interactions, as the palmitic chains stabilize the protein structure and appear to enhance its capacity to sort and

perturb lipids at' the interface (Gonzalez-Horta *et al.*, 2008; Qanbar *et al.*, 1996). While SP-C's palmitoylation is critical for many of its functions, it has been observed that this modification is not required for interfacial lipid adsorption but is necessary to sustain lipid sorting under high compression rates. This includes the ability to induce interdigitated phases and enhance lipid phase segregation, which are thought to contribute to the efficient remodeling of surfactant films during the respiratory cycle (Roldan *et al.*, 2017). Furthermore, the protein's ability to dimerize through specific motifs in its C-terminal segment may play a role in its function (Kairys *et al.*, 2004).

SP-C also exhibits a particular interaction with cholesterol, a key surfactant modulator. Cholesterol can impair surfactant function under certain conditions, but SP-C seems to at least partially counteract these effects, particularly when it is palmitoylated (Gómez-Gil, Schürch, *et al.*, 2009). Evidence suggests that SP-C improves cholesterol miscibility in surfactant-mimicking membranes and can fragment lipid bilayers into small vesicles where cholesterol accumulates. These properties imply a potential role for SP-C in cholesterol mobilization and pulmonary homeostasis, though the exact mechanisms underlying these interactions remain unknown (Roldan *et al.*, 2016). Additionally, SP-C and cholesterol appear to cooperate to modulate surfactant activity, with SP-C possibly stabilizing surfactant functionality at high compression rates when cholesterol and SP-B are present (Baumgart *et al.*, 2010; Bernardino de la Serna *et al.*, 2004).

Immune Function

SP-C plays several roles in modulating immune responses in the lung, complementing its biophysical functions in surfactant dynamics. A key immunomodulatory activity of SP-C involves its ability to bind bacterial lipopolysaccharides (LPS), facilitating their interaction with the CD14 receptor on macrophages (Augusto *et al.*, 2001; Augusto *et al.*, 2002; Augusto, Synguelakis, Johansson, *et al.*, 2003; Olmeda *et al.*, 2017). This binding may enhance the recognition and clearance of Gram-negative bacterial components by the immune system. Detailed analyses suggest that the N-terminal domain of SP-C binds specifically to the lipid A moiety of LPS, while the C-terminal domain may stabilize the protein's conformation, optimizing its interaction with LPS and CD14 (Augusto *et al.*, 2002; Augusto, Synguelakis, Johansson, *et al.*, 2003). SP-C may also modulate LPS-induced cytokine production via TLR-4 signaling in macrophages, potentially by reducing the receptor's affinity for LPS through a complex interplay with CD14 (Augusto, Synguelakis, Johansson, *et al.*, 2003; Chaby *et al.*, 2005). Alternatively, it has been proposed that SP-C mediates CD14-independent LPS handling, where its N-terminal segment could transfer LPS into liposomes,

preventing its binding to TLR-4 and thereby reducing cytokine production (Garcia-Verdugo *et al.*, 2009).

SP-C deficiency has been associated with increased inflammatory responses in SP-C knockout (KO) mice, including exacerbated macrophage accumulation and elevated levels of pro-inflammatory cytokines such as IL-1β, IL-6, and TNF-α upon LPS challenge (Glasser *et al.*, 2013). These findings suggest that SP-C may help to limit excessive inflammatory signaling in the lung. Furthermore, SP-C's anti-inflammatory activity has been observed under pathogen-free conditions, indicating that it may contribute to resolving inflammation even in the absence of infection (Jin *et al.*, 2018).

SP-C also appears to influence the function of alveolar macrophages and cholesterol metabolism. Evidence suggests that SP-C may regulate the uptake and handling of oxidized cholesterol and phospholipid species by alveolar macrophages, potentially mitigating pro-inflammatory signaling and NLRP3 inflammasome activation (Ertunc & Hotamisligil, 2016). In SP-C-deficient models, increased uptake of oxidized surfactant components by alveolar macrophages has been observed, which could contribute to the formation of foamy macrophages in the lungs of affected individuals (Glasser *et al.*, 2003; Hamvas *et al.*, 2004). This disrupted cholesterol metabolism may play a role in the pathogenesis of SP-C-related lung diseases, such as interstitial lung disease and pulmonary fibrosis (Lawson *et al.*, 2004; Salerno *et al.*, 2016).

SP-C's interaction with cholesterol may also impact surfactant dynamics. It has been proposed that SP-C could fragment lipid bilayers into small, highly curved vesicles, facilitating the accumulation and mobilization of cholesterol within surfactant reservoirs (Roldan *et al.*, 2016). This activity may contribute to maintaining surfactant homeostasis and ensuring proper membrane fluidity and stability during compression and expansion cycles. The palmitoylation state of SP-C has been reported to affect these interactions, potentially influencing its ability to restore surfactant function in cholesterol-impaired systems (Gómez-Gil, Pérez-Gil, *et al.*, 2009; Gómez-Gil, Schürch, *et al.*, 2009).

In summary, SP-C likely plays a versatile role in lung immunity, balancing host defense mechanisms and inflammatory responses while modulating alveolar macrophage function and cholesterol metabolism. These activities may contribute to maintaining immune homeostasis and protecting against surfactant dysfunction, although the underlying molecular mechanisms require further investigation.

Alveolar homeostasis

As mentioned before, the constituents of pulmonary surfactant are synthesized in lamellar bodies (LBs), which are specific organelles produced by AECII. Once in the alveolar space, the components of PS traverse the hypophase to reach the air-liquid interface (Olmeda *et al.*, 2017), where they are exposed to a highly oxidative environment that, over time, alters their structure and function. Consequently, in healthy lungs, a balance between PS secretion and processing/recycling is maintained.

This homeostasis in the lung is likely regulated by the activity of type II alveolar epithelial cells and alveolar macrophages (AMϕ), as both cell types contribute to the internalization of excess PS and its subsequent catabolism (**Figure 11**).

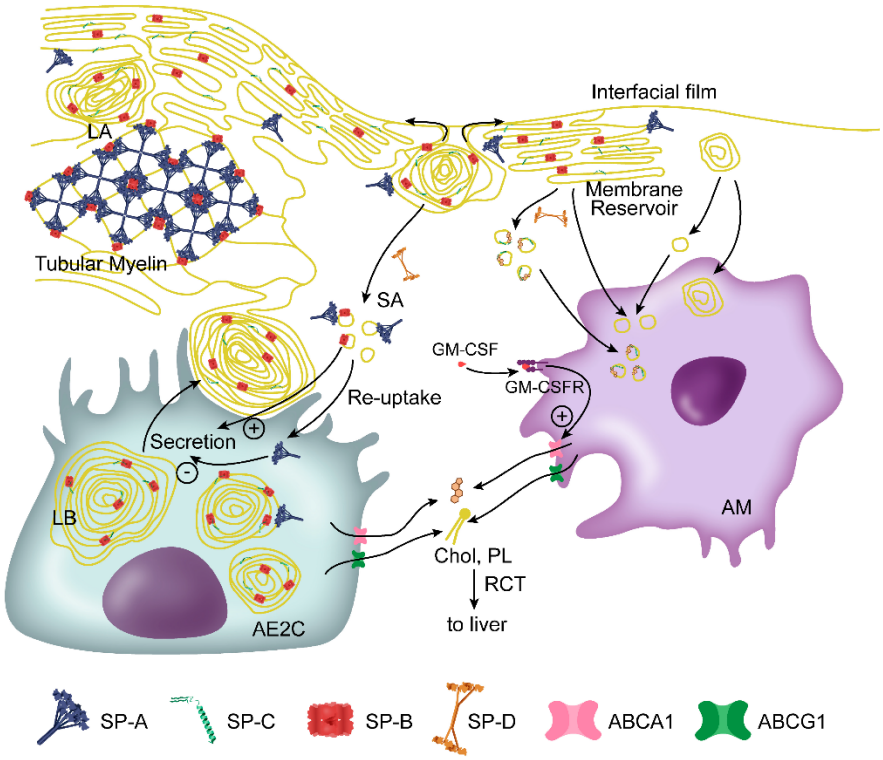

Figure 11: Schematic representation of the pulmonary surfactant lifecycle involving type II alveolar epithelial cell (AECII) and alveolar macrophages (AM). *The AE2C (type II alveolar epithelial cells) synthesizes and secretes surfactant components, stored in lamellar bodies (LBs), into the alveolar space. These components adsorb onto the air-liquid interface, forming a surfactant film crucial for reducing surface tension. Alveolar macrophages process excess surfactant and participate in its recycling. Various molecules, such as SP-A, SP-B, SP-C, and SP-D, play critical roles in the surfactant's structural and functional integrity. Proteins like ABCA1 and ABCG1 are involved in cholesterol and phospholipid transport, while GM-CSF signaling modulates surfactant secretion and recycling, maintaining lung homeostasis. Illustration from Cañadas et al. (2020).*

Synthesis and secretion of pulmonary surfactant

Lipid synthesis

Pulmonary surfactant lipids are synthesized through both de novo pathways and remodeling mechanisms, ensuring the production of the necessary components

for proper surfactant function. These pathways are tightly regulated and influenced by environmental conditions and physiological needs (Olmeda *et al.*, 2017).

The de novo synthesis of phosphatidylcholine (PC), the primary phospholipid in pulmonary surfactant, occurs via the Kennedy pathway. This process includes the phosphorylation of choline by choline kinase (CK), its conversion to CDP-choline by CTP:phosphocholine cytidyltransferase (CCT), and the final synthesis of PC by choline phosphotransferase (CPT). The latter step depends on the conversion of phosphatidic acid (PA) to diacylglycerol (DAG) by phosphatidic acid phosphatase (PAP) (Pol *et al.*, 2014). CCT is the rate-limiting enzyme in this pathway, and its regulation is critical for surfactant biosynthesis during lung development and in the postnatal period (Tian *et al.*, 2007; Wang *et al.*, 2005).

During fetal development, de novo synthesis is upregulated to meet the high demand for surfactant at birth. Glucocorticoids have been shown to stimulate fatty acid synthase (FAS) and other enzymes involved in fatty acid and PC biosynthesis, highlighting the hormonal regulation of surfactant lipid production during lung maturation (Agassandian & Mallampalli, 2013; Liggins, 1969).

The remodeling pathway, or Lands cycle, plays a predominant role in the synthesis of dipalmitoylphosphatidylcholine (DPPC), the most important surfactant phospholipid. This pathway begins with the deacylation of monounsaturated PC by phospholipase A2 (PLA2), producing lysophosphatidylcholine (lyso-PC). Lyso-PC is then reacylated with saturated fatty acids (e.g., palmitic acid) by acyl-CoA:lysophosphatidylcholine acyltransferase (LPCAT1), generating DPPC (Bridges *et al.*, 2010). LPCAT1 is crucial for surfactant function because it ensures the availability of saturated PC species required for reducing alveolar surface tension to minimal levels.

LPCAT1 also integrates de novo synthesis and remodeling pathways, potentially increasing activity during high surfactant demand. This may lead to reduced de novo synthesis by promoting CPT degradation, limiting the production of non-surfactant PC species and prioritizing DPPC synthesis (Butler & Mallampalli, 2010).

Peroxiredoxin 6, a bifunctional enzyme with both PLA2 and LPCAT activities, has been implicated in the remodeling of DPPC. Located in lamellar bodies, this enzyme enables the complete remodeling pathway to occur within these organelles. In addition to its role in DPPC synthesis, peroxiredoxin 6 contributes to the degradation of internalized DPPC, providing lyso-PC substrates for remodeling (Fisher & Dodia, 1996; Fisher & Dodia, 2001). Its glutathione peroxidase activity may also protect the lung by repairing peroxidized membranes (Chen *et al.*, 2006).

Phosphatidylglycerol (PG), the second most abundant surfactant phospholipid, is synthesized de novo via CDP-diacylglycerol and remodeled into dipalmitoylphosphatidylglycerol (DPPG) through LPCAT1 activity (Nakanishi *et al.*, 2006). PG plays a dual role as a structural component and as a regulator of innate immunity, modulating the activity of cationic surfactant proteins SP-B and SP-C (Chavarha *et al.*, 2013; Parra *et al.*, 2013). Its ability to form mechanically resistant films and selectively interact with SP-B underlines its functional significance (Olmeda *et al.*, 2015; Pérez-Gil *et al.*, 1995).

Cholesterol, the most abundant neutral lipid in surfactant, is derived from circulating lipoproteins or synthesized within AECII. Lamellar bodies contain cholesterol-binding proteins NPC1 and NPC2, which may regulate cholesterol content and trafficking via the Niemann-Pick C pathway (Roszell *et al.*, 2012). Cholesterol levels in surfactant can vary with environmental conditions, such as body temperature or exercise, suggesting an adaptive regulatory mechanism (Doyle *et al.*, 1994; Orgeig *et al.*, 2003; Suri *et al.*, 2012). However, an excess of cholesterol, as observed in acute respiratory distress syndrome (ARDS), has been associated with impaired surfactant function, though whether this is a cause or consequence remains unclear (Vockeroth *et al.*, 2010).

Protein synthesis

The synthesis and maturation of pulmonary surfactant proteins involve intricate processes of transcription, translation, and post-translational modifications, with distinct pathways for hydrophilic and hydrophobic proteins.

SP-A and SP-D are synthesized as propeptides in alveolar type II cells, undergoing glycosylation, hydroxylation, and oligomerization in the endoplasmic reticulum (ER) and Golgi apparatus (Crouch, 1998; Weaver & Whitsett, 1991). SP-D secretion appears to follow a constitutive pathway independent of lamellar body trafficking. For SP-A, there is still debate regarding its secretion route. Some studies suggest that newly synthesized SP-A is secreted directly into the alveolar space via lamellar bodies, while others propose that the SP-A present in lamellar bodies derives from protein previously endocytosed from the alveolar space (Fisher *et al.*, 1994; Ochs *et al.*, 2002; Osanai *et al.*, 1998; Schmiedl *et al.*, 2005).

SP-B is encoded by the *SFTPB* gene located on chromosome 2, and its expression is regulated by the transcription factor TTF-1 (thyroid transcription factor 1) (Lopez-Rodriguez & Pérez-Gil, 2014). The initial translation produces a 381-amino-acid preprotein, which is translocated into the endoplasmic reticulum (ER) as a 42 kDa proprotein (proSP-B) comprising three domains: the mature SP-B sequence (proSP-$B_{201-279}$) and N- and C-terminal propeptides (proSP-B_{1-200} and proSP-$B_{280-381}$), respectively). The propeptides likely serve a chaperone-like function, protecting the hydrophobic core of the mature protein during trafficking through the aqueous

intracellular environment (Akinbi *et al.*, 1997; Guttentag *et al.*, 1998; Serrano *et al.*, 2007).

The proteolytic processing of proSP-B occurs sequentially through the endosomal pathway, involving enzymatic cleavage in multivesicular bodies (MVBs), intermediate composite bodies, and lamellar bodies (LBs). This processing relies on a pH gradient along the pathway (Pérez-Gil & Frick, 2024), with acidic conditions (down to pH 5.5) activating proteases such as cathepsin H, napsin A, and pepsinogen C (Brasch, Johnen, *et al.*, 2004; Gerson *et al.*, 2008; Guttentag *et al.*, 2003). These enzymes cleave proSP-B into its mature 8 kDa form, while the N-terminal fragment of the propeptide is also transported to the LBs (**Figure 12**). The N-terminal domain of the precursor has been shown to exhibit microbicidal activity, possibly due to its saposin-like domain, which resembles antimicrobial peptides like granulysin (Brasch, Johnen, *et al.*, 2004; Yang *et al.*, 2010).

The C-terminal propeptide of SP-B may contribute to the formation and maintenance of LBs. Studies in transgenic mice expressing a truncated form of SP-B lacking the C-terminal propeptide revealed increased surfactant pool sizes and enlarged LBs, suggesting a role in surfactant storage and biogenesis (Akinbi *et al.*, 1997). Additionally, the saposin-like domain of the C-terminal fragment has been proposed to possess antimicrobial properties, further contributing to host defense (Perez-Gil & Weaver, 2010).

SP-C is encoded by the *SFTPC* gene on chromosome 8 and is also regulated by TTF-1. The precursor, proSP-C, is synthesized as a 21 kDa protein consisting of the hydrophobic mature sequence (proSP-C_{24-58}) flanked by N- and C-terminal propeptides (proSP-C_{1-23} and proSP-C_{59-197}, respectively). The proprotein is inserted into the ER in a type II orientation, with the N-terminal segment facing the cytoplasm and the C-terminal segment located within the ER lumen (Beers & Mulugeta, 2005; Keller *et al.*, 1991; Mulugeta & Beers, 2003).

The C-terminal propeptide (proSP-C_{59-197}) contains a BRICHOS domain (from Bri protein associated with familial British dementia, chondromodulin, and proSP-C), which may act as a chaperone, facilitating proper folding of the mature SP-C α-helix and stabilizing it until acylation of the protein (Johansson *et al.*, 2009; Perez-Gil & Weaver, 2010; Sánchez-Pulido *et al.*, 2002). Palmitoylation occurs at cysteine residues 5 and 6 of the mature SP-C sequence through an unidentified palmitoyl transferase, being the N-terminal close to the membrane (Gustafsson *et al.*, 2001). Palmitoylation is essential for proSP-C trafficking to the trans-Golgi network, where proteolytic processing begins (Beers & Lomax, 1995; Vorbroker *et al.*, 1992).

The processing of proSP-C involves sequential cleavage of the C- and N-terminal segments by proteases, including cathepsin H and pepsinogen C (Beers *et al.*, 1994). The C-terminal BRICHOS domain is first removed in the medial Golgi,

resulting in an intermediate 16 kDa peptide. Additional cleavage steps of N-terminal segment (essential for protein sorting) occur in MVBs and composite bodies (Johnson *et al.*, 2001), yielding a 7 kDa intermediate that eventually matures into the 4.2 kDa SP-C found in LBs (Beers & Mulugeta, 2005; Brasch *et al.*, 2002; Guttentag *et al.*, 2003). SP-B is required for the proper cleavage of proSP-C in MVBs and LBs, potentially by facilitating the orientation of proSP-C for proteolytic exposure. Mature SP-C primarily resides in LBs, where it integrates with surfactant phospholipids for secretion into the alveolar space (**Figure 12**) (Vorbroker *et al.*, 1995).

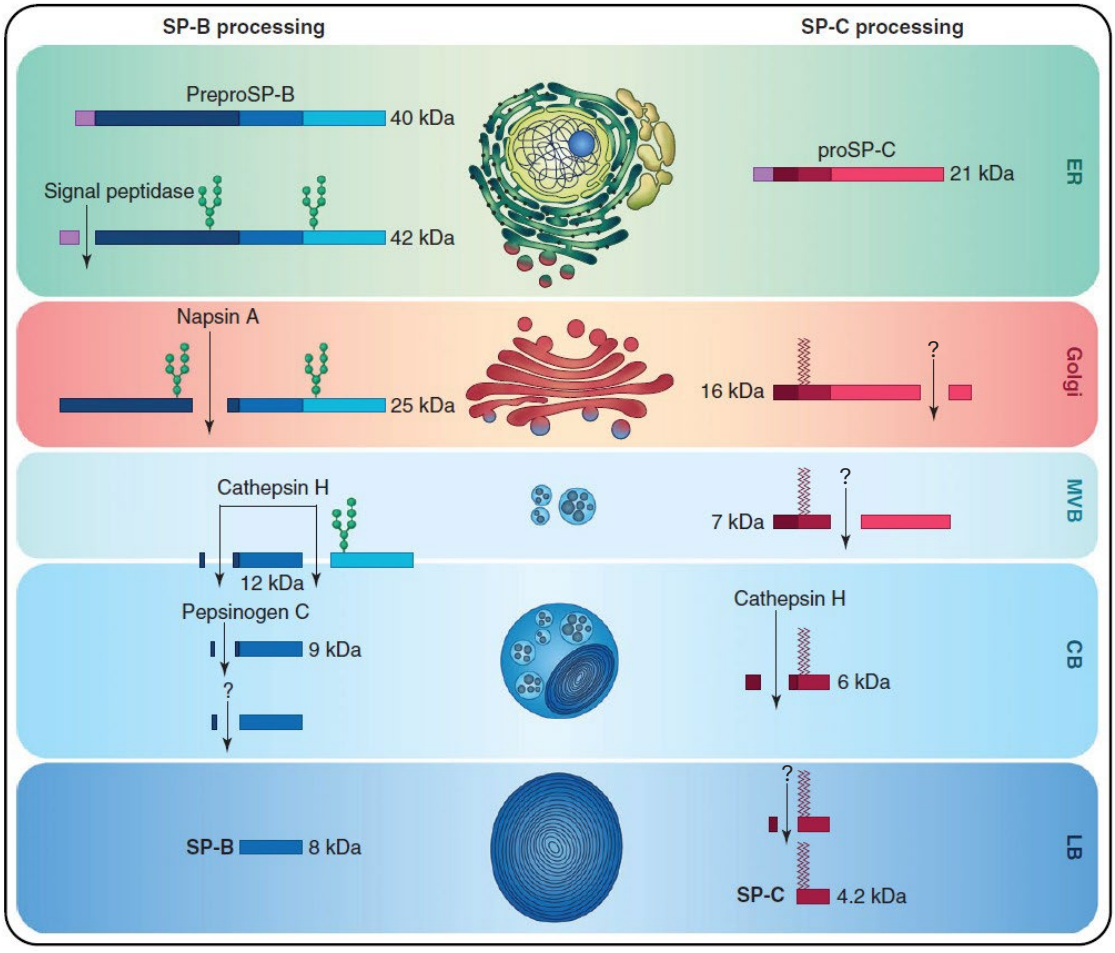

Figure 12: Synthesis and processing of hydrophobic surfactant proteins SP-B and SP-C. *Both SP-B and SP-C are synthesised as large precursors proSP-B and proSP-C, which are sequentially cleaved along the exocytosis pathway (ER, endoplasmic reticulum; MVB, multivesicular bodies; CB, composite bodies; LB, lamellar bodies) until they are assembled as lipid/protein complexes into lamellar bodies for their secretion. ?, Cleavage step promoted by a yet unknown protease. Illustration from García-Álvarez et al. (2019)*

Assembly and secretion of lamellar bodies

Lipids and proteins are transported to LBs via distinct mechanisms. Hydrophobic surfactant proteins SP-B and SP-C are transferred through multivesicular bodies (MVBs) during their maturation process, while lipid transport remains less

understood. Experimental evidence suggests that newly synthesized lipids may bypass vesicular pathways and instead rely on non-vesicular transport mechanisms. For instance, phosphatidylcholine (PC) transport from the ER to LBs may involve the phospholipid transport protein StarD10 (Lin *et al.*, 2015) and the ATP-binding cassette transporter A3 (ABCA3), which localizes to the limiting membrane of LBs and transfers lipids into their lumen at the expense of ATP hydrolysis (Ban *et al.*, 2007; Cheong *et al.*, 2007).

ABCA3 is essential for LB biogenesis, enabling the assembly of densely packed lipid-protein structures. The energy provided by ATP hydrolysis may facilitate the formation of highly dehydrated and non-lamellar phases, which contribute to the rapid and efficient interfacial adsorption of surfactant upon secretion (Castillo-Sánchez *et al.*, 2022; Cerrada *et al.*, 2015; Malacrida *et al.*, 2016). SP-B plays a complementary role in LB biogenesis by promoting membrane-membrane interactions, ensuring the proper organization of surfactant membranes within LBs (Stahlman *et al.*, 2000).

Surfactant secretion occurs through LB exocytosis, initiated by the fusion of the LB limiting membrane with the plasma membrane of AECII. Mechanical stretching of alveoli during inspiration is the primary physiological stimulus for this process, which increases cytoplasmic calcium concentrations ($[Ca^{2+}]c$) in AECII (Nicholas *et al.*, 1982). The calcium signal is supplied both from intracellular stores and via extracellular calcium entry through TRPV2 channels (Frick *et al.*, 2004). Additionally, ATP release from type I alveolar cells (AECI) during mechanical stretching can stimulate surfactant secretion in neighboring AECII through purinergic signaling (Frick *et al.*, 2004). Other agents, such as β2-adrenergic agonists and purinergic receptor agonists, also promote surfactant exocytosis through pathways involving protein kinase A (PKA), protein kinase C (PKC), and Ca^{2+}/calmodulin-dependent protein kinase (CaMK) (Rooney, 2001)(Rooney, 2001).

Once secreted, LBs retain their densely packed organization in the alveolar fluid as lamellar body-like particles (LBPs). These particles unravel upon contact with the air-liquid interface, facilitated by the coordinated action of SP-B and SP-C (Hobi *et al.*, 2016; Ravasio *et al.*, 2010). The unraveling process enables the efficient formation of the interfacial surfactant film, crucial for reducing surface tension. In some cases, LBPs may transition into other structures, such as tubular myelin—a lattice-like network of membranes formed by SP-A, SP-B, and calcium. While tubular myelin was historically considered an intermediate structure required for interfacial film formation, various studies suggest that it is not essential for surfactant function in vivo (Ikegami, Korfhagen, *et al.*, 1998; Sato & Kishikawa, 2001). Instead, LBPs, large vesicles, or lipid aggregates may directly adsorb to the air-liquid interface, ensuring surfactant functionality.

Recycling and degradation of pulmonary surfactant

Surfactant recycling and degradation are essential processes for maintaining surfactant homeostasis and alveolar function. Once secreted, surfactant components, including lipids and proteins, are long-lived molecules with a half-life ranging from 10 to several tens of hours. Surfactant clearance involves both the recycling and catabolism of its components, primarily mediated by type II alveolar epithelial cells (AECII) cells and alveolar macrophages (AMϕ) (Günther *et al.*, 1999; Olmeda *et al.*, 2017).

Recycling by AECII

AECII are responsible for approximately 65% of surfactant clearance (Rider *et al.*, 1992). Surfactant lipids and proteins are recycled through pathways mediated by SP-A, which binds to small surfactant aggregates and interacts with specific receptors, potentially P63, on the AECII membrane (Bates, 2010). This interaction promotes internalization via a clathrin-dependent mechanism, leading to sorting in early endosomes and transfer to lamellar bodies in a calmodulin-dependent process (Wissel *et al.*, 2001). An alternative actin-dependent pathway also contributes to lipid uptake by AECII, although this mechanism appears to play a minor role in recycling (Bates *et al.*, 2008).

Not all SP-A is recycled; a portion follows an actin-dependent degradation route, highlighting the dual pathways for protein fate in AECII (Nakanishi *et al.*, 2006). In the absence of SP-A, clathrin-mediated endocytosis becomes the primary recycling mechanism (Bates *et al.*, 2008). Additionally, SP-C may aid in recycling by inducing membrane fragmentation and forming small lipoprotein vesicles enriched in cholesterol, which are internalized by AECII or alveolar macrophages (Roldan *et al.*, 2016; Ruwisch *et al.*, 2020).

Role of Alveolar Macrophages in Degradation

Alveolar macrophages are critical for metabolizing 20–30% of surfactant components, including oxidized or damaged lipids and proteins (Lopez-Rodriguez & Pérez-Gil, 2014; Olmeda *et al.*, 2017; Wright & Clements, 1987). These cells degrade surfactant lipids primarily through phospholipase A2 (PLA2) activity. Altered macrophage function, as seen in conditions such as pulmonary alveolar proteinosis (PAP), results in impaired lipid degradation and the accumulation of lipids in the alveolar fluid, leading to the formation of "foamy macrophages" characterized by intracellular lipid droplets (Trapnell *et al.*, 2003). GM-CSF (granulocyte-macrophage colony-stimulating factor) plays a key role in regulating macrophage-mediated surfactant clearance (Trapnell & Whitsett, 2002).

SP-D modulates lipid uptake by promoting the transformation of large surfactant aggregates into smaller, less functional aggregates, which are preferentially

cleared by AECII and macrophages (Ikegami *et al.*, 2009). This activity may involve binding to phosphatidylinositol, though the precise mechanism remains unclear. SP-C, in conjunction with cholesterol, has been shown to enhance lipid uptake by alveolar macrophages, contributing to the intracellular accumulation of lipids in droplets while localizing SP-C to defined regions of the plasma membrane (Ruwisch *et al.*, 2020; Sehlmeyer *et al.*, 2020).

Degradation of Spent Surfactant

During respiratory cycles, surfactant at the air-liquid interface undergoes compression-expansion dynamics, resulting in compositional changes and the progressive loss of material. Spent surfactant is thus released from the interfacial film as small aggregates, which are directed toward AECII and macrophages for clearance (Günther *et al.*, 1999). Surfactant degradation is essential to remove oxidized or inactivated components, particularly those exposed to harmful environmental agents, as mentioned before. While lipid degradation primarily occurs through PLA2 activity in both cell types, AECII also eliminates excess phosphatidylcholine via basolateral transport mediated by ABCA1 (Bortnick *et al.*, 2003; Zhou *et al.*, 2004).

Surfactant Turnover

The turnover rate of surfactant pools, defined as the time required for their replenishment by newly secreted material, ranges from 4 to 11 hours in alveolar fluid (Wright & Clements, 1987). This continuous renewal ensures that fully functional surfactant is available at the interface, maintaining alveolar stability and efficient respiratory mechanics. Although SP-D and SP-C facilitate the regulation of lipid uptake and recycling (Ikegami *et al.*, 2009; Roldan *et al.*, 2016; Ruwisch *et al.*, 2020), further studies are needed to clarify the detailed mechanisms of these processes.

3.

OBJECTIVES

3.Objectives

Pulmonary surfactant is a complex mixture of lipids and proteins that reduces surface tension at the alveolar surface, preventing collapse during respiration. Among its protein components, surfactant protein C (SP-C) plays a key role in stabilizing and reorganizing lipid membranes, thus ensuring the structural and functional integrity of the surfactant.

The main objective of this thesis is to **explore the role of SP-C in the recycling and processing of pulmonary surfactant, processes that are crucial for alveolar homeostasis, as well as to investigate the molecular mechanisms underlying these processes**. In order to achieve this goal, the following specific objectives have been outlined:

1. To investigate propensity of SP-C to form dimers and oligomers, assessing protein-protein interactions through Bimolecular Fluorescence Complementation (BiFC) assays and fluorescence spectroscopy. This will include an analysis of how factors such as lipid composition, specific structural motifs, and palmitoylation status influence these interactions.
2. To study the ability of SP-C to induce membrane fragmentation using synthetic and native lipid systems. Techniques such as Nanoparticle Tracking Analysis (NTA), Tunable Resistive Pulse Sensing (TRPS), and the use of giant unilamellar vesicles (GUVs) will be employed to analyze SP-C distribution and effects in membranes and to assess SP-C-promoted overall membrane characteristics.
3. To analyze the role of SP-C in surfactant homeostasis, exploring its contribution to the recycling, uptake, and intracellular processing of lipids and proteins by different alveolar cell types. This objective will involve the use of confocal microscopy to visualize the localization and dynamics of vesicles within cells, as well as cellular models to evaluate SP-C's capacity to promote vesicle uptake by alveolar epithelial type II cells and alveolar macrophages.

4.

MATERIALS AND METHODS

Materials

Reagents and synthetic molecules

All reagents and chemicals were supplied by Merck (Darmstadt, Germany) and synthetic lipids by Avanti Polar Lipids (Alabaster, AL, USA) unless otherwise indicated. Chloroform and methanol were acquired from LabScan (Bangkok, Thailand).

DNA constructs

DNA coding for the proteins of interest, detailed in **Table 1**, was flanked by NotI recognition site in vector backbone pMA-RQ (AmpR). All of them were purchased from Thermo Fisher Scientific (Waltham, MA, USA). Each DNA construct was amplified using the PCR technique as described in Section 2.1 and subsequently purified with the NZYTech DNA Purification Kit (NZYTech, Lisbon, Portugal).

Table 1. Protein sequences codified by DNA constructs.

Protein	Sequence
proSP-C	N- and C-terminal propeptides (proSP-C_{1-23} and proSP-C_{59-197}, including mature SP-C (proSP-C_{24-58})
SP-C	FGI**PCCP**VHLKRLLIVVVVVLIVVVIVG**ALLMG**L
sSP-C	HLGRVKPCICFPVVVAVGVLMLIVVLVIVVLLLGI
SP-C (C →A)	FGIP<u>AA</u>PVHLKRLLIVVVVVLIVVVIVG**ALLMGL**
SP-C (A, G → I)	FGIPCCPVHLKRLLIVVVVVLIVVVIVG<u>I</u>LLM<u>I</u>L

Bold letters indicate dimerization motifs. Underlined are mutated residues with respect to wildtype sequence.

Sequences codifying the N-terminal (VN) or C-terminal (VC) segments of Venus Fluorescent Protein (VFP) were contained whitin BiFC plasmids (pBiFC-VN155 and pBiFC-VC155, respectively). These plasmids include downstream of VN or VC sequence encoding either GpA or mutated GpA and were provided by Dr. Ismael Mingarro from University of Valencia (Grau *et al.*, 2017). Due to BRICHOS domain at the C-terminal propeptide of proSP-C being necessary for the proper processing and folding of the protein, a DNA construct codifying the sequence of mature SP-C and the C-terminal domain was used. In addition, a DNA construct codifying just the mature SP-C and DNA constructs codifying mutant version of the mature SP-C were also used. Scrambled SP-C preserves the same number of amino acids as the mature SP-C and the hydrophobic α-helical segment at the C-terminal region of the mature protein.

To fuse the DNA fragments obtained by PCR with VN or VC, NotI restriction sites were used (**Figure 1**). The digestion reaction was performed in a 50 µL volume containing 1X CutSmart® Buffer, 0.3 µg of DNA fragments, 2 U of NotI (New

England Biolabs, Ipswich, MA, USA), and autoclaved MilliQ water, incubated at 37 °C overnight. Simultaneously, BiFC plasmids were digested using 3 U of NotI for 2 µg of plasmid DNA under the same conditions as the DNA fragments. It was stopped incubating the digestion mixture at 65 °C during 20 min. Digested DNA fragments were purified using NZYTech DNA Purification Kit (NZYTech, Lisbon, Portugal). To prevent self-ligation, the digested plasmids were dephosphorylated by incubating them with 5 units of alkaline phosphatase (New England Biolabs, Ipswich, MA, USA) for 20 minutes at 37°C. The dephosphorylation reaction was inactivated by incubating the mixture at 75°C for 5 minutes. Then the digested plasmids were subjected to 1.5% agarose gel electrophoresis as described in Section 2.2 and were purified from the agarose gel fragment using the NZYGelpure commercial kit (NZYTech, Lisbon, Portugal) following the manufacturer's protocol.

The DNA fragments encoding the proteins of interest and the plasmid fragments digested with NotI were ligated at a 1:5 molar ratio using 0.5 ng/µL concentration of plasmid vector and T4 DNA ligase (Thermo Fisher Scientific, Waltham, MA, USA; **Figure 1**). The ligation was performed at 37 °C for 1 hour, followed by incubation at 4 °C overnight in a mixture consisting of 1X ligation buffer (50 mM Tris-HCl, 10 mM MgCl2, 1 mM ATP, 10 mM dithiothreitol (DTT), pH 7.5) and 0.5 U of T4 DNA ligase in a final volume of 10 µL. The ligated DNA molecules were transformed into One-Shot™ TOP10 *E. coli* cells, as described in Section 2.2.

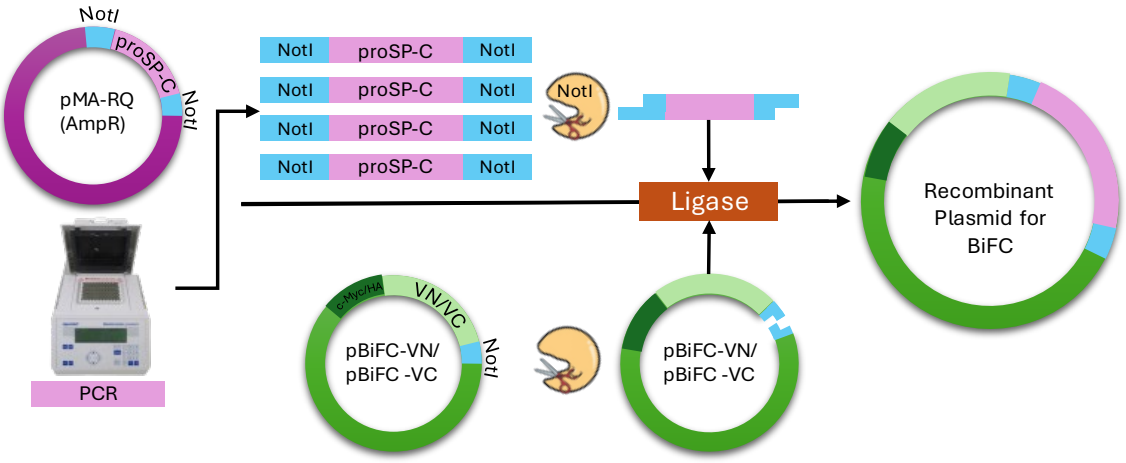

Figure 1: Schematic Representation of DNA Construct Production for BiFC Assays

Transformed bacteria were cultured overnight at 37 °C in 10 mL of LB medium containing 100 µg/ml of ampicillin. Plasmid DNA from these bacteria was purified using plasmid DNA purification kit from Macherey-Nagel (NucleoSpin® Plasmid Transfection-grade; Düren, Germany) according to the manufacturer's instructions and sequenced using the Sanger method with the M13 Reverse Primer. These plasmids were then used in the BiFC assays, as detailed in Section 2.4.

Lipids from native pulmonary surfactant

Pulmonary surfactant was isolated from bronchoalveolar lavage fluid (BALF) obtained from fresh porcine lungs as described by Taeusch *et al*. (2005). Each respiratory aparatus was lavaged with approximately 2.5 L of cold buffer solution (150 mM NaCl and 5 mM Tris, pH 7.4), introducing it via the trachea and followed by gentle massaging to detach the pulmonary surfactant from the lung walls. BALF was filtered through gauze and centrifugated at 1000g for 5 minutes at 4 °C to remove cellular debris. Supernatants were combined and stored at -20 °C until further purification. To purify PS, the BALF was thawn at 4 °C and ultra centrifugated at 10000g, 4 °C for 1 hour. Supernatant was discarded and pellet containing membrane complexes was resuspended in 16% NaBr, 0.9% NaCl solution and homogenized using a Potter. A NaBr density gradient was prepared by layering 5 mL of the homogenized pellet, followed by 7.3 mL of 13% NaBr, 0.9% NaCl solution and 3 mL of 0.9% NaCl solution, from bottom to top in the ultracentrifuge tube. The gradient was ultra centrifugated in a swinging angle rotor at 120000g, at 4 °C for 2 h. Pulmonary surfactant membrane complexes, along with some interacting proteins such as immunoglobulins, settled between the less dense solution (0.9% NaCl) and the intermediate density solution (13% NaBr, 0.9% NaCl). Therefore, the 0.9% NaCl solution was carefully removed, and the surfactant membrane complexes were collected and resuspended in 0.9% NaCl using a Potter homogenizer. Then, this purified whole natural pulmonary surfactant was aliquoted, frozen in liquid N_2 and stored at -80 °C.

The hydrophobic components of pulmonary surfactant were isolated using an organic extraction protocol as described by Bligh and Dyer (1959) (Section 2.5). Lipids and hydrophobic proteins present in the organic extract (OE) were then concentrated using a rotary evaporator and subjected to chromatographic separation on a Sephadex LH20 (GE Healthcare, Little Chalfont, United Kingdom) size-exclusion column equilibrated with chloroform-methanol (2:1, v/v). The absorbance of the eluted fractions was monitored at 240 nm and 280 nm to differentiate between proteins and lipids. The first peak corresponded to the hydrophobic proteins SP-B and SP-C, the second peak to phospholipids, and the third peak to neutral lipids. Fractions corresponding to lipids were pooled and stored at -20 °C, collectively referred to as lipid surfactant (LS). Lipid concentration was measured by phosphorus quantification (section 2.6).

SP-B and SP-C isolation

Hydrophobics surfactant proteins SP-B and SP-C were isolated from minced porcine lungs, as described in Pérez-Gil *et al*. (1993), to have better yienlding compared to BALF. Each minced lung was lavage with 0.5 L of cold buffer solution (150 mM NaCl and 5 mM Tris, pH 7.4) and filtered through double-layered gauze.

The fluid was then centrifuged at 1000g, 4 °C, for 5 minutes to remove tissue traces and cells. The resulting supernatant was centrifuged at 3000g, 4 °C for 2 hours to sediment large membrane complexes containing SP-B and SP-C. Pellets were collected and could be stored if needed in B29 tubes at -20 °C. Both hydrophobic proteins were isolated together as described above (Section 1.3) by performing an organic extraction followed by chromatographic separation using Sephadex LH-20 resin, but in this case, only the fractions containing the proteins corresponding to the first peak were collected, as the fractions containing lipids (second and third peak) not only include pulmonary surfactant lipids but also those from alveolar tissues. To isolate SP-B and SP-C proteins, the protein fraction obtained from the LH20 column was initially concentrated using a rotary evaporator. This was followed by chromatographic separation on a Sephadex LH60 column equilibrated with a chloroform-methanol (1:1, v/v) solution containing 0.05% 0.1 N HCl, which minimizes protein-resin interactions. Absorbance of the resulting fractions was measured at wavelengths of 240 nm and 280 nm. First peak corresponds to SP-B and second to SP-C. Fractions corresponding to each protein were pooled and stored in vials at -20 °C. Protein concentration was measured by aminoacid analysis (section 2.7), and its purity was verified by an electrophoretic analysis (section 2.8).

Production and purification of human recombinant SP-C

The purification protocol followed is described in Lukovic *et al*. (2006), with modifications from Roldan *et al*. (2015). First, *Escherichia coli* BL21 (DE3) bacteria were transformed with the recombinant vector pET-11a, which includes recombinant human SP-C (rhSP-C) flanked by a thrombin cleavage site, glycine linker, nuclease, and a histidine tag (**Figure 2**).

Figure 2: Schematic representation of the chimeric protein containing rhSP-C expressed in bacteria

The transformed bacteria were incubated overnight at 37°C on LB-Agar plates containing 100 µg/ml ampicillin as a selection marker. A transformed colony was selected for pre-culture in LB medium with 100 µg/ml ampicillin. After overnight incubation at 37°C shaking at 250 rpm, the bacterial culture was diluted to an initial OD_{600} of 0.1 in 4 L of 2XTY medium (16 g/L tryptone, 10 g/L yeast extract, and 5 g/L NaCl) with 100 µg/ml ampicillin. The culture was grown at 37°C at 250 rpm shaking until an OD_{600} of 0.4–0.5 was reached. Overexpression of the fusion protein was induced by adding 1 mM IPTG and incubating the culture for 3 hours at 37°C at 250 rpm shaking. Bacteria were centrifugated at 1000g, 4 °C for 20 minutes and pellet was stored at -80 °C until used. Every step since now was perfomed in cold with ice or at 4 °C in case temperature could be set. Pellet was thaw and resuspended in lysis buffer (10 mM Tris, 150 mM NaCl, 100 mM

phenylmethylsulphonyl fluoride serine (PMSF), 0.5 % (w/v) N-lauryl sarcosine sodium salt (NLS), 1X protease inhibition cocktail, a spoonful of lysozyme from chicken egg white (Honeywell Fluka™, Charlotte, NC, USA), and a spoonful of DNAse (Roche, Basel, CH), pH 7.0) with continuous stirring for 30 min. Bacterial lysis was complemented with sonication using an ultrasonic probe sonicator (Hierlcher UP200; Hierlcher Ultrasonics, Teltow, Germany). The sonication procedure consisted of three cycles of 1 min (1 s pulse, 1 s rest) at 50 % amplitude with 1 min resting intervals on ice between them. Lysed cells were centrifuged at 12,800 g for 20 minutes at 4°C in a Beckman Optima XL-90 ultracentrifuge (Beckman Coulter S.L.U., Brea, CA, USA) to separate the soluble fraction containing the rhSP-C protein from bacterial debris. The fusion protein, including rhSP-C, was isolated using a 5 mL HisTrap™ Fast Flow column (Cytiva, Marlborough, MA, USA) taking advantage of the histidine tag present in the fusion protein. HisTrap™ FF is a prepacked column specifically designed for the preparative purification of histidine-tagged recombinant proteins through immobilized metal ion affinity chromatography (IMAC). It is packed with Ni Sepharose™ 6 Fast Flow, immobilized with a chelating ligand charged with Ni^{2+} ions, which efficiently capture most histidine-tagged proteins. All solutions and the soluble fraction used during chromatography were filtered through a 0.22 μm syringe filter (Guangzhou Jet Bio-Filtration Co., Ltd., Guangzhou, P.R. China). The column was equilibrated with 3 column volumes of 50 mM Tris, 150 mM NaCl, and 0.5% NLS, pH 7. The soluble fraction, to which imidazole was added to a final concentration of 10 mM to reduce nonspecific binding of proteins to the column resin, was passed through the column, resulting in the retention of histidine-rich proteins by the Ni^{2+} resine. Low-affinity proteins were removed by washing the column with 25 column volumes of washing buffer (50 mM Tris, 150 mM NaCl, 30 mM imidazole, 0.2% NLS, pH 7). The fusion protein was eluted using 5 column volumes of elution buffer containing a high concentration of imidazole (50 mM Tris, 150 mM NaCl, 500 mM imidazole, 0.2% NLS, pH 7) in 1 mL fractions. Absorbance at 280 nm was measured for each fraction, and the fractions were subjected to electrophoresis. The presence of fusion protein was confirmed via Coomassie staining. Fractions containing the fusion protein were dialyzed overnight at 4°C in a buffer (50 mM Tris, 150 mM NaCl, 0.2% NLS, pH 7) using membranes with a 10 kDa molecular weight cut-off (Snake-Skin™, Thermo Fisher Scientific, Waltham, MA, USA) to remove residual imidazole from the previous chromatography step. The fusion protein was then cleaved using 0.5 units of thrombin (Novagen®, Merck Millipore, Burlington, MA, USA) per mg of protein, incubated in cleavage buffer (20 mM Tris, 150 mM NaCl, pH 8.4) at 4°C overnight to isolate rhSP-C. Phosphatidylcholine from egg yolk was added to the cleavage solution at a 5:1 ratio (w/w), to prevent the irreversible self-aggregation of the protein in the absence of lipids, followed by organic extraction, as described by Bligh and Dyer

(1959), omitting the flocculation step to prevent rhSP-C aggregation. The organic phase was subjected to size-exclusion chromatography using Sephadex LH-20 resin equilibrated with a chloroform-methanol (1:1, v/v) solution containing 0.05% 0.1 N HCl to separate rhSP-C from lipids. Fractions containing rhSP-C were collected and stored at -20°C. Protein concentration, purity, and structure were assessed by amino acid analysis, western blotting, and circular dichroism, respectively.

Protein labelling

For different fluorescence experiments, the N-terminal end of SP-C or rhSP-C was labelled with BODIPY-FL NHS ester (D2184, Invitrogen, ThermoFisher Scientific, Waltham, MA, USA) or Marina Blue® NHS ester (1242-5, Fluoroprobes) probes as described (Cabré *et al.*, 2018) with some modifications. For all labeling reactions except for rhSP-C conjugated with Marina Blue, the apparent pH of both pure proteins in the organic solvent (chloroform/methanol, 1:1, v/v) was adjusted to 7.1 with the appropriate amount of 50 mM Tris in methanol. To label rSP-C with Marina Blue, the solution containing pure rhSP-C was slightly alkalinized (pH 7.5). Then, the required probe was incubated overnight at 4ºC with pure proteins in a 5:1 probe/protein molar ratio. The labelling procedure was stopped by decreasing the apparent pH to 2 with HCl. Finally, the samples were loaded onto a Sephadex LH-20 resin equilibrated with chloroform/methanol (1:1, v/v) acidified with a 0.5% of HCl (0.1 N) to separate the labelled protein from free probe. Protein concentration was finally quantified by amino acid analysis.

The amount of dye conjugated to each protein was calculated using the Lambert–Beer law where the molar extinction coefficients (ε) used were ε504nm = 82 × 103 M^{-1} cm^{-1} for BODIPY-FL and ε_{365nm} = 19 × 103 M^{-1} cm^{-1} for Marina Blue (Haugland, 2002). The final dye:protein molar ratios (D/P) determined for the fluorescently-labelled proteins were D/P = 0.5 for BODIPY-FL/SP-C, D/P = 0.8 for BODIPY-FL/rSP-C, D/P = 0.5 for Marina Blue/SP-C, and D/P = 0.7 for Marina Blue/rSP-C, respectively.

To check whether the introduction of the fluorescent probes could alter protein conformation, we obtained the circular dichroism (CD) spectra of the different proteins reconstituted in micelles of lysophosphatidylcholine (LPC).

Synthetic peptides

All synthetic peptides used in this thesis were solid phase-assisted synthetized in the laboratory of Prof. David Andreu, at Pompeu Fabra University (Barcelona, Spain) and are described in **Table 2**.

Table 2: Peptides mimicking different SP-C regions.

Peptide	Sequence	GRAVY index
SP-C	FGIPCCPVHLKRLLIVVVVVVLIVVVIVGALLMGL	2.46
SP-$C_{1–13}$	FGIPCCPVHLKRL$_{amide}$	0.685
(AL)SP-$C_{11–35}$	KRALAALAALAAGGLLIVGALLMGL	1.816
mSP-$C_{1–13}$(C →A)	FGIPAAPVHLKRL$_{amide}$	0.577
mSP-$C_{1–13}$ (C →F)	FGIPFFPVHLKRL$_{amide}$	0.731
m(AL)SP-$C_{11–35}$ (A,G →I)	KRALAALAALAAGGLLIVGILLMIL	2.120

Lipid and lipid/protein preparations

Four lipid systems were used: (1) 1-palmitoyl-2-oleoyl-*sn*-glycero-3-phosphocholine (POPC); (2) a synthetic lipid mixture (LM) composed of DPPC (1,2-dipalmitoyl-*sn*-glycero-3-phosphocholine), POPC and POPG (1-palmitoyl-2-oleoyl-*sn*-glycero-3-phosphoglycerol) (50/25/15, w/w/w); (3) a synthetic non charged lipid mixture without POPG (NLM) and (4) the surfactant lipid fraction (LS) obtained from native PS. For cytometry and epifluorescence microscopy experiments a lipid fluorescence was added to the mixture, rhodamine-DOPE.

Lipid and lipid/protein MLV samples were prepared by co-drying a proper amount of lipid and fluorescently labelled and/or non-labelled protein under a stream of nitrogen that was finally subjected to vacuum during 2 h using SpeedVac™ Vacuum Concentrator (Savant SC250EXP, Thermo Fisher Scientific, Waltham, MA, USA). The dried lipid or lipid/protein samples were then suspended in Tris buffer (5 mM Tris, 150 mM NaCl pH 7) at 45°C, frozen with liquid nitrogen, and thawed in a bath at 45°C. Five freeze/thaw cycles were performed with vortexing between each cycle to obtain the desired MLVs (Traïkia *et al.*, 2000). In some cases, the dry material was reconstituted adding Tris buffer to each tube and shaking them intermittently at 41 °C for 1 h to get multilamellar suspensions. The phospholipid concentration for each sample was determined by phosphorus analysis upon phospholipid mineralization as described by Rouser *et al*. (1966) (section 2.6).

In some cases, mutant Re 595 (source strain 49284, Mw = 2500 g/mol) lipopolysaccharide from *Salmonella enterica* serotype Minnesota was co-dried with lipid or lipid/protein mixtures to prepare vesicles containing LPS.

Small and large unilamellar vesicles

The rehydrated samples were extruded through polycarbonate membranes with different pore sizes, 50 nm and 200 nm, in a mini-extruder (Avanti Polar Lipids) to

get SUVs and LUVs, respectively. Vesicles were used as soon as possible and maintained in cold on ice.

Giant unilamellar vesicles

Giant unilamellar vesicles were prepared using the standard electroformation protocol (Mathivet *et al.*, 1996). The fabrication chamber was composed of two 1-mm spaced conductor indium tin oxide (ITO)-coated slides (7.5 × 2.5 cm2; 15–25 Ω sq−1 surface resistivity). GUVs were prepared by transferring a volume of 10 µL of the lipid mixture in chloroform (0.5 mg mL^{-1}) onto each ITO-coated slide. Samples were dried at room temperature, rehydrated in 300 mM sucrose solution and the electrodes were connected to an 3 MHz function generator (10 Hz, 3 Vp-p, AIM-TTI Instruments, Huntingdon, UK) for 3 h at room temperature if transition phase temperature is below 15 °C, otherwise at 45 °C for 16 h. Lipids mixture were supplemented with 0.2 % (w/w) Rho-DOPE.

Cell Cultures

HEK 293T (ATCC CRL-3216), a kidney embryonic-derived cell line, was cultured in Dulbecco's modified Eagle medium (DMEM). MH-S (ATCC CRL-2019) is an alveolar macrophage derived cell line that was cultured in Roswell Park Memorial Institute 1640 medium. A549 (ATCC CCL-185) is a type II alveolar epithelial-derived cell line that was cultured in DMEM supplemented with F-12 nutrient mixture. All media were supplemented with 10% heat-inactivated fetal bovine serum and 50 units/mL of penicillin/streptomycin. Cells were cultured at 37 °C in a 5% CO_2 humid atmosphere. For bimolecular fluorescence complementation (BiFC), epifluorescence microscopy and flow cytometry assays, cells were grown in 24-well plates (Thermo Scientific, Waltham, MA, USA). For western blot, cells were cultured in 6-well plates (Thermo Scientific, Waltham, MA, USA).

Methods

Polymerase Chain Reaction (PCR)

DNA fragments corresponding to protein of interested described in **Table 1** contained in plasmid vector were amplified by PCR using a Mastercycler® gradient thermocycler (Eppendorf, Hamburg, Germany) and *Pyrococcus furiosus* (Pfu) DNA polymerase (Thermo Fisher Scientific, Waltham, MA, USA). The PCR master mix included 4% (v/v) dimethyl sulfoxide (DMSO), 1X Pfu DNA polymerase buffer (20 mM Tris-HCl pH 8.8 at 25°C, 10 mM $(NH_4)_2SO_4$, 10 mM KCl, 1 mg/mL bovine serum albumin (BSA), 1% (v/v) Triton X-100, 20 mM MgSO4), 1X GC enhancer (New England Biolabs, Ipswich, MA, USA), 0.045 ng/µL plasmid DNA template, 0.2 µM of each DNA primer (**Table 3**), 0.25 µM deoxynucleotide triphosphates (dNTPs) mix (New England Biolabs, Ipswich, MA, USA), and 0.02 U/µL Pfu DNA polymerase. The PCR program consisted of an initial denaturation step at 95°C for 5 minutes,

followed by 35 cycles of 1 minute at 95°C for denaturation, 1 minute at the annealing temperature (64–70°C gradient for optimal primer-template hybridization), and 1 minute at 72°C for extension. A final elongation step at 72°C for 5 minutes completed the reaction.

Table 3: Oligonucleotides sequences for each DNA sample used for PCR

	Primers	Sequence	Tm (°C)
proSP-C	Forward	GCGGCCGCTTTGGCATTCCCTGCTGC	85.2
	Reverse	GCGGCCGCCTAGATGTAGTAGAGCGG	76.4
mSP-C	Forward	ATAAGAATGCGGCCGCTTTGGCATTCCCTGCTGC	85
	Reverse	ATGCCAAAGCGGCCGCCTAGAGACCCATGAGC	84.8
sSP-C	Forward	TGGTGTAGGCGGCCGCCATCTGGGCCGCGTGA	87.2
	Reverse	ATAAGAATGCGGCCGCCTAAATGCCCAGCAGCAG	86.8
mSP-C (C → A)	Forward	TTCTCTAGGCGGCCGCTTTGGCATTCCCGCAG	86.1
	Reverse	ATGCCAAAGCGGCCGCCTAGAGACCCATGAGC	84.8
mSP-C (A, G → I)	Forward	ATAAGAATGCGGCCGCTTTGGCATTCCCTGCTGC	85
	Reverse	ATGCCAAAGCGGCCGCCTAGAGAATCATGAGCAG	83.6

Agarose electrophoresis

Agarose gel electrophoresis was employed to separate DNA molecules following restriction enzyme digestion and to check amplification of DNA made by PCR. 1.5% (w/v) agarose gel was prepared in TAE buffer (40 mM Tris-acetate, 1 mM EDTA, pH 8.0). To perform agarose electrophoresis, DNA samples were mixed with Blue/Orange Loading Dye (0.4% orange G, 0.03% bromophenol blue, 0.03% xylene cyanol FF, 15% Ficoll® 400, 1.0 mM Tris-HCl, pH 7.5, and 50 mM EDTA, pH 8.0) (Promega Corporation, Madison, WI, USA) and loaded into the wells of the agarose gel, which had been submerged in TAE buffer. Electrophoresis was carried out at 100V for 1 h using a Mini-Sub® Cell GT system (Bio-Rad Laboratories, Inc., Hercules, CA, USA). DNA samples were run alongside molecular size markers: a 100 bp DNA ladder (Promega Corporation, Madison, WI, USA) for shorter fragments, and a Quick-Load® 1 kb DNA ladder (New England Biolabs, Ipswich, MA, USA) for larger fragments. Following electrophoresis, the gels were stained by immersion in a 1X GelRed® solution (Biotium, Fremont, CA, USA), prepared in distilled water, for 20 minutes. DNA bands were visualized under UV light using the ENDURO™ GDS Gel Documentation System (Labnet International Inc., Edison, NJ, USA).

Transformation

Bacterial transformation was carried out using One Shot® Top 10 competent *E. coli* cells or the BL21 (DE3) strain. This protocol was applied to each plasmid DNA construct, with all steps performed under sterile conditions using a Bunsen burner. As a negative control, a vial was transformed with sterile water. A vial

containing 50 µL of competent cells, stored at -80°C, was thawed on ice. During this time, sterile LB broth (Lennox International Inc., Richardson, TX, USA) and LB agar plates containing the selection antibiotic (ampicillin, AppliChem GmbH, Darmstadt, Germany) were equilibrated to room temperature. Subsequently, 20-100 ng of plasmid DNA were added to the thawed competent cells and incubated on ice for 30 minutes. Heat shock was applied for 90 seconds at 42°C to facilitate DNA uptake by temporarily destabilizing the bacterial cell membrane, allowing the plasmid DNA to enter the cell. This was followed by a 2-minute incubation on ice to restore membrane integrity. Afterward, 250 µL of LB broth (International Inc.) were added to the vial, which was then incubated in a thermomixer (Eppendorf, Hamburg, Germany) at 37°C with shaking at 350 rpm for 1 hour to allow for the expression of antibiotic resistance genes. A 50 µL aliquot of the cell suspension was plated onto an LB agar plate containing 0.1 mg/mL of the selection antibiotic and incubated overnight at 37°C. A single transformed colony was selected and cultured in 10 mL of LB broth supplemented with 100 µg/mL ampicillin. The resulting culture was stored at -80°C by adding 300 µL of glycerol to 700 µL of concentrated bacterial culture. This stored culture could be used later for plasmid DNA extraction using the Macherey-Nagel NucleoSpin® Plasmid Transfection-grade purification kit (Macherey-Nagel GmbH & Co. KG, Düren, Germany), or for rhSP-C protein purification.

Bimolecular Fluorescence Complementation (BiFC)

To assess the interaction between SP-C molecules, a bimolecular fluorescence complementation (BiFC) assay was performed. In this technique, the Venus Fluorescent Protein (VFP) is split into two non-fluorescent fragments: the N-terminal (VN, residues 1-154, I152L) and the C-terminal (VC, residues 155-238, A206K). These VFP fragments are fused to the proteins of interest. If two proteins (or domains) interact stably, their respective VFP fragments reassemble, forming a functional VFP that emits fluorescence, serving as an indicator of oligomerization (**Figure 3**). In addition to proSP-C, mature SP-C, scrambled SP-C constructs, and specific SP-C mutants, BiFC plasmids containing the transmembrane segments of GpA and a mutated GpA dimerization motif (GpA G→I) were used as positive and negative controls, respectively (**Table 1**). To normalize the results, a pair consisting of the basic leucine zipper domains of the transcription factors Jun (bJun) and Fos (bFos) fused to VN or VC, respectively, was included (García-Murria *et al*., 2019). A plasmid encoding Renilla reniformis luciferase under the CMV promoter (pRL-CMV, Promega Corporation, Madison, WI, USA) was co-transfected as a control for transfection efficiency.

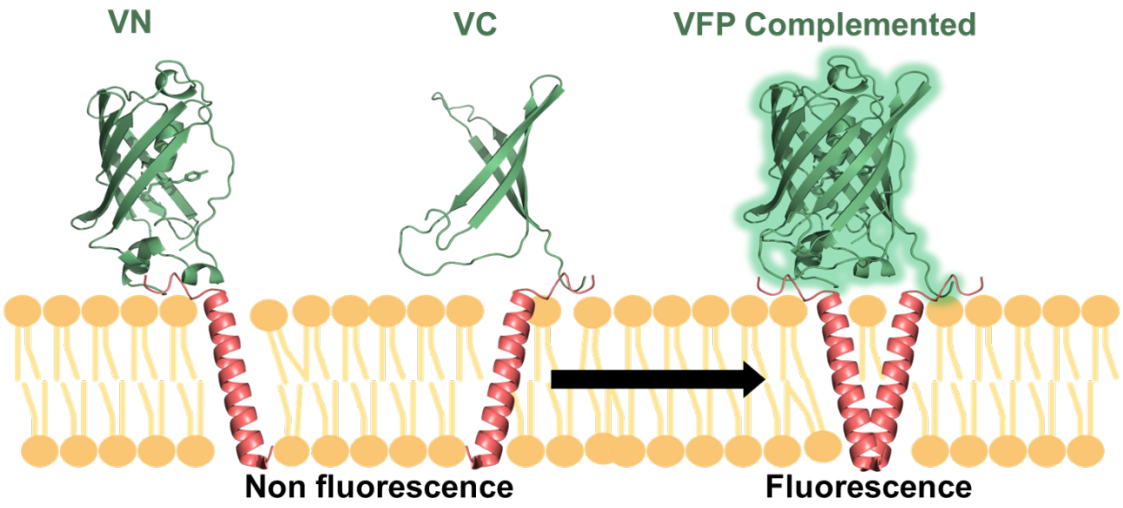

Figure 3: **Scheme of a BIFC assay for dimerization of SP-C molecules**. Two proteins carrying the VN or VC segments of VFP are expressed in cell membranes. Upon interaction of both molecules, the functional VFP is reassembled, and its fluorescence can be detected

VN and VC BiFC plasmids encoding the different constructs were transfected into HEK 293T cells using Lipofectamine 2000 (Invitrogen, Carlsbad, CA, USA) as the transfection reagent and Opti-MEM® (Gibco, Carlsbad, CA, USA) as the transfection medium. One day prior to transfection, 100,000 HEK 293T cells were plated in 500 µL of growth medium to achieve 30-50% confluency at the time of transfection. Two hours before transfection, the growth medium was replaced with 400 µL of Opti-MEM®. For each sample, 250 ng of VN and VC BiFC plasmids were mixed in 50 µL of Opti-MEM® with 15 ng of pRL plasmid. Simultaneously, 1.5 µL of Lipofectamine 2000 were diluted in 50 µL of Opti-MEM® and incubated for 5 minutes at room temperature. After incubation, the diluted plasmids were combined with the diluted Lipofectamine 2000, mixed, and incubated for 20 minutes at room temperature. The resulting DNA-Lipofectamine complexes were then added to each well containing cells and medium. Cells were incubated at 37°C in a humidified atmosphere with 5% CO2. After 4 hours, the cells were washed with phosphate-buffered saline (PBS) and the medium was replaced with DMEM. After 48 hours, the cells were sequentially washed with PBS, and fluorescence data were acquired using a FLUOstar OPTIMA Microplate Reader fluorometer (BMG Labtech, Ortenberg, Germany). Following fluorescence measurement, the cells were lysed, and luminescence was measured using the Renilla Luciferase Glow Assay Kit (Thermo Fisher Scientific, Waltham, MA, USA).

Organic extraction

A lipid extraction was performed from the different samples using the Bligh & Dyer method (Bligh & Dyer, 1959). To achieve this, the materials used were first delipidized by washing with chloroform-methanol (2:1, v/v) to prevent contamination from non-surfactant lipids. Subsequently, the sample was mixed

with chloroform and methanol (2:1, v/v) and vortexed for 30 seconds, resulting in a monophasic system of $CHCl_3$:CH_3OH. The sample was then heated to induce protein flocculation, and chloroform and MilliQ water in a 1:1 (v/v) ratio to the initial sample volume were added, vortexed for 30 seconds, and centrifuged at 600g, 4 °C for 5 min. This allowed for the separation of the organic phase (lower fraction) and the aqueous phase (upper fraction). The organic phase was collected, and the aqueous phase underwent two additional organic extractions by adding 2 volumes of chloroform relative to the initial volume sample, vortexing for 30 seconds, and centrifuging under the same conditions as in the previous step. After these steps, the organic phase was collected and stored at -20 °C.

Phosphorus quantification

Phosphorus quantification is used to determine the number of moles of phosphate, and therefore of phospholipids, present in a solution by interpolating the samples on a standard curve. To mineralize phosphate from phospholipids, the samples were dried in clean glass test tubes and subsequently incubated for 30 minutes in the presence of 70% perchloric acid in a sand bath at 240-260 °C with the tubes capped with glass ampoules to avoid evaporation. To quantify the phosphorus colorimetrically, 3.5 ml of MilliQ water, 0.5 ml of 2.5% ammonium molybdate, and 0.5 ml of 10% ascorbic acid were sequentially added. After each addition, the mixture was vortexed. The samples were then incubated in a thermal bath at 100 °C to facilitate the reduction of phosphomolybdic acid to phosphomolybdate, which gives the solution a blue color, the intensity of which depends on the amount of phosphomolybdate formed. The reaction was stopped using an ice water bath, and the absorbance was measured at 820 nm. A calibration curve was prepared with known amounts of phosphorus using a stock solution of dipotassium phosphate (K_2HPO_4) to interpolate the amount of phosphorus present in the samples.

Amino acid analysis

Amino acid quantification is a method used to determine protein concentration by measuring the hydrolyzed residues of a protein after separation via HPLC (High Performance Liquid Chromatography). This methodology is employed because SP-C, in addition to being very small, lacks aromatic amino acids, making techniques such as the Lowry or Bradford methods unsuitable. To isolate the amino acids, an acid hydrolysis in the absence of oxygen is required, for which 100 µL of 6N HCl, 0.1% phenol (w/v) were added to 300 µL of dried protein (approximately 10-20 ng). The tubes were sealed under vacuum using a vacuum pump, and amino acid hydrolysis was performed by incubating the sample in an oven at 100 °C for 24 hours. The acid solution contained a known amount of exogenous amino acid (*nor*leucine) as intrinsecal standard. The acid was then evaporated using a

nitrogen stream, followed by two washes with MilliQ water and drying in a SpeedVac™ Vacuum Concentrator (Savant SC250EXP Thermo Fisher Scientific, Waltham, MS). Finally, a citrated buffer (0.2M sodium citrate, pH 2.2) was added to solubilize samples, and injedted in an aminoacid analyzer system HPLC was performed. From the chromatogram, the concentrations of the different amino acids were determined, allowing for the calculation of the SP-B and SP-C and rhSP-C protein concentrations.

Electrophoretic analysis

SDS-PAGE

This analysis enabled the separation of proteins using polyacrylamide gel electrophoresis (PAGE) in the presence of sodium dodecyl sulfate (SDS). The polyacrylamide gel concentration was optimized based on the molecular weight of the target proteins, utilizing either 16% or 12% acrylamide. Organic samples were first dried and reconstituted in loading buffer containing 0.03% bromophenol blue, 2% SDS, 10% glycerol, and β-mercaptoethanol, while aqueous samples were combined with a concentrated loading buffer to ensure equivalent final composition across all samples. To promote complete denaturation, the samples were incubated at 95 °C for 5 minutes prior to electrophoresis. Following denaturation, the protein samples, along with a molecular weight marker (Precision Plus Protein Dual Color Standards, Thermo Fisher Scientific, Waltham, MA, USA), were loaded onto the polyacrylamide gel. Electrophoretic separation was conducted at a constant voltage of 100 V for 1 hour, ensuring effective separation of proteins based on molecular weight. After SDS-PAGE, gels were stained by Coomassie Brilliant Blue R-250 or silver nitrate or were transferred to the appropriate membranes for protein immunodetection.

Coomassie staining

Coomassie staining was used to detect the fusion protein containing rhSP-C. Gels were incubated in a solution containing 1 mg/ml Coomassie Brilliant Blue R-250, 50% methanol and 10% acetic acid for 30 minutes. Destaining with 10% acetic acid, 45% methanol solution revealed blue stained bands.

Sylver staining

The silver staining was performed because SP-B, SP-C, and rhSP-C proteins do not stain well with Coomassie Blue. First, the gel is fixed using a solution of 40% ethanol and 10% acetic acid, which immobilizes proteins by dehydrating and precipitating them within the polyacrylamide matrix. Subsequently, the gel is sensitized with a mixture of 30% ethanol, 0.5% glutaraldehyde, 12.6 mM sodium thiosulfate and 0.8 M sodium acetate. In this step, ethanol continues the dehydration process, while glutaraldehyde cross-links proteins, creating reactive aldehyde groups. Sodium thiosulfate enhances the sensitivity by interacting with

silver ions to form silver-sulfide complexes, and sodium acetate buffers the solution to optimize protein stability. The gel is then washed with MilliQ water to remove residual chemicals, ensuring uniform silver ion deposition. In the staining step, proteins bind silver ions (Ag^+) from a solution of 0.6 mM silver nitrate, with 0.04% formaldehyde acting as a reducing agent that initiates the reduction of Ag^+ to metallic silver (Ag^0) at the protein sites. Protein bands become visible during development with 0.2 M sodium carbonate and 0.02% formaldehyde, where sodium carbonate provides an alkaline environment for further reduction of Ag^+ to Ag^0, enhancing the visibility of the protein bands as silver deposits accumulate. Finally, the reaction was stopped using a solution of 50 mM EDTA, pH 8.0, which chelates remaining unbound silver ions, preventing overdevelopment and reducing background staining.

Western blot

For protein immunodetection, a western blot was carried out. Proteins were transferred onto polyvinylidene fluoride (PVDF) membrane using a wet transfer system for 1 hour at 300 mA. The membrane was subsequently incubated for 2 hours in a blocking solution containing PBS-T (PBS with 0.1% Tween 20) and 5% skimmed milk to minimize non-specific binding. Following the blocking step, the membrane was incubated overnight at 4°C with primary antibodies. After incubation, the membrane was washed four times for 15 minutes with PBS-T. It was then incubated for 2 hours at room temperature with a secondary HRP-conjugated antibody. Four additional 15-minute washes were performed before visualizing protein bands using chemiluminescence. Chemiluminescence detection was conducted with BM Chemiluminescence Blotting Substrate (Roche, Basel, Switzerland) and visualized using the ImageQuant LAS 500 system (GE Healthcare, Chicago, IL, USA).

For the immunodetection of hydrophobic proteins such as SP-B, SP-C, and rhSP-C, rabbit anti-SP-B and anti-SP-C antibodies (Sevenhills Bioreagents, Cincinnati, OH, USA) were used at a 1:5000 dilution in blocking solution, followed by incubation with an HRP-conjugated swine anti-rabbit antibody (Dako, Agilent Technologies, Santa Clara, CA, USA) at a 1:5000 dilution. For VN and VC protein detection, rabbit anti-c-myc and anti-HA antibodies were used at a 1:1000 dilution, respectively, followed by HRP-conjugated swine anti-mouse IgG (Cell Signaling Technology, Danvers, MA, USA.) at a 1:2500 dilution and HRP-conjugated swine anti-rabbit IgG (Dako, Agilent Technologies, Santa Clara, CA, USA) at a 1:5000 dilution.

Circular Dichroism

Proper amounts of each protein, labelled and non-labelled SP-C and rhSP-C, and LPC were dried in a 1:7 (protein:lipid) mass ratio under a stream of nitrogen and

then under vacuum for 2 h and samples were resuspended in PBS (4.4 mM KH_2PO_4, 5.6 mM Na_2HPO_4, 50 mM NaCl, pH 6.8) through five cycles of freeze with liquid nitrogen and thaw at 25°C, vortexing 30 s between each cycle. Quartz cells of 0.1 cm optical path were used to record the CD spectra in a JASCO J-715 Circular Dichroism CD Spectrometer (JASCO Corporation, Tokyo, Japan) at 25°C. Data analysis was performed with Spectra Manager Software and the BestSel™ online tool was used to achieve CD deconvolution. All the CD spectra were consistent with a mainly alpha-helical conformation for all the protein forms studied, palmitoylated and non-palmitoylated, with and without fluorescent groups attached.

Fluorescence spectroscopy

Fluorescence is widely recognized as one of the most versatile and sensitive techniques in biological and chemical sciences due to its ability to detect molecules at extremely low concentrations. This phenomenon, part of photoluminescence, relies on the property of certain molecules, known as fluorophores, to emit light after absorbing electromagnetic radiation, primarily in the visible and ultraviolet regions of the spectrum. Luminescence encompasses light-emitting phenomena that do not require high temperatures, and it can be classified based on the energy source that excites the emitting molecule. Within photoluminescence, fluorescence is a fast process, with emission times on the order of nanoseconds, distinguishing it from phosphorescence, where emission is delayed and can continue from milliseconds to minutes after the excitatory stimulus has ceased (Lakowicz & Masters, 2008).

The molecular mechanism of fluorescence involves the absorption of photons by a molecule, promoting electrons to excited electronic states. Once in these states, the molecule may lose part of this energy through non-radiative mechanisms, such as vibrational relaxation, transferring heat to surrounding molecules. Subsequently, the molecule emits photons of lower energy than those initially absorbed, resulting in light emission at a longer wavelength. This phenomenon is known as the Stokes shift. The Jablonski diagram is a fundamental tool for describing the electronic states of molecules and the possible transitions between them. This diagram illustrates how an electron can be promoted from the ground singlet state (S0) to higher excited states (S1 or S2) upon absorption of radiation and how, through internal conversion and vibrational relaxation, the molecule returns to its ground state, releasing energy in the form of fluorescence (**Figure 4**).

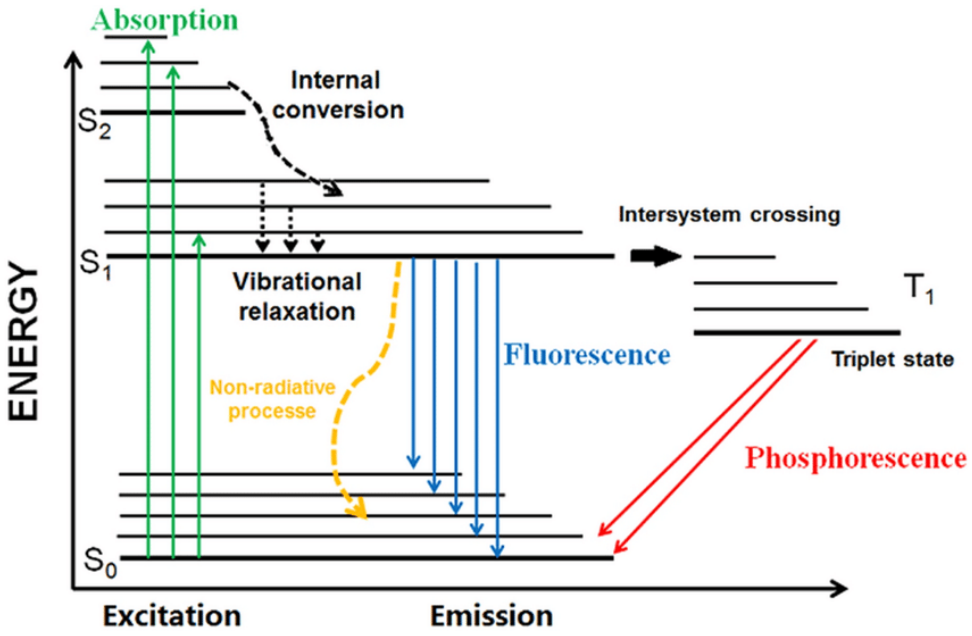

Figure 4: Perrin Jablonski diagram of fluorescence and phosphorescence. *Illustration from Schweizer et al. (2021).*

The fluorescence lifetime and quantum yield are two of the most important characteristics of a fluorophore. Quantum yield represents the ratio of emitted photons to absorbed photons. Substances with high quantum yields, close to unity, such as rhodamines, exhibit the brightest emissions. The lifetime determines the amount of time available for the excited state of the fluorophore to interact or diffuse in its environment, thus influencing the information extracted from its emission.

These concepts are best understood through a simplified Jablonski diagram, as shown in **Figure 5**, which illustrates the processes responsible for returning the fluorophore to its ground state. Of particular interest are the emissive rate (Γ) and the non-radiative decay rate to S_0(k_{nr}). The fluorescence quantum yield is the ratio of emitted photons to absorbed photons, expressed as:

$$Q = \frac{\Gamma}{\Gamma + k_{nr}} Q$$

Both the emissive rate (Γ) and the non-radiative decay rate (knr) contribute to the depopulation of the excited state. The fraction of fluorophores that decay via emission, and therefore the quantum yield, depends on the balance between these two rates.

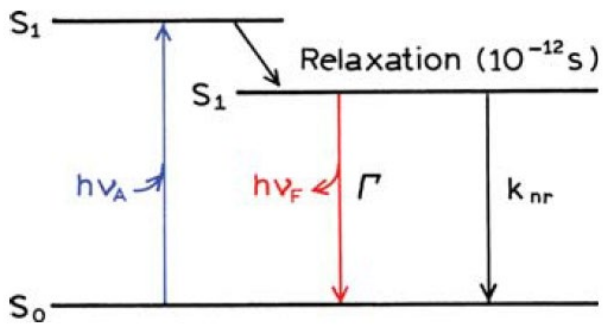

Figure 5: A simplified Jablonski diagram. Illustration from Lakowicz (2006).

The fluorescence lifetime is defined as the average time the molecule spends in the excited state before returning to the ground state. For the fluorophore depicted in **Figure 5**, the lifetime is given by:

$$\tau = \frac{1}{\Gamma + k_{nr}} \quad (1)$$

This model provides insight into how radiative and non-radiative processes influence the deactivation dynamics of the fluorophore.

Quenching

The de-excitation process of a fluorophore can be influenced by various molecular interactions. A relevant phenomenon is *quenching*, where certain agents, known as "quenchers", interfere with the photon emission process, dissipating the energy of the excited state as heat. For collisional quenching the decrease in intensity is described by the well-known Stern-Volmer equation:

$$\frac{F_0}{F} = 1 + K[Q] = 1 + k_q \tau_0 [Q]$$

In this expression *K* is the Stern-Volmer quenching constant, *k*q is the bimolecular quenching constant, τ0 is the unquenched lifetime, and [*Q*] is the quencher concentration. The Stern-Volmer quenching constant *K* indicates the sensitivity of the fluorophore to a quencher, with lower values when embedded in macromolecules and higher values when free in solution or on the surface of biomolecules.

This process is useful in biochemical studies to investigate molecular interactions, such as protein-protein interactions or conformational changes in macromolecules.

Anisotropy fluorescence

Fluorescence anisotropy is a measurement of the degree of polarization of emitted light and provides insights into the rotational mobility of fluorophores. Anisotropy

measurements are particularly useful for investigating protein-protein interactions, membrane fluidity, and performing immunoassays for a variety of substances. These measurements rely on the principle of photoselective excitation, where fluorophores absorb photons, whose electric vectors are aligned parallel to the fluorophore's transition dipole moment. This transition dipole moment has a specific orientation relative to the molecular axis, and in isotropic solutions, fluorophores are randomly oriented. However, upon excitation with polarized light, only those fluorophore molecules with an absorption dipole parallel to the excitation electric vector are selectively excited, allowing for detailed analysis of molecular dynamics and interactions (**Figure 6**).

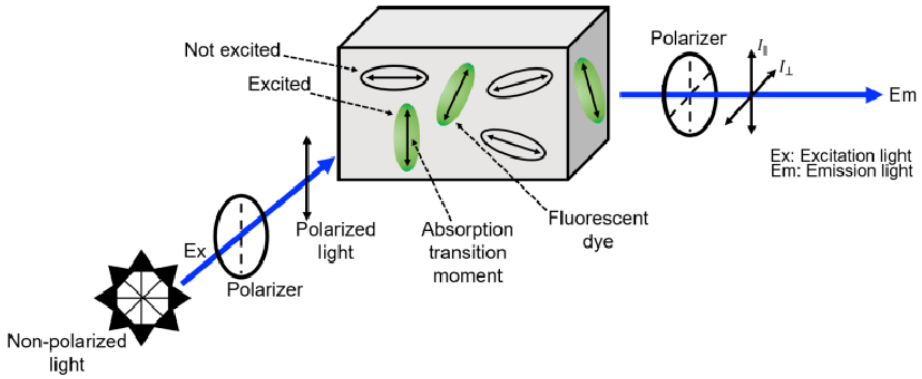

Figure 6: Schematic of fluorescence anisotropy. Pictorial from Jain et al. (2021)

The fluorescence anisotropy (r) and polarization (P) are defined by

$$r = \frac{I_{\parallel} - I_{\perp}}{I_{\parallel} + 2I_{\perp}}$$

$$P = \frac{I_{\parallel} - I_{\perp}}{I_{\parallel} + I_{\perp}}$$

Where $I_{\parallel}$ and $I_{\perp}$ are the fluorescence intensities of the vertically (||) and horizontally (⊥) polarized emission, when the sample is excited with vertically polarized light.

Förster Resonance Energy Transfer (FRET)

Förster Resonance Energy Transfer (FRET) is a process that occurs when the emission spectrum of a fluorophore, known as the donor, overlaps with the absorption spectrum of another molecule, referred to as the acceptor. The efficiency of energy transfer depends on two key factors: the distance between the donor and acceptor molecules, and the degree of spectral overlap between their respective emission and absorption spectra (**Figure 7**).

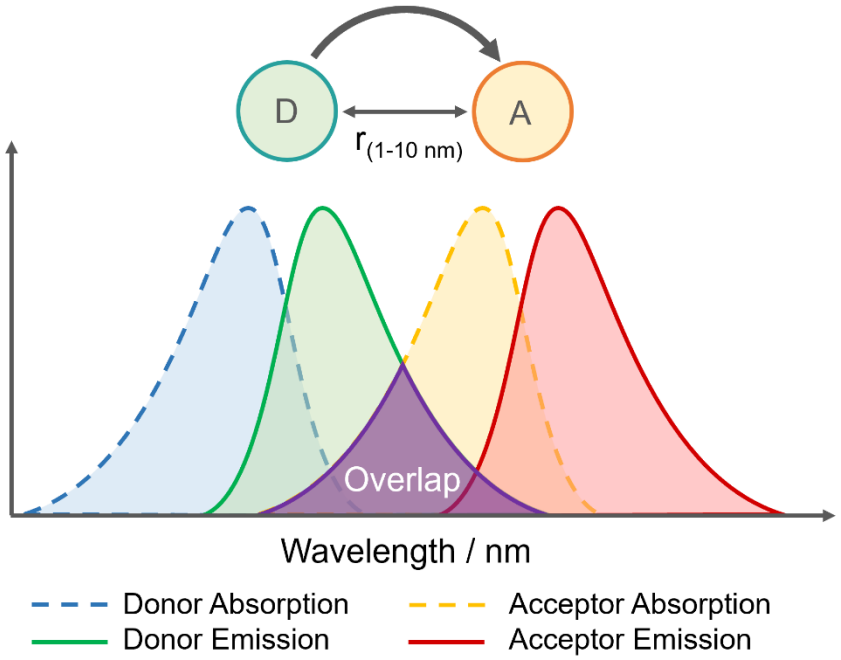

Figure 7. Requirements for quenching and Förster Resonance Energy Transfer (FRET) *(Edinburgh Instruments, 2024)*

This overlap is conveniently quantified using the Förster distance (R_0), which represents the distance at which energy transfer efficiency is 50%. The rate of energy transfer, $k_T(r)$, is determined by both the spectral overlap and the donor-acceptor separation distance,

$$k_T(r) = \frac{1}{\tau_D}\left(\frac{R_0}{r}\right)^6$$

where r is the distance between the donor (D) and acceptor (A) and τ is the lifetime of the donor in the absence of energy transfer. The efficiency of energy transfer for a single donor–acceptor pair at a fixed distance is

$$E = \frac{R_0^6}{R_0^6 + r^6}$$

The extent of energy transfer depends on the distance r between the donor and acceptor molecules. Förster distances, typically ranging from 30 to 60 Å, are similar in scale to the size of biological macromolecules, making FRET a valuable "spectroscopic ruler" for measuring distances between sites within proteins and other biomolecular structures.

Steady-State and Time Resolved Fluorescence

Fluorescence measurements can be classified into two main types: steady-state and time-resolved. Steady-state measurements, the most commonly used, involve constant illumination of the sample with a continuous light source, while recording

the resulting emission intensity or spectrum. Due to the nanosecond timescale of fluorescence, steady-state is quickly achieved after illumination. Time-resolved measurements, on the other hand, capture the dynamics of fluorescence, such as intensity or anisotropy decays. In this method, the sample is exposed to short light pulses, with pulse durations shorter than the fluorescence decay time, and the decay is monitored using high-speed detection systems that measure intensity changes on a nanosecond scale.

Steady-state fluorescence measurements provide an average of the time-resolved phenomena, integrating the intensity decay over time. For example, for a fluorophore with a single decay time (τ) and rotational correlation time (θ), the intensity and anisotropy decays are described by:

$$I(t) = I_0 e^{-t/\tau} \; and \; r(t) = r_0 e^{-t/\theta}$$

where I_0 and r_0 are the initial intensity and anisotropy immediately after excitation. The steady-state anisotropy (*r*) is obtained by averaging r*(t)* over the intensity decay, ensuring that the anisotropy remains independent of total intensity. This leads to the Perrin equation, which connects steady-state anisotropy to rotational dynamics.

Similarly, steady-state intensity (I_{SS}) is proportional to the fluorescence lifetime, as it averages the decay time, although influenced by fluorophore concentration and instrumental factors. While steady-state measurements are simple and practical, they often fail to capture critical molecular details.

Time-resolved measurements, though more complex and requiring specialized instrumentation, provide far more detailed molecular insights. Anisotropy decays, for example, can reveal the shape and flexibility of macromolecules, information that is lost in steady-state measurements, which reduce the decay to a single anisotropy value. Likewise, time-resolved intensity decays can expose multiple conformational states or distinguish between different decay times, which are averaged out in steady-state measurements.

Time-resolved methods are especially valuable in systems involving energy transfer or quenching, as they can distinguish between mechanisms like diffusion or formation of complexes. Ultimately, time-resolved fluorescence measurements unlock molecular information that remains hidden in steady-state observations, making them essential for in-depth fluorescence analysis.

In this thesis, the fluorescence self-quenching and hetero-FRET studies were carried out by performing both steady-state and time-resolved fluorescence measurements of the MLVs containing variable surface concentrations of the fluorescently labelled native and recombinant SP-C protein at 25 °C. Three lipid systems were used: 1) POPC; 2) LM composed of DPPC, POPC and POPG

(50:25:15, w:w:w) and 3) the lipid surfactant (LS) fraction obtained from native PS. MLVs were obtained through freeze-thawing process, as described in section 1.8. For the fluorescence self-quenching assays, variable concentrations of BODIPY SP-C or BODIPY rSP-C (namely 1.25 μM, 2 μM, 3.5 μM, 5 μM and 7.5 μM in reference to the fluorophore concentration) were co-solubilized with 1 mM of the desired lipids in order to obtain the fluorescently-labeled protein-loaded MLVs. For the hetero- Förster Resonance Energy Transfer (FRET) studies, the systems used were similar to the self-quenching assays. However, in this case, a FRET donor, Marina Blue SP-C or Marina Blue rSP-C (5μM of fluorescently-labeled protein), was also added to prepare the protein-containing MLVs.

Steady-state fluorescence measurements were conducted using a Horiba-Jobin Yvon Fluorolog 3-22 spectrofluorometer (Tokyo, Japan) with 0.5 × 0.5 cm quartz cuvettes. The samples were excited at 470 nm, and the fluorescence emission was recorded between 480 nm and 600 nm with slit widths set to 1 nm. Following the acquisition of fluorescence spectra, anisotropy measurements were performed in five replicates. The samples were excited at 470 nm, and the polarized emission was detected at 515 nm with an integration time of 0.5 seconds per measurement.

Steady-state anisotropy, $\langle r \rangle$, was determined according to Lakowicz (2006):

$$< r >= \frac{I_{VV} - G \cdot I_{VH}}{I_{VV} + 2G \cdot I_{VH}}$$

where I_{VV} and I_{VH} represent the vertical and horizontal components of the fluorescence emission with vertical excitation. The G factor, defined as $G = \frac{I_{HV}}{I_{HH}}$, is an instrumental correction factor accounting for the differences in transmission efficiency of the monochromators based on the polarization of the incoming light. The G factor was calculated using the horizontal excitation and emission components (I_{HV} and I_{HH}, respectively).

For the time-resolved fluorescence measurements, a time-correlated single-photon counting system was used (de Almeida et al., 2005; Loura et al., 1996a). In this setup, the instrumental G factor is assumed to be 1, since the polarized components of the fluorescent light were depolarized before reaching the entrance slit of the monochromator. Marina Blue-labeled proteins were excited at 340 nm using the second harmonic of a secondary dye laser (DCM from the Coherent DCM 700 series), while BODIPY-labeled proteins were excited at 488 nm using a ps laser diode (Becker & Hickl, Berlin, Germany, BPS-488-SM series). Emission was recorded at 455 nm for Marina Blue and 515 nm for BODIPY-labeled proteins.

For Time-resolved measurements the fluorescence intensity decay curves, $I(t)$, were described by a sum of discrete exponential terms (Lakowicz, 2006):

$$I(t) = \sum_{i=1}^{n} \alpha_i e^{(-t/\tau_i)}$$

where α_i and τ_i are the amplitude and the lifetime of the ith decay component, respectively of fluorescence. The decay parameters, α_i and τ_i, through iterative convolution of the fluorescence decay y $I(t)$ with the instrumental response function, IRF(t), and fitting to the experimental data, $I_{exp}(t)$.

Anisotropy decay parameters were subsequently derived by simultaneously fitting $I_{VV}(t)$ and $I_{VH}(t)$ through iterative convolution with the IRF, using the following relations:

$$I_{VV}(t) = \frac{I(t)}{3}[1 + 2r(t)]$$

$$I_{VH}(t) = \frac{I(t)}{3}[1 - r(t)]$$

with the IRF and globally fitting to the experimental parallel and perpendicular polarized components of the fluorescence. These fits were performed globally for the experimental parallel and perpendicular polarized components of the fluorescence.

Data analysis was carried out using the TRFA data processor Advanced Version 1.4 from Scientific Software Technologies Center (Belarusian State University, Minsk) (Marquardt, 1963). The goodness of the fits was judged from the experimental χ^2 value ($\chi^2 < 1.5$ indicating adequate fitting), weighted residuals and autocorrelation plots.

Tunable resistive pulse sensing setup

To investigate the effect of SP-C on membrane fragmentation, 200 nm synthetic LUVs containing varying concentrations of this protein, as well as synthetic peptides, were characterized using Tunable Resistive Pulse Sensing (TRPS) with a qNano Gold instrument (Izon Science Ltd., Oxford, UK). The qNano Gold system measures individual particles based on their size, concentration, and zeta potential, employing the TRPS technique. This method works by establishing an electrical current flow between an upper and lower chamber through a nanometer-sized pore (nanopore), which is continuously monitored via a computer-based system. When a particle traverses the nanopore, it temporarily interrupts the electron flow, leading to a disruption in the baseline current. The magnitude of this disruption correlates with particle size, the duration of the current drop reflects particle velocity (an indirect measure of zeta potential), and the frequency of interruptions provides information on particle concentration

(**Figure 8**). Calibration was performed using standard particles of known size, concentration, and zeta potential. The nanopore utilized in this study was NP100 (Izon Science Ltd., Oxford, UK), with a detection range of 50-330 nm. Data were standardized using CPC100 calibration particles (110 nm diameter, $1.1x10^{13}$ particles/mL; Izon Science Ltd., Oxford, UK), and internal controls were performed with CPC200 particles (210 nm diameter, $1x10^{12}$ particles/mL; Izon Science Ltd. Oxford, UK).

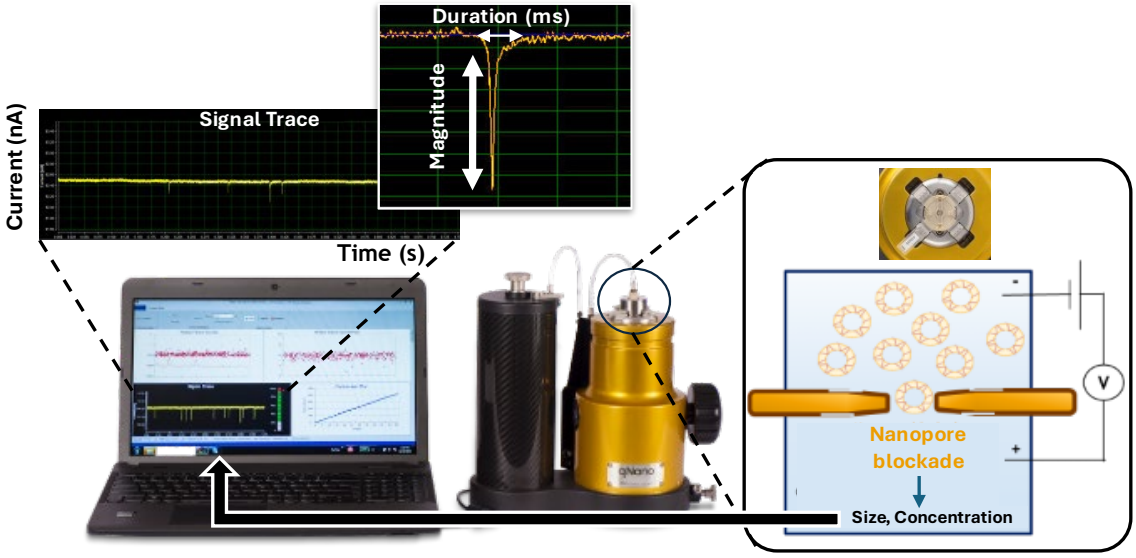

Figure 8: Tunable Resistive Pulse Sensing (TRPS) Device - qNano. *Experimental Principle: An electric current is established across a nanopore, where particle passage causes size-dependent fluctuations in current intensity. Each particle's transit results in a measurable decay in current proportional to its size.*

Under applied pressure, particle flow is governed by convective transport from regions of higher to lower concentration, allowing for the determination of both particle size and concentration under these conditions. Sample measurements were taken at pressures of 10 mm H_2O and 15 mm H_2O.

Zeta potential, also known as electrokinetic potential, is a key indicator of colloidal stability, representing the potential at the shear plane of particles. Zeta potential values provide insight into colloidal behavior: particles are considered unstable when the zeta potential is between ±10 mV, relatively unstable between 10 and 20 mV in absolute terms, moderately stable between 20 and 30 mV, and highly stable when exceeding 30 mV (Bhattacharjee, 2016). In this experiment, the applied pressure was kept low, so particle movement was primarily driven by the electrical current. Negatively charged particles migrated towards the positively charged lower chamber, where their zeta potential was measured. The applied pressure during zeta potential measurements ranged from 0 mm H_2O to 1 mm H_2O.

Nanoparticle tracking analysis

Due to limit detection of TRPS technique and the difficult hand use, 200 nm LUVs at 1 µg/ml were also characterized using Nanoparticle Tracking Analysis (NTA), developed by NanoSight Ltd. (Malvern Instruments Ltd., Malvern, Worcestershire, UK). This is a technique for real-time visualization of nanoparticles using laser-illuminated microscopy. A laser beam is directed through an optical prism, which refracts and focuses the beam into an intense illumination zone where nanoparticles become visible (**Figure 9**). The technique captures the Brownian motion of nanoparticles suspended in liquid. Detection is achieved using either a charge-coupled device (CCD) camera or, more recently, a complementary metal–oxide–semiconductor (CMOS) sensor, which converts optical signals into electronic data. Modern CMOS sensors, with their higher frame rates, are particularly well-suited for this application. The captured video, showing the movement of individual particles, is analyzed by NTA software, which calculates the distance travelled by each particle. By incorporating the temperature and viscosity of the solvent, the particle diameter is determined using a modified Stokes–Einstein equation. The detection limits of NTA vary based on the refractive index (Ri) of the nanoparticles: for particles with a high Ri, such as colloidal gold, the lower size limit is approximately 10 nm, while for particles of biological origin with a lower Ri, it is around 30 nm. The upper size limit is constrained by the diminishing Brownian motion of larger particles, making it difficult to track particles beyond approximately 1 µm in diameter. The measurement was performed at 25 °C using the NanoSight NS300 (Malvern Instruments Ltd., Malvern, Worcestershire, UK), illuminating the sample vesicles with a 405 nm laser, producing light scattering that was recorded by a CCD or CMOS camera. Five 60-second videos were captured for each sample. The data were analyzed using NTA 3.0 software, which processed the video sequence to obtain the number of particles, their trajectories, size, and particle concentration.

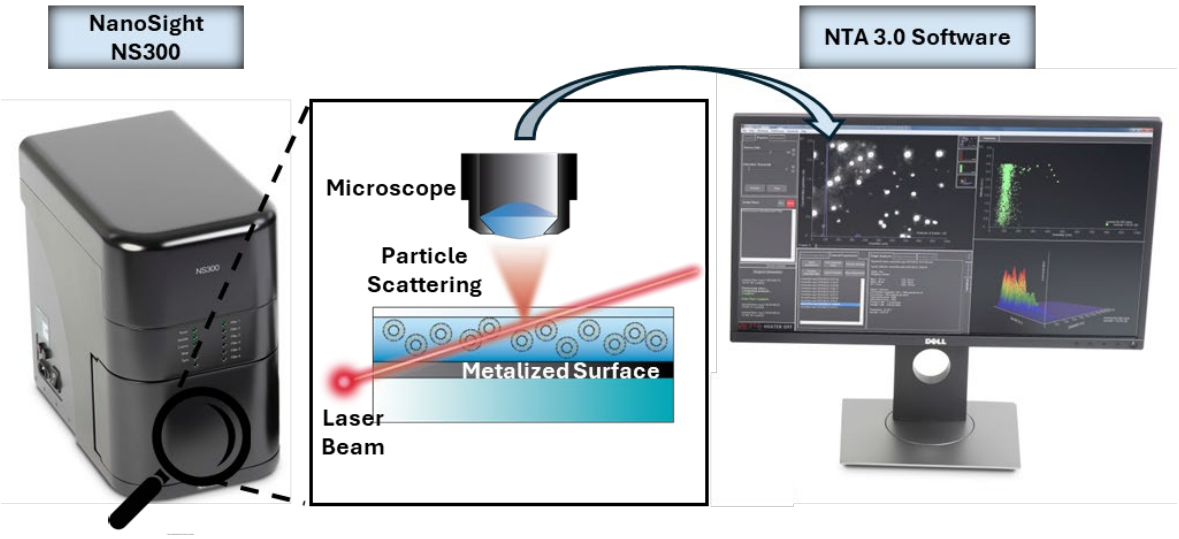

Figure 9: Overview of the Nanosight NS300 System with NTA 3.0 Software. *The figure illustrates the Nanosight NS300 setup for nanoparticle tracking analysis (NTA). The system includes a schematic of the microscope's function, showing how particles are illuminated by a laser beam. The scattered light from the particles is captured and visualized on a screen running the NTA 3.0 software. The software interface displays real-time videos of the particles, along with detailed data on their size distribution and concentration within the sample.*

Flow cytometry

Flow cytometry is a widely employed technique for both qualitative and quantitative analysis of cellular properties. It enables the simultaneous assessment of cell size (measured by Forward Scatter, FSC), internal complexity (measured by Side Scatter, SSC), and the detection of specific markers. This is accomplished through the analysis of optical properties and the application of various fluorescent probes. In the cytometer, a laminar flow ensures that individual cells pass sequentially through a beam of monochromatic light. At the point of intersection, light is scattered in multiple directions and collected by the cytometer's optical system. The signal is amplified by photomultiplier tubes, while specific wavelengths are filtered through dichroic mirrors and detectors, allowing precise characterization of samples based on fluorescence intensity for specific fluorochromes. The relative proportion of positive events or cells, compared to the total number of events, is calculated. Data are typically presented as histograms or two-dimensional dot plots.

In this study, alveolar cells were seeded in 24-well plates and incubated overnight as described earlier. For the MH-S cell line, 150,000 cells were cultured, whereas for the A549 cell line, 100,000 cells were grown. To analyze vesicle uptake mediated by SP-C, the cells were incubated for 2 hours with 10 µg of various types of fluorescently labelled lipid vesicles. Following incubation, the cells were washed with PBS, and the pellet obtained from 5-minute centrifugation at 1500 rpm was fixed with 0.5% paraformaldehyde (PFA). Flow cytometry data were acquired using an LSRFortessa Cytometer (BD Biosciences, San Jose, CA, USA),

recording 10,000 events per sample, and analyzed using FlowJo software v10 (BD Biosciences, San Jose, CA, USA). Rhodamine fluorescence was measured with the PE 575/26 filter, while BODIPY fluorescence was detected using the FITC 525/30 filter. Results were normalized to the background fluorescence of untreated control cells.

Imaging techniques

Epifluorescence microscopy

To determine wheter the fluorescent vesicles were engulfed by alveolar cells, epifluorescence microscopy was used. Fluorescence microscopy enables the visualization of fluorescent probes by utilizing a high-intensity light source that emits across a broad spectrum, ranging from ultraviolet to visible light. In the case of an epifluorescence microscope, the optical components are arranged so that the specimen is illuminated from above, allowing for efficient excitation of the fluorescent markers.

Prior to SUV incorporation, UV-sterile glass slides were placed in 24-well plates and the cells were plated. After 16 h, cells were incubated under culture conditions for 2 h with 10 µg of fluorescent SUVs. Then, cells were washed several times with PBS and fixed with 4% paraformaldehyde (PFA) for 15 min and incubated with 4',6-diamidino-2-phenylindole (DAPI) for 45 min. Then, glass slides were visualized by fluorescence microscope Leica DM-4000B (Leica Microsystems, Wetzlar, Germany) with DAPI and TX2 fluorescence filters and recorded with a digital camera C10600-10B ORCA-R2 (Hamamatsu, Shizuoka, Japan).

Confocal microscopy

The main feature of confocal microscopy is its ability to collect and detect light emitted by fluorescent molecules located within the same plane in a three-dimensional space. This is achieved by utilizing a laser as the light source, which emits collimated radiation that maintains a perfectly linear propagation. This monochromatic light specifically illuminates the sample with high intensity and stability, allowing for subcellular resolution at a microscopic level. In addition, confocal microscopes are equipped with a component known as the 'confocal pinhole aperture'. This small opening in the light detection filter blocks out light coming from out-of-focus planes in the sample. As a result, only information from the focused region, referred to as the 'primary image plane' or 'focal plane', is captured, while information from other planes is eliminated. This leads to significantly improved image quality and allows for virtual optical sectioning of the sample.

The operating principle of a confocal microscope is similar to that of an epifluorescence microscope, as both rely on the phenomenon of fluorescence. However, the key difference lies in the presence of the confocal pinhole in confocal microscopy, which is absent in epifluorescence microscopy. In confocal microscopy, the laser light scans the sample point by point, and the pinhole aperture ensures that only light from each focal plane reaches the detector. This enables the reconstruction of high-resolution, three-dimensional images by stacking these optical sections. The confocal setup not only enhances the optical resolution but also minimizes background noise and provides clearer images with better contrast, especially for thick samples or complex structures.

Ih this thesis confocal mycroscopy was used to characterize the effect of SP-C on membranas of GUVs and to study the colocalization of acid organelles with fluorescent SUVs, which uptake depends on SP-C concentration.

GUVs characterization

Samples were prepared by mixing 20 µL of electroformed GUVs with 200 µL of a 300 mM glucose solution to prevent GUV dispersion. Confocal images were acquired using a Nikon Ti-E inverted microscope, equipped with a Nikon C2 scanning confocal module and a Nikon Plan Apo 100X NA 1.45 oil immersion objective (Nikon, Tokyo Japan). Appropriate filter cubes were used for fluorescence detection. Image acquisition was carried out with the Nikon NIS-Elements software package, and subsequent analysis was performed using FIJI.

Colocalization assays

A549 and MH-S cells were cultured on circular coverslips placed in 24-well plates. The same experiment was conducted for both cell lines. To label acidic organelles (lysosomes and lamellar bodies), the fluorescent probe Lysotracker Red DND-99 was used, prepared by diluting the necessary volume in the appropriate culture medium for each cell line to reach a final concentration of 75 nM. Cells were incubated with 10 µg of various types of fluorescently protein labelled 50 nm SUVs and Lysotracker Red for 2 hours at 37°C. After incubation, the cells were washed three times with PBS and fixed with 0.5% paraformaldehyde (PFA). Additionally, nuclei were stained with DAPI as described above to provide clear localization of the cells. The coverslips were then examined using a confocal laser scanning microscope FluoView-1200, Olympus, equipped with three fluorescence detectors FITC-A, TxRed, and DAPI (Olympus, Tokyo, Japan).

5.

RESULTS

The fluorescence spectroscopies experiments included in the present chapter were done in collaboration with Prof. Manuel Prieto from iBB Institute for Bioengineering and Bioscience (IST, Universidade de Lisboa, Lisbon, Portugal) and published in the following article:

Morán-Lalangui M, Coutinho A, Prieto M, Fedorov A, Pérez-Gil J, Loura LMS, García-Álvarez B. **"Exploring protein-protein interactions and oligomerization state of pulmonary surfactant protein C (SP-C) through FRET and fluorescence self-quenching."**

Protein Sci. 2024 Jan;33(1):e4835. doi: 10.1002/pro.4835. PMID: 37984447; PMCID: PMC10731621.

Some BiFC experiments were published in the following article:

Barriga A, Morán-Lalangui M, Castillo-Sánchez JC, Mingarro I, Pérez-Gil J, García-Álvarez B. **"Role of pulmonary surfactant protein Sp-C dimerization on membrane fragmentation: An emergent mechanism involved in lung defense and homeostasis"**.

Biochim Biophys Acta Biomembr. 2021 Jun 1;1863(6):183572. doi: 10.1016/j.bbamem.2021.183572. Epub 2021 Feb 4. PMID: 33548215.

EBSA Biophysics in Europe

U LISBOA | UNIVERSIDADE DE LISBOA

CHAPTER 1:

ANALYSIS OF THE OLIGOMERIZATION STATE OF SP-C: OLIGOMER STOICHIOMETRY AND PROTEIN-PROTEIN INTERACTIONS

Introduction

Understanding the molecular interactions and structural dynamics of proteins within cellular and lipid environments is crucial for elucidating their functional roles in biological systems. This chapter focuses on the propensity of the pulmonary surfactant protein SP-C to form dimers and higher-order oligomers. Pulmonary surfactant plays an essential role in reducing alveolar surface tension, thereby facilitating efficient gas exchange during the respiratory cycle (Clements, 1977; Haagsman & Van Golde, 1991). SP-C, a highly hydrophobic transmembrane protein, contributes to the stabilization and dynamic regulation of the surfactant interfacial lipid film during breathing (Baumgart *et al.*, 2009; Johansson, Szyperski, *et al.*, 1994). Previous studies have suggested that SP-C's ability to dimerize may influence the structural properties of membranes, potentially inducing stress or curvature that alters the membrane architecture and affects lipid dynamics and distribution (Roldan *et al.*, 2016). Despite its significance, the mechanisms driving SP-C dimerization and aggregation, as well as the structural and environmental factors influencing these processes, remain insufficiently understood.

Protein-protein interactions, including dimerization and oligomerization, can be influenced by various factors, such as the lipid environment, post-translational modifications, and local membrane organization. SP-C is particularly intriguing due to its unique structure, which includes an extremely rigid valine-rich α-helical transmembrane domain, a palmitoylated N-terminal segment, and motifs believed to mediate protein-protein interactions (Creuwels *et al.*, 1995; Pérez-Gil *et al.*, 1992). The presence of palmitoyl chains is hypothesized to stabilize the protein's insertion into the lipid bilayer and may modulate its interaction with neighboring proteins (Baumgart *et al.*, 2010). However, alterations in the lipid composition of membranes or the eventual absence of palmitoylation can lead to changes in SP-C's behavior, potentially promoting the formation of dimers or aggregates (Korolainen *et al.*, 2022; Roldan *et al.*, 2015).

Previous studies have suggested that SP-C dimerization may be mediated by specific motifs, such as the highly conserved AxxxG sequence in the transmembrane domain or the PCCP sequence in the N-terminal segment (Kairys *et al.*, 2004; Luy *et al.*, 2004). These motifs may facilitate interactions through hydrogen bonds, van der Waals forces, or, in the case of the PCCP motif, the formation of disulfide bonds. However, the physiological relevance and structural implications of SP-C dimerization remain not fully understood. While some studies have observed SP-C dimers in vivo or under experimental conditions, others have reported that SP-C primarily exists as a monomer in functional surfactant systems (Creuwels *et al.*, 1995; Horowitz *et al.*, 1993; Wang *et al.*, 2002). This discrepancy

underscores the need for a more comprehensive investigation of the factors influencing SP-C oligomerization.

This chapter investigates the oligomerization state of SP-C using a combination of experimental approaches, including Bimolecular Fluorescence Complementation (BiFC) assays, fluorescence self-quenching, and Förster Resonance Energy Transfer (FRET) studies. The BiFC technique enables the visualization of protein-protein interactions within a cellular context, providing insights into the dimerization of SP-C in live cells. The use of synthetic lipid systems that mimic pulmonary surfactant environments enables a detailed analysis of SP-C behavior in controlled conditions, isolating the effects of lipid composition and membrane phase separation. Through fluorescence self-quenching and FRET analyses, we examine the lateral diffusion, aggregation, and compartmentalization of SP-C in membranes, shedding light on the interplay between protein structure, lipid environment, and dimerization propensity.

This work also examines the role of palmitoylation in the structural stability and oligomerization of SP-C. Non-palmitoylated recombinant SP-C (rSP-C) was studied to evaluate how the absence of palmitoyl groups influences protein-protein interactions and membrane behavior. Palmitoylation has been proposed to reduce the tilting of SP-C's α-helical domain within the bilayer and to promote deeper insertion of its N-terminal segment, factors that may affect its interaction with other proteins (Baumgart *et al.*, 2010; Roldan *et al.*, 2015). By comparing native SP-C solated from natural sources with rSP-C, this study aims to differentiate the contributions of palmitoylation from those of other structural features in driving SP-C dimerization and aggregation.

The findings presented in this chapter have important implications for understanding the physiological and pathological roles of SP-C oligomerization. Protein aggregation in pulmonary surfactant may contribute to membrane remodeling, vesicle formation, and surfactant recycling-processes that are critical for maintaining alveolar homeostasis (Cañadas *et al.*, 2020; Roldan *et al.*, 2016; Ruwisch *et al.*, 2020). Conversely, aberrant aggregation of SP-C, potentially induced by lung injury or oxidative stress, may impair surfactant function and contribute to respiratory disorders (Johansson, 2001). This chapter aims to provide a comprehensive analysis of SP-C interactions, offering new insights into the molecular basis of its behavior in different environments and its potential roles in both health and disease.

Results

Oligomerization state of SP-C in a cellular context using Bimolecular Fluorescence Complementation

To evaluate the interaction between SP-C molecules, a bimolecular fluorescence complementation (BiFC) assay was employed, as detailed in the Materials and Methods section. In brief, fusion proteins were designed in which either the N-terminal (VN) or C-terminal (VC) fragment of the Venus fluorescent protein (VFP) was fused to the sequences encoding the proteins whose dimerization state is being studied as well as proteins used as controls. These fragments were connected via a flexible linker. Upon successful dimerization of the studied proteins, the reconstitution of the VFP was achieved, resulting in the restoration of its fluorescence signal. Thus, this complementation serves as an indicator of protein-protein interactions in a cellular context.

Initially, we used the well-established heterodimer Fos-Jun as a transfection control in HEK293T cells and as normalization factor. However, since our goal was to study the homodimerization of SP-C, we employed the well-characterized transmembrane protein glycophorin A (GpA) as a more suitable control. In addition, its dimerization motif, GxxxG (where 'x' represents any amino acid) is analogous to the putative motif proposed for dimerization of SP-C (GxxxA) (Kairys *et al.*, 2004). To specifically examine the contribution of this dimerization motif, we employed a truncated chimeric variant of GpA, comprising only the transmembrane domain, with all non-essential residues substituted by leucine, thereby isolating the GxxxG motif's role in dimerization (Grau *et al.*, 2017). As a negative control, we utilized a mutated variant of this GpA construct (GpA G→I), in which the glycine residues critical to dimerization were replaced with isoleucine (Grau *et al.*, 2017), thereby disrupting the interaction. This experimental approach was utilized to study the dimerization of both proSP-C, the precursor of mature SP-C containing the C-terminal BriCHOS domain required for proper folding, and mature SP-C (mSP-C).

Fluorescence levels obtained from lysates of HEK 293T cells transfected with proSP-C or mSP-C pairs were significantly higher than those transfected with the negative control GpA G→I or with the positive control GpA (**Figure 1.1A**). indicating the self-interaction between both proteins, each with itself. This increase in fluorescence indicates a robust interaction between both proSP-C and mSP-C, each forming homodimers. As no statistically significant difference was detected between proSP-C and mSP-C, constructs with mutations in either of the proposed dimerization motifs, PCCP and AxxxG, mSP-C (C→A) and mSP-C (A,G→I) respectively, were used. Furthermore, a scrambled version of mSP-C (sSP-C), were introduced to further investigate protein-protein interaction of SP-C. In this case,

fluorescence levels from these mutated variants, including the scrambled construct, remained comparable to the wild-type mSP-C (**Figure 1.1B**). To explain these findings, the expression levels of each construct were assessed, revealing a marginally higher expression of VN and VC fusion proteins in mSP-C and its mutants compared to the controls and proSP-C. However, the precise impact of this differential expression on the assay outcomes could not be definitively determined.

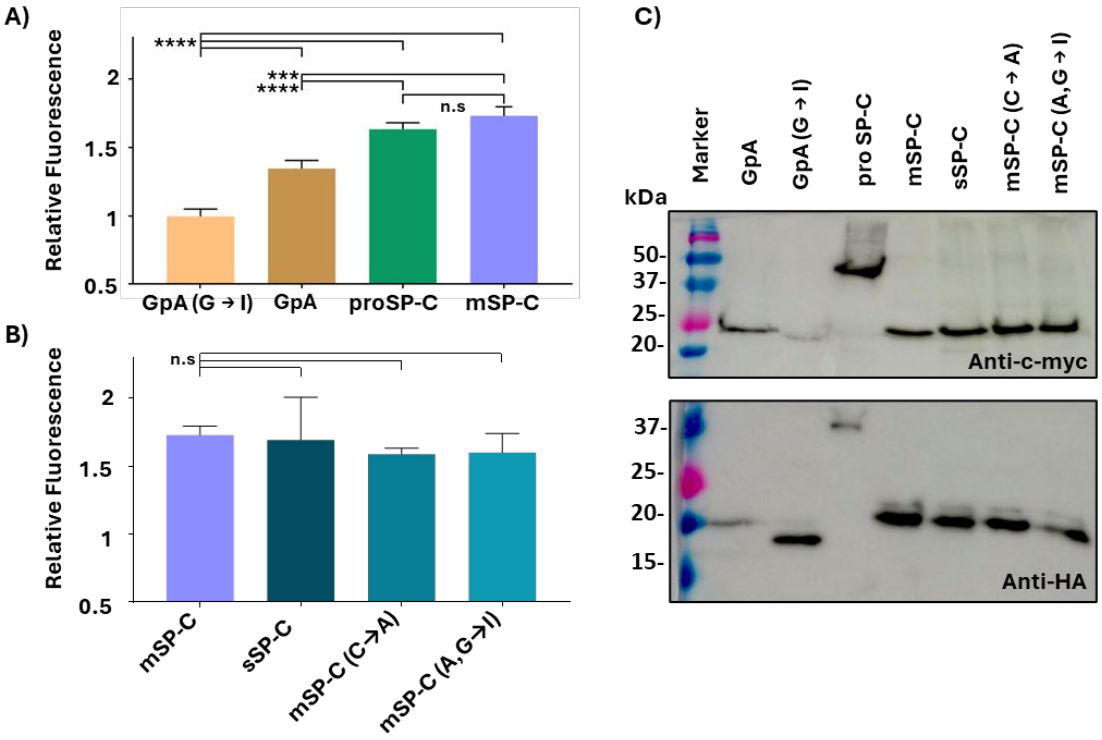

Figure 1.1: BiFC assays to explore dimerization of mature SP-C and proSP-C. A) *Fluorescence derived from BiFC assays using different potential homodimeric systems in HEK 293T cells.* ***B)*** *Fluorescence derived from BiFC assays using a scrambled version of SP-C (sSP-C) and mutations in the potential proposed dimerization motifs of mature SP-C. Results are expressed as the ratio of the fluorescence value for each sample with respect to obtained using Fos/Jun dimers. All values are expressed as means ± S.D. Statistical analyses were performed using an unpaired Student's t-test. Significant p-values are depicted as asterisks (n.s, not significant; ***, p<0.001; ****, p<0.0001). C) Western blot analysis of lysates from HEK 293T cells transfected with constructs encoding the Venus N-terminal (VN) and C-terminal (VC) fragments fused to the proteins of interest. The presence of these fusion proteins was confirmed using anti-c-myc antibodies, which recognize VN, and anti-HA antibodies, which recognize VC, providing validation for the expression of the constructs utilized in this experiment.*

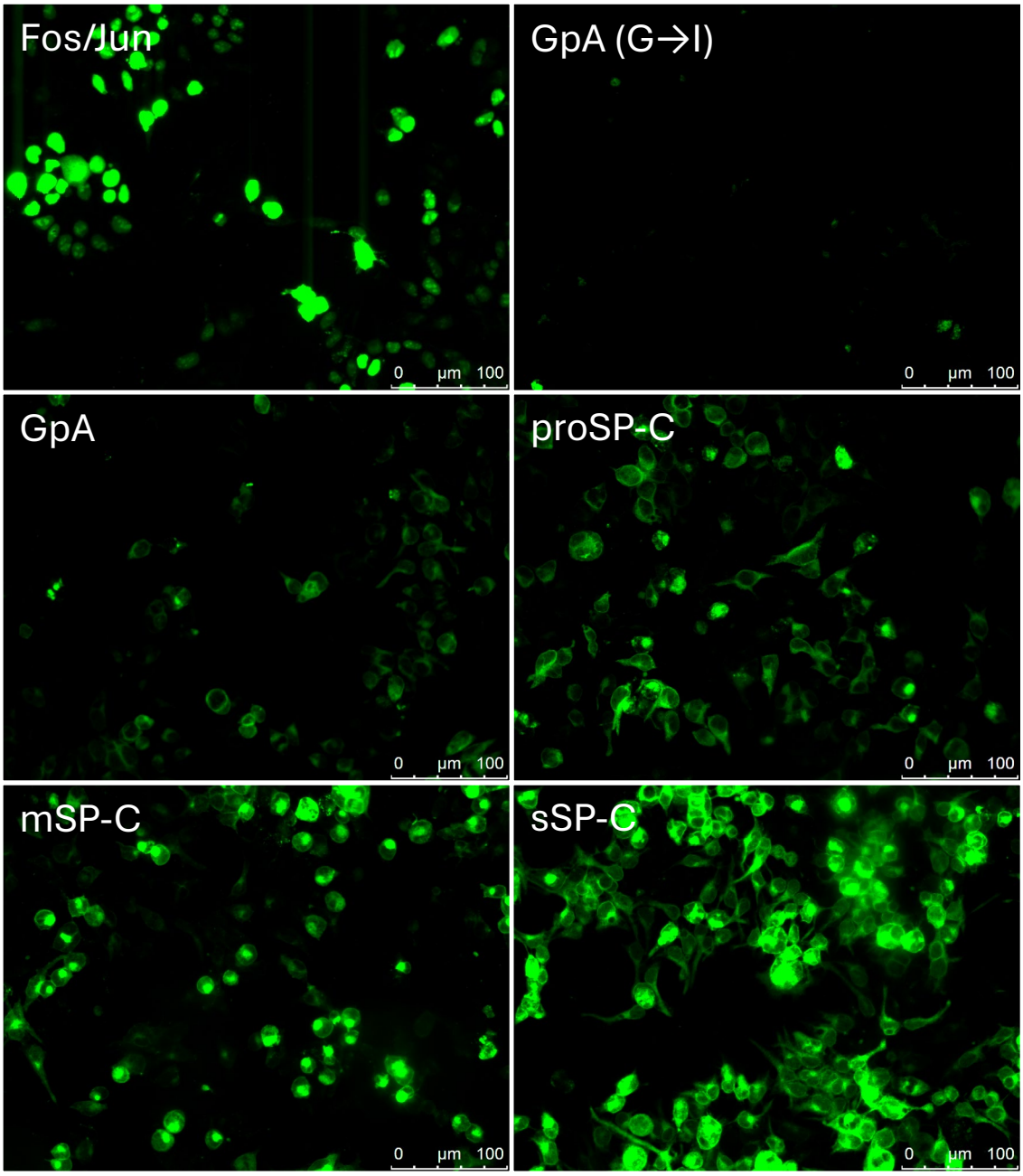

Figure 1.2. Cellular fluorescence derived from Bimolecular Fluorescence Complementation (BiFC). *Representative micrographs of HEK293T cells following transfection and expression of VN and VC fusion proteins linked to the protein Jun, Fos, respectively, and GpA (G→I), GpA, proSP-C, mSP-C and sSP-C, as indicated in the figure. In all micrographs, fluorescence corresponding to the reconstitution of Venus fluorescent protein (VFP) is depicted in green, reflecting successful protein-protein interactions.*

Additionally, cellular fluorescence was analyzed via fluorescence microscopy to assess the localization of protein interactions during expression. Fos/Jun is a nuclear heterodimer, therefore its localization is expected to be nuclear. In contrast, the other constructs correspond to transmembrane proteins and should be primarily located to cellular membranes. Improper folding could disrupt their trafficking, potentially leading to their accumulation in the perinuclear region, particularly within the endoplasmic reticulum. As shown in **Figure 1.2**, cells transfected with Fos/Jun exhibited high levels of fluorescence derived from BiFC in

the nucleus, consistent with previous reports of nuclear localization. In contrast, GpA (G→I), a negative control, displayed fluorescence only in discrete punctate regions in a small subset of cells. Conversely, GpA demonstrated robust fluorescence corresponding to VFP reassembly, primarily localized at the cell membrane. Concerning the proteins whose dimerization wanted to be studied, proSP-C, which includes the BriCHOS domain needed for a proper folding during SP-C synthesis, shows a fluorescence pattern similar to GpA, although some high fluorescent dots were observed, which could suggest the partial confinement of VN/VC linked to proSP-C in specific regions such as the nucleus. The micrograph corresponding to cells expressing VN and VC linked to mSP-C displays an increased number of fluorescent spots, indicating a higher level of nonspecific reconstitution of VFP. However, fluorescence is also observed along the membrane, suggesting the formation of some specific dimers at this location. This is also observed in cells transfected with sSP-C, but with significantly higher levels of fluorescence, both in the concentrated fluorescent spots, presumably located in the nucleus, and in membrane-associated systems. This suggests a greater capacity for self-interaction and for nonspecific aggregation, likely due to the high concentration of the protein in confined areas, as similarly observed with the GpA mutant, GpA (G→I).

In conclusion, only the samples corresponding to proSP-C exhibit expression levels comparable to the control proteins (**Figure 1.1C**) and its fluorescence pattern closely resembles that of GpA (**Figure 1.2**). This suggests that proSP-C is capable of forming highly stable dimers within membranes and, unlike mSP-C and its variants, does not show evidence of extensive aggregation in perinuclear spaces indicating BRiCHOS contained in proSP-C is essential for proper trafficking of the protein. Because of this, to study the oligomerization state of the mature SP-C protein, it is necessary to perform the experiments in synthetic systems, otherwise SP-C would aggregate in a non-specific manner, as observed in this work.

SP-C homodimer formation studied by self-quenching and FRET studies

The oligomerization state of SP-C in synthetic membrane systems has been studied using fluorescence spectroscopy techniques. We have performed self-quenching and FRET assays to analyze dimerization of native palmitoylated SP-C and of a non-palmitoylated recombinant version of SP-C (rSP-C) using fluorescently labeled versions of either protein reconstituted in different lipid systems mimicking pulmonary surfactant environments: (i) POPC membranes, in an entirely fluid disordered state; (ii) DPPC/POPC/POPG (50:25:15 w/w/w) mixed membranes, somehow mimicking in a simplified version the lipid composition of pulmonary surfactant and a likely coexistence of disordered and ordered phases, and (iii) membranes made of deproteinized full lipid surfactant (LS) directly

extracted from native pulmonary surfactant. This complex mixture a major fraction of DPPC, other phospholipids and neutral lipids such as cholesterol.

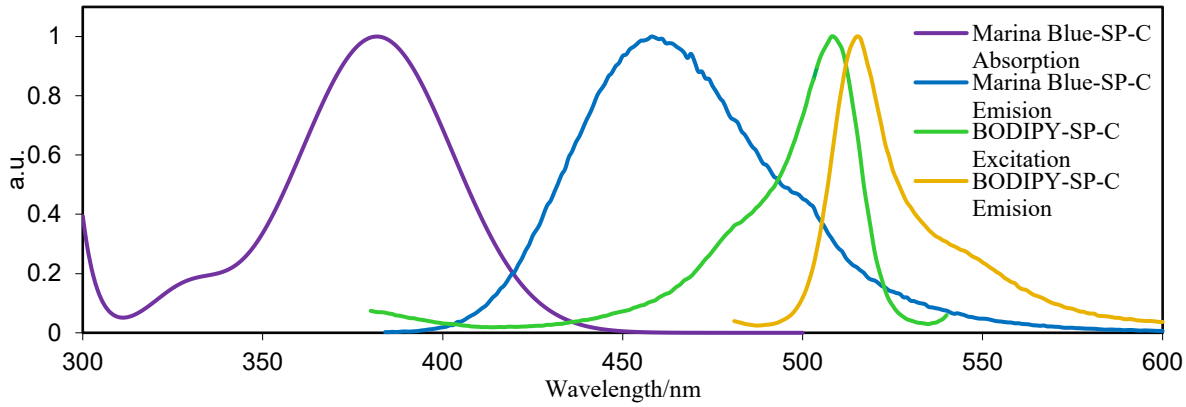

Figure 1.3: Normalized spectra of Marina Blue SP-C and BODIPY SP-C in POPC membranes. *The spectra were obtained with 0.5 mol % of Marina Blue SP-C, and 0.125 mol% of BODIPY SP-C in 1 mM POPC vesicles.*

The absorption and emission spectra of SP-C labelled with Marina Blue or BODIPY-FL fluorophores upon incorporation into POPC bilayers under diluted conditions at 25 °C are depicted in **Figure 1.3**. No significant spectral alterations were detected for BODIPY SP-C compared to BODIPY SP-B [44], and these spectral profiles are also identical to the ones obtained with the recombinant SP-C protein, rSP-C (results not shown). Upon direct inspection of the spectra in **Figure 1.3**, a large overlap between Marina Blue fluorescence emission and BODIPY-FL absorption spectra can be detected, allowing for an efficient FRET interaction. Incorporating fluorophores into a protein could influence its intrinsic structure. To explore this issue, we have performed Circular Dichroism (CD) measurements. Deconvolution of spectra profiles have shown that the probe does not disrupt the essentially the α-helical structure of the protein.

The photophysical characterization of these two derivatized proteins is presented in **Table 1** and **Figure 1.4**. The fluorescence intensity decay of Marina Blue SP-C is well described by three exponentials, with an additional faster component when compared to previous data (Cabré *et al.*, 2018). A similar behavior was obtained for the fluorescence anisotropy decay of Marina Blue SP-C, where the previous limiting anisotropy is now translated by a very long rotational correlation time ϕ=21.0 ns (**Figure 1.4**). For the BODIPY SP-C, its fluorescence intensity decay is successfully described by a single exponential of τ= 6.0 ns, and a long rotational correlation time of ϕ=14.1 ns is necessary to adequately fit its fluorescence anisotropy decay. It should be stressed that these results are essentially comparable to the ones previously described in (Cabré *et al.*, 2018), and the small

differences are essentially due to a better instrumental time-resolution, allowing for the detection of ultrafast components in the fluorescence intensity decays.

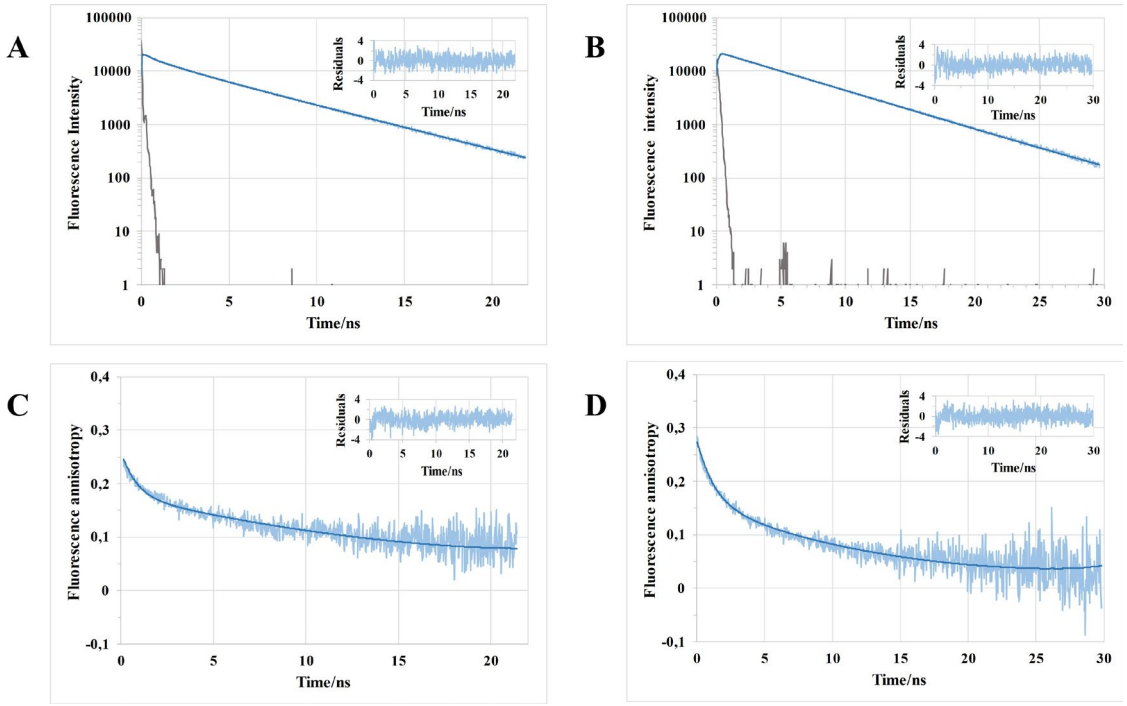

Figure 1.4: Fluorescence intensity and anisotropy decays of Marina Blue SP-C and BODIPY SP-C in POPC membranes. *(A and B) Fluorescence intensity and (C and D) anisotropy decays of (A and C) Marina Blue SP-C and (B and D) BODIPY SP-C in POPC vesicles. Solid dark lines represent the best fitting curves using the fitting parameters summarized in* ***Table 1****. The distributions of residues are shown in the inset plots.*

Table 1: Fluorescence intensity and anisotropy decay fitting parameters for fluorescently-labeled Marina Blue SP-C and BODIPY SP-C in POPC membranes.

		Marina Blue SP-C	BODIPY SP-C
Fluorescence intensity decay parameters	τ_1/ns	0.23 (0.26)	6.0 (1.0)
	τ_2/ns	1.9 (0.17)	-
	τ_3/ns	5.3 (0.57)	-
	χ^2	1.088	1.115
Fluorescence anisotropy decay parameters	ϕ_1/ns	0.79 (0.3)	1.2 (0.43)
	ϕ_2/ns	21.0 (0.69)	14.1 (0.57)
	χ^2	1.205	1.219

The parameters (with normalized amplitudes inside parentheses) have been determined in samples containing 0.5 mol% Marina Blue SP-C or 0.125 mol% BODIPY SP-C in 1 mM POPC vesicles. τ_i are the lifetimes components and ϕ_i the rotational correlation times. See text for further details.

Protein lateral diffusion and compartmentalization from time-resolved self-quenching

The self-quenching (SQ) of emission of the BODIPY fluorophore upon aggregation and π-stacking interactions has been reported often in the literature (e.g., (Kang *et al.*, 2022; Liu *et al.*, 2019; Pakhomov *et al.*, 2017)). In the present work, we used both time-resolved and steady-state self-quenching (TRSQ and SSSQ, respectively) as means to probe the lateral diffusion/compartmentalization (from TRSQ) and aggregation (from SSSQ) of the two fluorescently-labeled proteins in the different lipid systems. We address the former in this subsection.

The dependence of BODIPY SP-C and BODIPY rSP-C mean fluorescence lifetimes on their membrane concentrations were analyzed using a Stern-Volmer equation:

$$\bar{\tau}_0 / \bar{\tau} = 1 + k_q \langle \tau_0 \rangle [\mathrm{Q}] \tag{1}$$

where [Q] is the fluorophore concentration in the lipid phase (equal to that of the fluorescently-labeled protein, corrected for the corresponding labeling ratio), $\bar{\tau}$ is the amplitude-averaged mean fluorescence lifetime,

$$\bar{\tau} = \sum_i \alpha_i \tau_i \tag{2}$$

and <τ> is the intensity-averaged mean fluorescence lifetime,

$$\langle \tau \rangle = \frac{\sum_i \alpha_i \tau_i^2}{\sum_i \alpha_i \tau_i} \tag{3}$$

The subscript "0" indicates values extrapolated to infinite dilution. The main fitting parameter in the Stern-Volmer plots is the bimolecular collisional quenching rate constant, k_q. According to the approximation of Umberger and Lamer (Umberger & LaMer, 1945), it is related to the self-diffusion coefficient *D* through

$$k_q = 4\pi N_A (2R_c)(2D)\left(1 + \frac{2R_c}{\sqrt{2 < \tau_0 > D}}\right) \quad (4)$$

where N_A is the Avogadro constant and R_c is the collisional radius, which for self-quenching equals to twice the fluorophore radius.

Stern-Volmer plots for the different systems under study are depicted in **Figure 1.5**. Note the enlarged ordinate scale in the right plots, indicative of a larger extent of self-quenching for rSP-C, especially in the LM (mixture of DPPC/POPC/POPG, 50/25/15 w/w/w) and LS (lipid surfactant) systems. **Table** shows the corresponding *D* values obtained from solving the non-linear Eq. 4 (with R_c= 1.0 nm), as well as their 90% confidence intervals. The diffusion coefficient measured for BODIPY SP-C in POPC is typical of a membrane-inserted protein, being in fact similar to that previously obtained for BODIPY SP-B in the same system (Cabré *et al.*, 2018), and of the order of what is expected for phospholipids in fluid disordered bilayers (~10^{-7} cm^2/s (Filippov *et al.*, 2003, 2004)). A similar extent of dynamic self-quenching, and consequently a similar *D* value, was measured for BODIPY SP-C in the LM system. At variance, for LS membranes, a larger degree of quenching occurred within the same concentration range, implying a higher diffusion coefficient by approximately an order of magnitude. Such value is unrealistically high for lateral diffusion in lipid bilayers, and reflects compartmentalization of SP-C, resulting in much higher effective SP-C concentrations available for dynamic self-quenching than expected from the bulk membrane concentration in this system.

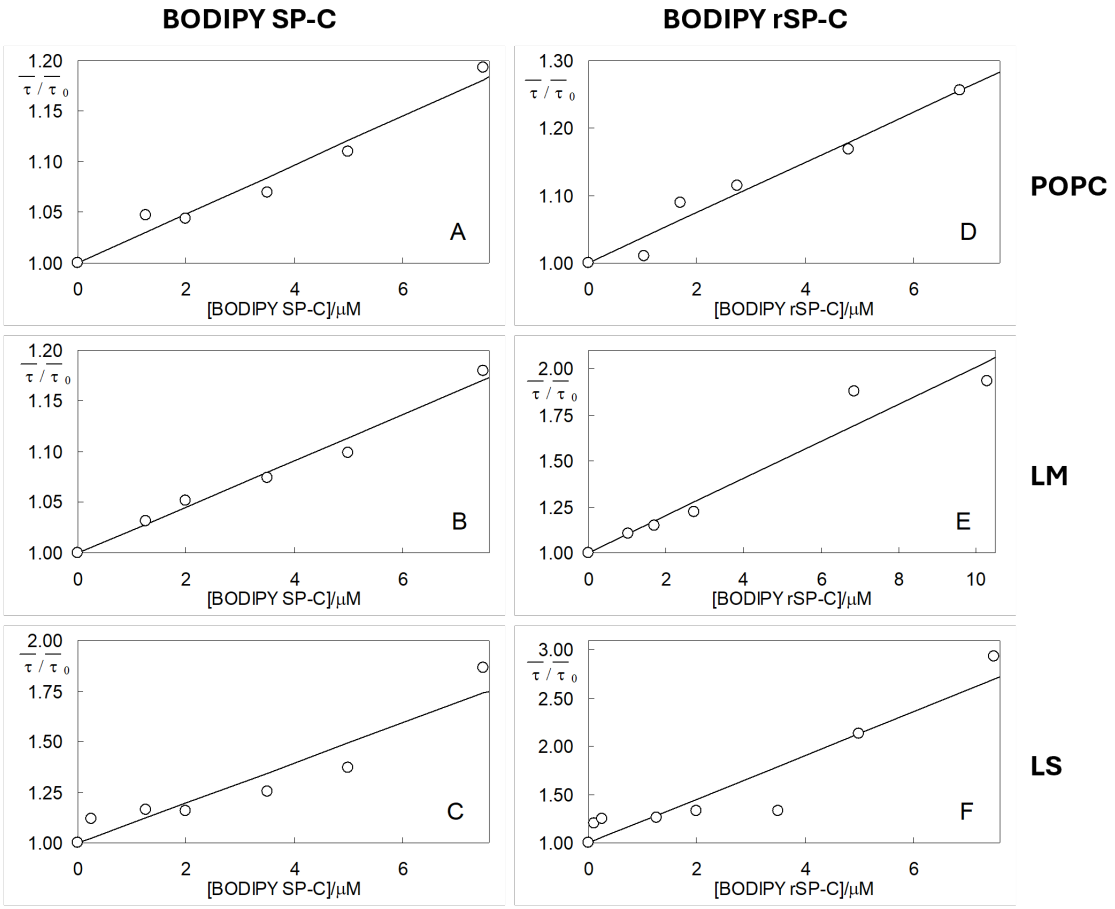

Figure 1.5: Dynamic self-quenching of BODIPY SP-C and rSP-C in membranes. *Stern-Volmer plots for the dynamic self-quenching studies of BODIPY SP-C (A-C) or BODIPY rSP-C (D-F) in POPC (A,D), DPPC/POPC/POPG lipid mixture (B, E) or LS (lipid surfactant) (C, F). The solid lines are the best fits of Eq. 1 to the experimental data of* $\overline{t} / \overline{t}_0$ *ratios (circles) as a function of the concentration of the fluorescently-labeled protein used in each case. Note the enlarged ordinate scale in the right plots, indicative of a larger extent of self-quenching for BODIPY rSP-C.*

Table 2: Lateral diffusion coefficients of BODIPY SP-C and BODIPY rSP-C in membranes.

System	*D* (10^{-7} cm^2/s)	
	BODIPY SP-C	**BODIPY rSP-C**
POPC	1.92 ([1.39; 2.52])	**4.03 ([2.97; 5.19])**
LM	1.55 ([1.23; 1.90])	**15.7 ([11.0; 20.8])**
LS	**16.3 ([10.8; 22.1])**	**51.2 ([42.1; 60.5])**

The coefficient D (10^{-7} cm^2/s) has been obtained from Eq. 4 after fitting Eq. 1 to the Stern-Volmer plots of ***Figure 1.5*** *for either protein in POPC, LM (DPPC/POPC/POPG lipid mixture) or LS (lung surfactant lipid fraction). 90% confidence intervals are given inside parentheses.*

Turning now to BODIPY rSP-C, an approximately two-fold increase in *D* was observed in POPC compared to the value obtained for the palmitoylated protein.

This slightly faster lateral diffusion of BODIPY rSP-C compared to BODIPY SP-C could be rationalized on account of the lack of the membrane-inserted acyl chain. On the other hand, compared to POPC, the apparent diffusion coefficient of BODIPY rSP-C is increased by a factor of ≅4 and ≅15 in LM and LS vesicles, respectively. While the results obtained for both proteins in LS are qualitatively similar, the higher apparent diffusion coefficient in LM compared to POPC reveals that BODIPY rSP-C probably has a confined distribution in this lipid system, contrarily to its palmitoylated counterpart.

Protein aggregation from steady-state self-quenching

SSSQ of BODIPY-labeled membrane proteins was monitored at λ_{em} = 550 nm, following excitation at λ_{em} = 470 nm (**Figure 1.6**). The measured fluorescence intensities I_F were analyzed first with a formalism that combined dynamical with static quenching, the latter being described by an active sphere term, which accounts for transient statistical nonfluorescent contact pairs, formed at the moment of excitation, but not involved in complexes formation (i.e., with interaction energy below the thermal value) (Cabré *et al.*, 2018; Fernandes *et al.*, 2003):

$$I_F = \frac{C[F]}{1/\overline{\tau}_0 + k_q[F]} \exp(-VN_A[F]) \quad (5)$$

In this equation, V is the active sphere volume and C is a multiplying factor. From this analysis, we concluded that no aggregation of BODIPY SP-C was apparent in POPC or LM bilayers (a V = 0 being recovered), while a low degree of aggregation was observed for this protein in LS, compatible with formation of statistical contact pairs (active sphere radius $R = (3V/(4\pi))^{1/3}$ = 8.9 Å). Conversely, for BODIPY rSP-C, higher active sphere radii were retrieved in all systems, namely 13.8 Å, 26.7 Å and 18.7 Å for POPC, LM and LS, respectively. Such values, namely the latter two, are higher than the expected interfluorophore distances for a contact dimer, indicating a higher extent of aggregation than what could be justifiably rationalized as statistical pairs. This led us to alternatively consider a dimerization scheme,

$$2F_1 \rightleftharpoons F_2, K = [F_2]/[F_1]^2, [F] = [F_1] + 2[F_2] \quad (6)$$

where F_1 and F_2 represent monomeric and dimeric fluorophore species, and [F] is the total fluorophore concentration. Under these circumstances, the fluorescence intensity will be given by

$$I_F = \frac{C[\mathrm{F}_1]}{1/\bar{\tau}_0 + k_q[\mathrm{F}]} \tag{7}$$

Solving Eq. 6 for $[F_1]$ (for given *K* and [F] values), and inserting in Eq. 7 leads to (Fernandes *et al.*, 2003):

$$I_F = \frac{C}{1/\bar{\tau}_0 + k_q[\mathrm{F}]}\frac{-1+\sqrt{1+8K[\mathrm{F}]}}{4K} \tag{8}$$

This equation holds for the hypothetical situation of a complete protein labeling with fluorophore. However, in the case of incomplete protein labeling, such as in the present situation, three different combinations are possible for dimers, namely labeled/labeled, labeled/unlabeled, and unlabeled/unlabeled protein pairs. Only formation of the first one leads to self-quenching of BODIPY. Under this situation, the concentration of protein in each form can be obtained for a given *K* value by numerically solving a set of nonlinear equations, as detailed below.

Let F_1, F_2 and F_t be the monomeric, homodimeric and total concentration of protein, respectively. The assumption of a dimerization equilibrium (with association constant *K*) implies that

$$F_2 = K F_1^2 \tag{9}$$

An identical relationship (with the same assumed association constant) applies to unlabeled proteins, replacing F_1 and F_2 by the corresponding monomeric and dimeric "dark" protein concentrations, D_1 and D_2 respectively:

$$D_2 = K D_1^2 \tag{10}$$

Dimers involving one labeled and another unlabeled protein unit can also be formed, with concentration *FD*, assumingly with the same association constant:

$$FD = K F_1 D_1 \tag{11}$$

Concentration balances hold for both labeled and unlabeled proteins, that is

$$F_t = F_1 + 2F_2 + FD \tag{12}$$

and

$$D_t = D_1 + 2D_2 + FD \tag{13}$$

where D_t is the total unlabeled protein concentration. Note that F_t and D_t are known from the experimental analytical protein concentration and the labeling ratio r. This leaves us with a set of five equations with the five unknowns F_1, F_2, D_1, D_2 and FD. Applying simple algebra, one can reduce this set to one of two nonlinear equations on the two variables F_1 and D_1, which can be written as a vector equation:

$$\mathbf{f}(F_1, D_1) = \begin{bmatrix} f_1(F_1, D_1) \\ f_2(F_1, D_1) \end{bmatrix} = \begin{bmatrix} KD_1F_1 + F_1 - F_t + 2KF_1^2 \\ F_t - D_t - F_1 + D_1 - 2KF_1^2 + 2KD_1^2 \end{bmatrix} = \begin{bmatrix} 0 \\ 0 \end{bmatrix} \tag{14}$$

Starting from an initial approximation $\mathbf{f}(F_1^{(0)}, D_1^{(0)})$, one can solve the vector equation iteratively, using the Newton-Raphson method:

$$\begin{bmatrix} F_1^{(i+1)} \\ D_1^{(i+1)} \end{bmatrix} = \begin{bmatrix} F_1^{(i)} \\ D_1^{(i)} \end{bmatrix} - \left(\begin{bmatrix} \frac{\partial f_1}{\partial F_1} & \frac{\partial f_1}{\partial D_1} \\ \frac{\partial f_2}{\partial F_1} & \frac{\partial f_2}{\partial D_1} \end{bmatrix} \right)^{-1}_{F_1^{(i)}, D_1^{(i)}} \begin{bmatrix} f_1(F_1^{(i)}, D_1^{(i)}) \\ f_2(F_1^{(i)}, D_1^{(i)}) \end{bmatrix} \tag{15}$$

where the Jacobian matrix is given by

$$\mathbf{J_F} = \left(\begin{bmatrix} \frac{\partial f_1}{\partial F_1} & \frac{\partial f_1}{\partial D_1} \\ \frac{\partial f_2}{\partial F_1} & \frac{\partial f_2}{\partial D_1} \end{bmatrix} \right) = \begin{bmatrix} KD_1 + 1 + 4KF_1 & kF_1 \\ -1 - 4KF_1 & 1 + 4KD_1 \end{bmatrix} \tag{16}$$

Implementation of the method was carried out in a Microsoft Excel worksheet, with inversion of the Jacobian matrix in each iteration, from its determinant and adjugate matrix:

$$(\mathbf{J_F})^{-1} = \frac{1}{\det(\mathbf{J_F})}\left(\begin{bmatrix} \frac{\partial f_2}{\partial D_1} & -\frac{\partial f_1}{\partial D_1} \\ -\frac{\partial f_2}{\partial F_1} & \frac{\partial f_1}{\partial F_1} \end{bmatrix}\right) \quad (17)$$

As initial guesses, $F_1^{(0)} = F_t/2$ and $D_1^{(0)} = (1 - r)F_1^{(0)}$ were used. To all practical purposes, the method converged after five iterations in all cases.

Summing the concentration of the two species with a single labeled protein (either true monomers or unlabeled/labeled dimers) and inserting that sum in the numerator of Eq. 7 (in the place of $[F_1]$), the theoretical fluorescence intensity is obtained as a function of total protein, and from fitting of this variation to the experimental I_F, one recovers K (as well as C), which, in turn, allows estimation of the variable concentrations of the monomeric and dimeric species.

For the situations where the sphere of action formalism indicated the possibility of aggregation, namely BODIPY SP-C in LS or BODIPY rSP-C in POPC, LM or LS membranes, we used the dimer equilibrium formalism, to obtain K = 1.0 M^{-1}, 3.9 M^{-1}, 438 M^{-1} and 16.6 M^{-1}, respectively. For these systems, the corresponding panels of **Figure 1.6** (C, D, E and F, respectively) show the fraction of monomeric labeled protein as a function of total fluorescently-labeled protein.

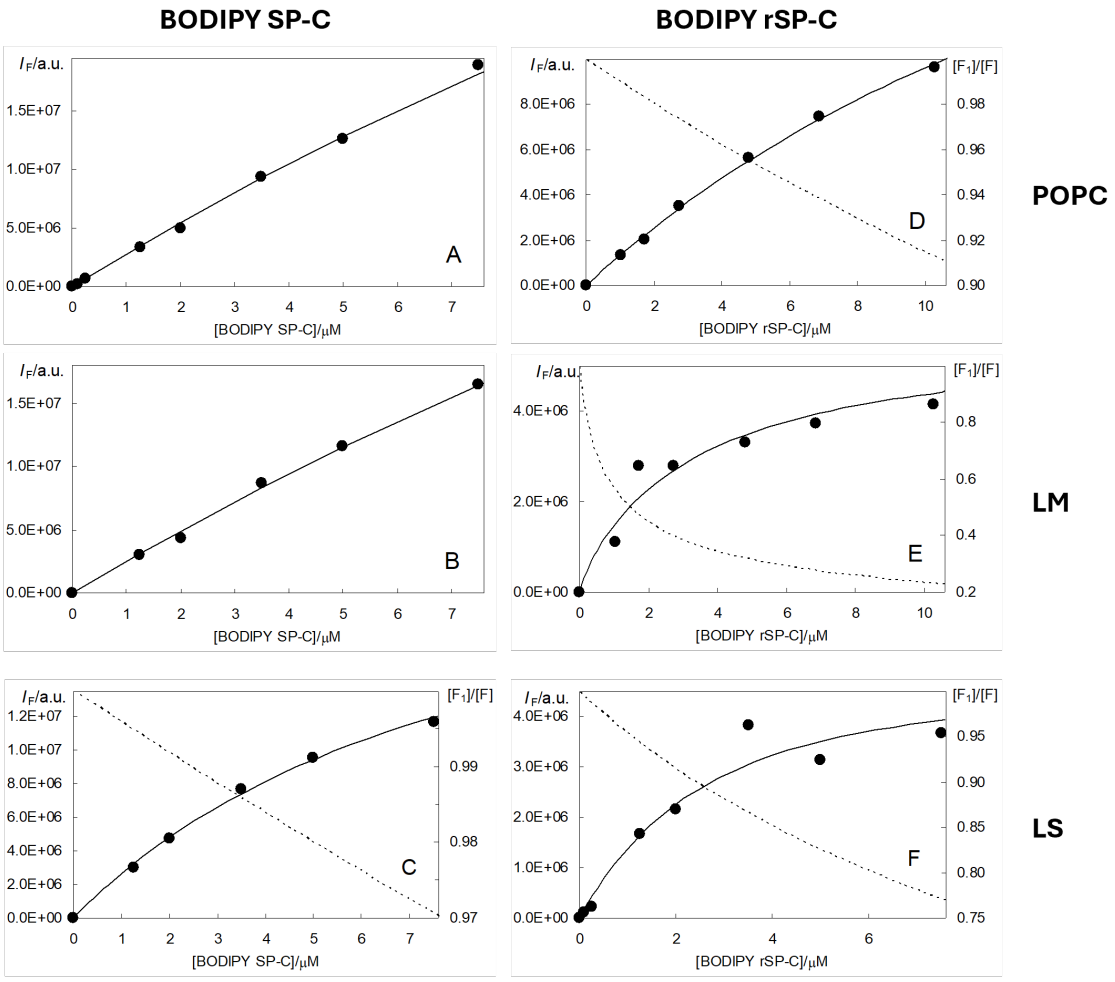

***Figure 1.6: Steady-state fluorescence of BODIPY SP-C and BODIPY rSP-C in membranes**. Steady-state fluorescence intensity (I_F; circles) of BODIPY SP-C (A-C) or BODIPY rSP-C (D-F) in POPC (A, D), DPPC/POPC/POPG lipid mixture (B, E) or pulmonary surfactant lipid fraction (C, F). The solid lines are the best fits to a combined dynamic and static quenching mechanism, with an active sphere (A, B; V = 0 in Eq. 5) or dimerization equilibrium (C-F; Eq. 7, see text for K values in each case) formalism. In the latter situation, the fractions of monomeric labeled protein, $[F_1]/[F]$, are plotted as dotted lines, referring to the secondary ordinate axes of the corresponding panels.*

A critical comment should be made here about the quenching models and the best fit values recovered: (i) there is some scatter in the data for plots E and F; (ii) there is anti-correlation between the two sources of quenching, meaning that an underestimation of the dynamic component may be counterbalanced by an overestimation of the static one, and vice-versa; (iii) although the fits in **Figure 1.6** are satisfactory, higher order aggregates cannot be ruled out; and finally (iv) for simplicity, it is assumed that the quenching efficiency of dimers involving fluorescent units is strictly unity. Still, it can be concluded that these results point to an essentially monomeric distribution of BODIPY SP-C in all systems (a very slight degree of aggregation is apparent only in LS), in contrast to BODIPY rSP-C, for which aggregation can be inferred, most significantly in the LM and LS systems.

Protein lateral membrane distribution from time-resolved FRET measurements

The time-resolved emission of Marina Blue SP-C and Marina Blue rSP-C was measured in the absence and in the presence of varying membrane concentrations of BODIPY SP-C and BODIPY rSP-C, respectively. As clearly seen in **Figure 1.3**, the emission spectrum of Marina Blue and the absorption spectrum of BODIPY display considerable overlap. This allows for an efficient FRET between protein molecules labeled with the two fluorophores, with a Förster distance of 4.93 nm as previously determined (Cabré *et al.*, 2018).

For each lipid system, the fluorescence intensity decays of samples with donor only (vesicles loaded with 5 μM Marina Blue SP-C or Marina Blue rSP-C) and donor + acceptor (vesicles loaded with 5 μM Marina Blue SP-C or Marina Blue rSP-C, and varying concentrations of BODIPY SP-C or BODIPY rSP-C) were measured. For each acceptor concentration, the donor-only sample received a concentration of the corresponding unlabeled protein equal to that of the BODIPY-labeled protein in the corresponding donor + acceptor sample. These two decays were analyzed globally, with linkage of the common decay parameters, as described previously in our study of SP-C/SP-B interactions (Cabré *et al.*, 2018). In that work, we also established as the best FRET model a formalism that allows for the possibility of two populations (relative amounts A_1 and A_2) of non-equivalent donors, transferring excitation energy to corresponding populations of acceptors (with local two-dimensional concentrations c_1 and c_2, respectively). Each donor molecule can undergo FRET to acceptors located in the same bilayer leaflet (cis FRET) or in the opposite one (trans FRET), at a transverse distance h = 3.4 nm (see

Fig. 7 of Cabré *et al* (2018) (Cabré *et al*., 2018)). The donor decay in the presence of acceptor, $i_{DA}(t)$, is described by

$$i_{DA}(t) = i_D(t)\left[A_1\rho_{cis,1}(t)\rho_{trans,1}(t) + A_2\rho_{cis,2}(t)\rho_{trans,2}(t)\right] \quad (18)$$

where $i_D(t)$ is the donor decay in the absence of acceptor (described as a sum of up to three exponentials), and the ρ functions, given by

$$\rho_{cis,i}(t) = \exp\left(-c_i t^{1/3}\right) \quad (19)$$

and

$$\rho_{trans,i}(t) = \exp\left\{-\frac{2\,c_i}{\Gamma(2/3)\cdot b}\int_0^1\left[1 - \exp(-t\,b^3\,\alpha^6)\right]\alpha^{-3}\,d\alpha\right\} \quad (20)$$

are the *cis* and *trans* FRET terms that apply to donor and acceptor population *i* (*i* = 1, 2).

In the latter equation, Γ is the complete gamma function and $b = (R_0/h)/\langle\tau_D\rangle^{1/3}$ (Davenport *et al*., 1985).

From the recovered acceptor concentrations c_1 and c_2, an overall acceptor concentration $\langle c\rangle$ may be calculated obtained by averaging with weights given by the relative amount of donors ($q = A_2/A_1$):

$$\langle c\rangle = (c_1 + qc_2)/(1+q) \quad (21)$$

which can be compared with the theoretical expectation, obtained from the two-dimensional acceptor concentration *n* (molecules/unit area) (Loura et al., 1996b; Loura et al., 2000):

$$c = n\Gamma(2/3)\pi R_0^2 / \langle\tau_D\rangle^{1/3} \quad (22)$$

As an example, **Figure 1.7** shows experimental decays, fitting curves, as well as residual distributions and residual autocorrelations, for the Marina Blue SP-C/BODIPY SP-C FRET pair in POPC. The corresponding best fit parameters are given in **Table 3**, while the ones for the Marina Blue rSP-C/BODIPY rSP-C FRET pair are shown in **Table 4**.

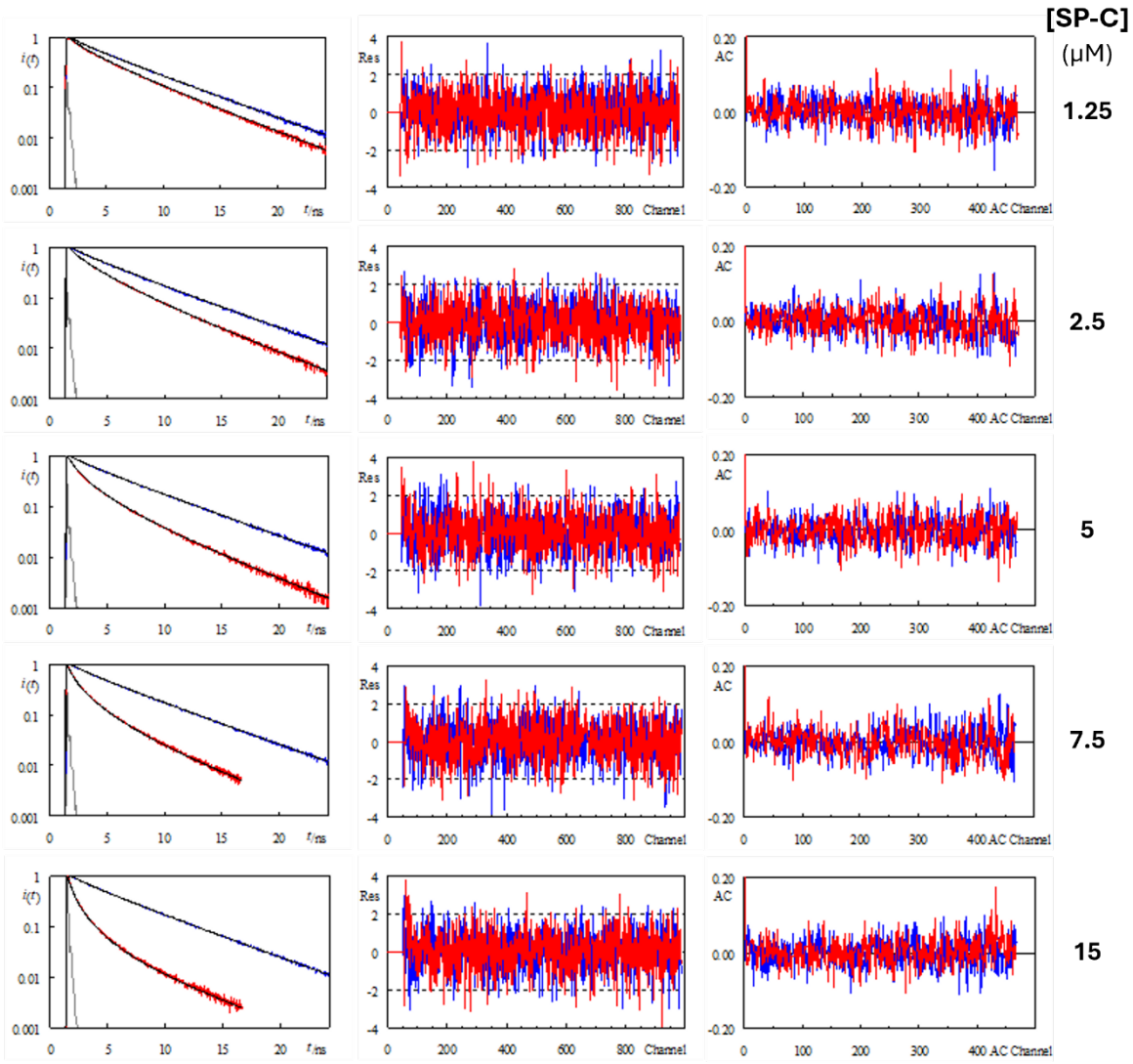

Figure 1.7: Fluorescence intensity decays of Marina Blue SP-C in POPC membranes in the presence of unlabeled or BODIPY-labeled SP-C. *Fluorescence intensity decays of Marina Blue SP-C (5 μM) in POPC vesicles (1 mM), in the presence of unlabeled SP-C (blue lines) or BODIPY SP-C (red lines), of concentration (either unlabeled or labeled with BODIPY), from top to bottom: 1.25, 2.5, 5, 7.5 and 15 μM. In the left panels, the fitting curves (Eqs. 18-20) to each data set and the instrumental response function are also shown (in black and gray, respectively). The middle and right plots in each row show the residuals and residual auto-correlation plots for the corresponding concentration of unlabeled (blue) or BODIPY-labeled (red) SP-C.*

Table 3: Time-resolved fluorescence data from FRET between Marina Blue SP-C and BODIPY SP-C in POPC membranes.

[BODIPY SP-C]/μM	1.25	2.5	5	7.5	15
Freely adjusted c_1 and c_2 parameters					
Recovered c_1/ns^{-3}	0.161	0.280	0.606	0.842	1.206
Recovered c_2/ns^{-3}	2.594	0.279	0.024	0.088	0.000
Recovered q	0.0297	0.856	0.0565	0.0732	0.0264
Calculated <c>/ns^{-3} (Eq. 22)	0.23	0.28	0.57	0.79	1.18
Global χ^2 (considering both donor-only and donor-plus-acceptor decay for each [BODIPY SP-C])	1.11	1.06	1.28	1.27	1.20
Fixed $c_2 = 0$					
Recovered c_1/ns^{-3}	0.162	0.280	0.601	0.811	1.206
Recovered q	0.000	0.000	0.0488	0.0459	0.0264
Calculated <c>/ns^{-3} (Eq. 22)	0.16	0.28	0.57	0.78	1.18
Global χ^2 (considering both donor-only and donor-plus-acceptor decay for each [BODIPY SP-C])	1.11	1.06	1.28	1.27	1.20

*Data obtained from plots in **Figure 1.7**.*

Table 4: Time-resolved fluorescence data of FRET between Marina Blue rSP-C and BODIPY rSP-C in POPC membranes.

[BODIPY rSP-C]/μM	1.25	2.5	5	7.5	15
Freely adjusted c_1 and c_2 parameters					
Recovered c_1/ns^{-3}	0.089	0.178	0.290	0.262	0.367
Recovered c_2/ns^{-3}	0.089	0.178	0.290	0.520	1.024
Recovered q	0.773	0.867	2.14	2.16	0.927
Calculated <c>/ns^{-3} (Eq. 22)	0.089	0.18	0.29	0.44	0.68
Global χ^2 (considering both donor-only and donor-plus-acceptor decay for each [BODIPY rSP-C])	1.06	1.27	1.35	0.97	1.18
Fixed c_2 = 0					
Recovered c_1/ns^{-3}	0.089	0.178	0.290	0.441	0.611
Recovered q	0.000	0.000	0.000	0.0324	0.0571
Calculated <c>/ns^{-3} (Eq. 22)	0.09	0.18	0.29	0.43	0.58
Global χ^2 (considering both donor-only and donor-plus-acceptor decay for each [BODIPY rSP-C])	1.06	1.27	1.35	0.98	1.24

*Data obtained from plots in **Figure 1.7**.*

While both the fitted curves of **Figure 1.7** and the fitting parameters in **Table 3** and **Table 4** concern the analysis of the ongoing hetero-FRET between the MB- and BODIPY-labeled proteins within the framework of Eqs. 18-20 (with two non-equivalent populations of labeled protein), it should be noted that, for both the fluorescently-labeled SP-C and rSP-C in POPC, the decays of the most dilute samples could be successfully analyzed with a simple formalism, considering a single population. This is clear in the approximately equal c_1 and c_2 values obtained for [BODIPY SP-C] = 2.5 μM (**Table 3**; even though this is not the case for 1.25 μM, consideration of a single population would lead to an identically good fit,

with c = 0.162 ns^{-3} and global χ^2= 1.11) and [BODIPY rSP-C] = 1.25, 2.5 and 5 μM (**Table 4**). However, using higher acceptor concentrations leads to donor fluorescence intensity decays that can only be successfully analyzed by allowing for a second population. For fluorescently-labeled SP-C (**Table 3**), this is apparent in a small (<8%) fraction of isolated donors, i.e., reporting a decreased local concentration of acceptors ($c_2 << c_1$). We believe that this result is not very significant, since the calculated average concentration, $<c>$, remains close to the c_1 value; the residual c_2 component could arise from an imperfect linkage of the donor and acceptor decay samples. Significantly, when c_2 is fixed to zero, the quality of the global fits is not affected, and the recovered isolated donor fractions are consistently < 5%.

To some extent, this situation is also verified for rSP-C (**Table 4**). However, somewhat differently for the highest concentrations, when both c_1 and c_2 are optimized, their recovered values are finite, differing by a factor of 2-3, with comparable amplitudes (q is neither very small nor very large, indicating significant contributions of both populations), which points to a slightly more heterogeneous population. This result would be expected for a phase-separated lipid system, with two coexisting phases, with differences in distribution of donor- and acceptor-labeled proteins according to their respective preferences. This is actually what is observed for the Marina Blue SP-C/BODIPY SP-C FRET pair in the LM and LS systems, where two populations of donors are inferred, one sensing acceptor depletion (0.1 $ns^{-3} < c_1 < 0.4$ ns^{-3}), while the other reports a local higher acceptor concentration (1.5 $ns^{-3} < c_2 < 3.6$ ns^{-3}), compatible with a partition coefficient of acceptor between these two phases of c_2/c_1 (Loura & Prieto, 2000) ≅ 10 (**Table 5** and **Table 6).**

Table 5: Analysis of time-resolved fluorescence data of FRET between Marina Blue SP-C and BODIPY SP-C in DPPC/POPC/POPG lipid mixture.

[BODIPY SP-C]/μM	1.25	2.5	5	7.5	15
Freely adjusted c_1 and c_2 parameters					
Recovered c_1/ns^{-3}	0.135	0.228	0.385	0.368	0.136
Recovered c_2/ns^{-3}	3.478	2.708	2.423	1.667	2.009
Recovered q	0.330	0.383	0.675	1.30	6.15
Calculated <c>/ns^{-3} (Eq. 13)	0.96	0.92	1.21	1.10	1.75
Global χ^2 (considering both donor-only and donor-plus-acceptor decay for each [BODIPY SP-C])	1.15	1.01	1.14	1.20	1.32
Fixed c_2 = 0					
Recovered c_1/ns^{-3}	0.200	0.332	0.557	0.786	1.549
Recovered q	0.235	0.158	0.0774	0.0957	0.114
Calculated <c>/ns^{-3} (Eq. 13)	0.16	0.29	0.52	0.72	1.39
Global χ^2 (considering both donor-only and donor-plus-acceptor decay for each [BODIPY SP-C])	1.27	1.23	1.71	1.76	1.76

Table 6: Analysis of time-resolved fluorescence data of FRET between Marina Blue SP-C and BODIPY SP-C in pulmonary surfactant lipid fraction.

[BODIPY SP-C]/μM	1.25	2.5	5	7.5	15
Freely adjusted c_1 and c_2 parameters					
Recovered c_1/ns^{-3}	0.096	0.186	0.350	0.271	0.263
Recovered c_2/ns^{-3}	3.047	3.599	2.185	2.654	2.082
Recovered q	0.291	0.358	0.524	2.09	4.16
Calculated <c>/ns^{-3} (Eq. 13)	0.76	1.09	0.98	1.88	1.73
Global χ^2 (considering both donor-only and donor-plus-acceptor decay for each [BODIPY SP-C])	1.17	1.07	1.03	1.06	1.11
Fixed c_2 = 0					
Recovered c_1/ns^{-3}	0.190	0.232	0.510	0.881	1.257
Recovered q	0.499	0.105	0.0911	0.201	0.105
Calculated <c>/ns^{-3} (Eq. 13)	0.13	0.21	0.47	0.73	1.14
Global χ^2 (considering both donor-only and donor-plus-acceptor decay for each [BODIPY SP-C])	1.34	1.31	1.29	2.59	2.13

In the case of fluorescently-labeled SP-C in these more complex membrane systems, composed of both unsaturated and saturated phospholipids and (in the case of LS) cholesterol, an underlying heterogeneous lipid organization is expected. This is not the case for rSP-C in single-component POPC membranes, where the recovery of two distinct and significant populations can only be interpreted as a non-homogeneous distribution of protein at high concentrations, with possible coexistence of monomers and aggregates, which would account for the lower and higher c values, respectively.

From Eq. 22, a linear dependence of *c* on the analytical acceptor surface concentration *n* is expected. *n* (molecules/Å^2) can be readily calculated from the probe:lipid ratio divided by the lipid molecular area (taken as 66 Å^2 for POPC; (Filipe *et al.*, 2015)), and used to obtain theoretical estimates of *c*. The latter are compared with the <*c*> values recovered from the decay fits of Marina Blue SP-C and rSP-C in POPC (**Figure 1.8A-B**). Taking into account that the theoretical line in **Figure 1.8A** is not a fit (but the direct result of applying Eq. 22 with independently obtained parameters), there is good agreement between the theoretical line and the recovered <*c*> values for SP-C, with linear dependence of the latter on protein concentration being kept up to 7.5 μM (or lipid:protein = 133). Deviations from the theoretical line may stem from several factors, including uncertainty in absolute lipid or protein concentrations, as well as lipid molecular area. Only for very high protein concentration (15 μM, or lipid:protein = 67) a clear deviation from linearity to <*c*> lower values becomes apparent, probably indicating onset of aggregation. Similar behaviors were observed for this protein in the other lipid systems (**Figure 1.8C-D**). In contrast, for rSP-C in POPC, this deviation occurs at lower concentrations, pointing to higher propensity for protein aggregation.

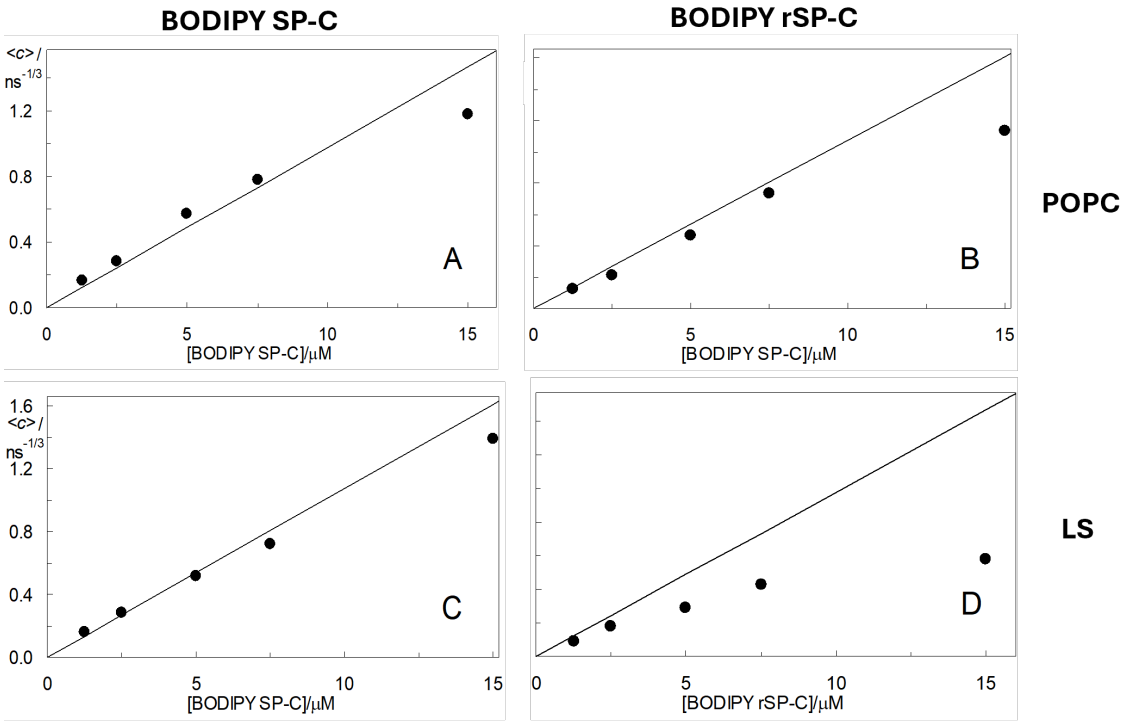

Figure 1.8: Overall surface acceptor concentrations as a function of BODIPY rSP-C content as determined by FRET data. *Overall acceptor concentrations <c> (circles) recovered from fitting Eqs. 18-20 to the time resolved FRET data, with fixed c_2 = 0. A: fluorescently-labeled SP-C in POPC (**Table 3**); B): fluorescently-labeled rSP-C in POPC (**Table 4**). C: SP-C in DPPC/POPC/POPG lipid mixture (**Table 5**); D: SP-C in pulmonary surfactant lipid fraction (**Table 6**). The lines are the theoretical values calculated from the actual acceptor concentrations with Eq. 22 (straight line), using the spectroscopic R_0 = 4.93 nm value, and an area/POPC lipid molecule = 0.66 nm^2 (Filipe et al., 2015).*

While the fitting of FRET models to the decays provides important clues regarding the organization of SP-C and rSP-C in the different lipid systems, a simpler, more immediate, and model-independent analysis may be carried out by comparing the FRET efficiencies obtained from time-resolved data, using amplitude averaged lifetimes $\overline{t}$ (Eq. 2),

$$E_{TR} = 1 - \bar{\tau}_{DA} / \bar{\tau}_{D} \tag{23}$$

with those determined, in the same samples, from steady-state measurements, using fluorescence intensities *I*:

$$E_{SS} = 1 - I_{DA} / I_{D} \tag{24}$$

In both equations, "D" and "DA" denote the donor-only and the donor + acceptor samples, respectively. The presence of donor-acceptor aggregation would give rise to donors quenched with 100% efficiency, invisible in the time-resolved experiment, but whose lack of emission would be reflected in a reduced I_{DA} in the steady-state measurement. This situation would, in turn, be manifested as $E_{SS} > E_{TR}$. Conversely, the absence of a systematic order relation between E_{SS} and E_{TR} would point to absence of extensive donor-acceptor (and thus protein) aggregation.

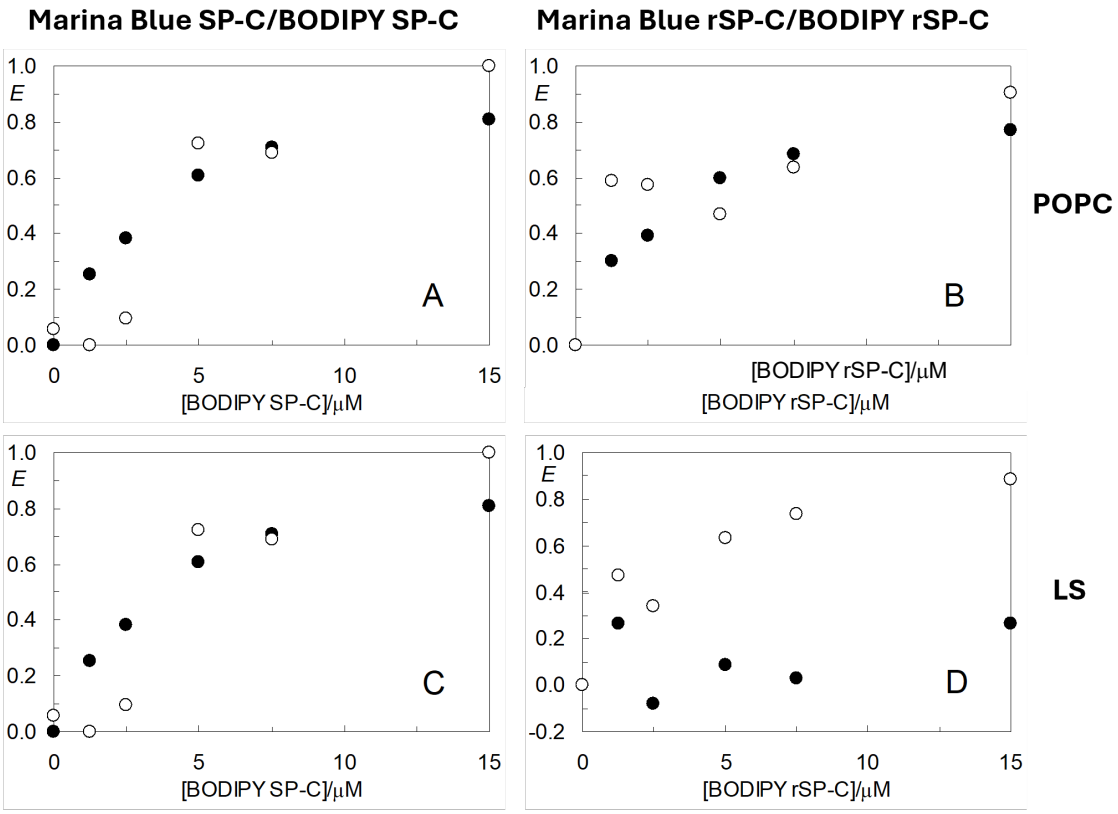

Figure 1.9: FRET efficiencies from Marine Blue SP-C to BODIPY SP-C or rSP-C as calculated from time resolved and steady-state fluorescence. *FRET efficiency E calculated from time-resolved (E_{TR}; filled circles) or steady-state (E_{SS}; open circles) fluorescence experiments with Marine Blue SP-C/BODIPY SP-C (A, C) or Marina Blue rSP-C/BODIPY rSP-C (B, D) donor-acceptor pairs, are compared in the plots, in POPC (A, B) or LS (C, D) membrane systems.*

Analysis of **Figure 1.9** reveals a monotonic variation of E_{TR}, except for rSPC in LS (**Figure 1.9D**), while data for E_{SS} is largely scattered. This is unsurprising, since the latter depends critically on donor concentration, which is an additional cause of experimental uncertainty. Still, it can be safely concluded that in both POPC and LS membrane systems, the variations of E_{SS} and E_{TR} for the SP-C-based FRET pair have a similar trend of variation (**Figure 1.9A, Figure 1.9C**). This is not the case for the rSP-C-based FRET pair. In POPC, E_{SS} and E_{TR} are close, and only at lower acceptor concentrations the higher E_{SS} points out to some extent of static quenching of Marina Blue rSP-C by BODIPY rSP-C, likely caused by aggregation. On the other hand, for LS (**Figure 1.9D**), E_{TR} displays an erratic dependence on acceptor concentration, around low values, denoting inefficient FRET. This contrasts with the corresponding E_{SS} variation, which shows the expected sublinear increase to values close to unity for high acceptor concentration. This behavior can be interpreted as extensive static quenching of most donor fluorophores by acceptors, indicative of aggregation. The TR data reflect that the "surviving" donors, probably monomers segregated from the quenched aggregates, reside mostly in an acceptor-deprived microenvironment, and FRET from them is inefficient.

Discussion

The homodimerization of SP-C has been explored in previous *in silico* and experimental studies, where either the full sequence or the structure of the studied protein differed slightly from that of native SP-C (Kairys *et al.*, 2004; Korolainen *et al.*, 2022; Wang *et al.*, 2002). In this chapter, we have investigated SP-C/SP-C interactions using BiFC assays. Fusion proteins containing SP-C were produced in HEK293T cells, a well-established human embryonic kidney cell line, chosen as the expression system due to its ease of transfection (Tan *et al.*, 2021).

Fluorescence levels resulting from dimerization between proSP-C or SP-C molecules were significantly higher than those observed with the prototypical homodimer system of GpA (Grau *et al.*, 2017) (**Figure 1.1A**). These findings suggest a strong homotypic interaction between SP-C molecules. However, it is important to note that BiFC assays for homodimeric proteins inherently present a 50% chance that SP-C molecules will interact with another molecule fused to the same VFP fragment (either VN or VC), potentially forming an unproductive homodimer that does not generate fluorescence. Thus, our approach could potentially underestimate the ability of SP-C to form homodimers, although this limitation is applied also to GpA homodimers. Working with membrane proteins introduces additional complexities, particularly due to the difficulty in controlling the orientation of proteins within bilayers (i.e., whether the N-terminus is oriented inward or outward). Consequently, some SP-C molecules might miss the opportunity to interact if their orientation is reversed. Nevertheless, in our model — especially for proSP-C— nearly all molecules should be oriented as they would be during natural synthesis, since our construct includes the juxtamembrane basic residues and the C-terminal pro-peptide necessary for proper orientation and folding of SP-C (Mulugeta & Beers, 2003; Mulugeta *et al.*, 2015). Given this, we would expect proSP-C fluorescence levels to be higher than those of SP-C. However, since the fluorescence levels were similar, it suggests that SP-C is likely oriented in the same manner as proSP-C, unless the absence of the C-terminal pro-peptide or another factor accounts for the observed fluorescence levels in SP-C.

We have investigated the contribution of the proposed dimerization motifs within the SP-C structure, specifically the AxxxG sequence at the C-terminal and the PCCP motif at the N-terminal ends (Creuwels *et al.*, 1995; Kairys *et al.*, 2004; Luy *et al.*, 2004; Plasencia *et al.*, 2001; Plasencia *et al.*, 2004). Interestingly, the fluorescence levels resulting from VFP reassembly due to homodimerization of mutated SP-C variants, as well as that of the scrambled version of SP-C, were similar to those observed for mature SP-C molecules (**Figure 1.1B**). This result cannot be associated to a true dimerization as a consequence of specific protein-protein interactions but could be attributed to the concentration of the fusion

protein in the nucleus or in a membrane-bound organelle, where the proximity of VN and VC fragments facilitates VFP reassembly but rather due to their high local concentration, as observed in **Figure 1.2**. It is likely that most of these molecules exhibit altered trafficking, preventing them from reaching the cell membrane as expected. These findings are consistent with reported data by Wang *et al*. (2002) where A549, a lung epithelial cell line transfected with DNA encoding mature region of SP-C fused to Enhanced Green Fluorescent Protein (EGFP/SP-C (24-58)) showed retention of the corresponding protein in proximal compartments. Moreover, these cells formed perinuclear aggregates, similar to those observed with the mutated proSP-C variants used in that study.

In contrast, A549 transfected with EGFP/SP-C (1–194) DNA, which encodes full length proSP-C fused to EGFP, demonstrated efficient translocation of the protein to CD63-positive cytosolic compartments, which are associated with multivesicular and lamellar bodies. In our study, fluorescence was observed in the plasma membrane indicating proper trafficking of proSP-C molecules. This observation is significant because the HEK293T cells, platform of transfection used in our experiments, do not present lamellar bodies. The dimerization of proSP-C molecules likely occurs through the mature SP-C region, as confirmed by chemical cross-linking experiments conducted by Wang *et al*. (2002).

In the current study, the BiFC technique revealed certain limitations in investigating SP-C dimerization. Firstly, the use of the SP-C precursor (proSP-C) is essential, as the mature SP-C alone leads to improper trafficking. Moreover, the cells used in these assays lack lamellar bodies, the organelles responsible for proSP-C processing. Even when A549 cells are employed, post-translational modifications such as N-terminal double palmitoylation of SP-C cannot be assured (Wang *et al*., 2002). Additionally, the plasma membranes of HEK293T cells, while containing a nature mixture of phospholipids and cholesterol, do not have the high concentrations of DPPC and other specific lipids typical of pulmonary surfactant (Haagsman & Van Golde, 1991; Pérez-Gil *et al*., 1992). The difference in lipid composition may affect the distribution of SP-C within the membrane and potentially interfere with its ability to interact and dimerize correctly.

To avoid these problems, we performed fluorescence self-quenching and FRET studies using synthetic MLVs containing different lipid systems, incorporating either native SP-C. We also used a non-palmitoylated recombinant version of SP-C (rSP-C), as expressed in bacteria lacking the palmitoylation machinery, to explore the effect of acylation in the possible dimerization of SP-C. Our analysis from fluorescence intensities from steady-state self-quenching assays reveals that SP-C does not appear to oligomerize within fluid POPC membranes, where

compartmentalization is not feasible. This result is consistent with the finding of Horowitz and collaborators (Horowitz *et al*., 1993) who observed that SP-C remains uniformly distributed in DPPC:DMPG (7:1) membranes when the temperatures exceeds the melting temperature of the membranes, suggesting that SP-C dimerization requires lipid phase separation. Therefore, we also investigated the oligomerization state of SP-C in membranes with lipid composition that mimics PS (LM) and in membranes with the full lipid complexity of PS, referred here as LS. A key difference between these two systems is the presence of cholesterol, which is only found in LS, where it regulates the fluidity of segregated ordered-like membrane domains (Doole *et al*., 2022). Regarding LM membranes, our results from self-quenching assays using only BODIPY-labeled SP-C are similar to those obtained in POPC membranes. However, two populations of donors were determined (**Table 5**) suggesting that SP-C could be compartmentalized. A similar observation occurs in LS membranes, but in this lipid system, dimerization constants derived from steady-state self-quenching indicate that SP-C monomers show minimal aggregation, with only 3% of dimers present at higher BODIPY SP-C concentrations (**Figure 1.6C**). Research performed by Horowitz *et al*. (1993) at temperatures below phase transition in different synthetic lipid systems showed increased energy transfer between NBD SP-C and EITC SP-C. However, they could not distinguish between true protein oligomerization and the potential formation of membrane patches enriched in SP-C as a result of the phase separation, due to the lower sensibility of the equipment used. Based on these studies, it could be concluded that SP-C is likely mainly monomeric, although it could form a small proportion of dimers when significant lipid phase separation occurs. Some simulation studies have suggested that SP-C could form dimers, but these studies were simulating only the behavior of the α-helical segment of SP-C (Kairys *et al*., 2004) or of the entire SP-C molecule without palmitoylation (Korolainen *et al*., 2022). Our investigations as well as the work of Wang *et al*. (2002) using proSP-C, also support the idea that SP-C interacts with itself. However, the palmitoylation state of that recombinant protein was not analyzed. We have conducted complementary experiments to the examine potential protein oligomerization of non-palmitoylated rSP-C.

The structure and properties of this recombinant version were thoroughly studied by Baumgart *et al*. (Baumgart *et al*., 2010). It has been proposed that the palmitic chains of native SP-C may facilitate a deeper insertion of the protein's N-terminal segment into membrane layers and reduce the degree of tilting of the protein within lipid bilayers (Roldan *et al*., 2015). As a result, rSP-C may experience different structural constraints within the membrane, potentially leading to the formation of a higher proportion of dimers compared to native SP-C. Alternatively, a partial mismatch between the less tilted protein end and the membrane

thickness could promote greater segregation of the protein from the lipids, thereby favoring protein-protein interactions.

All the parameters obtained suggest that rSP-C is capable of forming dimers even in POPC membranes, with 9% of dimers observed (**Figure 1.6D**). The lateral diffusion coefficient calculated using Stern-Vomer equation is higher than that determined for the palmitoylated BODIPY-labeled SP-C in POPC membranes (**Table 2**). Steady-state self-quenching of rSP-C in POPC membranes revealed the presence of aggregation, with a dimerization constant higher than that found for SP-C in LS membranes. Therefore, we conclude that there are more dimers of rSP-C in POPC membranes than dimers of SP-C in LS membranes, where phase segregation is more pronounced. Additionally, according to time-resolved FRET data (**Figure 1.8A-B**), the concentration of rSP-C required for aggregation is lower than the corresponding concentration of SP-C. This result is consistent with the characterization of a dimeric form of a recombinant mutant protein rSP-C (FFI) using high resolution NMR spectroscopy (Johansson, Szyperski, *et al.*, 1994). To further investigate the influence of phase separation, where rSP-C molecules would be closer due to compartmentalization, LM and LS systems were employed. In both systems, the presence of dimers is higher in rSP-C than determined for the same protein in POPC membranes (**Table 7**). The lateral diffusion coefficient obtained from Stern-Volmer equation for BODIPY-labeled rSP-C in LS membranes is higher than that in the LM system, potentially indicating a greater segregation of lipid domains, enhanced interaction between rSP-C monomers, or a combination of both processes. Based on the SP-C state observed in the three lipid systems studied here, the membranes of LS membranes appear to be the most compartmentalized. Consequently, the formation of rSP-C dimers would be expected to be particularly favored in LS membranes. In contrast, the concentration of rSP-C required for protein-protein interaction is the lowest in LM system (**Table 7**). This suggests that while phase separation promotes oligomerization, it may not be solely dependent on the degree of compartmentalization but could also be influenced by the nature of the segregated phases or specific protein/lipid interactions, amongst other factors.

Taken all together, it would be interesting to determine if proSP-C expressed by HEK293T is palmitoylated or not, due crucial role of palmitic chains of SP-C in interfering on protein-protein interaction at low concentrations of SP-C.

Table 7: Evidences from fluorescence experiments regarding the oligomeric state of SP-C

Lipid system	SP-C	rSP-C
POPC	• *Self-quenching*: diffusion similar to host lipid, no evidence for aggregation. • *FRET*: essentially uniform distribution. Small (<5%) fraction of isolated labeled protein for higher concentrations (L/P < 200).	• *Self-quenching*: two-fold faster apparent diffusion compared to SP-C. Static quenching indicates slight evidence for aggregation at high concentrations (~8% protein dimerized at L/P = 100). • *FRET*: essentially uniform distribution for low concentrations. Heterogeneous distribution for L/P < 200: two donor populations with two- to three-fold differences in local acceptor concentration.
LM (DPPC/POPC/POPG lipid mixture)	• *Self-quenching*: diffusion similar to POPC, no evidence for aggregation. • *FRET*: protein distribution in two different environments, with local concentrations differing by ~one order of magnitude, underlying lipid phase coexistence	• *Self-quenching*: faster apparent diffusion, by one order of magnitude compared to POPC, compatible with compartmentalization. Static quenching indicates clear aggregation, with ~50% protein dimerized at L/P = 500.
LS (Lipid Surfactant)	• *Self-quenching*: faster apparent diffusion, by one order of magnitude compared to the same protein in POPC and LM, compatible with compartmentalization. However, no evidence for aggregation from steady-state data, apart from statistical contacts. • *FRET*: protein distribution in two different environments, with local concentrations differing by ~one order of magnitude, underlying lipid phase coexistence	• *Self-quenching*: faster apparent diffusion, by one order of magnitude compared to POPC compatible with compartmentalization. Static quenching indicates clear aggregation, with ~50% protein dimerized at L/P = 200. • *FRET*: efficient donor quenching detected in steady-state data, virtually undetectable in time-resolved conditions (formation of highly quenched aggregates, leaving "surviving" fluorophores isolated).

The main structural difference between rSP-C and SP-C is the palmitoylation state. Considering the degree of aggregation detected in POPC membranes, it seems that palmitoylation could prevent, at least partially, the interaction among SP-C monomers. Our results suggest that rSP-C could tend to form more dimers than SP-C, for which dimerization could not be completely established. Despite of this, dimers of native palmitoylated SP-C have been observed, in a minimal proportion, during purification of this protein in different species, such as bovine, canine, porcine, or rat SP-C (Baatz *et al.*, 1992; Creuwels *et al.*, 1995; Luy *et al.*, 2004; Wang *et al.*, 2002). The secondary structure proposed for the SP-C preparations analyzed in those studies were β-sheet for the bovine protein and α-helical for the canine protein. Thus, one could expect that the amino acids implied in the formation of the possible homodimers would be different depending on the protein secondary structure or dimerization precedes conformational shift from α-helical to β-sheet structure. In Baatz and collaborators' assays (Baatz *et al.*, 1992), the yielding of fatty acids liberated upon deacylation was lower in SP-C dimers, pointing out that the cysteines in the PCCP motif within the N-terminal segment of SP-C could participate in intermolecular disulfide bonds. Whether the potential formation of intermolecular disulfides precedes or is rather a consequence of protein dimerization/oligomerization, remains to be established. Regarding the formation of dimers in α-helical canine SP-C, it was observed in a non-acylated form of 7 kDa, indicating again the generation of a dimer through intermolecular disulfide binding in the PCCP motif as defined in Creuwels *et al* (Creuwels *et al.*, 1995). In NMR studies with porcine SP-C, two sets of resonances were resolved at the C-terminal segment of the protein, suggesting the potential coexistence of monomers and dimers (Johansson, Szyperski, *et al.*, 1994). Because of that, Luy and collaborators investigated a recombinant mutant form of SP-C shifting the PCCP sequence to PFFI (Luy *et al.*, 2004). That work supported the three-state model proposed previously for SP-C (Szyperski *et al.*, 1998): 1) monomeric α-helix, 2) dimeric α-helix and 3) β-sheet fibrils. Such dimeric α-helical structure would not be formed through disulfide bonds due to the absence of cysteines in the sequence of mutant rSP-C (FFI). This interaction could be performed through hydrogen bonds or Van der Waals forces implying the AxxxG motif or the recently proposed region V21xxxVxxxGxxxM33 (Kairys *et al.*, 2004; Korolainen *et al.*, 2022). All these studies seem to suggest a connection between SP-C depalmitoylation and the formation of dimers/oligomers. Our results in the present study indicate that, beyond the potential formation of disulfide bonds, the lack of palmitic chains at the N-terminal moiety of the SP-C structure could be a factor promoting by itself protein-protein interactions and the stabilization of higher order oligomers.

FRET studies performed in this Thesis could not determine the secondary structure of SP-C dimers/oligomers. Currently, the physiological implication of

dimerization is not defined. SP-C dimer adopting an α-helix structure could be embedded in the membrane bilayer in an analogous fashion to the monomer, and would be able to achieve the insertion of phospholipids into the interfacial monolayer as well as SP-C monomers, with a slight difference in the kinetics (Creuwels *et al*., 1995). It has been hypothesized that SP-C dimers might adopt a rigid transmembrane V-shaped structure that would trigger membrane fragmentation (Roldan *et al*., 2016).Recently, Korolainen *et al* have proposed three plausible different structures for non-palmitoylated SP-C homodimers according with its stability or lowest free energy calculated from MD simulations: 1) parallel dimer; 2) inverted V-shape dimer and 3) V-shape dimer. Our results from rSP-C self-quenching would imply the formation of rSP-C dimers but considering the distance between the N-terminal end of the molecules of rSP-C in the inverted V-shape topology, this structure seems improbable. The most compatible conformation would be the parallel dimer, although the V-shape dimer cannot be discarded. Vesicles possibly produced by SP-C-promoted membrane fission could be endocytosed by alveolar macrophages or AT2 cells (Sehlmeyer *et al*., 2020). In this way, α-helical stable or transient SP-C dimers could participate in processing and homeostasis of different fractions of surfactant in the alveoli. Our results suggest that dimerization of SP-C could be minimal and would depend on phase separation and protein concentration (**Table 7**). However, during breathing, local lipid composition, as well as compartmentalization degree and SP-C concentration, is constantly changing in both membranes and interfacial multilayered films of surfactant (Keating *et al*., 2012; Pastrana-Rios *et al*., 1994). Conversely to α-helix SP-C dimers, the functional behavior of those with a β-sheet structure functions has not been characterized in detail. It has been proposed that they could end forming a β-barrel, similar to some transmembrane proteins such as porin, affecting the lipid transference between bilayers and monolayers during breathing-like compression-expansion dynamics (Baatz *et al*., 1992).

In conclusion, the results of this chapter suggest that palmitoylation could be important to stabilize the monomeric α-helical conformation of SP-C, which is likely optimal to perform the role of the protein to stabilize the interfacial surfactant films along the demanding breathing dynamics. Eventual depalmitoylation as a consequence of lung injury and oxidation, accumulation of the protein to high densities because of membrane compartmentalization and other potential factors could end in the extensive formation of protein dimers and other possible higher order oligomers that could affect function to extents that need to be analyzed in detail and that could be associated with certain pathologic situations. It has been proposed that protein oligomerization could be associated with membrane remodeling and the fragmentation of surfactant layers into small vesicles enriched in SP-C, which could thus be prone to uptake by alveolar

macrophages or alveolar pneumocytes. The palmitoylation state of SP-C could then serve as part of the sensors triggering surfactant recycling, the metabolism that maintains alveolar homeostasis.

The study presented in this chapter started as a continuation of the experiments performed by Dr. Alejandro Barriga and part of the experiments were published in the following article:

Barriga A, Morán-Lalangui M, Castillo-Sánchez JC, Mingarro I, Pérez-Gil J, García-Álvarez B. **"Role of pulmonary surfactant protein Sp-C dimerization on membrane fragmentation: An emergent mechanism involved in lung defense and homeostasis."**

Biochim Biophys Acta Biomembr. 2021 Jun 1;1863(6):183572. doi: 10.1016/j.bbamem.2021.183572. Epub 2021 Feb 4. PMID: 33548215.

NTA assays were performed in Gregorio Marañon Hospital thanks to Dr. Beatriz Salinas Rodríguez from Biomedical Imaging and Instrumentation Group.

CHAPTER 2:

MECHANISTIC INSIGHTS INTO SP-C MEDIATED MEMBRANE FRAGMENTATION AND LIPID REMODELING IN PULMONARY SURFACTANT SYSTEMS

Introduction

The human respiratory process, a cyclical and sequential mechanism, alternates between inspiration and expiration. During inspiration, the air-liquid interfacial surface covering the alveolar epithelium expands, while during expiration, this surface contracts. These dynamic cyclic fluctuations of expansion and compression directly affect pulmonary surfactant membranes and films, which are critical for maintaining alveolar stability and preventing lung collapse during respiration (Pérez-Gil, 2008; Serrano & Pérez-Gil, 2006). Pulmonary surfactant, predominantly composed of lipids and specific proteins, acts as a crucial biophysical interface that reduces surface tension and facilitates efficient gas exchange. Its hydrophobic proteins, SP-B and SP-C are essential for the structural organization and functional performance of surfactant membranes (Parra *et al.*, 2011; Pérez-Gil *et al.*, 1995; Serrano & Pérez-Gil, 2006).

SP-C could alter lipid packing, influencing lipid lateral mobility and distribution, increasing membrane permeability, and promoting lipid adsorption at air-liquid interfaces as well as lipid transfer among various lipid structures (Morrow, Taneva, *et al.*, 1993; Parra *et al.*, 2013; Pérez-Gil *et al.*, 1995; Plasencia *et al.*, 2001; Possmayer *et al.*, 2001; Roldan *et al.*, 2017). Furthermore, SP-C would enable the reversible formation of multilayered stacks interconnected with the interfacial phospholipid monolayer, capturing compressed surfactant material during expiration and redistributing it upon inspiration (Amrein *et al.*, 1997; Keating *et al.*, 2012; von Nahmen *et al.*, 1997). This functionality is strongly associated with SP-C's palmitoylation, a post-translational modification that stabilizes the interactions of the protein with highly compressed interfacial films (Lukovic *et al.*, 2012; Plasencia *et al.*, 2001).

The interplay between SP-C and cholesterol, both critical modulators of surfactant properties, further highlights the complexity of SP-C functionality (Roldan *et al.*, 2017). Cholesterol modulates membrane fluidity and phase segregation, influencing surfactant behavior in both positive and negative ways depending on its proportion (Bernardino de la Serna *et al.*, 2004; Gunasekara *et al.*, 2005). Notably, SP-C enhances cholesterol miscibility in surfactant-mimicking membranes, and its configuration in bilayers is affected by the presence of cholesterol (Gómez-Gil, Pérez-Gil, *et al.*, 2009). This reciprocal relationship likely plays a pivotal role in regulating surfactant activity, though the precise molecular mechanisms that remain under investigation.

From a structural perspective, SP-C's functionality relies primarily on its rigid transmembrane helix, which mediates hydrophobic interactions with lipids, disrupting and reorganizing membrane architecture (Baumgart *et al.*, 2010). Additionally, its positively charged N-terminal segment establishes critical

electrostatic interactions with anionic phospholipids crucial in surfactant, such as phosphatidylglycerol, inducing packing defects that enhance membrane remodeling and vesicle aggregation (Plasencia *et al.*, 2004). The palmitoyl chains attached to this segment are thought to couple the protein's motion with membrane dynamics, improving its efficiency in lipid organization (Gonzalez-Horta *et al.*, 2008).

An emerging hypothesis proposes that SP-C's ability to induce membrane curvature—a key step in surfactant dynamics—may be driven by protein dimerization. This dimerization appears to depend on the lipid environment, phase segregation, and the local concentration of SP-C (Results Chapter 1). During expiration, membrane compression may lead to localized SP-C accumulation, increasing the probability of dimerization and facilitating membrane curvature and segregation/fragmentation. However, as observed in Chapter 1, SP-C primarily exists in its monomeric form at low concentrations, suggesting that its functional activity is highly regulated by its concentration and the surrounding lipid context.

SP-C's ability to fragment membranes has been demonstrated using large unilamellar vesicles (LUVs), where it reduces vesicle size from 200 nm to 30 nm through membrane fission (Roldan *et al.*, 2016). However, this activity is highly concentration-dependent, with significant effects observed only at concentrations substantially higher than those typically present in natural surfactant. Determining the minimum SP-C concentration required for effective membrane fragmentation is essential for understanding its role in surfactant dynamics and extracellular metabolism.

This chapter investigates the factors influencing SP-C's ability to induce membrane fragmentation, focusing on its concentration, palmitoylation state, and the lipid composition of the membranes. Experiments were performed using LUVs composed of synthetic lipid mixtures that emulate pulmonary surfactant composition, as well as native lipid extracts containing cholesterol and other relevant molecules. SP-C and rSP-C (a recombinant non-palmitoylated SP-C variant) were incorporated to assess their differential impacts on membrane fragmentation.

Advanced biophysical techniques, including nanoparticle tracking analysis (NTA) and tunable resistive pulse sensing (TRPS), were employed to characterize the size and concentration of fragmented vesicles, providing quantitative insights into the dynamics of membrane remodeling. Additionally, confocal microscopy was used to examine the distribution and localization of SP-C in giant unilamellar vesicles (GUVs), leveraging fluorescent markers to visualize protein-lipid interactions.

To elucidate the mechanistic underpinnings of SP-C's activity, peptides mimicking the N- and C-terminal regions of SP-C were synthesized, including mutant variants

designed to disrupt the proposed dimerization motifs PCCP and AxxxG (Chapter 1).

These experimental approaches aim to reveal the contributions of SP-C, its palmitoylation state, lipid environment, and propensity for dimerization to membrane remodeling. The findings presented in this chapter offer a comprehensive and integrated perspective on SP-C's role in maintaining alveolar homeostasis and pulmonary surfactant activity, thereby advancing our understanding of its molecular mechanisms in both health and disease.

Results

Effect of SP-C in membrane fragmentation.

We conducted a series of TRPS experiments on LUVs composed of the synthetic lipid mixture DPPC/POPC/POPG (50/25/15, w/w/w), which roughly mimics the lipid composition of pulmonary surfactant in terms of saturated/unsaturated and zwitterionic/anionic phospholipids, systematically varying the SP-C content to evaluate its role in promoting vesicle fission. In these assays, the particles are driven to move through a nanopore that connects the compartment where the sample is loaded with a collector space, with an electric current being established and monitored between both compartments. When a particle travels through the nanopore, a transient current blockade is registered as a peak in electrical resistance. Thus, by monitoring and analysing the frequency, magnitude, and duration of the transient blockades, we can assess the particle concentration, size, and zeta potential, respectively.

The results of a representative TRPS experiment using LUVs containing SP-C is depicted in **Figure 2.1A**, where both the size and concentration of the LUVS for every SP-C composition are represented. One of the major limitations of this approach is that the blockades caused by particles smaller than 50 nm are indistinguishable from the normal current noise. However, we harnessed this drawback to determine the reduction of LUVs size to entities with sizes lower than 50 nm. Hence, although all LUVs were produced using 200 nm extrusion membranes, a reduction in size due to SP-C membrane fragmentation would be observed as a decrease in particle concentration in the analysed range (50 – 300 nm).

Our results show that the particle concentration steeply drop when a SP-C content of 7.5% or higher was included into the vesicles, whereas lower SP-C amounts did not produce significant effects (**Figure 2.1B**). We performed a phosphorus quantification for each sample to confirm that the presence of SP-C did not affect the phospholipid amounts present in the LUVs after all the manufacturing process (**Figure 2.2**). The apparent average diameter of the vesicles progressively increases

with the addition of SP-C to the vesicle composition, which may suggest that the smaller vesicles produced by membrane fragmentation aggregate either with each other or with larger vesicles (**Figure 2.1C**). In addition, a direct correlation was observed between the content of SP-C in the LUVs and the decrease of zeta potential (**Figure 2.1D**). Zeta potential represents the charge at the interface between the vesicle surface and the surrounding liquid medium, serving as an indicator of colloidal dispersion stability. The reduction in zeta potential suggests decreased electrostatic stability, leading to an increased propensity for vesicle aggregation, which may be associated with the observed increase in apparent diameter of the nanoparticles bearing SP-C. Taken together, these results support a one-step mechanism instead of a gradual process for SP-C-induced membrane fragmentation as particle concentration of LUVs containing 5% or 2.5% SP-C is similar to those LUVs without protein.

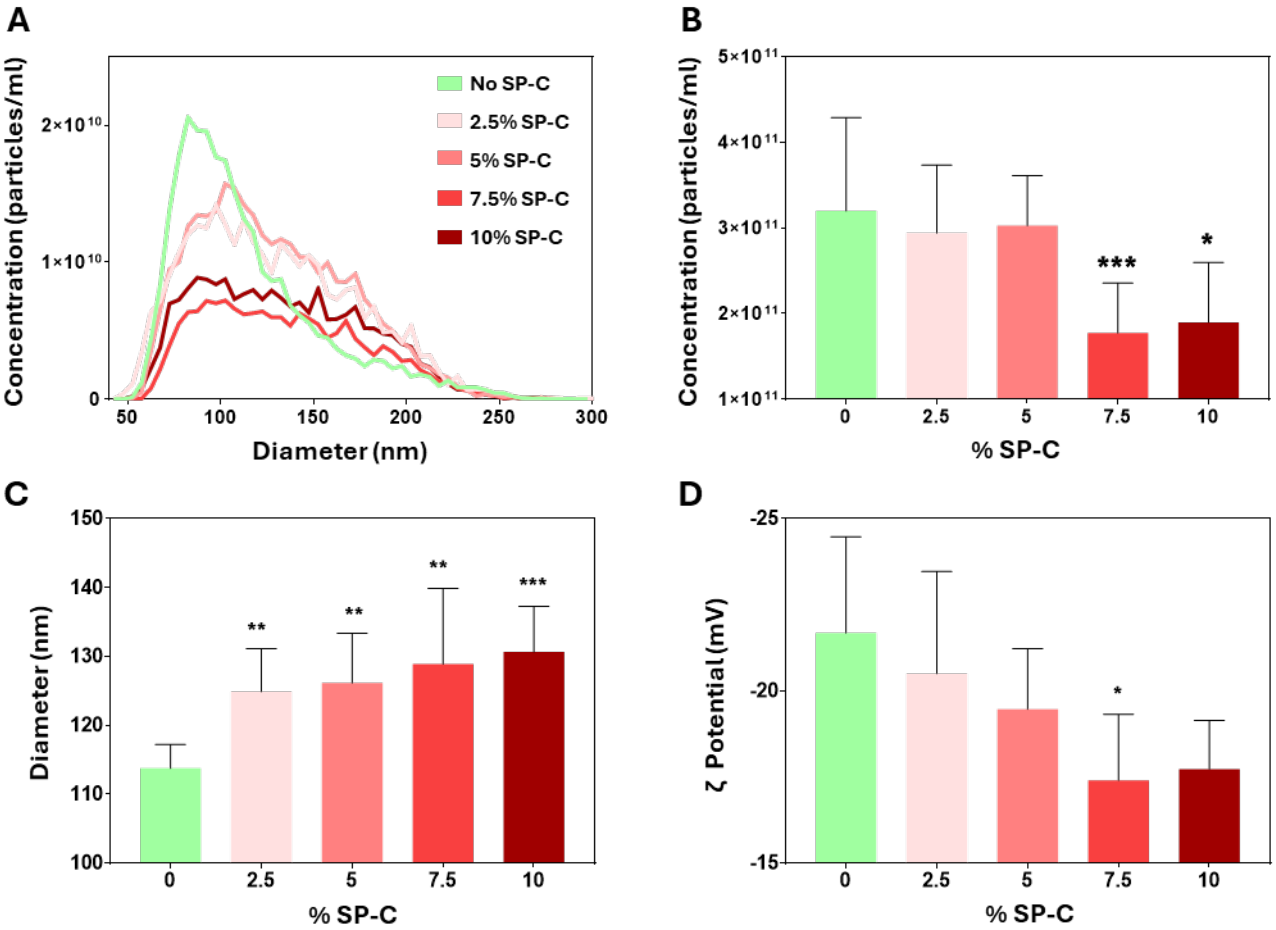

Figure 2.1: Membrane fragmentation in SP-C-loaded LUVs as detected by TRPS. **A)** Representative data of a TRPS experiment where the LUV diameter vs. LUV concentration is plotted. The data represent the profile of particles between 50-300 nm originated from LUVs containing different SP-C proportion (expressed as the percentage of total mass). **B)** Concentration of 50-300 nm particles from LUVs bearing different SP-C percentage of total mass. **C**) Mean diameter of particles from LUVs bearing different SP-C percentage of total mass. **D)** ζ potential of particles originated from LUVs bearing different SP-C percentage of total mass. All values are expressed as means ± S.D. Statistical analyses were performed using an unpaired Student's T-test. Significant p-values are depicted as asterisks (*, $p < 0.05$; **, $p < 0.01$; ***, $p < 0.001$).

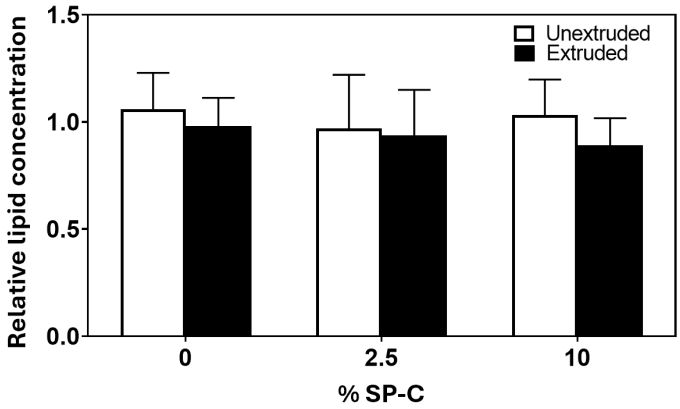

Figure 2.2: Relative lipid concentration of vesicles bearing different content of SP-C. *White bars represent unextruded MLVs, while black bars represent extruded MLVs with 200nm membrane pore size, also referred to as LUVs. Data were normalized to the theoretical concentration of the prepared vesicles. All values are expressed as means ± S.D. Statistical analyses were performed using an unpaired Student's t-test.*

Once the content of SP-C required for a significant membrane vesicle size was established, we have investigated the impact of the palmitoylation state of SP-C as well as lipid composition of vesicles in SP-C-induced fission. Due to the limitations and complex handling of the TRPS technique, this study was conducted using nanoparticle tracking analysis (NTA) assays. NTA is used for measuring the size, concentration, and movement of nanoparticles in suspension by combining light scattering with Brownian motion principles. Particles are illuminated by a laser and the scattering light allows individual particles to be visualized using a microscope connected to a video camera and tracked as they move randomly due to Brownian motion. The speed of this movement, inversely related to particle size, is analyzed to calculate particle diameter using the Stokes-Einstein equation and particle concentration is determined by counting the particles in the field of view. 200 nm LUVs composed of three different lipid systems containing 7.5% by mass of palmitoylated protein (native SP-C) or its non-palmitoylated recombinant version (rSP-C) were characterized. The lipid mixtures used were: (1) a synthetic lipid mixture (LM) that models pulmonary surfactant membranes due to its charge and ratio of saturated to unsaturated lipids, consisting of DPPC, POPC, and POPG in a 50/25/15 weight ratio; (2) a non-charged synthetic lipid mixture (ncLM) of DPPC and POPC in a 60/30 weight ratio, selected to study the effect of SP-C in the absence of electrostatic interactions with the anionic lipid POPG, as SP-C has a positive charge and could otherwise interact with it; and (3) the full lipid fraction of native pulmonary surfactant (LS) which also includes neutral lipids as cholesterol.

Figure 2.3 shows representative frames from videos captured by the microscope-associated camera, illustrating distinguishable differences in particle concentration. As previously mentioned, particle size is inferred by tracking Brownian motion, with detection relying on light scattering intensity. Due to the relatively low refractive index of the studied LUVs, light scattering is limited,

making detection and tracking of very small vesicles challenging. The images corresponding to the LM and nLM lipid mixtures display increased background signal due to the microscope's focal plane

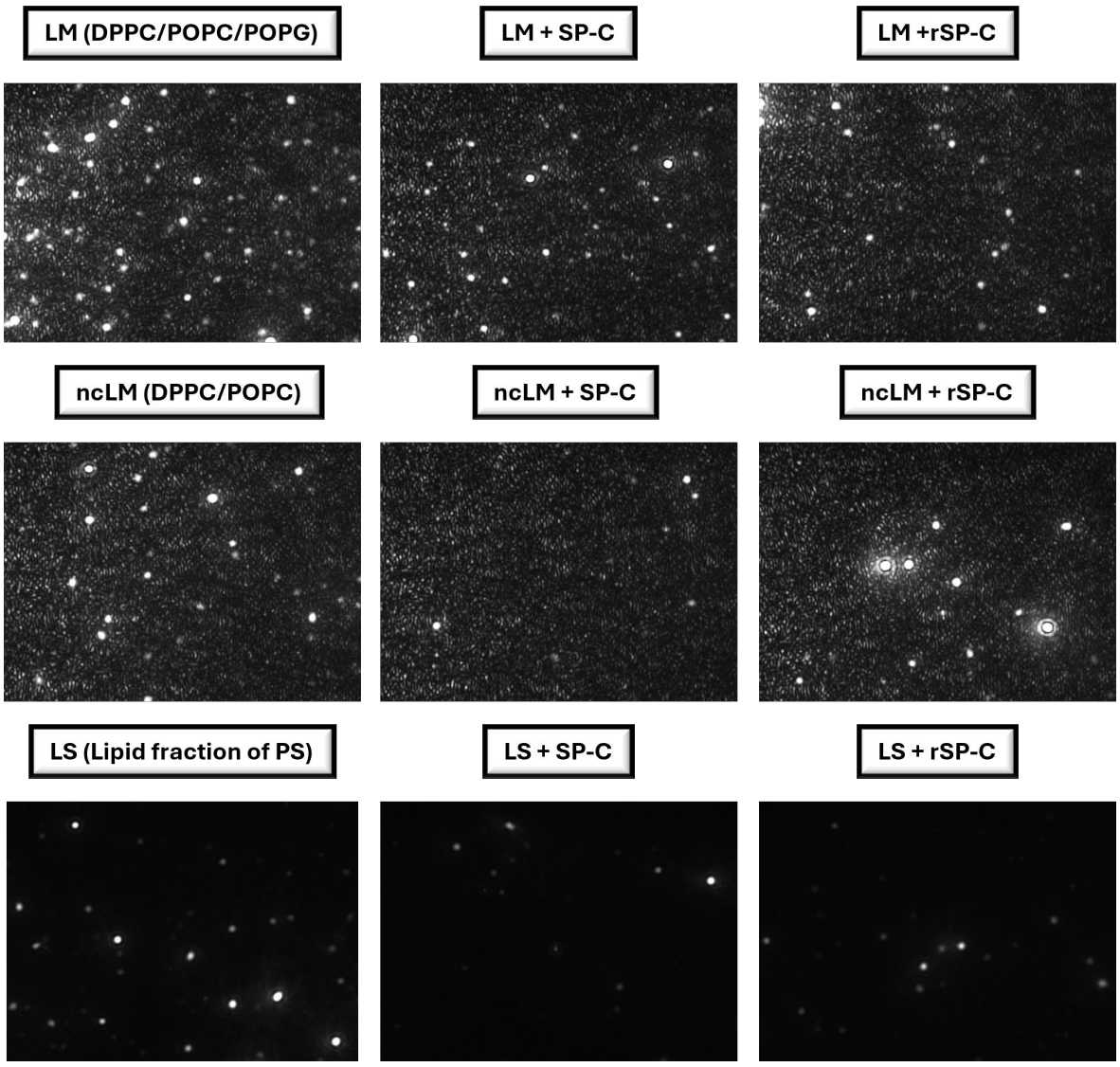

Figure 2.3: Representative images of vesicles with different lipid composition and protein conditions from video files recorded by NTA software using a camara associated to a microscope. *Each image corresponds to a specific condition, indicated by the label above each frame. Vesicles are composed of various lipid mixtures: LM (DPPC/POPC/POPG, 50/25/15, w/w/w), LM with SP-C (LM + SP-C), and LM with recombinant non-palmitoylated SP-C (LM + rSP-C); ncLM (non-charged lipid mixture of DPPC/POPC, 60/30, w/w), ncLM with SP-C (ncLM + SP-C), and ncLM with recombinant non-palmitoylated SP-C (ncLM + rSP-C); LS (lipid fraction of pulmonary surfactant), LS with SP-C (LS + SP-C), and LS with recombinant non-palmitoylated SP-C (LS + rSP-C). In all conditions with proteins, SP-C or its recombinant version (rSP-C) are present at 7.5% with respect to the total mass percentage in the vesicles. The bright white spots represent individual vesicles, which were tracked to determine their diameter size using the Stokes-Einstein equation.*

After 60 seconds of recording particle movement, their size and concentration were determined using the Nanosight NTA software (**Figure 2.4**). The concentration profile by particle diameter shown in **Figure 2.4A** reveals that presence of proteins causes a decrease in particle concentration independently of

lipid composition. In the LM system, however, this decrease is minimal, though a shift toward larger diameters is observed likely due to particle aggregation.

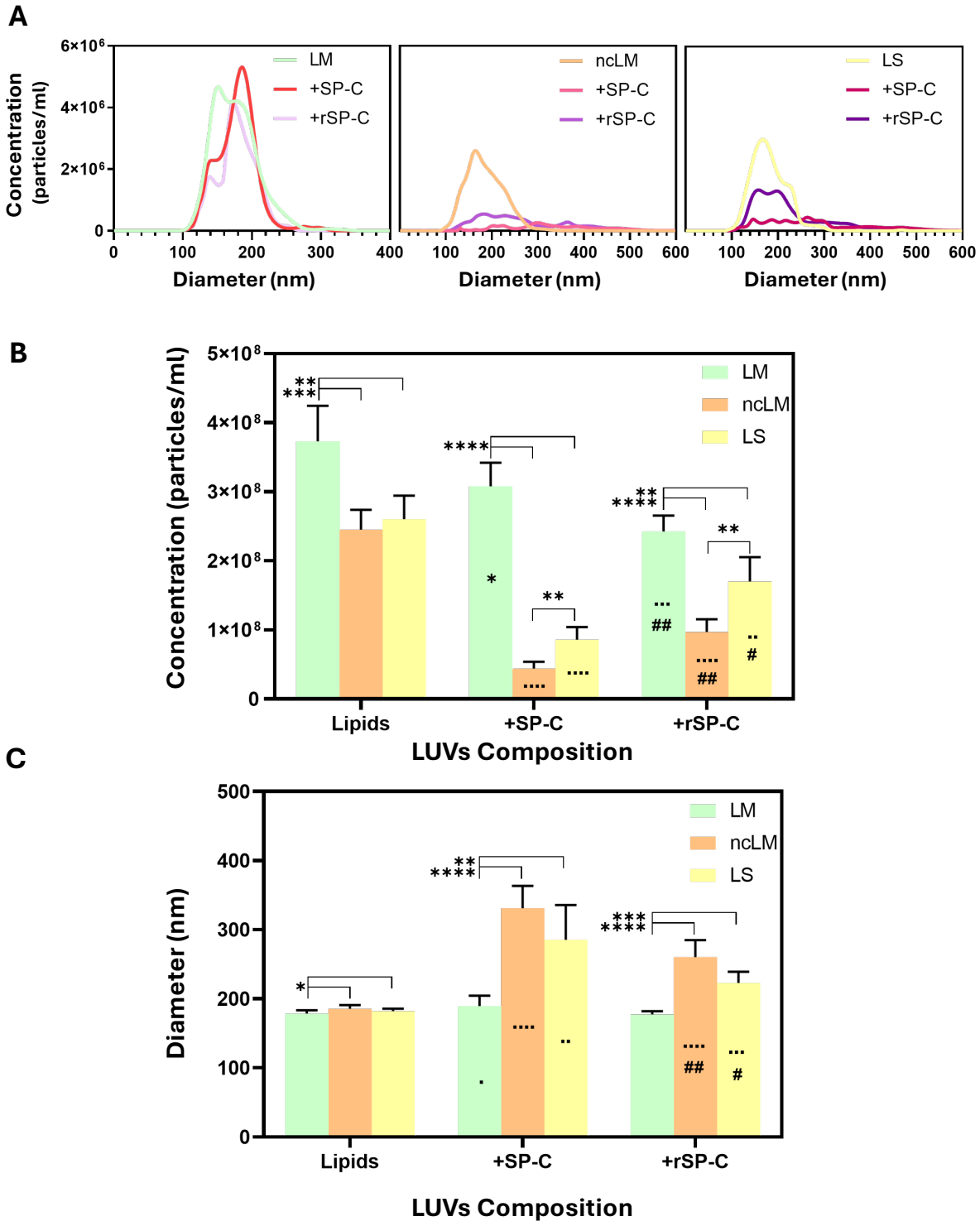

Figure 2.4: Membrane fragmentation produced by SP-C as detected using NTA technique. *Particle tracking results are summarized regarding size and concentration of particles detected in each sample.* ***A)*** *Particle size distribution graphs, displaying particle concentration across sizes ranging from 10 nm to 1000 nm for each lipid system. Although this size range is detectable by the technique, the low refractive index of the vesicles in our samples limits the detection of very small vesicles.* ***B)*** *Total particle concentration, irrespective of size, for all sample groups. Light green bars represent LUVs composed of LM, orange bars represent LUVs composed of*

ncLM, and yellow bars represent LUVs composed of LS. In the X axis, it is specified whether the sample contains only lipids or incorporates SP-C or rSP-C. ***C)*** *Similar to B), but indicating the apparent average diameter of the particles, as smaller particles are typically not detected due to their low scattering intensity. Statistically significant differences between lipid systems are denoted by boxes with asterisks indicating the level of significance. Differences within the same lipid system across different conditions are marked by symbols within each bar: asterisks denote significant differences relative to vesicles composed only of lipids, while the hashtag symbol represents significant differences between vesicles containing SP-C and rSP-C. All values are expressed as means ± S.D. Statistical analyses were performed using an unpaired Significant p-values are indicated* as asterisks, squares and hashtags (*, ▪, #, p<0.05; **,▪▪, ##, p< 0.01; ***, ▪▪▪ p < 0.001; ****, ▪▪▪▪, p < 0.0001).

In order to compare better the effects of protein and lipid composition, the total particle concentration and the apparent average diameter of particles are presented in **Figure 2.4B** and **Figure 2.4C**, respectively. Concentration particle corresponding to LM vesicles are higher than those corresponding to ncLM and LS vesicles which may indicates that LM vesicles are more stable, giving rise to a similar phospholipid content in every condition. Furthermore, the effect of SP-C on membrane fragmentation inferred from the decrease in particle concentration appears to be substantially lower in the LM + SP-C system, as indicated by its higher particle concentration compared to the other lipid systems. Analysis of the concentrations for vesicles containing SP-C in the ncLM or LS system shows that vesicles with an ncLM lipid composition undergo greater fragmentation than those composed of LS. A similar tendency is observed with the non-palmitoylated protein version, rSP-C, although the reduction in particle concentration is less pronounced. These results would indicate that lipid composition has a high impact in the ability of SP-C to fragmentate membranes likely because SP-C interacts differently depending on lipid properties.

Regarding the effect of palmitoylation, it can be observed that in vesicles composed of the model lipid mixture LM, those containing rSP-C exhibit a lower particle concentration, suggesting that depalmitoylation promotes membrane fragmentation in this lipid system may be as a consequence of more favorable self-interaction of the protein (detailed in chapter 1). However, in the other lipid systems, the opposite is observed, as the particle concentration increases in both cases compared to the corresponding containing SP-C.

The apparent average diameter of particles from ncLM and LS vesicles is slightly larger than that of LM vesicles (**Figure 2.4C**). These results, in addition to the lower particle concentration, suggest that lipid composition by itself influences vesicle production. Furthermore, lipid composition appears to be more impactful than the presence of SP-C in LM vesicles, as no significant size differences are observed between LM vesicles with or without the protein. The reduction in particle concentration is also more pronounced between ncLM or LS vesicles and LM vesicles than between LM vesicles with and without SP-C. The effect of SP-C and its non-palmitoylated version rSP-C in reduction of vesicle concentration and

therefore membrane fragmentation is increased when LUVs are composed by ncLM or LS because of larger diameter of particles, being largest when they are composed by ncLM and SP-C. These data are consistent with results from **Figure 2.4B.** Taken all data together our results suggest that SP-C's electrostatic interactions, along with potential phase separation within the lipid fraction of pulmonary surfactant, play crucial roles in driving membrane fission. It is also noteworthy that the presence of POPG in the lipid fraction may attenuate SP-C's fission-inducing effect through electrostatic interactions, yet a significant reduction in particle concentration is still observed.

Protein distribution in membranes

To investigate the distribution of SP-C within the membrane, we generated Giant Unilamellar Vesicles (GUVs) via the electroformation method. The membranes were labeled with rhodamine-DOPE to visualize the lipid bilayer, while SP-C localization was monitored using BODIPY-labeled SP-C. Confocal microscopy images were acquired at 21 ±1°C, the temperature at which the optical setup is optimized.

In **Figures 2.5A**, GUVs composed solely of LM (DPPC/POPC/POPG/rhodamine-DOPE, 50/25/15/0.2, w/w/w) are observed. These vesicles are large and exhibit an irregular, circle-like morphology, indicative of lipid phase separation within the mixture. Additionally, no signal corresponding to BODIPY-labeled SP-C is detected under these conditions (**Figure 2.5A**), confirming the absence of overlap between the red and green channels.

When 1% BODIPY-labeled SP-C is incorporated into the GUV composition, the vesicles exhibit a smoother surface (**Figure 2.5B**) indicative of a more fluid character induced by the protein in the bilayers. The lipid and protein signals overlap, and the vesicles are smaller and more polydisperse compared to those without SP-C (**Figure 2.5B vs. 2.5A**). This suggests a possible membrane fragmentation induced by SP-C.

This effect becomes more pronounced in GUVs composed of 10% SP-C, with 1% of which being BODIPY-labeled. Under this condition, fewer vesicles are observed, and they appear predominantly circular and smooth, suggesting a general fluid character and the loss of phase separation (**Figure 2.5C**). Fluorescence levels corresponding to BODIPY-labeled SP-C are slightly higher in GUVs containing 10% SP-C compared to those with only 1%, despite the same labeling amount. In contrast, lipid fluorescence appears significantly lower (**Figure 2.5C vs. 2.5B**). The merged lipid and protein signal in GUVs containing 10% SP-C is predominantly green (**Figure 2.5C**), unlike GUVs with 1% SP-C, which display a mixture of red and green, with red fluorescence being more prominent (**Figure 2.5B**).

These observations suggest that 10% SP-C induces significant lipid refinement, leading to the complete loss of phase separation and potentially causing membrane fragmentation, as evidenced by the reduced vesicle size.

The effect of non-palmitoylated rSP-C was also evaluated using BODIPY-labeled rSP-C. In GUVs containing 1% BODIPY-rSP-C, minimal effects were observed. The vesicles remained large and irregular, and the green fluorescence signal was very weak (**Figure 2.5D**), indicating limited presence of the protein into the lipid bilayers. When 9% unlabeled rSP-C was added to the composition, a higher number of smaller vesicles with irregular morphology was observed. This suggests increased fragmentation of the GUVs and enhanced incorporation of BODIPY-labeled rSP-C into the membrane (**Figure 2.5E**). The merged red and green channels displayed a color pattern similar to that observed in GUVs with 1% SP-C (**Figure 2.5E vs.2.5B**), indicating that the effect of rSP-C on the membrane is weaker or qualitatively different from that of native SP-C.

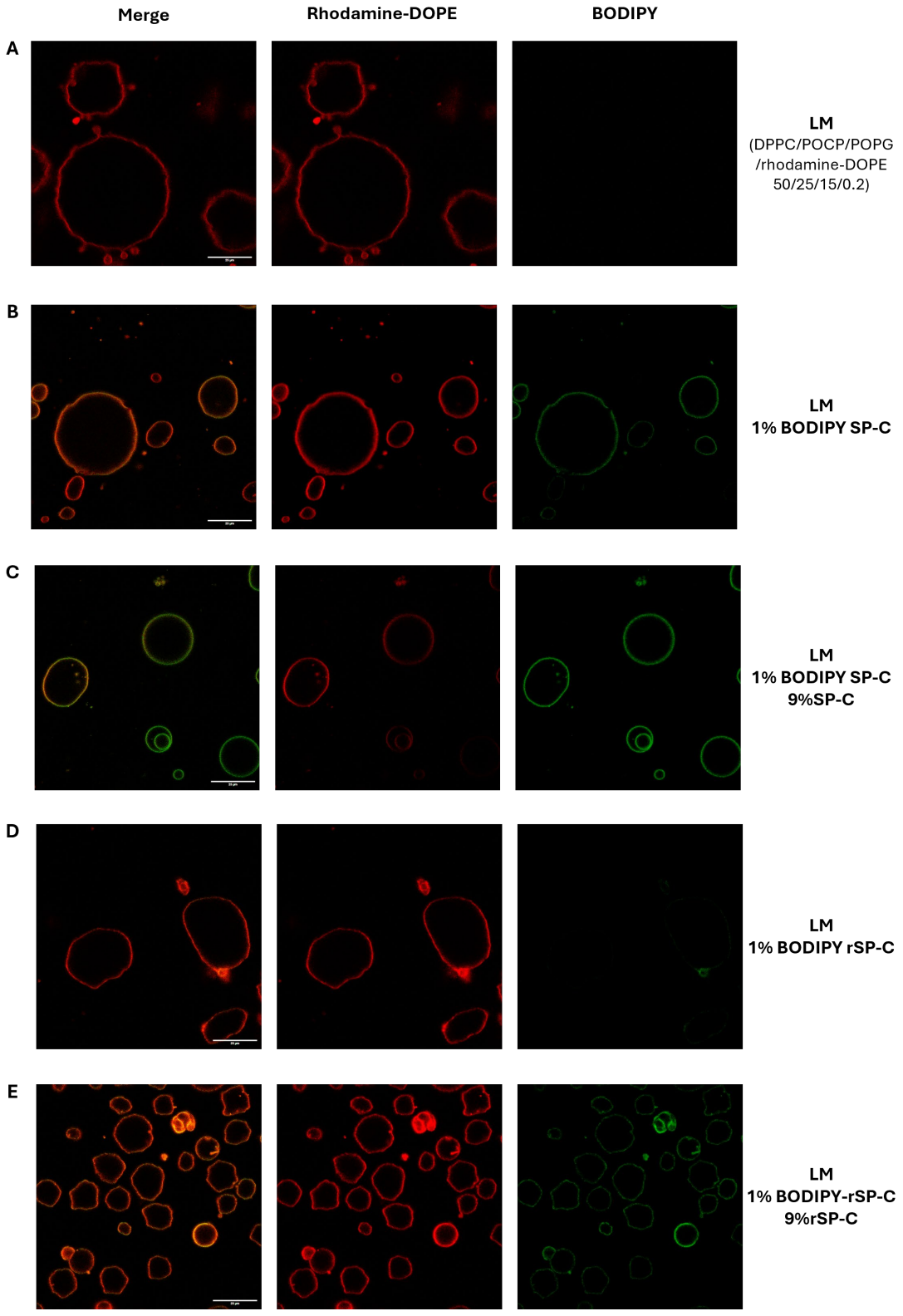

Figure 2.5: Confocal microscopy images of Giant Unilamellar Vesicles (GUVs) showing the distribution of rhodamine-DOPE (red) and BODIPY-labeled SP-C (green). A) *GUVs composed of the lipid model mixture (DPPC/POPC/POPG, 50/25/15, w/w/w) labeled with 0.2% rhodamine-DOPE.* ***B)*** *GUVs composed of the lipid model mixture with 0.2% rhodamine-DOPE and 1% BODIPY-labeled SP-C.* ***C)*** *GUVs composed of the lipid model mixture with 0.2% rhodamine-DOPE, 1% BODIPY-labeled SP-C, and 9% native (unlabeled) SP-C.* ***D)*** *GUVs composed of the lipid model mixture with 0.2% rhodamine-DOPE and 1% BODIPY-labeled rSP-C (non-palmitoylated recombinant SP-C variant).* ***E)*** *GUVs composed of the lipid model mixture with 0.2% rhodamine-*

DOPE, 1% BODIPY-labeled rSP-C, and 9% unlabeled rSP-C. The figure displays the merged fluorescence channels of rhodamine-DOPE and the BODIPY-labeled protein (left), the individual channel of rhodamine-DOPE (middle), and the individual channel of the BODIPY-labeled protein (right). White scale bars correspond to 25 μm.

The NTA experiments performed in this chapter suggest that lipid composition critically affects vesicle fragmentation, prompting the analysis of GUVs composed of a non-charged lipid mixture (ncLM: DPPC/POPC/rhodamine-DOPE, 60/30/0.2, w/w/w) (**Figure 2.6**).

In GUVs composed solely of ncLM, micrographs revealed vesicles approximately 20µm in size, with an oval morphology and small protusions, indicative of phase separation (**Figure 2.6A**). These features resemble those observed in vesicles composed of DPPC/POPC/POPG, but with a smaller overall size (**Figure 2.5A**).

The addition of 1% BODIPY-labeled SP-C to the ncLM composition resulted in vesicles with highly heterogeneous sizes and lipid-protein distributions. The vesicles exhibited distinct fluorescence patterns, with some being predominantly green, others showing an intermediate mix of red (rhodamine-DOPE) and green (BODIPY-labeled SP-C), and some appearing primarily red (**Figure 2.6B**). The protein distribution within these vesicles was also variable; in some of them, BODIPY-labeled SP-C was homogeneously distributed across the membrane, while in others, it was localized at specific regions (**Figure 2.6B**). This heterogeneity suggests intermediate levels of phase segregation and of it being fragmented, with some vesicles displaying lipids lacking phase separation possibly due to SP-C-induced fragmentation, while others remain unaffected.

GUVs containing 10% SP-C, of which 1% was BODIPY-labeled SP-C, exhibited a distinct morphology. These vesicles were oval but smoother, with a higher concentration of labeled protein in the membrane (**Figure 2.6C**). Additionally, the level of BODIPY-labeled SP-C incorporation was significantly higher in these vesicles compared to those without unlabeled SP-C (**Figure 2.6C** vs. **Figure 2.6B**), suggesting enhanced protein-membrane interaction and lipid redistribution in the presence of higher SP-C concentrations.

A comparative analysis of GUVs containing 1% BODIPY-labeled SP-C across synthetic lipid systems revealed greater size polydispersity in GUVs lacking POPG (ncLM) compared to those containing it (LM) (**Figure 2.6B vs. Figure 2.5B**). This finding supports the hypothesis that electrostatic interactions between SP-C and membrane lipids modulate fragmentation, as observed in NTA experiments.

These results highlight the critical role of lipid composition and SP-C in determining vesicle morphology, size distribution, and phase separation, emphasizing the mechanistic differences induced by the presence or absence of charged lipids in the membrane system.

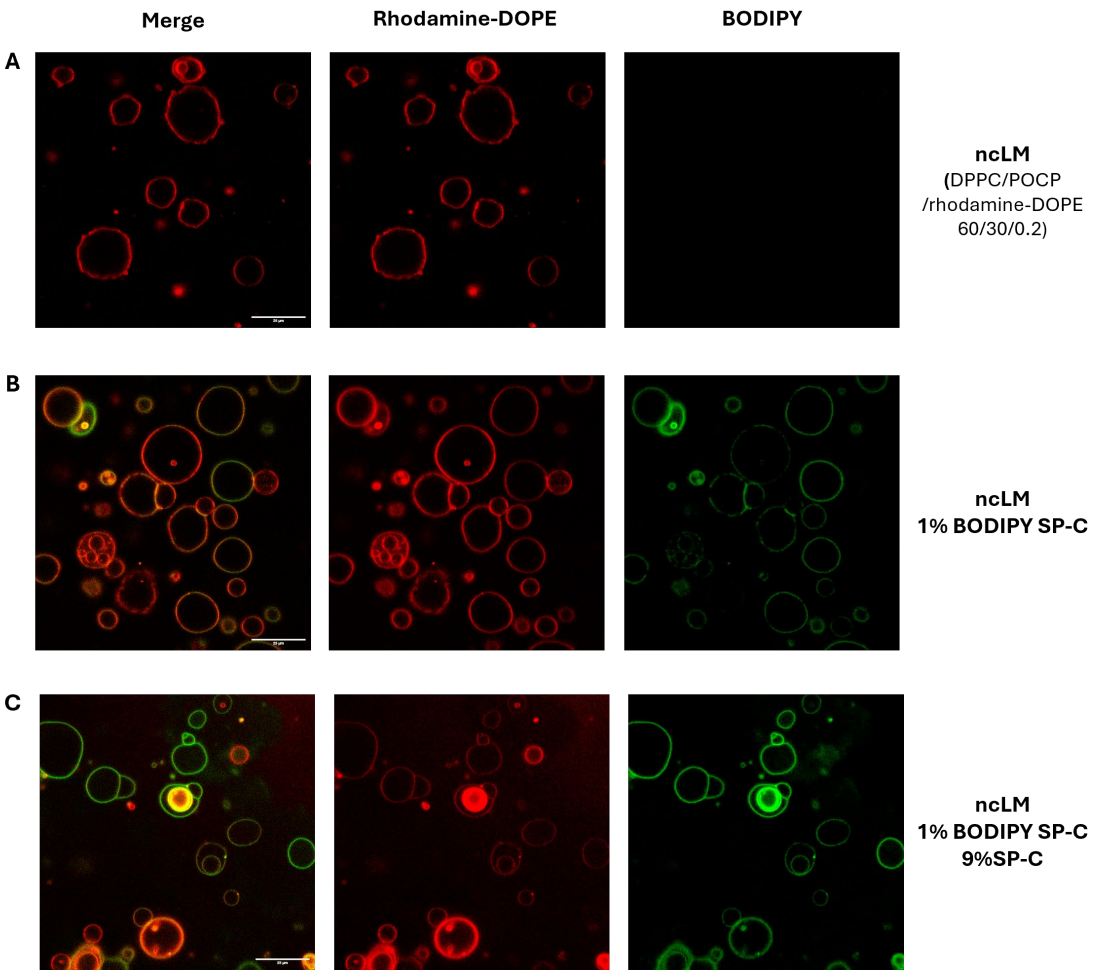

Figure 2.6: Confocal microscopy images of Giant Unilamellar Vesicles (GUVs) showing the distribution of rhodamine-DOPE (red) and BODIPY-labeled SP-C (green). A) *GUVs composed of the non-charged lipid mixture (DPPC/POPC, 60/30, w/w) labeled with 0.2% rhodamine-DOPE.* ***B)*** *GUVs composed of the non-charged lipid mixture with 0.2% rhodamine-DOPE and 1% BODIPY-labeled SP-C.* ***C)*** *GUVs composed of the lipid model m non-charged lipid mixture with 0.2% rhodamine-DOPE, 1% BODIPY-labeled SP-C, and 9% native (unlabeled) SP-C. The figure displays the merged fluorescence channels of rhodamine-DOPE and the BODIPY-labeled protein (left), the individual channel of rhodamine-DOPE (middle), and the individual channel of the BODIPY-labeled protein (right). White scale bars correspond to 25 µm.*

GUVs formed exclusively from the lipid fraction of pulmonary surfactant exhibited instability, with only a small number of vesicles being successfully generated. These vesicles tended to aggregate, forming clusters ranging in size from approximately 25 µm to smaller vesicles. Remarkably, their membranes appeared smooth and uniform, lacking the irregularities typically associated with phase separation (**Figure 2.7A**).

Incorporating 1% BODIPY-labeled SP-C into the composition resulted in the formation of a few large, rounded GUVs (15-25 µm). However, the distribution of both the lipid (rhodamine-DOPE, red channel) and the protein (BODIPY-labeled SP-C, green channel) was heterogeneous across the membrane (**Figure 2.7B**). The overlapping signals produced yellowish fluorescence, indicating a higher concentration of SP-C in certain areas of the membrane compared to lipids.

Aggregates, similar to those observed in the absence of protein were still visible in the top-left corner, suggesting partial clustering (**Figure 2.7D**).

Increasing the protein concentration to 10% SP-C (including 1% BODIPY-labeled SP-C) produced smaller (~7 μm), highly circular GUVs. These vesicles exhibited intense fluorescence in both the lipid and protein channels (**Figure 2.7C**), suggesting high concentrations of both components within the membrane. This pattern would imply that SP-C promotes membrane fragmentation, resulting in vesicles enriched in both BODIPY-labeled SP-C and rhodamine-DOPE, potentially leading to the segregation and concentration of these molecules.

The role of palmitoylation was also investigated comparing the behavior of non-palmitoylated rSP-C. GUVs containing 1% or 10% rSP-C (both BODIPY-labeled and unlabeled) formed larger, aggregated vesicles with irregular morphologies (**Figure 2.7D**). At higher protein concentrations, a greater number of vesicles was observed, many of which appeared to adhere to one another (**Figure 2.7E**). This contrasts with the behavior of native SP-C, which would promote membrane fragmentation and the formation of smaller, independent vesicles.

These findings highlight the critical role of palmitoylation in SP-C action. While native SP-C would induce membrane fission and the formation of independent vesicles, rSP-C appears to be less effective at inducing fragmentation. Instead, rSP-C seems to favor vesicle aggregation and adhesion, likely due to the absence of palmitic acid chains, which are essential for stabilizing protein-membrane interactions as alternative to protein-protein interactions.

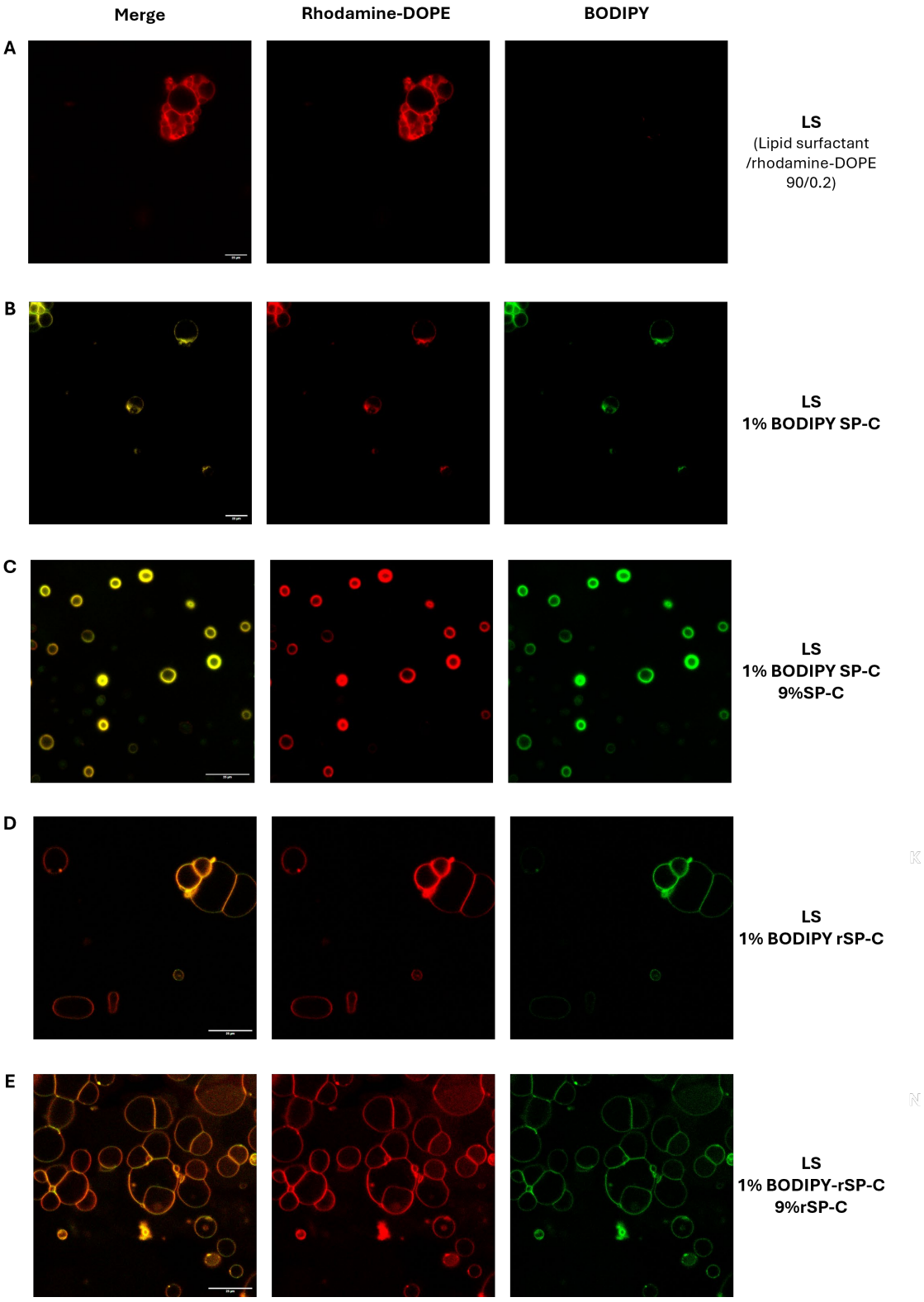

Figure 2.7: Confocal microscopy images of Giant Unilamellar Vesicles (GUVs) composed of the lipid surfactant (LS) fraction showing the distribution of rhodamine-DOPE (red) and BODIPY-labeled SP-C (green). A) *GUVs composed of the lipid surfactant (LS) fraction obtained from native PS labeled with 0.2% rhodamine-DOPE.* ***B)*** *GUVs composed of the lipid surfactant (LS) fraction with 0.2% rhodamine-DOPE and 1% BODIPY-labeled SP-C.* ***C)*** *GUVs composed of the lipid model mixture with 0.2% rhodamine-DOPE, 1% BODIPY-labeled SP-C, and 9% native (unlabeled) SP-C.* ***D)*** *GUVs composed of the lipid model mixture with 0.2% rhodamine-DOPE and 1% BODIPY-labeled rSP-C (non-palmitoylated recombinant SP-C variant).* ***E)***

GUVs composed of the lipid model mixture with 0.2% rhodamine-DOPE, 1% BODIPY-labeled rSP-C, and 9% unlabeled rSP-C. The figure displays the merged fluorescence channels of rhodamine-DOPE and the BODIPY-labeled protein (left), the individual channel of rhodamine-DOPE (middle), and the individual channel of the BODIPY-labeled protein (right) White scale bars correspond to 25 µm.

Contribution of N- and C-terminal regions in SP-C contribution to membrane fragmentation

To elucidate the contribution of particular segments of SP-C in the potential fragmentation of LUVs, we designed different peptides mimicking each section of the protein that contained potential dimerization motifs (**Table 1**). SP-$C_{1\text{-}13}$ peptide comprises the N-terminal region and the first leucine residue of the transmembrane segment. The carboxyl-end of this peptide was substituted for an amidated end to mimic its context within the whole protein and therefore allowing for its partial integration into the lipid bilayer. On the other hand, (AL)SP-$C_{11\text{-}35}$ peptide was an analogue of the whole transmembrane region in which valine residues were replaced by alanine and leucine residues. Thus, this peptide could display an α-helical conformation, while possible effects that could influence membrane fission —such as membrane stiffness or propensity to adopt to β-sheet conformations— might be prevented. GRAVY (grand average of hydropathy) indexes for each peptide, as well as for the full SP-C sequence, were calculated and summarized in **Table 1.**

Table 4: Peptides mimicking different SP-C regions.

Peptide	Sequence	GRAVY index
SP-C	FGI**PCCP**VHLKRLLIVVVVVVLIVVVIVGALLMGL	2.46
SP-$C_{1–13}$	FGI**PCCP**VHLKRL$_{amide}$	0.685
(AL)SP-$C_{11–35}$	KRALAALAALAAGGLLIVG**ALLMGL**	1.816
mA-SP-$C_{1–13}$(C →A)	FGIP*AA*PVHLKRL$_{amide}$	0.577
mF-SP-$C_{1–13}$ (C →F)	FGIP*FF*PVHLKRL$_{amide}$	0.731
m(AL)SP-$C_{11–35}$ (A,G →I)	KRALAALAALAAGGLLIVG*I*LLM*I*L	2.120

** Putative dimerization domains are highlighted in bold letters and aminoacid substitution are in cursive.*

A representative figure of a TRPS experiment with LM LUVs containing these peptides is shown in **Figure 2.8A**. For these assays, we used LUVs with either no SP-C or 7.5% of SP-C, as it was the assessed minimum protein concentration causing effective reduction of particle concentration. When the peptides were

included by itself into the LUVs, in the absence of SP-C, no effect on the particle concentration or their average diameter was detected (**Figure 2.8B-C**). However, when the peptides were included in LUVs containing an additional 7.5% of SP-C, a further significant decrease in concentration and an increase in average diameter were observed. This effect was slightly higher when LUVs contained the (AL)SP-C_{11-35} peptide. These results determined that both ends of SP-C apparently contribute

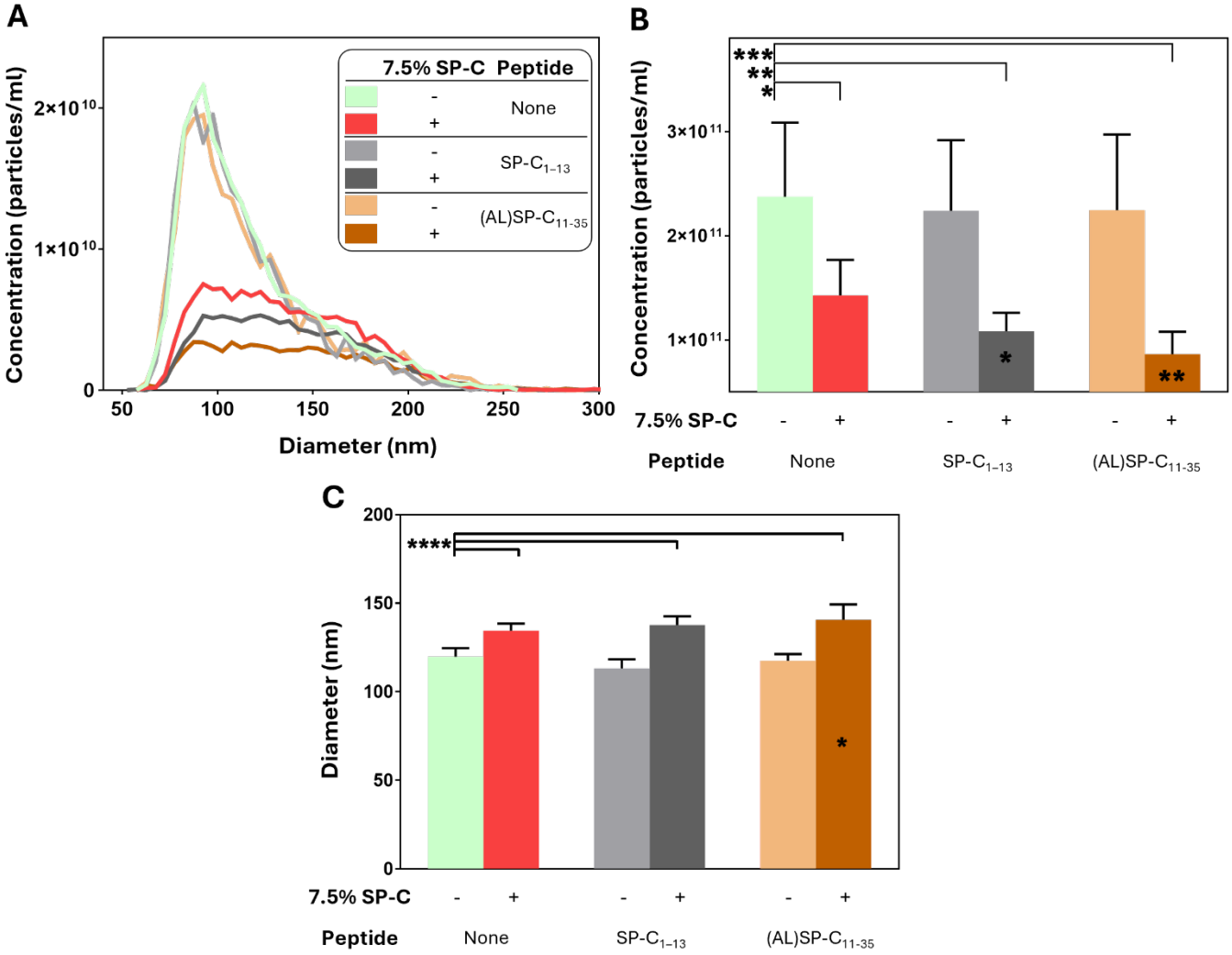

Figure 2.8: TRPS experiments using LM LUVs with peptides mimicking different SP-C regions, in the absence or presence of native SP-C. A) *Representative histograms of a TRPS experiment where the LUV size vs. LUV concentration is plotted. The data represent the profile in the range of 50-300 nm of LUVs comprising different compositions, as indicated in the legend (- and + represent absence or presence of 7.5% protein/lipid by mass of porcine purified SP-C).* ***B)*** *Concentration of 50-300 nm LUVs bearing different compositions, as indicated below.* ***C)*** *Apparent average diameter of LUVs bearing different compositions, as indicated below. Statistically significant differences between samples and LUVs composed just by lipids are denoted by boxes with asterisks. Asterisks within the bars shows statistical difference between LUVs bearing SP-C when samples are significantly different to LUVs not bearing protein. Significant p-values are depicted as asterisks (*, $p < 0.05$; **, $p < 0.01$; *** $p < 0.001$; ****, $p < 0.0001$).*

to enhance the observed membrane fission, but only when the whole SP-C is present.

To assess whether dimerization motifs contribute to the synergistic effect with SP-C in membrane fragmentation, peptides with modified dimerization motifs were designed. Two mutants of the N-terminal segment were created: 1) mA-SP-$C_{1–13}$(C →A), in which cysteines in the PCCP motif were replaced by alanines, chosen for their small size, low reactivity, and minimal steric hindrance; and 2) mF-SP-$C_{1–13}$ (C →F), where cysteines were substituted by phenylalanines, as the structure of phenylalanine might effectively mimic, at least partially, that of palmitoylated cysteins. For the proposed motif at the C-terminal end, we developed the m(AL)SP-$C_{11–35}$ (A,G →I) mutant replacing alanine and glycine residues in the AxxxG sequence by isoleucines. This substitution of small and flexible residues by branched amino acids was designed to introduce steric hindrance, preventing the close approach of α-helices and thereby likely inhibiting dimer formation (Grau *et al.*, 2017; Lemmon *et al.*, 1992).

We have characterized the concentration and size of vesicles composed of LM or LS containing native SP-C, and/or synthetic peptides through NTA. **Figure 2.9** presents the results obtained with peptides emulating the N-terminal end and its mutants. Similar to the TRPS technique results (**Figure 2.8**), the particle concentration and size remain constant in the LM LUVs containing the SP-$C_{1–13}$. Same trend was observed using mutant peptide mF-SP-$C_{1–13}$ (C →F). Moreover, when vesicles include any of the peptides, regardless of their sequence, along with 7.5% SP-C, a synergistic effect is observed in SP-C's fragmentation capability. This is reflected in a significant decrease in particle concentration, although it does not impact on the apparent average diameter of particles (**Figure 2.9**). It is worth indicating that LM LUVs bearing the peptide in which cysteines were replaced by alanine, mA-SP-$C_{1–13}$ (C →A), an even greater reduction in particle concentration than that induced by SP-C alone is observed. This suggests an intrinsic effect of this peptide on particle stability. This effect is further supported by an increase in the apparent size of vesicles, greater than that observed in vesicles composed solely of lipids, which could indicate a higher aggregation capacity of the particles (**Figure 2.8**). Thus, the decrease in particle concentration in LUVs containing both SP-C and mA-SP-$C_{1–13}$ (C →A) could be attributed exclusively to the effect of SP-C and not to a synergistic interaction between this peptide and SP-C (**Figure 2.9**).

Regarding lipid composition, vesicles composed of LS do not exhibit the trends observed in LM. In this lipid system, none of the N-terminal peptides, with or without substitutions, caused alterations in the studied parameters, neither in particle concentration nor in their average size. In all cases a decrease in particle concentration and an increase in the apparent mean diameter of LUVs with SP-C and peptide, compared to those containing only peptides, was observed, suggesting greater fragmentation. However, when compared to vesicles containing

only SP-C, a higher particle concentration is observed, indicating that these peptides might interfere with the membrane fission effect of SP-C.

In summary, mutations in the PCCP proposed dimerization motif do not appear to significantly impact on SP-C's membrane fragmentation capability; rather, a key factor seems to be the presence of the peptide itself, regardless of its sequence. However, lipid composition is crucial in determining whether the effect with SP-C is synergistic, as observed in LM LUVs, or antagonistic, as seen in LUVs made of LS.

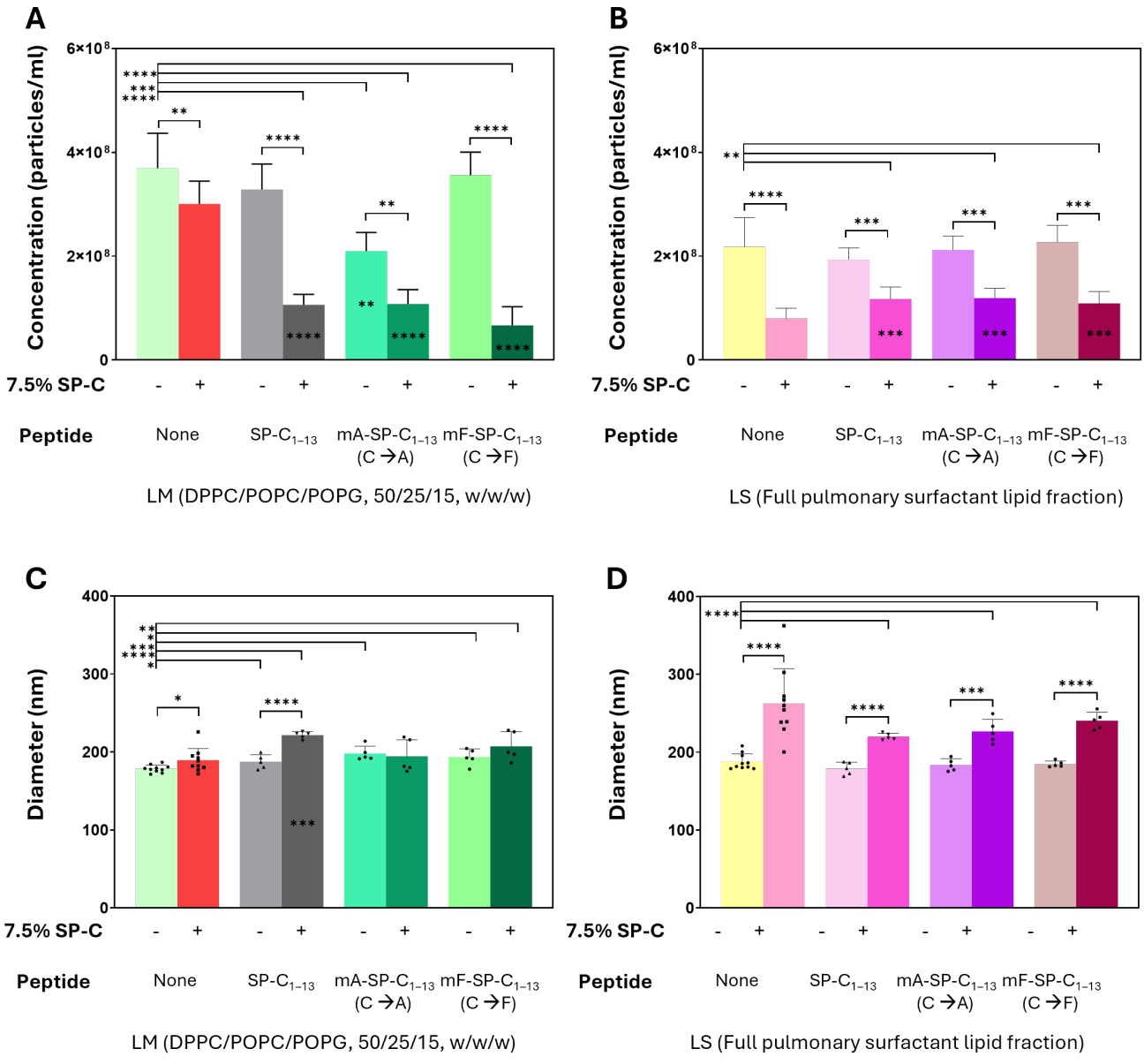

Figure 2.9: NTA characterization of LUVs containing peptides mimicking the N-terminal region of SP-C, in the absence or presence of native SP-C, with different lipid compositions. *The concentration and apparent mean particle size of LUVs with various lipid compositions are shown.* ***A)*** *and* ***C)*** *LUVs with a lipid composition of DPPC/POPC/POPG in a 50/25/15 mass ratio.* ***B)*** *and* ***D)*** *LUVs are composed of the full lipid fraction derived from purified pulmonary surfactant obtained from porcine bronchoalveolar lavage fluid. Particle concentration is shown in A) and B), while apparent mean diameter is presented in C) and D). Each condition includes LUVs composed solely of lipids or with 7.5% SP-C by mass relative to lipids, as indicated by "–" (absence) or "+" (presence) in the legend. The different N-terminal peptides used are: SP-C$_{1–13}$ (a peptide analogous to the*

native N-terminal region of SP-C), mA-SP-$C_{1–13}$(C → A), where cysteines in the PCCP motif are replaced with alanine, and mF-SP-$C_{1–13}$(C → F), where cysteines are replaced with phenylalanine, as shown in the legend. Significant differences are indicated with asterisks next to or above boxes, representing comparisons between specific samples. Asterisks within bars indicate statistically significant differences for samples that differ lipid + SP-C conditions. If a sample is significantly different from lipid + SP-C but not from lipid-only, no significance is indicated. Significant p-values are depicted as asterisks (, p<0.05; **, p<0.01; *** p<0.001; p<0.0001).*

The study results on the role of the C-terminal end and the potential dimerization motif AxxxG in SP-C-induced membrane fragmentation are shown in **Figure 2.10**. For vesicles composed of LM and the (AL)SP-C_{11-35} peptide, which mimics the C-terminal region, particle concentration remains comparable to that observed in LUVs containing only lipids, indicating no immediate impact of the peptide alone. However, when this peptide is combined with SP-C, a pronounced reduction in particle concentration is observed, alongside a notable increase in the average apparent particle size compared to vesicles containing only SP-C (**Figure 2.10**). These results align with prior findings obtained using TRPS (**Figure 2.8**).

In contrast, the peptide with substitutions in the AxxxG sequence, m(AL)SP-C_{11-35} (A,G →I), does not induce any observable changes in particle characteristics, with both concentration and diameter of particles being similar to those of vesicles composed solely of lipids. When m(AL)SP-C_{11-35} (A,G →I) is included alongside SP-C in the vesicles, there are not changes, suggesting that SP-C-induced fragmentation may be inhibited under these conditions.

For vesicles composed of LS, the C-terminal peptides alone do not produce any measurable alterations in particle parameters (**Figure 2.10**). Moreover, although the combined presence of SP-C and the peptides leads to a reduction in particle concentration, this reduction is equivalent to that seen in vesicles containing only SP-C. This result implies that, in LS-composed vesicles, C-terminal peptides, whether or not they have substitutions in the proposed AxxxG dimerization motif, may not enhance or alter the fragmentation effect of SP-C.

Altogether, these findings indicate that in certain lipid systems, such as LM, the AxxxG motif appears to play a critical role in SP-C-driven vesicle fragmentation. However, in a more complex lipid system, like LS, the potential SP-C fragmentation effect observed as a decrease in particle concentration seems unaffected, even in the presence of analogous peptides that include or lack substitutions in the AxxxG motif. This suggests that the lipid environment is a determining factor as well as it was for dimerization of native SP-C.

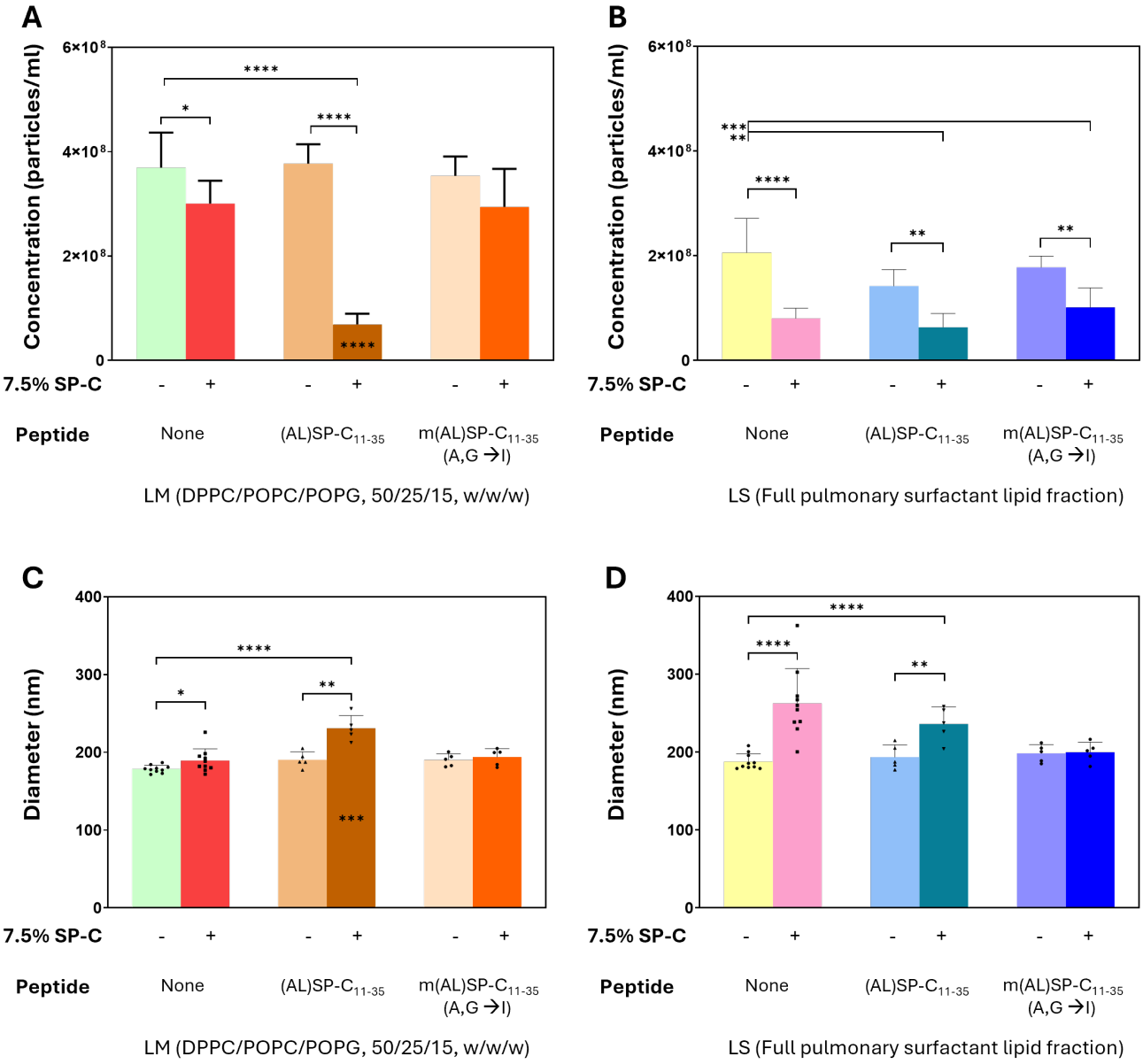

Figure 2.10: NTA characterization of LUVs containing peptides mimicking the C-terminal region of SP-C, in the absence or presence of native SP-C, with different lipid compositions. *The concentration and apparent mean particle size of LUVs with various lipid compositions are shown.* ***A)*** *and* ***C)*** *LUVs with a lipid composition of DPPC/POPC/POPG in a 50/25/15 mass ratio.* ***B)*** *and* ***D)*** *LUVs are composed of the full lipid fraction derived from purified pulmonary surfactant obtained from porcine bronchoalveolar lavage fluid. Particle concentration is shown in A) and B), while apparent mean diameter is presented in C) and D). Each condition includes LUVs composed solely of lipids or with 7.5% SP-C by mass relative to lipids, as indicated by "–" (absence) or "+" (presence) in the legend. The different C-terminal peptides used are: (AL)SP-C$_{11-35}$ (a peptide analogous to the native C-terminal region of SP-C) and m(AL)SP-C$_{11-35}$ (A, G→ I), where alanine and glycine of AxxxG proposed motif is substituted with isoleucines. Significant differences are indicated with asterisks next to or above boxes, representing comparisons between specific samples. Asterisks within bars indicate statistically significant differences for samples that differ lipid + SP-C conditions. If a sample is significantly different from lipid + SP-C but not from lipid-only, no significance is indicated. Significant p-values are depicted as asterisks (*, p<0.05; **, p<0.01; *** p<0.001; p<0.0001).*

Discussion

The ability of SP-C to induce membrane curvature has been a well-documented phenomenon, particularly in studies conducted with GUVs composed of POPC, where its potential to alter membrane morphology was clearly demonstrated (Parra *et al.*, 2011). This effect may facilitate membrane fragmentation, leading to the formation of small, highly curved vesicles. To test this hypothesis, Roldan *et al*. (2016) analyzed vesicles by DLS, observing a significant reduction in vesicle size. This finding was confirmed by Cryo-EM, which revealed the presence of small, curved vesicles in the presence of the protein, while vesicles without the protein showed no changes. These results highlight SP-C's ability to generate small, curved vesicles, regardless of lipid composition and the palmitoylation state of the SP-C protein. In this chapter, TRPS data provided valuable insights into the mechanisms underlying SP-C-induced membrane fragmentation. Given that TRPS systems are unable to detect particles with diameters smaller than 50 nm, the fragmentation effect induced by SP-C was assessed as a decrease in vesicle concentration when the resulting vesicles fell below this detection threshold. This phenomenon was particularly evident when 10% SP-C was incorporated into LUVs extruded through 200 nm membranes, as previously reported (Roldan *et al.*, 2015). TRPS systems also have an upper limit for detecting larger particles, but we confirmed that this limit was not reached, as it would be associated with a permanent nanopore blockade. It is important to note that effective membrane fission only occurs when SP-C is included at levels around 7.5% w/w into DPPC/POCP/POPG membranes. These results align with the idea that a minimum concentration of SP-C is required to form large, stiff oligomers capable of triggering the fission mechanism. As we have shown, this outcome is independent of the colloidal stability of the LUVs, as the decrease in the absolute values of ζ-potential appears to be proportional to the SP-C composition of LUVs. Since other factors influencing ζ-potential remain unchanged across sample, we hypothesize that this neutralization in ζ-potential may be linked to the presence of the cationic residues of SP-C in the outer region of SP-C, which likely counteract the negative charge of the polar heads of the phospholipids.

Once the minimum concentration of SP-C required to induce membrane fragmentation was established, the next phase of this study aimed to explore the influence of the lipid environment on this phenomenon. To achieve this, two distinct lipid systems were analyzed: non-charged lipid system (ncLM), consisting of DPPC and POPC in a 60/30 w/w ratio, and the lipid fraction of native pulmonary surfactant (LS), which features a more complex composition, including the presence of cholesterol. This comparative approach allowed us to investigate how the absence of charged lipids affects the interaction and functionality of SP-C,

particularly in comparison with lipid systems that more closely mimic the natural composition of pulmonary surfactant.

The characterization of vesicles made of these systems, both in the presence and absence of SP-C, was performed using NTA. This technique was chosen to address limitations encountered in TRPS, particularly for the detection of particles smaller than 50 nm. However, due to the low light-scattering properties of the vesicles, detecting small particles still remained a challenge. As in the TRPS experiments, a reduction in the concentration of detectable particles was interpreted as an indirect measure of increased membrane fragmentation. To address this limitation, it would have been advantageous to consider complementary techniques such as DLS or CryoEM. Given the potential impact of SP-C on membrane fragmentation, its presence is likely to induce polydispersity within the vesicle population. Consequently, methods such as size exclusion chromatography or gradient centrifugation assays could prove useful in resolving the heterogeneous populations generated by SP-C-induced fragmentation.

In both lipid systems (ncLM and LS), SP-C induced a substantial reduction in the concentration of vesicles, with potential fragmentation levels significantly higher than those observed in the model lipid system DPPC/POPC/POPG. However, observations made on giant unilamellar vesicles (GUVs) corresponding to each system revealed notable differences in terms of size, polydispersity, and distribution patterns of the fluorescently labeled protein BODIPY-SP-C and the lipid marker rhodamine-DOPE in the membranes. These differences suggest that the increase in membrane fragmentation may be mediated by distinct molecular mechanisms depending on the lipid environment.

The defining characteristic of the ncLM system is its lack of the anionic lipid POPG, a key component of the DPPC/POPC/POPG model. The absence of POPG prevents SP-C, a cationic protein, from establishing electrostatic interactions with the lipid headgroups. These interactions are critical for SP-C anchoring to lipid bilayers and monolayers, as previously demonstrated (Plasencia *et al.*, 2004). This lack of electrostatic stabilization likely facilitates greater membrane fragmentation in the ncLM system, as SP-C interacts less stably with the lipids. In contrast, the presence of POPG in the DPPC/POPC/POPG system appears to enhance membrane stability, requiring higher concentrations of SP-C to induce sufficient curvature for vesicle fission (Parra *et al.*, 2011; Pérez-Gil *et al.*, 1995). This stability is consistent with the proposed role of POPG in maintaining the structural integrity of surfactant membranes.

One of the key distinctions in the lipid composition of LS is the presence of cholesterol, the most abundant neutral lipid in pulmonary surfactant. Cholesterol is known to promote segregation between ordered and disordered fluid phases in

surfactant membranes and films (Bernardino de la Serna *et al.*, 2004; Keating *et al.*, 2007). This segregation has significant implications for membrane dynamics, particularly in surfactant systems. In Chapter 1, we demonstrated that LS membranes exhibited a tenfold increase in BODIPY-labeled SP-C diffusion coefficients compared to membranes composed of POPC or LM. This enhancement reflects greater lipid segregation and compartmentalization, consistent with the findings of Roldan *et al*. (2017) which further highlight the interplay between cholesterol and SP-C in membrane remodeling. SP-C has been widely recognized for its ability to modulate cholesterol distribution and mobility within membranes (Baumgart *et al.*, 2009; Plasencia *et al.*, 2008). This modulation has been associated with SP-C's capacity to induce membrane fragmentation, as observed in this chapter and previous studies (Parra *et al.*, 2013; Parra *et al.*, 2011; Roldan *et al.*, 2016) where it has been hypothesized that the curvature induced by SP-C facilitates the mobilization of cholesterol, which then integrated into the resulting vesicles. This process may represent a selective refinement mechanism that excludes unsaturated phospholipids and cholesterol from specific membrane domains. This phenomenon was clearly demonstrated in GUVs containing 10% SP-C, where fluorescence in micrographs revealed high concentrations of rhodamine-DOPE (an unsaturated lipid) and BODIPY-labeled SP-C in specific vesicle regions. Interestingly, while SP-C's modulatory role in membrane cholesterol distribution has been well documented, our findings indicate that cholesterol-containing membranes (LS) are more prone to fragmentation than cholesterol-free systems, such as DPPC/POPC/POPG mixtures. These results suggest a synergistic mechanism in which cholesterol contributes to membrane structural modulation, promoting SP-C confinement and increasing its local concentration. This localized enrichment of SP-C could facilitate membrane curvature and, ultimately, fragmentation. In turn, SP-C mobilizes cholesterol and unsaturated lipids, confining them within specific vesicle domains and regulating their distribution in pulmonary surfactant membranes. This dynamic interplay has been reported in previous studies (Baumgart *et al.*, 2009; Baumgart *et al.*, 2010; Gómez-Gil, Schürch, *et al.*, 2009) and is supported by our observations.

These findings underscore the significant impact of lipid composition on SP-C interactions and the underlying mechanisms of vesicle fragmentation. The distinct behaviors observed in ncLM and LS systems reflect how subtle differences in lipid composition could influence SP-C actions and its ability to modulate membrane structure. It could be valuable to determine the minimum SP-C concentration required for fragmentation in each lipid system, as these thresholds are likely lower for ncLM and LS compared to DPPC/POPC/POPG systems. This hypothesis is supported by the observation that GUVs with just 1% BODIPY-labeled SP-C exhibited significant protein localization within the membrane, suggesting that

lipid refinement and vesicle fragmentation had already occurred. Furthermore, it is important to consider that BODIPY labeling could affect SP-C's fragmentation efficiency, particularly if the N-terminal region plays a critical role in mediating these processes.

To further elucidate SP-C's functional mechanisms, this study also examined the contribution of the protein's palmitic chains, as well as the roles of its N- and C-terminal regions, to vesicle fragmentation.

Regarding the palmitoylation of the protein, it has been observed that, in all cases and regardless of the lipid composition of the membranes, rSP-C (non-palmitoylated) also induces a significant effect on vesicle fragmentation. This effect was reflected in the reduction of vesicle concentrations detected via NTA, consistent with the formation of vesicles of approximately 40 nm in size. These findings align with previous observations in POPC membranes containing 10% rSP-C, as described by Roldan *et al*. (2016), where such small vesicles were undetectable by NTA due to the system's detection limit. This supports the notion that, while palmitic acids play a crucial role in stabilizing and promoting the α-helical conformation of SP-C (Gustafsson *et al*., 2001; Johansson *et al*., 1995; Vandenbussche, Clercx, Curstedt, *et al*., 1992) the non-palmitoylated form retains the capacity to interact with membranes, likely through its helical segment or by alterations mediated via the N-terminal region (Plasencia *et al*., 2005; Plasencia *et al*., 2004; Qanbar *et al*., 1996; Wang *et al*., 1996).

As with SP-C, the extent of rSP-C-induced fragmentation varied across lipid systems, with a more pronounced effect observed in LS and ncLM membranes. This variability may be attributed to differences in lipid and protein compartmentalization as well as electrostatic interactions, as discussed in previous sections. Interestingly, given that rSP-C exhibits a higher propensity to form dimers (as detailed in Chapter 1), one might expect it to induce greater fragmentation compared to SP-C. However, the data suggest otherwise, likely due to the weaker membrane anchoring and reduced tilt of rSP-C within the bilayer (Baumgart *et al*., 2010; Roldan *et al*., 2015) or a different geometry imposed in non-acylated SP-C oligomers. These structural differences may result in lower membrane stress, thereby diminishing its ability to drive fragmentation.

Observations from GUVs composed of LM (DPPC/POPC/POPG) containing 10% rSP-C further corroborate this hypothesis. These GUVs displayed irregular morphologies, including oval shapes, rough surfaces, and small invaginations indicative of lipid phase segregation. This contrasts sharply with GUVs containing 10% palmitoylated SP-C, which exhibited homogenous membranes devoid of phase separation, suggesting a more efficient lipid refinement process associated with enhanced fragmentation. The reduced lipid refinement observed in rSP-C

systems suggests a less effective disruption of lipid domains, likely contributing to the observed differences in fragmentation efficiency.

Interestingly, NTA data revealed a higher level of fragmentation for rSP-C than SP-C in certain contexts, a finding that appears inconsistent with the previously mentioned observations. This discrepancy may arise from differences in analytical methods, limitations in detection sensitivity, or heterogeneity in the size distribution of the vesicles generated. These findings highlight the need for further experimentation to clarify the specific contribution of palmitoylation to SP-C-induced membrane fragmentation, particularly in LM systems.

Our NTA data suggest that palmitic chains slightly influence the fragmentation process, as SP-C-induced fragmentation is significantly higher in LS and ncLM lipid systems compared to rSP-C induced fragmentation. This could be due to the structural stabilization provided by the palmitic chains, which enhances the α-helical structure of SP-C, enabling more efficient interaction with membranes and promoting the curvature required for fission.

In LS lipid systems containing 10% rSP-C, most GUVs were observed to adhere to one another, forming aggregates. This phenomenon may reflect incomplete fragmentation, where membrane separation is insufficient, or strong interactions between rSP-C molecules in different membranes, potentially causing this variant to behave like an adhesion protein (Lipowsky, 2023; Schmid *et al.*, 2015; Tareste *et al.*, 2008). Such behavior underscores the complexity of SP-C dynamics in lipid systems and the impact of its acylation state on membrane remodeling processes.

In conclusion, while palmitoylation does not qualitatively alter SP-C's ability to fragment membranes at high concentrations, it significantly affects the extent of fragmentation. The greater fragmentation efficiency observed for palmitoylated SP-C highlights the importance of this modification in stabilizing its structure and optimizing its interactions within surfactant membranes. These findings suggest that palmitoylation may play a critical role in maintaining lipid homeostasis, particularly in pulmonary surfactant systems, where precise membrane remodeling is essential for functionality. Further investigations are needed to fully elucidate the mechanistic contributions of palmitic chains and their potential implications for therapeutic applications targeting SP-C functionality.

The roles of SP-C N- and C-terminal regions in vesicle fragmentation were studied to define the potential contribution of the proposed dimerization motifs (as described in Chapter 1) to membrane fragmentation, using peptides that emulate these regions of the protein. TRPS and NTA data from LUVs bearing the SP-C_{1-13} peptide showed that, despite having no effect on the vesicle concentration when applied alone, this peptide, in combination with full SP-C, exerts a synergistic effect on membrane fission. SP-C_{1-13} spans the outer N-terminal region of the

protein. Despite carrying the first leucine of the α-helix and an amide terminal modification, it is unlikely that this peptide could insert by itself deeply into the lipid bilayer due to its limited hydrophobicity (GRAVY index of 0.685). However, previous studies have shown that similar peptides comprising the N-terminus of SP-C interact spontaneously with lipid bilayers, arranging the amino acid chain parallel to the membrane surface even when they lack the palmitic groups (Plasencia *et al.*, 2004). Considering these data, it is reasonable to assume that this peptide interacts with native SP-C in the immediate vicinity of the bilayer, cooperatively inducing membrane fragmentation, possibly by facilitating the clustering of additional SP-C molecules. Similarly, synthetic peptides designed to include the PCCP motif from the mutated N-terminal fragment—either by substituting cysteines by alanines (mASP-C_{1-13} (C→A)) or cysteines by phenylalanines (mFSP-C_{1-13} (C→F) to mimic N-terminal palmitoylation—exhibit comparable behavior. This suggest that while the PCCP motif itself is not essential for SP-C clustering, the N-terminal region may play a critical role in modulating this process, even when minor modifications are introduced.

On the other hand, similar results were obtained with (AL)SP-C_{11-35} peptide: no changes were detected in LUVs containing only peptide, but when SP-C was included into the vesicle formulation, a cooperative effect on membrane fission was observed, even at greater extent than observed with SP-C_{1-13}. Given its sequence and its high GRAVY index, it is highly likely that (AL)SP-C_{11-35} adopts an α-helical conformation that spans the width of the membrane, except for the KR residues, which should remain exposed to the aqueous solvent. An interaction between the peptide and the whole protein through these positively charged amino acids, should be prevented a a consequence of electrostatic repulsion. Instead, the interaction could likely occurs via transmembrane residues and possibly through the AxxxG motif, similarly to what is observed in GpA (Kairys *et al.*, 2004). In this context, the findings with the mutant peptide in which alanine and glycine were substituted by isoleucines to prevent dimerization through steric hindrance, are contradictory. In membranes composed of LM, SP-C-mediated fragmentation was inhibited, resulting in vesicle concentrations similar to those observed in the absence of SP-C. However, in the purified lipid fraction of the native pulmonary surfactant (LS), a synergistic effect was still observed, albeit slightly (and not significantly) lower than that achieved with the C-terminal analog peptide (AL)SP-C11-35. This discrepancy could be attributed to the degree of lipid compartmentalization imposed by the dynamic interplay between cholesterol and SP-C. In the LS system, this interaction may overcome the steric hindrance introduced by the mutation, allowing the confined molecules to exert greater membrane stress than SP-C alone.

Nevertheless, it cannot be conclusively determined that the AxxxG motif actually acts as a definitive dimerization motif, although it seems plausible that it could contribute to the observed effects. Further investigations are required to elucidate its exact role in SP-C-mediated membrane remodeling and the observed synergistic effects. Taken together, all these results highlight that both ends of the SP-C are necessary, but not sufficient, for membrane fragmentation. Therefore, an integrated mechanism that simultaneously involves the two motifs in the full protein appears essential.

These findings underscore the critical role of SP-C in membrane fragmentation, a process intricately regulated by protein concentration, lipid composition, and interactions with components such as cholesterol and anionic lipids like POPG. SP-C's ability to remodel membranes is enhanced by palmitoylation, which stabilizes its α-helical structure and optimizes its interaction with lipid bilayers, while the non-palmitoylated form exhibits reduced efficiency. In cholesterol-rich environments, such as those existing in pulmonary surfactant systems, SP-C and cholesterol could engage in a synergistic relationship: SP-C-induced membrane curvature facilitates cholesterol redistribution, while cholesterol enhances membrane curvature and promotes SP-C confinement within specific domains. This interplay likely reflects a positive feedback mechanism that reinforces membrane remodeling.

During the respiratory cycle, the dynamic compression and expansion of alveolar membranes may create conditions conducive to the local accumulation of SP-C, where tilted, rigid α-helices could oligomerize to generate the membrane stress necessary for fission. This process leads to the formation of small vesicles enriched in SP-C and containing refined or selected lipids. These vesicles may subsequently be internalized by alveolar cells for recycling or processing of their components, highlighting SP-C's pivotal role not only in membrane remodeling but also in maintaining surfactant homeostasis within the alveoli. These results provide important insights into the molecular mechanisms underlying SP-C's function and its contribution to the dynamic regulation of pulmonary surfactant systems.

Flow cytometry assays were performed in Carlos III Health Institute under supervision of Dr. Mario Alia, coordinator of the cytometry unit of this institute.

Part of experiments included in this article were published at the following article:

Barriga A, Morán-Lalangui M, Castillo-Sánchez JC, Mingarro I, Pérez-Gil J, García-Álvarez B. **"Role of pulmonary surfactant protein Sp-C dimerization on membrane fragmentation: An emergent mechanism involved in lung defense and homeostasis."**

Biochim Biophys Acta Biomembr. 2021 Jun 1;1863(6):183572. doi: 10.1016/j.bbamem.2021.183572. Epub 2021 Feb 4. PMID: 33548215.

CHAPTER 3:

THE ROLE OF SP-C IN VESICLE UPTAKE AND INTRACELLULAR TRAFFICKING IN ALVEOLAR CELLS

Introduction

The uptake and trafficking of vesicles by alveolar cells are processes essential for pulmonary homeostasis and immune defense. These mechanisms support the recycling of surfactant components, the clearance of inhaled particles, and the preservation of alveolar integrity (Cañadas *et al.*, 2020). In this complex system, surfactant protein C (SP-C) may play a pivotal role, not only in enhancing the biophysical properties of pulmonary surfactant but also in mediating interactions between lipid vesicles and alveolar cells. As a matter of fact, the expression of the STFPC gene is tightly associated with the differentiation of the lung tissue(Korfhagen *et al.*, 1990; Wade *et al.*, 2006). SP-C's ability to fragment lipid membranes and facilitate vesicle formation (as discussed in Chapter 2), underscores its significant role in vesicle internalization across various lung cell types.

SP-C is primarily associated with type II alveolar epithelial cells (AECII) and probably with alveolar macrophages (AMϕ), where it plays a critical role in surfactant metabolism and immune regulation (Haagsman & Van Golde, 1991; Olmeda *et al.*, 2017; Weaver & Whitsett, 1991; Whitsett *et al.*, 2010). The palmitoylated N-terminal domain of SP-C facilitates interactions with lipid membranes, promoting membrane curvature and vesicle formation (Plasencia *et al.*, 2008; Qanbar *et al.*, 1996; Wang *et al.*, 1996). Beyond its structural functions, SP-C also interacts with lipopolysaccharides (LPS) through both hydrophobic and electrostatic forces. SP-C recognizes the lipid A region of LPS, targeting the terminal phosphate group at the reducing end of the lipid A disaccharide in alpha configuration, as well as the N-linked fatty acyl chain on the reducing glucosamine of lipid A. While these interactions do not require SP-C's palmitoyl chains, both the hydrophilic and hydrophobic regions of the protein are essential for specific LPS binding (Augusto *et al.*, 2001; Augusto *et al.*, 2002). This binding not only neutralizes LPS toxicity but may also facilitate its presentation to alveolar cells, thereby modulating the immune response and reducing the risk of endotoxin-induced inflammation (Garcia-Verdugo *et al.*, 2009; Väyrynen *et al.*, 2002).

Despite its well-documented role in surfactant function, the specific mechanisms by which SP-C influences vesicle uptake are not fully understood. Previous studies have suggested that SP-C enhances vesicle uptake by AMϕ, potentially through mechanisms involving membrane fragmentation and vesicle size reduction (Ikegami, Horowitz, *et al.*, 1998; Kelly *et al.*, 2011; Poelma *et al.*, 2004; Roldan *et al.*, 2016; Sane & Young, 1994; Schwendener *et al.*, 1984). However, its effects on AECII and its interactions with other surfactant proteins, such as SP-B, remain less explored. Similarly, the impact of lipid composition, vesicle size, and external factors, such as LPS, on SP-C mediated uptake warrants further investigation.

In this chapter, we provide a detailed analysis of the role of SP-C in vesicle uptake by alveolar-like cells, focusing on its interactions with different lipid compositions and its modulation by other surfactant proteins and external stimuli. Using alveolar macrophage-like MH-S cells and pneumocyte-derived A549 cells, we systematically investigate how SP-C concentration, vesicle size, and lipid composition influence the efficiency and specificity of vesicle internalization. Furthermore, we investigate the intracellular fate of SP-C, exploring its colocalization with acidic organelles, such as lysosomes and lamellar bodies, to understand its role in intracellular trafficking.

To address these questions, we employ advanced imaging techniques, including epifluorescence and confocal microscopy, combined with quantitative analyses such as flow cytometry. These methodologies allow us to investigate the role of SP-C mediated vesicle uptake at both cellular and molecular levels. By comparing the behaviors of palmitoylated native SP-C and its non-palmitoylated recombinant counterpart (rSP-C), we also assess the functional importance of SP-C's post-translational modifications in facilitating vesicle interactions.

This work builds on existing knowledge by integrating biophysical and cellular perspectives to elucidate the mechanisms underlying SP-C-mediated vesicle uptake. The findings presented here have broader implications for understanding the pulmonary surfactant system, particularly its role in immune modulation and homeostasis. Moreover, these insights may inform therapeutic strategies that utilize surfactant components for drug delivery or the treatment of surfactant-related disorders.

In summary, this chapter aims to deepen our understanding of SP-C's multifaceted roles in vesicle uptake and intracellular trafficking within alveolar-like cells. By linking its biophysical properties to cellular functions, we provide a comprehensive framework for investigating SP-C's contributions to pulmonary biology and its potential as a therapeutic target in respiratory diseases.

Results

Role of SP-C in vesicle uptake by alveolar cells

The vesicle uptake induced by SP-C was studied in cell lines derived from AMϕ (MH-S) or AECII (A549) through epifluorescence microscopy assays. Fluorescent LUVs composed by DPPC/POPC/POPG/rhodamine-DOPE (50/25/15/1; w/w/w/w) and 7.5% of SP-C by mass ratio were used to determine the level of vesicle endocytosis. Epifluorescence microscopy experiments showed no autofluorescence (**Figure 3.1A, D, G, J**) or vesicle association to the membrane in both cell lines (**Figure 3.1B-C and 3.1H-I**) due to absence of rhodamine signal when LUVs were immediately removed after incubation. A slight increase in

rhodamine-derived fluorescence in the cytoplasm of MH-S cells was observed when they were incubated for two hours with LUVs lacking SP-C, indicating the basal uptake level for these cells (**Figure 3.1E**). However, when cells were exposed to LUVs containing 7.5% SP-C, rhodamine-derived fluorescence uniformly increased in the cytoplasm of all MH-S cells (**Figure 3.1F**). Similar results were achieved with the A549 cell line: few cells showed a minor increase in fluorescence when incubated with LUVs lacking SP-C (**Figure 3.1K vs. 3.1E**), whereas a considerable increase in fluorescence internalization was observed when the cells were cultured with LUVs containing 7.5% of SP-C (**Figure 3.1L**). Furthermore, in this cell type, the fluorescence was concentrated in discrete perinuclear spots within the cytoplasm, probably reflecting the location of lamellar bodies in AECII which will be studied using colocalization assays in this chapter.

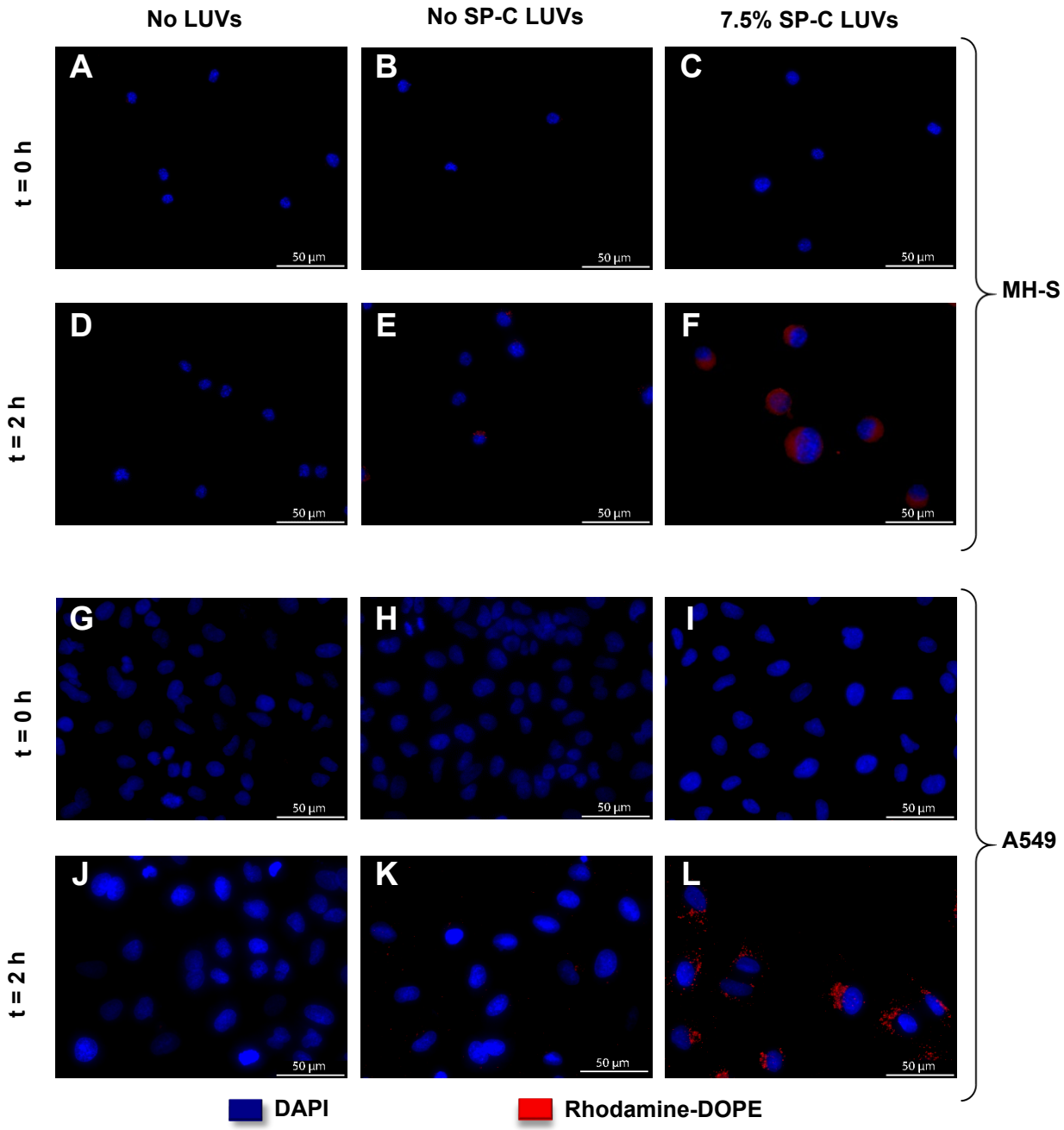

Figure 3.1. Endocytosis of LUVs by alveolar cell lines. A-F) Illustrative micrographs depicting MH-S cells (an AM-derived cell line) after being incubated for 0 or 2 hours with A,D) Tris buffer; B,E) 100 nm LUVs or C,F) 100 nm LUVs containing 7.5% SP-C. **G-L)** Illustrative micrographs depicting A549 cells (an AECII-derived cell line) after incubation for 0 or 2 hours with G,J) Tris buffer; H,K) 100 nm LUVs or I,L) 100 nm LUVs containing 7.5% SP-C. In all micrographs, nuclei were stained with DAPI (blue) while rhodamine-derived fluorescence of LUVs is represented in red.

We aimed to quantitatively determine the levels of fluorescence associated with LUV uptake. For this purpose, we performed flow cytometry assays using cells incubated with rhodamine-labeled LUVs, similar to the conditions used in the epifluorescence microscopy observations. However, we extended the set of conditions in these experiments to vesicles of different sizes (LUVs manufactured

using extrusion membranes of 50, 100 or 200 nm pore size). Moreover, besides LUVs containing no SP-C or the critical SP-C composition of 7.5%, we used vesicles including slightly more (10%) or less (5%) SP-C to assess the possible role of membrane fission in cellular uptake. Additionally, we included LUVs carrying physiological levels of the protein (1%). Representative experiments using this methodology with MH-S and A549 cells are presented in **Figure 3.2A and B**, respectively, where the resulting histograms of fluorescence intensity derived from cells incubated with 100 nm LUVs are shown.

These experiments were systematically repeated for MH-S, A549 and HEK 293T cells (kidney epithelial cells) using 50, 100 and 200 nm LUVs containing varying amount of SP-C. For all cell lines, a slight increase in fluorescence was detected when cells were incubated with LUVs lacking SP-C (**Figure 3.2C-K**). However, a distinct pattern for each cell line was observed when cells were incubated with LUVs containing different SP-C content. First, when these assays were performed using MH-S cells, a remarkable increase in fluorescence was observed, but only when SP-C concentrations reached 7.5% or higher (**Figure 3.2C-E**). These results may reflect the role of membrane fragmentation and the consequent reduction of vesicle size in facilitating cellular uptake. This effect was evident for all vesicles sizes tested, but it was especially pronounced with 50nm LUVs (**Figure 3.2C**). In contrast, while a notable fluorescence increase was observed in A549 cells, the overall levels of vesicle uptake increased with higher SP-C concentration (**Figure 3.2F-H**). Therefore, in these cells, phagocytosis appears to be dependent on the amount of SP-C present, rather than on the fragmentation mechanism. To confirm that vesicle uptake is specific of these cells, we performed the same set of experiments using the non-phagocytic HEK 293T cell line. Fluorescence levels showed no significant change when cells were incubated with LUVs containing no SP-C or low amounts of SP-C, with only a slight increase when using high SP-C concentrations (**Figure 3.2I-K**). These data would suggest that these vesicles are poorly incorporated into non-phagocytic cells and that the SP-C-dependent uptake mechanism is specific to alveolar phagocytic cells.

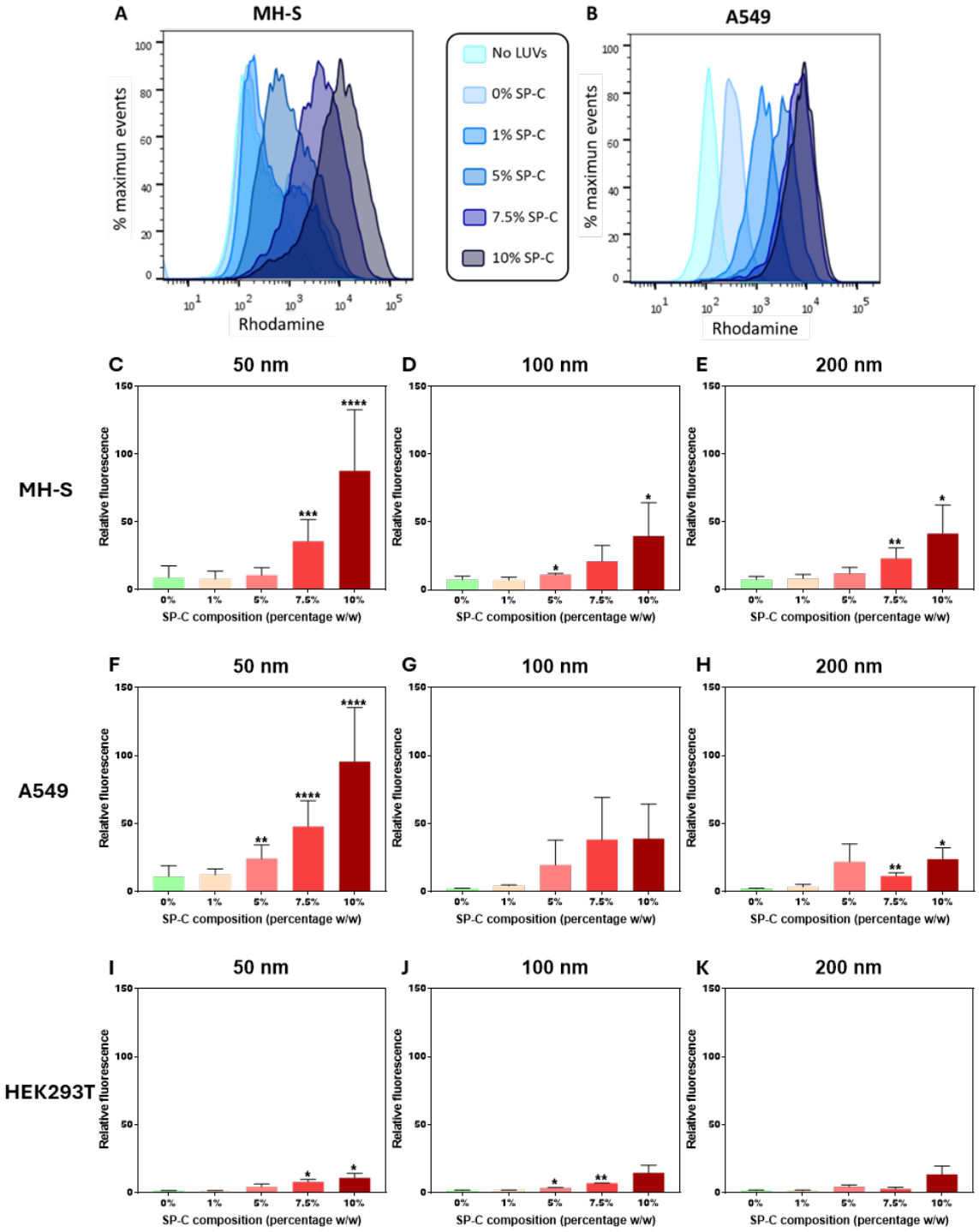

Figure 3.2: LUV uptake by alveolar cell lines. A) *Representative fluorescence histograms obtained using flow cytometry assays from MH-S cells or* ***B)*** *A549 cells incubated for 2 hours with rhodamine-labeled LUVs loading different SP-C content, as indicated in the legend.* ***C-E)*** *Mean fluorescence values obtained when MH-S cells were incubated for 2 hours with C) 50 nm, D) 100 nm, or E) 200 nm LUVS varying SP-C proportion.* ***F-H)*** *Mean fluorescence obtained when A549 cells were incubated for 2 hours with F) 50 nm, G) 100 nm, or H)200 nm LUVS varying SP-C proportion.* ***I-K)*** *Mean fluorescence obtained when HEK293T cells incubated for 2 hours with (I) 50 nm, (J) 100nm, or (K) 200 nm LUVS varying SP-C proportion. All values are expressed as means ± S.E.M. Statistical analyses were performed using an unpaired Student's t-test. Significant p-values compared to LUVs without SP-C are indicated by asterisks above the bars (*, $p < 0.05$; **, $p < 0.01$; ***, $p < 0.001$; ****, $p < 0.0001$).*

The non-palmitoylated recombinant human version of SP-C (rSP-C) was used to study the involvement of SP-C's palmitic chains in vesicle internalization. For this purpose, assays similar to those described above were performed using only vesicles of 50 nm diameter, as SP-C-mediated uptake is maximal at this size in both cell lines, which had a lipid composition of DPPC/POPC/POPG (50/25/15, w/w/w). As mentioned earlier, in A549 cells, the uptake appears to be dependent on SP-C concentration. To further investigate this, we have added an intermediate concentration (2.5%) in the protein mass ratio.

In the alveolar macrophage-derived cell line MH-S, unlike with native SP-C, an increase in rSP-C concentration did not enhance cell-associated fluorescence from the rhodamine-DOPE in the vesicles, even when concentration is higher than 7.5% by mass lipid ratio. The fluorescence remained comparable to that of cells incubated without protein, suggesting that SP-C palmitoylation is essential for vesicle uptake (**Figure 3.3A**). Similarly, in A549 cells, the non-palmitoylated rSP-C did not promote vesicle internalization (**Figure 3.3B**). Interestingly, fluorescence levels at 2.5% of SP-C were slightly higher that 1% though this difference was not statistically significant.

These results indicate that palmitoylation is indispensable for SP-C-mediated cellular endocytosis, likely facilitating membrane–membrane interactions or promoting increased vesicle fragmentation.

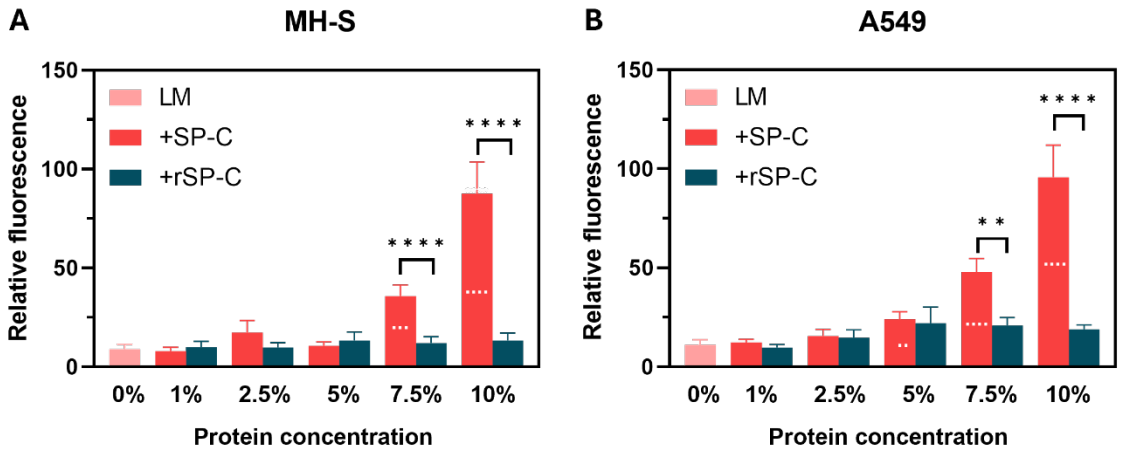

Figure 3.3: Contribution of palmitic chains in LUV uptake mediated by SP-C. A) *Mean fluorescence obtained using flow cytometry assays upon incubation of MH-S cells for 2 hours with rhodamine-labeled LUVs (50 nm) containing varying concentrations of native SP-C (in red) or non-palmitoylated recombinant rSP-C (in blue), as indicated in the legend. The lipid composition is LM (DPPC/POCP/POPG/rhodamine-DOPE, 50/25/15/1, w/w/w/w).* ***B)*** *Mean fluorescence intensity of A549 cells incubated under the same conditions as in panel (A). All values are expressed as means ± S.E.M. Statistically significant differences between palmitoylated SP-C and non-palmitoylated rSP-C are denoted by boxes, with asterisks indicating the level of significance. Comparisons between each concentration condition of SP-C or rSP-C and lipid vesicles without protein are marked by white squares within each bar. Statistical analyses were performed using an unpaired Student's t-test. Significance levels are denoted as follows**; ▪▪ $p < 0.01$; ▪▪▪ $p < 0.001$; ****; ▪▪▪▪ $p < 0.0001$.*

SP-C, due to its positive charge, interacts effectively with anionic lipids such as POPG, which are present in the lipid model mixtures used in previous experiments. As described in Chapter 2, SP-C fragmentation is significantly higher when large unilamellar vesicles (LUVs) are composed of a non-charged lipid mixture containing only DPPC and POPC (60/30, w/w). To explore this further, vesicle uptake experiments were conducted using the non-charged lipid mixture (ncLM) without POPG (DPPC/POPC/rhodamine-DOPE, 60/30, w/w/w).

Our results indicate that in MH-S cells, the absence of POPG in the vesicles leads to a marked increase in SP-C-mediated uptake of LUVs. This enhancement is evident at a minimum SP-C concentration of 2.5% in the ncLM system, whereas 7.5% SP-C is required to achieve comparable uptake levels in the POPG-containing lipid model system (LM). Notably, the fluorescence levels observed with 2.5% SP-C in the ncLM system exceed those obtained with 7.5% SP-C in the LM system. Furthermore, vesicles with 10% SP-C in the ncLM system produce fluorescence levels approximately 10 times higher than those observed with the same SP-C concentration in the LM system (**Figure 3.4A**). These results highlight the critical role of lipid composition in modulating SP-C-mediated vesicle uptake, particularly in immune cell types like MH-S.

In contrast, A549 cells show no apparent dependence on vesicle lipid composition for uptake. Similar fluorescence levels are observed at all SP-C concentrations and lipid compositions tested, supporting the hypothesis that vesicle uptake by A549 cells does not rely so much on SP-C fragmentation (**Figure 3.4B**). These findings highlight a clear difference in the mechanisms underlying SP-C-mediated vesicle uptake between MH-S and A549 cells.

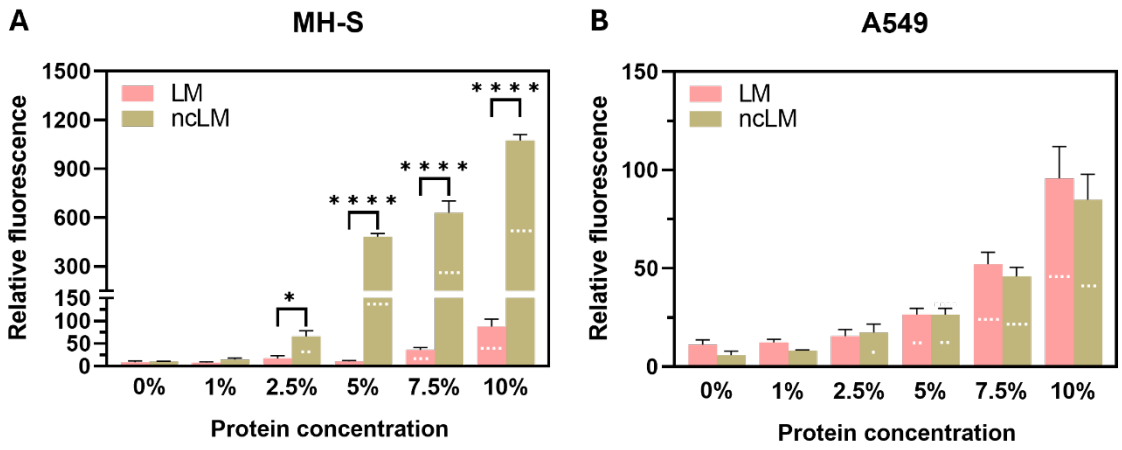

Figure 3.4: Impact of lipid composition on LUV uptake mediated by SP-C. A) *Mean fluorescence obtained using flow cytometry assays when MH-S cells were incubated for 2 hours with rhodamine-labeled LUVs of 50 nm containing varying concentrations of native SP-C, as indicated in the legend. The lipid compositions used were LM (DPPC/POPC/POPG/rhodamine-DOPE, 50/25/15/1, w/w/w) in pink and ncLM (DPPC/POPC/rhodamine-DOPE, 60/30/1, w/w/w) in brown.* ***B)*** *Mean fluorescence intensity of A549 cells incubated under the same conditions as in panel (A). All values are expressed as means ± S.E.M. Statistically significant differences between the different lipid mixture compositions are denoted by boxes, with asterisks*

*indicating the level of significance. Differences between each concentration condition of SP-C and its corresponding lipid vesicles without protein are marked by white squares within each bar. Statistical analyses were performed using an unpaired Student's t-test. Significance levels are denoted as follows: *,▪ $p < 0.5$, ▪▪ $p < 0.01$; ▪▪▪ $p < 0.001$; ****, ▪▪▪▪ $p < 0.0001$.*

Finally, the effect of lipid composition on vesicle uptake in the presence of rSP-C was studied. Native palmitoylated SP-C induced higher cellular fluorescence levels compared to rSP-C, confirming that palmitoylation is crucial for vesicle endocytosis by both A549 cells and MH-S cells, regardless of lipid composition (**Figure 3.5A-B**). However, it was observed that at 5% or 7.5% SP-C, depending on the specific cell type, rSP-C could promote the internalization of vesicles composed of ncLM in MH-S and A549 cells, respectively. In contrast, vesicles composed of the lipid model mixture, LM, were not internalized even at high concentrations of rSP-C (10% w/w). Therefore, lipid composition plays a key role in vesicle internalization. In this case, the absence of POPG enhances the effect of SP-C on uptake and allows the non-palmitoylated rSP-C to exert some activity.

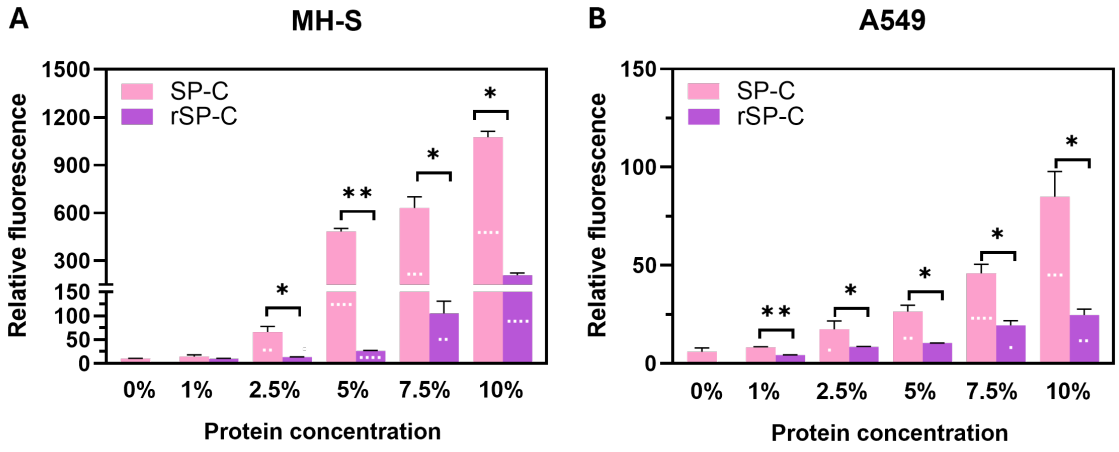

Figure 3.5: Contribution of palmitic chains to LUV uptake mediated by SP-C. A) *Mean fluorescence obtained using flow cytometry assays when MH-S cells were incubated for 2 hours with rhodamine-labeled LUVs of 50 nm containing varying concentrations of native SP-C (in pink) or non-palmitoylated recombinant rSP-C (in purple), as indicated in the legend, with the lipid composition being ncLM (DPPC/POCP/rhodamine-DOPE, 60/30/1, w/w/w).* ***B)*** *Mean fluorescence intensity of A549 cells incubated under the same conditions as in panel (A). All values are expressed as means ± S.E.M. Statistically significant differences between palmitoylated SP-C and non-palmitoylated rSP-C are denoted by boxes, with asterisks indicating the level of significance. Comparisons between each concentration of SP-C or rSP-C and lipid vesicles without protein are marked by white squares within each bar. Statistical analyses were performed using an unpaired Student's t-test. Significance levels are denoted as follows: **, ▪▪ $p < 0.01$; ▪▪▪ $p < 0.001$; ****, ▪▪▪▪ $p < 0.0001$.*

Effect of SP-B and LPS on SP-C-Dependent Vesicle Uptake

We have determined that SP-C promotes vesicle uptake by alveolar-like cells. To further investigate this phenomenon, we studied the combined effect of the hydrophobic surfactant proteins SP-C and SP-B. Preliminary uptake assays were performed using epifluorescence microscopy by incubating alveolar-like cells with 100 nm LUVs composed of LM (DPPC/POPC/POPG/rhodamine-DOPE, 50/25/15/1, w/w/w/w) with or without 10% SP-C and with/without 10% SP-B.

In MH-S cells, similar rhodamine-DOPE fluorescence intensities (in red) were observed whether the vesicles contained SP-C, SP-B, or both (**Figure 3.6B-D**). In contrast, no fluorescence was detected in the absence of proteins in the vesicles (**Figure 3.6A**), confirming the role of SP-C and SP-B in promoting vesicle uptake being. However, in A549 cells, vesicles containing both SP-C and SP-B produced significantly higher fluorescence intensities compared to those containing only SP-C (**Figure 3.6H vs 3.6F**). Micrographs of cells incubated with vesicles containing SP-C or SP-B exhibited fluorescence patterns distinct from those incubated with LUVs composed solely of LM, which showed no detectable fluorescence (**Figure 3.6E-G**). Furthermore, the morphology and distribution of rhodamine-DOPE fluorescence intensities (in red) differed noticeably in A549 cells depending on the protein loading. Cells incubated with SP-C-containing vesicles exhibited defined punctate fluorescence patterns, indicative of discrete vesicle uptake (**Figure 3.6F**). In contrast, cells incubated with vesicles containing both SP-C and SP-B displayed circular aggregates and a diffuse fluorescence distribution throughout the cell. This pattern suggests potential vesicle fusion and adherence to the cell membrane, making it unclear whether the vesicles are internalized or remain associated with the cell surface.

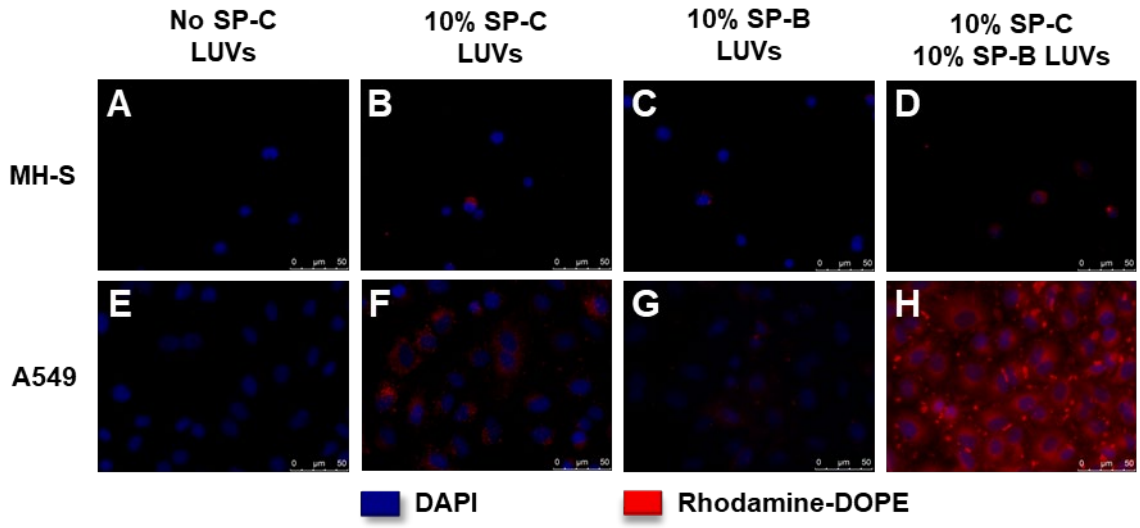

Figure 3.6: LUVs uptake by alveolar cell lines. A-D) *Illustrative micrographs depicting MH-S cells, an AM-derived cell line, and* ***E-H)*** *A549 cells, an AECII-derived cell line, after being incubated for 2 hours with A, E) Tris buffer; B, F) 100 nm LUVs containing 7.5% SP-C; C, G) 100 nm LUVs containing 10% SP-B, and D,H) 100 nm LUVs containing 10% SP-C and 10% SP-B. In all micrographs, nuclei were stained with DAPI (blue), while rhodamine-derived fluorescence of LUVs is represented in red.*

To further investigate the internalization of lipids and SP-C, analogous flow cytometry experiments were conducted using 50 nm vesicles with different lipid compositions, all of them including 1% of rhodamine-DOPE, where SP-C was fluorescently labeled with BODIPY (BSP-C).

The results obtained from MH-S cells were consistent with those observed via epifluorescence microscopy. Similarly to unlabeled SP-C, BSP-C increases rhodamine-DOPE fluorescence levels in MH-S cells across all lipid systems tested (**Figure 3.7A-C**). This effect is particularly pronounced when vesicles are composed of ncLM (DPPC/POPC/rhodamine-DOPE, 60/30/1, w/w/w) or the pulmonary surfactant lipid fraction (LS). Additionally, SP-B was found to slightly enhance vesicle uptake, irrespective of the lipid system (**Figure 3.7A-C**). However, BSP-C demonstrated a significantly greater effect, particularly when vesicles were composed of ncLM (**Figure 3.7B**), with an even more pronounced increase in fluorescence when vesicles were prepared with LS, the lipid fraction of surfactant (**Figure 3.7C**). In all lipid systems studied, lipid uptake was similar between cells incubated with LUVs containing BSP-C and LUVs containing both proteins, BSP-C and SP-B, indicating that SP-B does not interfere in vesicle uptake (**Figure 3.7A-C**).

In contrast, A549 cells did not exhibit the same pattern observed in epifluorescence microscopy. The combination of SP-B with BSP-C resulted in significantly lower cellular lipid fluorescence levels compared to vesicles containing SP-C alone in the LM lipid system (**Figure 3.7D**). In the ncLM and LS lipid systems, fluorescence levels were similar but not higher regardless of whether the vesicles contained both proteins or only SP-C. As observed in MH-S cells, SP-B promoted vesicle uptake although in a lesser extent that BSP-C in these epithelial cells (**Figure 3.7D-F**).

The uptake of the fluorescently labeled protein BSP-C in MH-S cells was found to be dependent on the lipid composition of the vesicles, similar to the observed cellular fluorescence levels corresponding to rhodamine-DOPE lipid. Cellular fluorescence associated with BODIPY was significantly higher when vesicles were composed of LS or ncLM compared to LM (**Figure 3.7G**). This highlights the critical role of lipid composition in protein uptake efficiency. Additionally, SP-B did not appear to affect BSP-C uptake, as no significant differences in fluorescence levels were observed between vesicles containing only BSP-C and those containing both BSP-C and SP-B. These findings suggest that SP-C plays a predominant role in protein uptake in this cell type, independent of SP-B.

In contrast, in A549 cells, where SP-C protein internalization does not depend on the lipid composition, fluorescence levels remain similar across all conditions tested in this assay. Notably, a decrease in BSP-C internalization by AECII-like A549 cells was observed when vesicles are composed of LM and SP-B (**Figure 3.7H**).

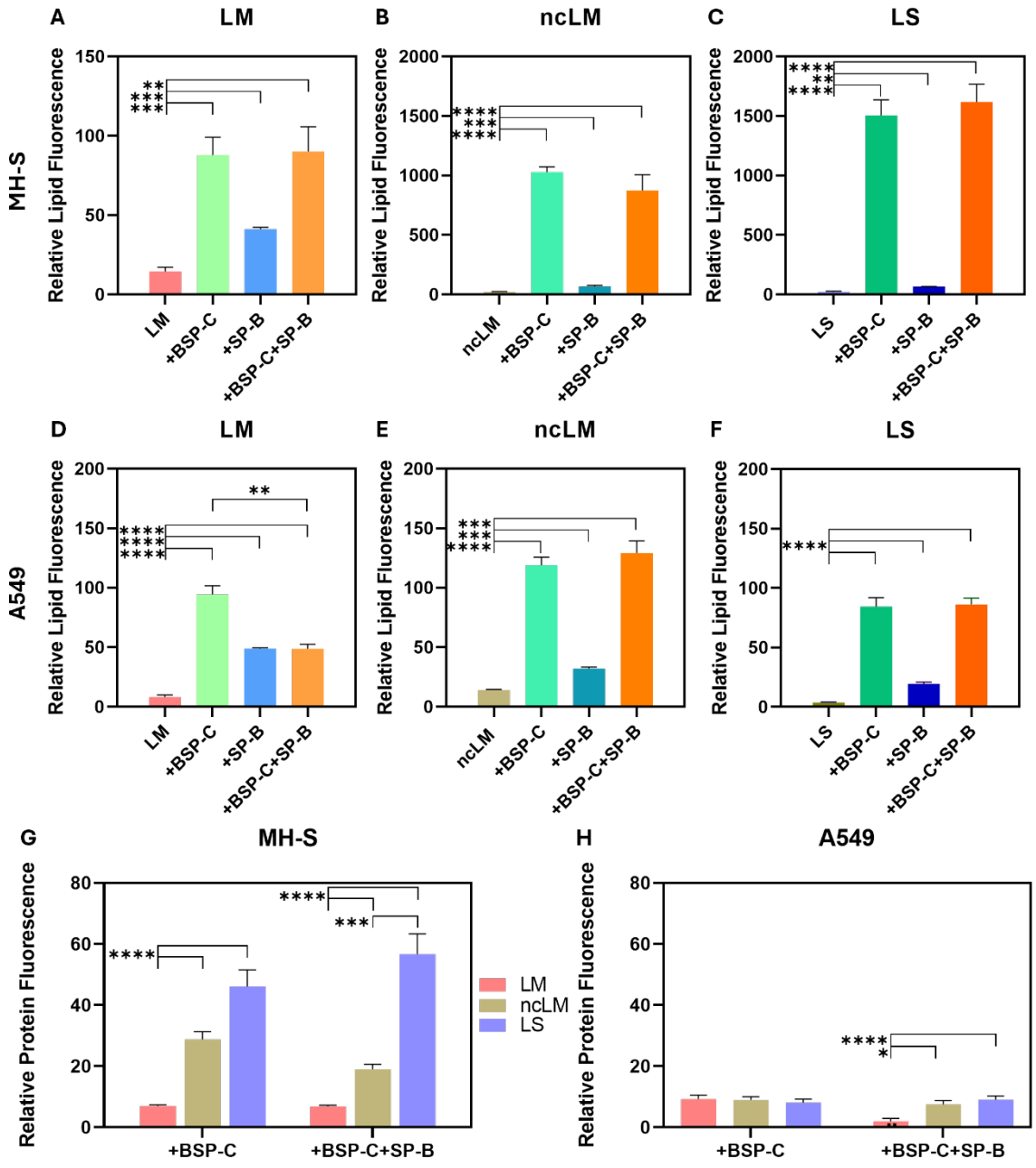

Figure 3.7: Effect of SP-B on LUVs uptake mediated by SP-C. *Mean fluorescence obtained using flow cytometry assays.* ***A-C)*** *Mean rhodamine-DOPE fluorescence in MH-S cells following a 2-hour incubation with 50 nm rhodamine-labeled LUVs containing BODIPY-labeled SP-C, SP-B, or both proteins. The lipid compositions of the vesicles were:* ***A)*** *LM (DPPC/POPC/POPG/rhodamine-DOPE, 50/25/15/1, w/w/w),* ***B)*** *ncLM (DPPC/POPC/rhodamine-DOPE, 60/30/1, w/w/w), and* ***C)*** *LS (lipid surfactant fraction).* ***D-F)*** *Mean rhodamine-DOPE fluorescence in A549 cells incubated under the same conditions as MH-S cells. The lipid compositions were:* ***D)*** *LM,* ***E)*** *ncLM, and* ***F)*** *LS.* ***G)*** *Mean fluorescence of BODIPY-labeled SP-C in MH-S cells after a 2-hour incubation with rhodamine-labeled LUVs containing BODIPY-labeled SP-C alone or in combination with SP-B. Vesicle lipid compositions were LM (brown), ncLM (brown), and LS (blue).* ***H)*** *Mean fluorescence of BODIPY-labeled SP-C in A549 cells under the same conditions as in panel G. Vesicle lipid compositions were LM (brown), ncLM (brown), and LS (blue). All values are expressed as means ± S.E.M. Statistically significant differences are highlighted with boxes, and asterisks indicate the level of significance. Comparisons between BODIPY-labeled SP-C and BODIPY-labeled SP-C plus SP-B are marked by squares within each bar. Statistical analyses were performed using an unpaired Student's t-test. Significance levels are denoted as follows: *, $p < 0.5$, ▪▪ $p < 0.01$; *** $p < 0.001$; **** $p < 0.0001$.*

To evaluate the potential synergistic action of SP-C and LPS Re 595 on vesicle uptake by alveolar cells, preliminary microscopy studies were performed. Alveolar-like cells were incubated with 50 nm vesicles composed of LM (DPPC/POPC/POPG/rhodamine-DOPE, 50/25/15/1, w/w/w/w) under four conditions: with or without 10% SP-C and with or without LPS at a molar ratio equivalent to 10% SP-C. No rhodamine-DOPE signal was detected inside either alveolar cell type when incubated with LUVs composed solely of lipids (**Figure 3.8A, E**).

In MH-S cells, LUVs composed solely of lipids appeared not to be internalized. The highest fluorescence intensity, corresponding to rhodamine-DOPE from the vesicles, was observed when LUVs contained both SP-C and LPS (**Figure 3.8D**). Uptake was also evident, although at lower levels, with vesicles containing SP-C or LPS alone (**Figure 3.8B-C**). These findings suggest that the combination of SP-C and LPS enhances vesicle uptake in MH-S cells.

In contrast, A549 cells displayed a different pattern. Vesicles containing SP-C alone resulted in the highest fluorescence intensity (**Figure 3.8F**). When LPS was combined with SP-C, a slight decrease in fluorescence was observed, and no fluorescence signal was detected in cells incubated with vesicles containing only lipids and LPS (**Figure 3.8F-G**). These results indicate that the presence of LPS inhibits SP-C-mediated vesicle uptake in A549 cells.

These outcomes highlight a cell-type-specific interaction between SP-C and LPS in vesicle uptake, suggesting that the effects of LPS are context-dependent and may modulate SP-C activity differently in immune cells (MH-S) and epithelial cells (A549).

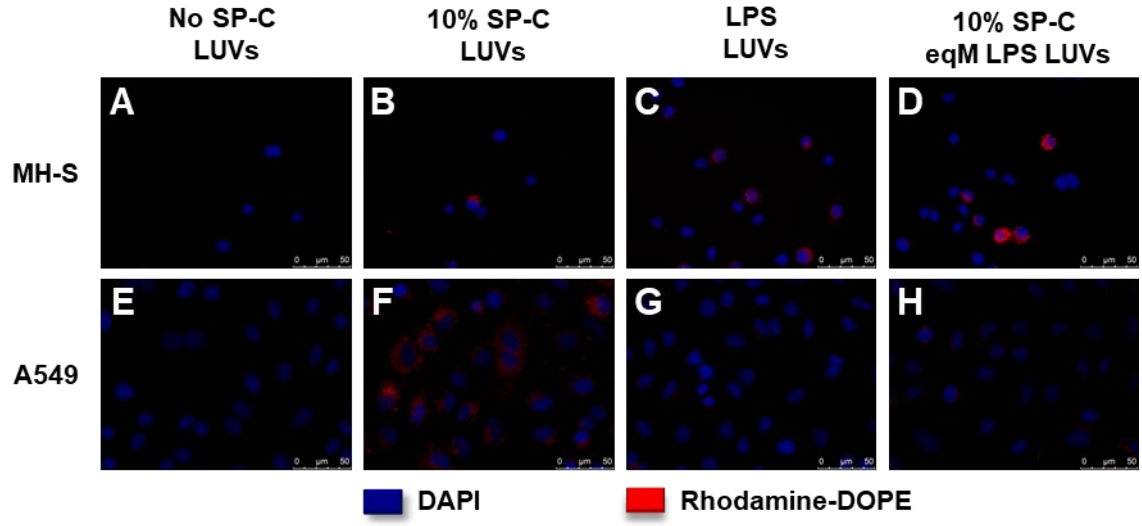

Figure 3.8: Uptake of LUVs by alveolar cell lines. A-D) *Representative micrographs depicting MH-S cells, an AM-derived cell line, and* ***E-H)*** *A549 cells, an AECII-derived cell line, after being incubated for 2 hours with: A,E) 100nm LUVs composed by DPPC/POPC/POPG/rhodamine-DOPE (50/25/15/1, w/w/w/w); B,F) 100 nm LUVs containing 10% SP-C; C,G) 100 nm LUVs containing LPS; and D,H) 100 nm LUVs containing 10% SP-C*

and equimolar LPS. In all micrographs, nuclei were stained with DAPI (blue), and rhodamine-derived fluorescence from LUVs is represented in red.

To evaluate the effect of LPS on SP-C-mediated vesicle internalization, fluorescent vesicle uptake experiments were performed using vesicles containing rhodamine-DOPE and 10% BSP-C. These vesicles were tested on two alveolar cell types, MH-S and A549, under conditions of different lipid composition.

LPS alone caused a modest increase in vesicle uptake by MH-S cells, although to a lesser extent than BODIPY-labeled SP-C. Interestingly, the combination of LPS and BSP-C in vesicles approximately doubled the uptake levels across all lipid systems (**Figure 3.9A-C**). This result suggests that MH-S cells may preferentially internalize vesicles containing LPS/BSP-C complexes. In contrast, in A549 cells incubated with vesicles of synthetic lipid composition (LM and ncLM), the presence of both LPS and BSP-C led to reduced rhodamine-DOPE fluorescence compared to vesicles containing BSP-C alone (**Figure 3.9D, E**). However, vesicles composed of the full surfactant lipid fraction (LS) showed increased rhodamine-DOPE fluorescence levels when both LPS and BSP-C were present, compared to vesicles containing only BSP-C (**Figure 3.9F**).

When analyzing BSP-C protein internalization by MH-S cells, a similar pattern to lipid uptake was observed. BSP-C uptake was significantly higher when the vesicle lipid composition was either ncLM or LS (**Figure 3.9A-B** vs. **Figure 3.9G**). Additionally, the combination of LPS and SP-C enhanced BSP-C-derived fluorescence compared to SP-C alone, with markedly higher levels observed in ncLM and LS lipid systems. Among these, LS vesicles yielded 50% higher BSP-C fluorescence than ncLM vesicles, highlighting the crucial role of lipid composition and LPS in BSP-C internalization by MH-S cells (**Figure 3.9G**).

In contrast, A549 cells showed no significant differences in BSP-C uptake across the different lipid compositions tested, as BSP-C fluorescence levels remained comparable (**Figure 3.9H**). However, in the presence of LPS, a slight increase in BSP-C fluorescence was observed, regardless of lipid composition. This behavior contrast with lipid uptake in A549 cells, where fluorescence levels decreased when LPS was combined with BSP-C, except in the LS lipid system (**Figure 3.9G vs. 3.9D-F**).

These results reveal critical differences in the mechanisms underlying vesicle internalization between MH-S and A549 cells. The data highlight the importance of LPS and lipid composition in BSP-C-mediated uptake, particularly in macrophage-like MH-S cells, while suggesting a contrasting inhibitory effect of LPS on SP-C-mediated uptake in epithelial A549 cells.

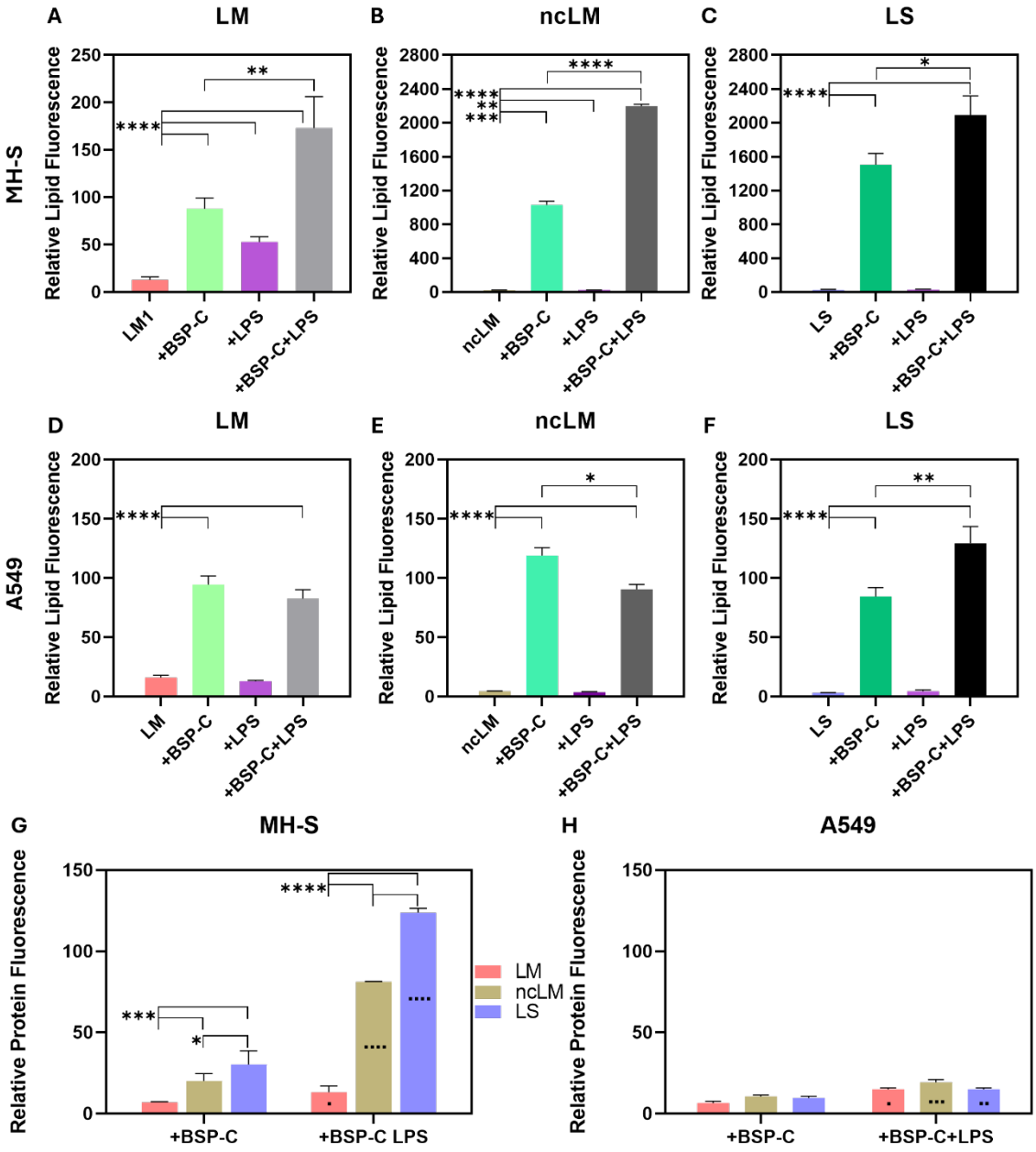

Figure 3.9: Impact of LPS on SP-C-Mediated Vesicle Internalization. *Mean fluorescence obtained using flow cytometry assays.* ***A-C)*** *Mean rhodamine-DOPE fluorescence in MH-S cells following a 2-hour incubation with 50 nm rhodamine-labeled LUVs containing BODIPY-labeled SP-C, LPS, or both. The lipid compositions of the vesicles were:* ***A)*** *LM (DPPC/POPC/POPG/rhodamine-DOPE, 50/25/15/1, w/w/w/w),* ***B)*** *ncLM (DPPC/POPC/rhodamine-DOPE, 60/30/1, w/w/w), and* ***C)*** *LS (lipid surfactant fraction).* ***D-F)*** *Mean rhodamine-DOPE fluorescence in A549 cells incubated under the same conditions as MH-S cells. The lipid compositions were:* ***D)*** *LM,* ***E)*** *ncLM, and* ***F)*** *LS.* ***G)*** *Mean fluorescence of BODIPY-labeled SP-C in MH-S cells after a 2-hour incubation with rhodamine-labeled LUVs containing BODIPY-labeled SP-C alone or in combination an equimolar concentration of LPS. Vesicle lipid compositions were LM (brown), ncLM (brown), and LS (blue).* ***H)*** *Mean fluorescence of BODIPY-labeled SP-C in A549 cells under the same conditions as in panel G. Vesicle lipid compositions were LM (brown), ncLM (brown), and LS (blue). All values are expressed as means ± S.E.M. Statistically significant differences are highlighted with boxes, and asterisks indicate the level of significance. Comparisons between BODIPY-labeled SP-C and BODIPY-labeled SP-C plus LPS are marked by squares within each bar. Statistical analyses were conducted using an unpaired Student's t-test. Significance levels are denoted as follows: *, ▪ $p < 0.5$, ▪▪ $p < 0.01$; **, ▪▪▪ $p < 0.001$; **** $p < 0.0001$.*

Intracellular Localization of SP-C and Its Colocalization with Acidic Organelles: Influence of Lipid Composition and LPS

Considering the flow cytometry results, which demonstrated increased uptake of lipid vesicles when SP-C was part of the composition, a laser confocal microscopy experiment was conducted to determine the localization of the protein after internalization by the cells. The aim was to assess whether colocalization ocurred between the signal from the protein, labeled with BODIPY, and acidic organelles-lysosomes and lamellar bodies, the latter being organelles present exclusively in AECII. Acidic organelles were labeled using the LysoTracker Red probe.

The experiment involved incubating either of the two cell types (MH-S or A549) for two hours with LysoTracker and SUV-type vesicles composed of one of three lipid systems: LM (DPPC/POPC/POPG, 50/25/15, w/w/w), ncLM (DPPC/POPC, 60/30, w/w), and LS (the full lipid fraction of pulmonary surfactant). The potential influence of LPS on colocalization was also assessed in both cell lines.

Quantitative colocalization results were analyzed using Manders' correlation coefficients (M1 and M2), which quantify the overlap between two fluorescence signals. The M1 coefficient indicates the proportion of green fluorescence (BODIPY-labeled SP-C) that overlaps with red fluorescence (lysosomes), while the M2 coefficient measures the proportion of red fluorescence (lysosomes) that overlaps with green fluorescence (BODIPY-labeled SP-C). Values closer to 1 indicate high colocalization, while values below 0.5 suggest limited overlap. Quantitative results obtained from confocal microscopy images (**Figures 3.10A and 3.11A**) are presented in **Figures 3.10B and 3.11B**.

For experiments conducted in AMϕ, the M1 correlation coefficient was greater than 0.85 in all cases. This indicates a significant overlap between the green BODIPY-labeled SP-C signal and the red lysosome signal, suggesting that SP-C predominantly localizes to lysosomes after internalization. However, the M2 correlation coefficient values were below 0.5, indicating that many lysosomes did not contain detectable SP-C, suggesting that only part of the acidic organelles were accessible to internalized SP-C (**Figure 3.10B**).

No significant differences were observed between lipid systems containing the protein in the absence of LPS, all three exhibited similar colocalization values. However, when LPS was included, LM and LS showed similar colocalization values, while ncLM exhibited significantly higher colocalization than both. Finally, comparisons within the same lipid system, with and without LPS, revealed no significant differences for LM and ncLM. However, in the LS system, colocalization decreased significantly upon the addition of LPS, suggesting a potential inhibitory effect of LPS on SP-C localization in lysosomes (**Figure 3.10B**).

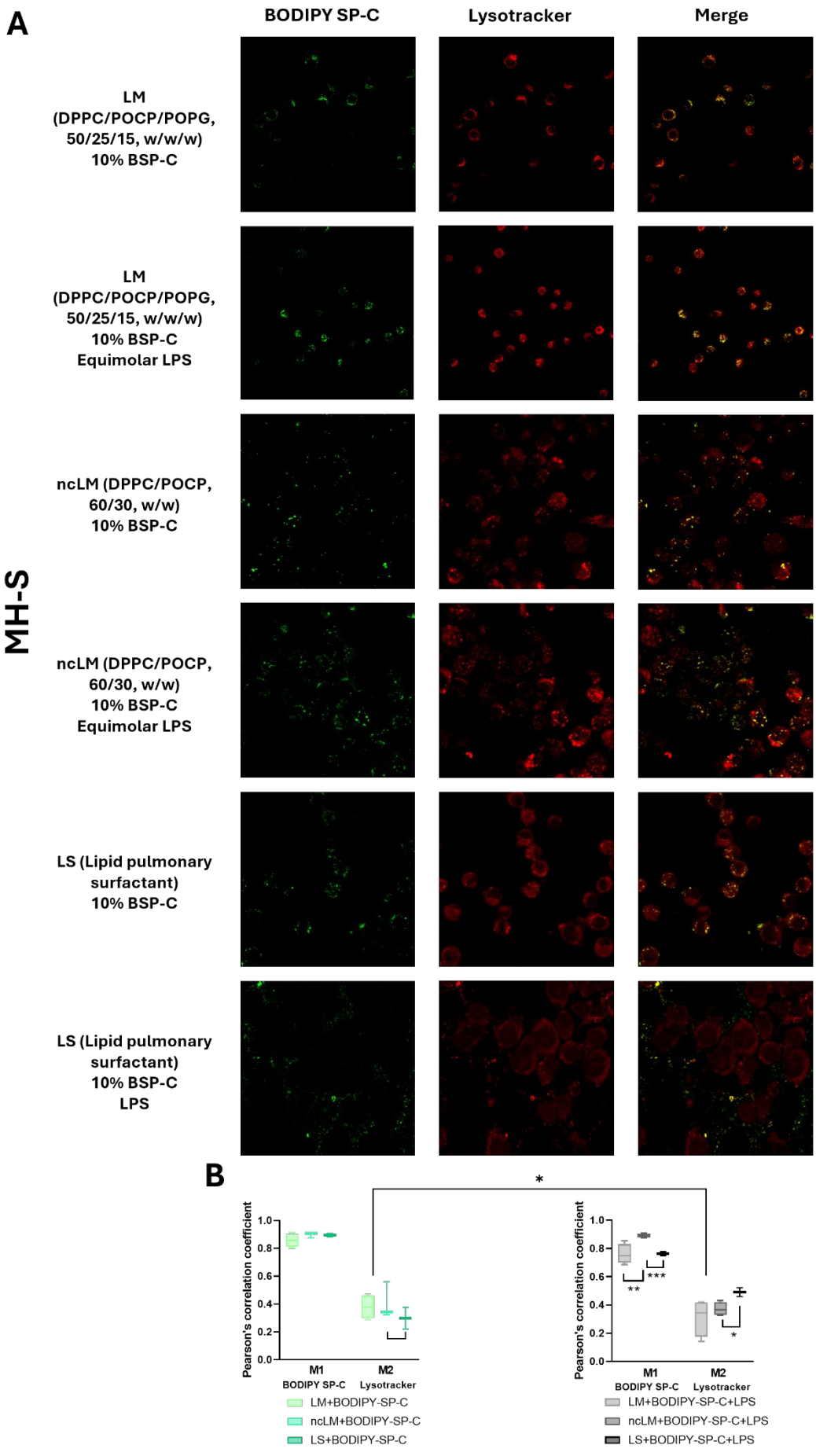
A
BODIPY SP-C
Lysotracker
Merge
MH-S
LM (DPPC/POCP/POPG, 50/25/15, w/w/w) 10% BSP-C
LM (DPPC/POCP/POPG, 50/25/15, w/w/w) 10% BSP-C Equimolar LPS
ncLM (DPPC/POCP, 60/30, w/w) 10% BSP-C
ncLM (DPPC/POCP, 60/30, w/w) 10% BSP-C Equimolar LPS
LS (Lipid pulmonary surfactant) 10% BSP-C
LS (Lipid pulmonary surfactant) 10% BSP-C LPS
B
Pearson's correlation coefficient
M1
BODIPY SP-C
M2
Lysotracker
LM+BODIPY-SP-C
ncLM+BODIPY-SP-C
LS+BODIPY-SP-C
LM+BODIPY-SP-C+LPS
ncLM+BODIPY-SP-C+LPS
LS+BODIPY-SP-C+LPS

Figure 3.10: Colocalization of acidic organelles and BODIPY-labeled SP-C in MH-S cells. *(A) Representative micrographs of MH-S cells incubated for 2 hours with LysoTracker Red (red signal) and fluorescently labeled vesicles containing BODIPY-labeled SP-C (green signal). Vesicle compositions are detailed in the figure legend. Images are Z-stack projections, with fluorescence values representing the average intensity of each slice. (B) Manders' Correlation Coefficients (M1 and M2) calculated using Fiji software from four independent images. Data quantify the colocalization between BODIPY-labeled SP-C and LysoTracker Red fluorescence.*

In A549 cells, M1 correlation coefficient values were also above 0.65 in all cases, indicating colocalization between the protein and acidic organelles. Comparing of colocalization values between lipid systems containing the protein in the absence of LPS revealed no significant differences between LM and ncLM. However, LS showed significantly higher colocalization to both (**Figure 3.11B**).

In lipid systems with LPS, LM and ncLM showed no significant differences in colocalization, nor did ncLM and LS. However, LS exhibited significantly higher colocalization than LM, suggesting that LS might promote SP-C localization more effectively when LPS is present. Comparison of colocalization values between the absence and presence of LPS within the same lipid system yielded results similar to those observed in MH-S cells. Only the colocalization coefficient for LS was significantly affected, showing a lower value when LPS was present compared to when it was absent.

These results indicate that SP-C localizes at acidic organelles in both cell types, as evidenced by the consistently high M1 coefficients. However, the extent of this colocalization varies depending on lipid composition and the presence of LPS. While MH-S cells show a preference for ncLM in the presence of LPS, A549 cells are less affected by LPS, except in the LS system, where LPS reduces colocalization. This suggests that LPS may modulate the intracellular trafficking and localization of SP-C, with effects that are dependent on both the lipid environment and the cell type.

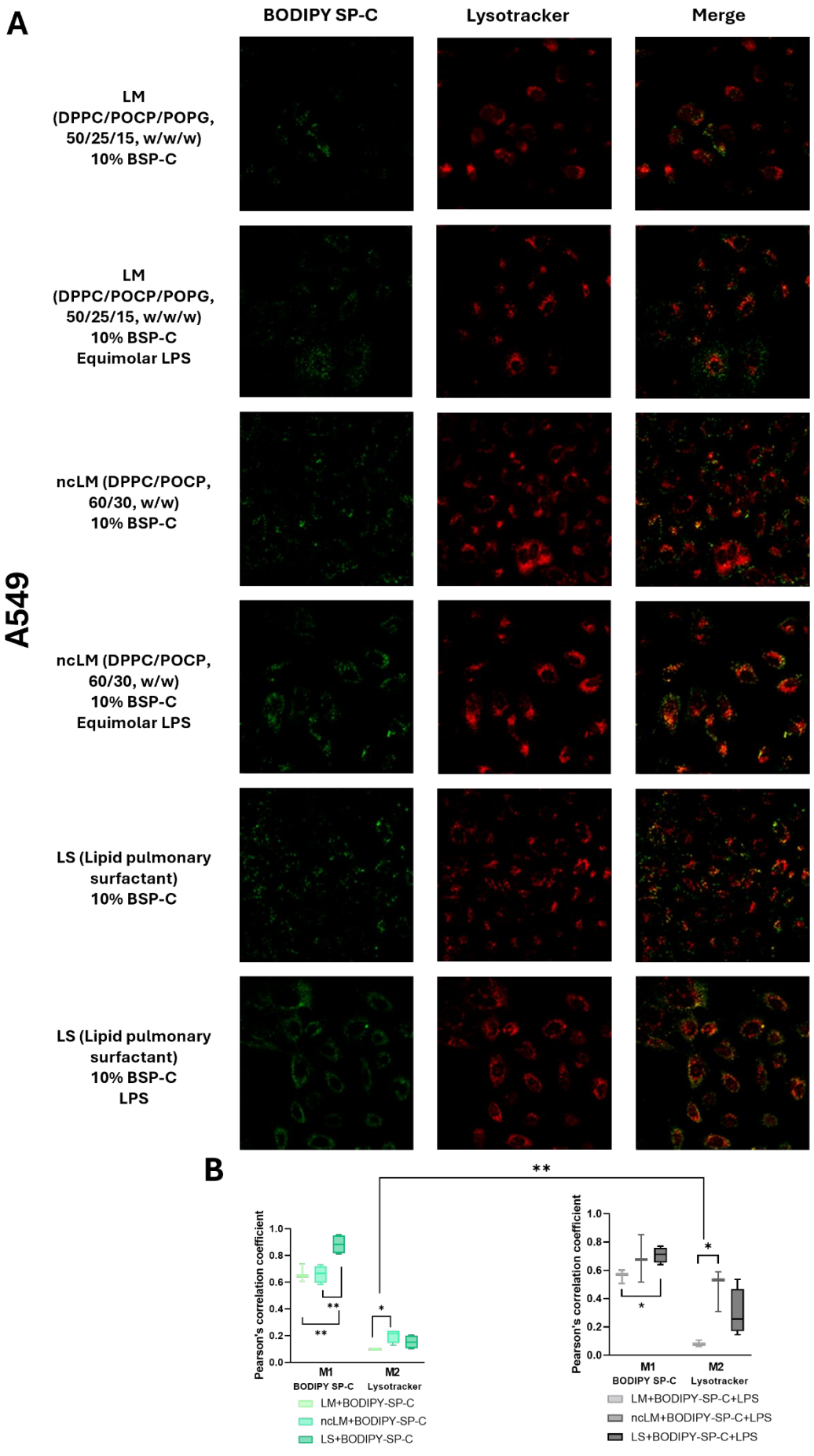
A
BODIPY SP-C
Lysotracker
Merge
LM (DPPC/POCP/POPG, 50/25/15, w/w/w) 10% BSP-C
LM (DPPC/POCP/POPG, 50/25/15, w/w/w) 10% BSP-C Equimolar LPS
ncLM (DPPC/POCP, 60/30, w/w) 10% BSP-C
ncLM (DPPC/POCP, 60/30, w/w) 10% BSP-C Equimolar LPS
LS (Lipid pulmonary surfactant) 10% BSP-C
LS (Lipid pulmonary surfactant) 10% BSP-C LPS
A549
B
Pearson's correlation coefficient
M1 BODIPY SP-C
M2 Lysotracker
LM+BODIPY-SP-C
ncLM+BODIPY-SP-C
LS+BODIPY-SP-C
LM+BODIPY-SP-C+LPS
ncLM+BODIPY-SP-C+LPS
LS+BODIPY-SP-C+LPS

Figure 3.11: Colocalization of acidic organelles and BODIPY-labeled SP-C in MH-S cells. A) *Representative micrographs of MH-S cells incubated for 2 hours with LysoTracker Red (red signal) and fluorescently labeled vesicles containing BODIPY-labeled SP-C (green signal). Vesicle compositions are detailed in the figure legend. Images are Z-stack projections, with fluorescence values representing the average intensity of each slice.* ***B)*** *Manders' Correlation Coefficients (M1 and M2) were calculated using Fiji software from four independent images. Data quantify the colocalization between BODIPY-labeled SP-C and LysoTracker Red fluorescence.*

Discussion

Alveolar macrophages (AMϕ) play a central role in the clearance of surfactant components and inhaled particles, making them critical for maintaining pulmonary homeostasis (Cañadas *et al.*, 2020; Olmeda *et al.*, 2017). Previous studies have suggested that the inclusion of SP-C in liposomes enhances their uptake by AMϕ (Poelma *et al.*, 2004), but the specific influence of SP-C concentration and the mechanisms underlying this effect had not been thoroughly explored.

In this study, we demonstrate that SP-C promotes vesicle uptake by AMϕ, with the effect becoming significant at concentrations exceeding 7.5%. Interestingly, this enhancement was independent of the initial vesicle size but was influenced by the lipid composition of the vesicles, as discussed below.

This uptake profile aligns with results from TRPS experiments (Chapter 2) revealing that 7.5% of SP-C (or higher) triggered membrane fragmentation in vesicles composed of DPPC/POPC/POPG, a synthetic mixture mimicking the lipid balance of lung surfactant, possibly generating small vesicles (~30–50 nm) (Roldan *et al.*, 2016). These small vesicles appear to act as efficient vehicles for AM-mediated clearance of substances, including potentially harmful materials (Roldan *et al.*, 2016). This fragmentation-driven mechanism correlates with increased vesicle uptake, as vesicle size is a critical determinant of endocytosis efficiency. Smaller vesicles are more readily internalized by macrophages, likely due to their compatibility with the size constraints of endocytic mechanisms (Kelly *et al.*, 2011; Schwendener *et al.*, 1984).

POPG has been described as essential for regulating the pulmonary immune system, particularly in reducing the release of inflammatory mediators like TNF-α and arachidonic acid in macrophages by competitively antagonizing ligand-dependent activation of toll-like receptors (TLRs) or blocking infection of epithelial cells by respiratory syncytial virus and influenza A virus (Hashimoto *et al.*, 2003; Kandasamy *et al.*, 2011; Numata *et al.*, 2010; Numata *et al.*, 2012). This regulation prevents macrophage activation into the M1 phenotype, associated with lower phagocytic activity (Chen *et al.*, 2023; Wang *et al.*, 2014). When experiments were conducted with vesicles lacking POPG (ncLM), a significant increase in fragmentation was observed, requiring only 2.5% SP-C for AMϕ uptake. This could be attributed to the role of POPG in regulating macrophage activation, as

previously noted. However, SP-C itself has been described as an inhibitor of pro-inflammatory mediator release (Augusto, Synguelakis, Espinassous, *et al*., 2003; Garcia-Verdugo *et al*., 2009). The observed increase in vesicle uptake does not appear to be driven by an inflammatory response but rather by SP-C's ability to induce membrane fragmentation. In the absence of POPG, SP-C could fragment membranes more efficiently, as described in Chapter 2, generating small vesicles. These small vesicles, due to their size and its enrichment in SP-C, are more likely to be engulfment by AMϕ, as detailed in this chapter. This highlights the dual role of SP-C in membrane remodeling and modulating vesicle-mediated clearance processes in the lung.

A similar pattern is observed with vesicles derived from the lipid fraction of native surfactant, where enhanced uptake may be attributed to the generation of small vesicles via SP-C-induced fragmentation (see Chapter 2). Additionally, the presence of cholesterol in these membranes could play a significant role, as described by Ruwisch *et al*. (2020). That study proposed an SP-C/cholesterol axis that regulates cholesterol metabolism and transport, influencing cellular function and preventing lipid accumulation. This regulation ensures lipid homeostasis by AMϕ and protects against fibrotic remodeling. Interestingly, no differences in uptake or fragmentation were observed between this system and vesicles lacking POPG, suggesting that AMϕ uptake is closely tied to SP-C-induced fragmentation and may primarily occur through endocytosis rather than receptor-mediated mechanisms. An alternative explanation for the increased uptake in this lipid system could be that POPG is inhibiting the endocytic activity of MH-S cells. However, in the lipid system derived from native surfactant, similar results are observed despite the presence of POPG, suggesting that its role may not be as decisive. The role of cholesterol in lipid composition and vesicle uptake warrants further investigation to determine whether AMϕ preferentially target cholesterol-rich vesicles. Vesicles with high cholesterol concentrations (20%) exhibited a similar uptake profile to those containing 10% SP-C, further emphasizing cholesterol's role in vesicle properties and macrophage interaction (Ruwisch *et al*., 2020). However, if AMϕ preferentially target cholesterol-rich vesicles remains unclear. Future studies investigating cholesterol's role in membrane fragmentation and macrophage uptake will provide valuable insights into the interplay between cholesterol, SP-C, and vesicle-mediated clearance.

Palmitoylation of SP-C appears to be a key factor in the uptake of vesicles by AMϕ, as vesicles enriched in rSP-C do not significantly promote this process in the DPPC/POPC/POPG lipid system. This result may be associated with the lower degree of membrane fragmentation observed in this system, which reduces the generation of small vesicles. While rSP-C does generate small vesicles in other lipid systems, their uptake is practically negligible compared to vesicles mediated

by palmitoylated SP-C. This behavior could be explained by rSP-C's lower affinity for lipid membranes. The palmitoylation of SP-C enhances its interaction with the lipid bilayer, increasing the stability and efficiency of protein-membrane binding (Baumgart *et al*., 2010; Johansson, 1998; Qanbar *et al*., 1996; Roldan *et al*., 2015). Without this modification, rSP-C appears unable to establish certain interactions with cellular membranes, hindering the recognition and uptake of vesicles by macrophages. These observations suggest that, although membrane fragmentation plays an important role in generating small vesicles, it is not the sole mechanism governing their endocytosis. Other processes, such as those involving scavenger receptors that mediate the uptake of oxidized lipoproteins, may also contribute (Ishiyama *et al*., 2011; McDonald & Levy, 2013; Rowland & Brandariz-Nuñez, 2024). This aspect warrants further investigation to fully understand the underlying mechanisms driving vesicle uptake by AMϕ.

It has been proposed that SP-C could interact with SP-B by modulating the structure of SP-B-formed pores in membranes, thereby maintaining appropriate permeability in native surfactant (Cabré *et al*., 2018; Martínez-Calle *et al*., 2021). This interaction suggests that the presence of both proteins might influence the uptake of phospholipids or SP-C by AMϕ. However, our experiments revealed fluorescence levels similar to those observed with SP-C alone, indicating that SP-B does not exert an antagonistic or synergistic effect on this process. This finding is significant, as the organic extract (OE) of pulmonary surfactant containing SP-B/SP-C is effective in drug delivery applications (Garcia-Mouton *et al*., 2019; Hidalgo *et al*., 2021) . A potential combined effect could be envisioned, where OE acts as a drug carrier while supplementation with SP-C enhances uptake. However, understanding the underlying mechanism is crucial, as if it relies on membrane fragmentation, the drug might be prematurely released before macrophage uptake occurs.

SP-B alone can stimulate the uptake of phospholipids, but only at very high concentrations and to a lesser extent than SP-C, consistent with previous studies (Merckx *et al*., 2018; Poelma *et al*., 2004; Rice *et al*., 1989; Sane & Young, 1994). These results highlight SP-C's superior efficiency in this context and open new avenues for exploring the combined use of both proteins in therapeutic applications.

Since SP-C has the ability to bind both LPS and the macrophage co-receptor CD14 (Chaby *et al*., 2005), small vesicles enriched with SP-C would transport this bacterial molecule to alveolar AMϕ. This is consistent with the observations in the present study, where a significant increase in cellular fluorescence corresponding to both lipids and BODIPY-labeled SP-C protein was detected, regardless of the lipid composition of the vesicles.

Although LPS is a potent activator of inflammation and a regulator of macrophage phagocytosis (Kirchhoff *et al.*, 2024), its processing and elimination could occur through non-inflammatory pathways due to the presence of SP-C. This protein can inhibit the release of inflammatory mediators, such as tumor necrosis factor-α (TNF-α) or nitric oxide (NO), as demonstrated previously (Augusto, Synguelakis, Espinassous, *et al.*, 2003; Garcia-Verdugo *et al.*, 2009). In this way, SP-C could help to prevent an exacerbated immune response in the lung to a molecule that is frequently and inhaled via small droplets or smoked in small amounts (Bals, 2005). This hypothesis is further supported by observations in SP-C-deficient mice, which developed a sustained inflammatory response after exposure to LPS (Glasser *et al.*, 2013). Future studies exploring the phenotype and functions of AMϕ exposed to SP-C-enriched vesicles carrying different molecules, such as inhaled drugs, will provide more comprehensive insights about potential defense-related mechanisms involving this protein.

We acknowledge that using the immortalized murine alveolar macrophage cell line MH-S in our study presents certain limitations. While the phagocytic behavior of this cell line closely resembles that of primary AMϕ, differences exist, such as variations in the expression of specific surface markers (Brenner *et al.*, 2016). Therefore, careful consideration is required when extrapolating these results to the behavior of primary AMϕ. Complementing these findings with experiments involving true primary AMϕ would provide a more comprehensive understanding of how macrophages respond to lipid vesicle uptake, thereby validating the observations reported here. Although A549 cells are widely used as an alveolar epithelial model, their adenocarcinoma origin and heterogeneity limit their physiological relevance. As they are not true AECII-derived, they do not fully replicate alveolar function, and their mixed epithelial and mesenchymal phenotype (Tièche *et al.*, 2019) affects key properties such as extravasation and invasion (Schmid *et al.*, 2024). To improve model accuracy, transitioning A549 cells to a chemically defined medium has been shown to induce a more AECI and AECII-like phenotype (Chary *et al.*, 2022). Alternatively, primary human AECII cells or iPSC-derived alveolar models may provide more physiologically relevant options.

Our results strongly support the hypothesis that fragmentation is the primary mechanism driving vesicle uptake by AMϕ, as differences in vesicle fragmentation among the lipid systems tested correlate with variations in both phospholipid and protein uptake. Interestingly, once internalized, SP-C predominantly localizes to acidic organelles, suggesting that the protein is processed post-uptake. However, it is important to note that SP-C was labeled with BODIPY for detection purposes, and this fluorescent marker could influence its localization within cellular compartments.

Although endocytosis facilitated by membrane fragmentation appears to be the dominant pathway, additional receptor-mediated mechanisms may complement this process. For instance, CD14 has been implicated in LPS uptake, suggesting that specific membrane receptors may play a role in vesicle internalization. Similarly, the absence of palmitic chains, which would prevent recognition by scavenger receptors, highlights the potential involvement of alternative pathways.

These findings underscore the complexity of SP-C-mediated vesicle uptake by AMϕ. Membrane fragmentation emerges as a key driver of this process, with lipid composition, cholesterol content, and SP-C palmitoylation playing critical roles. The potential interaction between SP-C and SP-B, as well as SP-C's ability to facilitate non-inflammatory LPS processing, further emphasizes its importance in surfactant function and immune regulation. Future studies exploring these mechanisms in greater detail will provide valuable insights into the therapeutic potential of SP-C and its interactions within the pulmonary environment.

The data obtained in this study reveal significant differences in how SP-C mediates vesicle uptake in AECII-like cells compared to AMϕ-like cells. In AECII, vesicle uptake is directly proportional to SP-C concentration and appears independent of vesicle size or SP-C-induced membrane fragmentation. This observation suggests that the internalization process in these cells is likely receptor-mediated, with SP-C playing a central role in recognition, rather than uptake being dictated by the biophysical properties of the vesicles. These findings are consistent with previous studies using SP-C-derived peptides, where vesicle uptake was also found to increase proportionally with SP-C levels (Rice *et al.*, 1989). Notably, vesicles prepared at 50 nm show the highest levels of uptake, likely due to their increased surface area exposing SP-C or the higher membrane curvature, which allows a better binding to membrane receptor (Iriondo *et al.*, 2022). Larger vesicles, such as those at 100 or 200 nm, may reduce the accessibility or presentation of SP-C, potentially limiting receptor binding and subsequent uptake (Khan *et al.*, 2019).

Unlike AMϕ, where lipid composition plays a crucial role in uptake efficiency, AECII show no apparent dependence on lipid composition for SP-C-mediated vesicle uptake. This suggests that the internalization process in AECII is less influenced by the biophysical properties of the vesicles, such as charge or fluidity, and more reliant on the presence and configuration of SP-C to possibly interact with cellular receptors.

Palmitoylation of SP-C plays a critical role in facilitating vesicle uptake by AECII, similar to its role in AMϕ. Vesicles containing non-palmitoylated SP-C (rSP-C) exhibit significantly reduced uptake, suggesting that the palmitic acids in SP-C contribute to receptor recognition or membrane-vesicle interaction. Given that SP-C's α-helix is embedded within the vesicle membrane, the N-terminal, which

contains the palmitoyl groups, is likely the primary site for interaction with cellular receptors or other recognition molecules (Johansson, 1998; Vandenbussche, Clercx, Curstedt, *et al.*, 1992). This aligns with previous studies highlighting the importance of SP-C's N-terminal region in binding interactions (Augusto *et al.*, 2002; Augusto, Synguelakis, Espinassous, *et al.*, 2003; Augusto, Synguelakis, Johansson, *et al.*, 2003; Bi *et al.*, 2002; Plasencia *et al.*, 2008; Plasencia *et al.*, 2004). Interestingly, at higher concentrations of rSP-C (7.5–10%) in all synthetic systems, a slight increase in cellular fluorescence was observed, suggesting that the N-terminal of SP-C is involved in the recognition of vesicles by AECII. Understanding how palmitoylation enhances SP-C binding affinity and receptor interaction will be crucial for elucidating the mechanisms underlying vesicle uptake.

While SP-B is less effective than SP-C in promoting lipid internalization, it appears to play a complementary role in vesicle formation and stability. The presence of SP-B alongside SP-C does not significantly alter SP-C-mediated uptake, suggesting that any interaction between the two proteins does not interfere with receptor recognition. This observation supports the hypothesis that SP-B/SP-C and SP-C function through distinct yet complementary mechanisms, with SP-B/SP-C primarily contributing to vesicle structure and SP-C facilitating receptor-driven internalization. Further studies are needed to investigate whether SP-B/SP-C interactions influence receptor binding or vesicle biophysical properties.

The interplay between SP-C and LPS in vesicle uptake offers additional insights into the functional versatility of SP-C. LPS alone does not promote lipid internalization in AECII, but when bound to SP-C, it does not inhibit SP-C-mediated uptake. This suggests that SP-C retains its functional role in vesicle recognition and internalization even in the presence of LPS. However, uptake levels vary across lipid compositions, suggesting that lateral lipid organization could modulate the interaction of SP-C/LPS complexes with SP-C receptors. For instance, DPPC/POPC vesicles combined with LPS show reduced uptake compared to those derived from native surfactant lipid fractions, which exhibit enhanced uptake. These variations may reflect differences in SP-C accessibility or its ability to maintain a functional conformation for receptor interaction (Garcia-Verdugo *et al.*, 2009; González-Horta, 2006). Structural studies focusing on the interplay between lipid organization, SP-C, and LPS would provide a deeper understanding of these dynamics.

Once internalized, SP-C predominantly localizes at lamellar bodies within AECII, as evidenced by microscopy data, consistent with previous studies (Horowitz *et al.*, 1997; Ikegami, Horowitz, *et al.*, 1998). Epifluorescence micrographs detecting internalized lipids suggest that these lipids are confined to specific organelles,

most likely lamellar bodies. However, the colocalization of these lipids with acidic organelles could not be confirmed using confocal microscopy in this study. Approximately 60–70% of the incorporated BODIPY-labeled SP-C colocalizes with lamellar bodies, indicating that SP-C and associated lipids are processed and stored within these organelles. The remaining SP-C likely localizes to other membranous compartments or to lamellar bodies undergoing fusion with the plasma membrane. It is important to note that while lamellar bodies are acidic organelles, their pH increases during the secretion of pulmonary surfactant complexes as soon as they fuse with the membrane (Dietl *et al*., 2012; Olmeda *et al*., 2017). This pH shift could explain why not all BODIPY-labeled SP-C was detected, as the fluorescent marker may be diminished in less acidic environments. This distribution pattern suggests that SP-C may play a role in both surfactant recycling and secretion processes. However, further studies are required to confirm the precise localization and processing pathways of SP-C and its associated lipids in AECII.

The use of A549 cells in this study offers valuable insights but poses certain limitations. Although A549 cells exhibit lamellar body-like structures, they may not fully replicate the recycling pathways observed in primary AECII (Foster *et al*., 1998). Primary cell cultures and in vivo models are essential for confirming the proposed pathways and assessing their physiological relevance. These models would also provide a more accurate representation of SP-C's role in surfactant recycling and its potential therapeutic applications.

Our findings suggest that SP-C plays critical roles in a recycling mechanism where vesicles deliver excess or waste materials to epithelial tissues, enabling AECII to re-synthesize and release surfactant with optimal composition and performance. This process likely involves the coordinated processing of both lipids and proteins, ensuring the homeostasis of the pulmonary surfactant system. Additionally, AMϕ may contribute to this recycling process by capturing and processing vesicles, thereby supporting surfactant turnover. While this hypothesis aligns with SP-C's observed role in maintaining surfactant homeostasis, further validation is needed.

Based on the results exposed in this Thesis, we propose a novel role for SP-C in the maintaining a functional PS system, as illustrated in **Figure 3.12**. According to this model, the dimerization of SP-C would initiate the formation of small vesicles, which effectively deliver substances from the interface to the alveolar cells exposed to the underlying hypophase. This process may be disrupted or absent in conditions associated with SP-C deficiency, which are often linked to impaired intracellular processing of proSP-C, leading to its accumulation within AECII (Nogee, 2004). Additionally, the relevance of this model is underscored by the abnormally elevated SP-C levels observed in patients with pulmonary alveolar

proteinosis (Brasch, Birzele, *et al.*, 2004). These elevated levels could represent a compensatory mechanism aimed at enhancing the activity of AMϕ.

These findings highlight the multifaceted role of SP-C in surfactant homeostasis, encompassing biophysical, cellular, and immune functions. Further studies focusing on receptor identification, the role of palmitoylation, and the structural basis of SP-C interactions with lipids and cells will be essential for fully understanding the mechanisms underlying its function. Expanding this knowledge will provide valuable insights into SP-C's potential as a therapeutic target in surfactant-related disorders.

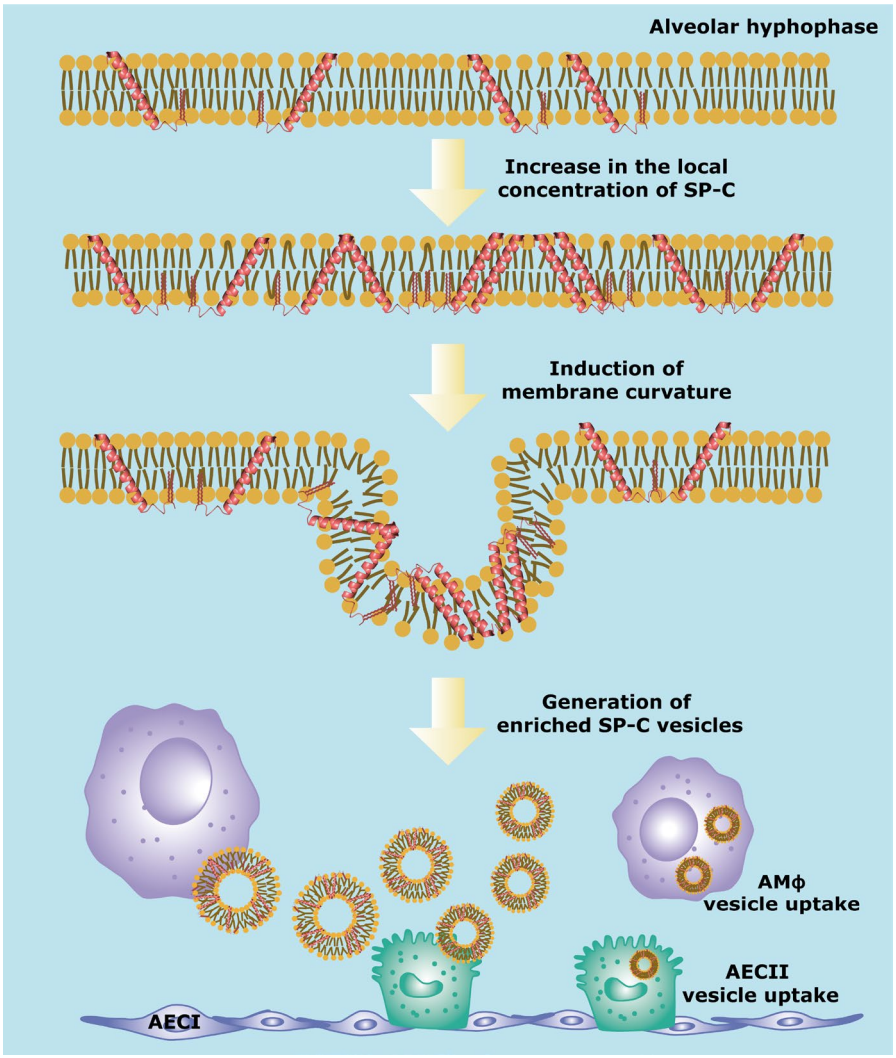

Figure 3.12. Surfactant alveolar homeostasis mediated by SP-C. SP-C present in the lipid bilayers of PS would occasionally reach local concentrations that could facilitate clustering and interaction between the different molecules. As a result, some dimers would be progressively established, inducing a curvature in the membrane that eventually would generate small vesicles. These SP-C enriched vesicles could carry diverse molecules to the hypophase, targeting different alveolar cells. Inhaled exogenous molecules that can be harmful, such as LPS, could then be processed and removed by AMϕ, while wasted or exceeding PS would be collected and recycled by AECII, contributing to the alveolar homeostasis.

6.
GENERAL DISCUSSION

Homeostasis refers to the physiological ability of organisms to maintain a stable internal environment despite external fluctuations (Cannon, 1932). In the lungs, homeostasis is primarily regulated by the alveolar epithelium, which consists of type I (AECI) and type II (AECII) alveolar epithelial cells. AECI cells provide a large surface area for efficient gas exchange (Crapo *et al*., 1982), while AECII cells play a critical role to alveolar homeostasis by producing and recycling pulmonary surfactant (Olmeda *et al*., 2017), which reduces surface tension and maintains alveolar integrity during respiratory cycles. This dual functionality is essential to preserve the mechanical stability of the alveolar structure and facilitate effective immune and inflammatory responses against to environmental insults (Ware & Matthay, 2000).

Pulmonary surfactant is a complex mixture of lipids and proteins critical for alveolar function (Goerke, 1998; Possmayer *et al*., 2001). Among these proteins, SP-C plays a pivotal role. This hydrophobic protein contributes to the stability and renewal of the surfactant lipid monolayer at the air–water interface, crucial for reducing surface tension during breathing (Pérez-Gil, 2008). SP-C's unique structural features, including its transmembrane α-helix and palmitoylated N-terminal, are essential for its function (Johansson, 1998; Johansson, Szyperski, *et al*., 1994; Vandenbussche, Clercx, Curstedt, *et al*., 1992). Palmitoylation enhances SP-C's insertion into lipid bilayers, increasing its tilt and potentially affecting its interaction with other surfactant components and proteins (Creuwels *et al*., 1993; Johansson *et al*., 1995; Roldan *et al*., 2015). The main function of SP-C in pulmonary surfactant is biophysical, although it may also be implicated in surfactant recycling and processing (Lopez-Rodriguez & Pérez-Gil, 2014; Olmeda *et al*., 2017; Sehlmeyer *et al*., 2020). Consequently, SP-C may play a role in recycling oxidized lipids at this interface or in the clearance of harmful inhaled particles, which has significant implications for maintaining alveolar homeostasis.

In this Doctoral Thesis, a comprehensive analysis of the functional and structural properties of SP-C within the pulmonary surfactant system has been conducted. This work has investigated key aspects such as SP-C's ability to form homodimers, its role in inducing membrane fragmentation, and its contribution to pulmonary homeostasis-properties that are likely interrelated. A central focus of the study has been the dimerization and oligomerization of SP-C, a process hypothesized to induce stress in lipid membranes, potentially triggering their fission and leading to the formation of highly curved, small vesicles (Chapters 1 and 2). These vesicles, enriched in SP-C, are subsequently internalized by alveolar-like cells for processing and/or recycling, a mechanism crucial for maintaining pulmonary surfactant performance, as discussed in Chapter 3 and proposed by Roldan *et al*. (2016).

6. General discussion

SP-C is predominantly monomeric at low concentrations in all lipid systems used in the fluorescence spectroscopy studies conducted in Chapter 1 of this work. This is consistent with the results of Horowitz *et al*. (1993). However, under conditions that lead to high protein concentration, such as compartmentalization induced by the lipid environment or membrane compression during respiratory cycles, SP-C undergoes changes (Horowitz *et al*., 1993; Keating *et al*., 2012; Roldan *et al*., 2017). This phenomenon was observed in samples with the highest concentration of BODIPY-labeled SP-C (7.5 μM or ~4% by mass relative to lipids) in the lipid system corresponding to the native lipid extract known as LS. These results underscore the importance of lipid environment properties for SP-C activity, highlighting how phase segregation facilitates compartmentalization and potentially promotes protein-protein interaction.

Palmitoylation plays a key role in SP-C dimer formation, as its absence facilitates dimerization even at low concentrations and in the absence of phase separation. Without palmitoylation, free cysteines can also form disulfide bonds with cysteines from other SP-C molecules, as documented in the canine isoform of SP-C (Creuwels *et al*., 1995). However, whether this propensity for dimerization has positive or negative effects remains unclear and largely depends on the secondary structure adopted by protein within the dimers. Specifically, a conformational change from α-helix to β-sheets may lead to the formation of amyloid-like aggregates associated with respiratory pathologies (Beers & Mulugeta, 2005; Johansson, 2001; Johansson *et al*., 2004). This underscores the importance of detailed structural and functional characterization of SP-C in the dimeric/oligomeric context. Such analysis is not only relevant from a biomedical perspective but also holds potential implications for optimizing recombinant proteins, whose development could significantly reduce the costs of producing the exogenous surfactant required to treat in neonates with surfactant deficiency and other respiratory diseases (Blanco & Pérez-Gil, 2007; Halliday, 2017; Lee *et al*., 1999; Pérez-Gil, 2022; Rebello *et al*., 2002). Understanding the mechanisms and consequences of SP-C dimerization is therefore crucial for advancing more efficient and accessible therapeutic strategies.

SP-C also plays a crucial role in membrane fragmentation (Chapter 2). To establish a connection between dimerization and membrane fragmentation, the roles of the N-terminal and C-terminal regions of SP-C in this process were investigated. Experiments using synthetic peptides mimicking these regions revealed a synergistic effect when combined with full-length SP-C, suggesting that both regions are necessary to maximize fragmentation. This effect may occur due to these peptides enhancing the local concentration of SP-C. However, mutations in the proposed dimerization motifs do not completely inhibit SP-C activity, indicating that other structural and lipid environmental factors also contribute to this

process. Another possible explanation is that the studied dimerization motifs are not as important as originally thought. Recently, Korolainen *et al*. (2022) proposed a much longer dimerization motif in the C-terminal helix (V^{21}xxxVxxxGxxxM^{33}) compared to the simpler A^{30}xxxG^{34} motif suggested by (Kairys *et al*., 2004). To validate these motifs, mutants based on these sequences should be generated, and their dimerization and fragmentation capacities studied.

Additionally, Chapter 2 demonstrates that the role of SP-C in membrane fission is influenced by factors such as lipid composition, palmitoylation status, and interactions with other components of the pulmonary surfactant system.

Lipid composition is crucial for the extent of membrane fragmentation. In the synthetic lipid model system (DPPC/POPC/POPG, 50/25/15, w/w/w), it has been confirmed that fragmentation occurs not gradually, but as a discrete mechanism, potentially linked to the local accumulation of SP-C and the generation of membrane stress. A 7.5% SP-C concentration is the minimum required to observe a significant decrease in particle concentration. This finding aligns with observations by Roldan *et al*. (2016), where 10% SP-C reduced the mean diameter of LUVs from the original 200 nm to 25–50 nm. However, in lipid model systems lacking POPG (ncLM) and in native lipid extracts (LS) the decrease in particle concentration at comparable protein concentration is higher than in LM. The presence of charged lipids, such as POPG, appears to provide electrostatic stability to the membranes, thereby reducing fragmentation. In other words, the absence of POPG facilitates fragmentation, likely due to a less stable interaction between SP-C and the membrane (Roldan *et al*., 2017; Takamoto *et al*., 2001). It would be interesting to investigate the dimerization capacity of SP-C in this system. If it mirrors the result observed using lipid surfactant (LS) derived from organic lipid extracts of PS, it could be inferred that there is a correlation between dimerization and fragmentation. The inclusion of cholesterol, a key component of pulmonary surfactant and present in LS, enhances fragmentation, possibly due to the interplay between SP-C and cholesterol. This interaction may induce lipid phase segregation and promote the localization, and potential accumulation, of both molecules in specific membrane domains (Bernardino de la Serna *et al*., 2004; Gómez-Gil, Schürch, *et al*., 2009; Roldan *et al*., 2017). This could support a role of SP-C in the movilization of cholesterol in and out from surfactant complexes. Fast changes in cholesterol proportions have been connected with the adaptation of the surfactant system to specific environmental conditions, such as different physiological temperatures or breathing regimes (Orgeig *et al*., 2003; Suri *et al*., 2012; Suri *et al*., 2013; Veldhuizen *et al*., 1998)

The palmitoylation state of SP-C also seems to play a fundamental role. The non-palmitoylated version of SP-C (rSP-C) retains the ability to fragment membranes,

although with reduced efficiency, despite its greater capacity for dimerization (Chapter 2). These findings suggest that dimers of native palmitoylated SP-C may differ structurally or functionally from non-palmitoylated rSP-C dimers. Alternatively, the role of palmitoylation in stabilizing the α-helical structure of SP-C could explain these observations. Optimizing SP-C's interaction with lipid membranes and enhancing membrane perturbation, palmitoylation may facilitate acquiring the curvature necessary for effective fragmentation (Gonzalez-Horta *et al.*, 2008; Lukovic *et al.*, 2012; Plasencia *et al.*, 2008; Roldan *et al.*, 2015).

The lipid vesicles enriched in SP-C generated through fragmentation, appear to be selectively refined in terms of composition by SP-C (Chapter 2). These vesicles, released into the hypophase (the layer beneath the air-liquid interface), would be available for subsequent internalization by alveolar cells, including pneumocyte-like cells and alveolar macrophage-like cells (Chapter 3). This refinement and internalization underscore the critical role of SP-C to sustain pulmonary surfactant dynamics, contributing both to the maintenance of surfantant performance and to alveolar homeostasis.

SP-C plays a fundamental role as a mediator in the formation, fragmentation, and internalization of lipid vesicles by alveolar macrophage-like cells, specifically the MH-S cell line. Notably, vesicle uptake is higher in lipid systems with greater fragmentation capacity. This finding underscores the close relationship between SP-C's ability to fragment membranes and its effectiveness in promoting the internalization of the vesicles generated. Importantly, the minimum proportion of SP-C required to induce membrane fragmentation aligns with that needed to facilitate vesicle uptake in the DPPC/POPC/POPG lipid system. This phenomenon demonstrates how SP-C-mediated fragmentation generates smaller vesicles, significantly enhancing their internalization by alveolar macrophages (Kelly *et al.*, 2011; Khan *et al.*, 2019; Schwendener *et al.*, 1984).

In A549 cells, an pneumocyte-like cell line, vesicle uptake increases proportionally with SP-C concentration. This observation suggests that factors beyond SP-C-induced fragmentation may influence internalization, as increased cellular fluorescence was also detected at low SP-C concentrations. Vesicle uptake occurs consistently across all lipid systems studied, regardless of their potential fragmentation capacity and even at low SP-C concentrations (2.5%). Based on these observations, it is likely that the uptake of SP-C is mediated by a membrane receptor that recognizes this protein as a ligand. However, to confirm this hypothesis and exclude the possibility of a nonspecific uptake mechanism, experiments assessing saturation and specificity are required. For saturation, the rate of internalization should reach a maximum at high ligand concentrations, indicating receptors limitation. For specificity, the interaction could be validated

using specific competitors or mutant SP-C variants incapable of binding to the receptor (Goldstein *et al.*, 1979; Mayor & Pagano, 2007; Sorkin & von Zastrow, 2009). These analyses would clarify whether the uptake occurs through a receptor-ligand mechanism or a nonspecific process.

The impact of palmitoylation on SP-C function was also evaluated in chapter 3, revealing it as a critical factor in facilitating vesicle internalization. The results demonstrate that the non-palmitoylated version of SP-C (rSP-C) exhibits significantly lower efficiency in this process, suggesting that palmitoylation enhances SP-C's interaction with cellular membranes. Furthermore, depalmitoylation negatively affects all functional properties of SP-C analyzed in this Thesis, as presented in Chapters 1, 2, and 3. These findings underscore the importance of this structural modification not only for the specific SP-C's biological function but also for maintaining alveolar homeostasis in general.

In addition to palmitoylation, other factors, such as interactions with the other hydrophobic surfactant protein SP-B and the presence of lipopolysaccharides (LPS), may modulate SP-C activity during vesicle internalization by alveolar cells (Augusto *et al.*, 2002; Cabré *et al.*, 2018; Martínez-Calle *et al.*, 2018).

SP-B and SP-C are essential components for reducing alveolar surface tension. Their combined presence in surfactant enhances the adsorption and spreading of phospholipids, promoting efficient surface film formation. Furthermore, both proteins have been shown to influence surfactant membrane permeability to polar molecules, ions, and membrane probes (Parra *et al.*, 2013; Parra *et al.*, 2011). Interactions between SP-B and SP-C appear to be mutually modulated, as studies have suggested that the oligomeric structure of SP-B plays a pivotal role in linking membrane permeability and surfactant biophysical functions (Martínez-Calle *et al.*, 2021). Interestingly, while the membrane fission action of SP-C is sometimes counteracted by SP-B's membrane fusion capabilities (Roldan *et al.*, 2016), this Thesis show that this interplay does not impact SP-C nor in alveolar macrophages which vesicle internalization has been related with SP-C-mediated vesicles uptake, either in alveolar macrophages, where vesicle internalization has been linked to SP-C's fragmentation capacity. Therefore, SP-B/SP-C interactions do not appear to interfere with SP-C's mechanism of internalization by alveolar cells. Further experiments are needed to fully elucidate the mechanisms underlying these observations. Nonetheless, current evidence suggests that SP-C plays a dominant role in protein uptake, independently of SP-B's presence, underscoring its critical function in this context.

On the other hand, the effects of LPS on SP-C activity appear to be cell type-specific. In alveolar macrophages, the combination of SP-C with LPS dramatically enhances vesicle internalization across all lipid systems studied. This suggests

that the SP-C/LPS interaction does not directly influence uptake, but that LPS may "drag" SP-C, facilitating its internalization. This finding underscores a potential immunomodulatory role of SP-C, as LPS typically triggers cytotoxic inflammatory responses. However, SP-C appears to modulate this response, reducing the secretion of pro-inflammatory agents by alveolar macrophages (Augusto, Synguelakis, Espinassous, *et al.*, 2003). This effect aligns with studies showing that SP-C-deficient mice are more susceptible to bacterial infections and to exacerbated inflammatory reactions, further emphasizing the importance of SP-C to modulate pulmonary immune defense (Glasser *et al.*, 2013; Glasser *et al.*, 2008; Glasser *et al.*, 2009; Thomas *et al.*, 2002).

Once internalized, SP-C predominantly localizes at acidic organelles such as lysosomes and lamellar bodies in type II alveolar epithelial cells. This localization pattern suggests that SP-C actively participates in the recycling and processing of pulmonary surfactant, processes critical for maintaining alveolar homeostasis (Crapo *et al.*, 1982). In macrophages, it could be hypothesized that SP-C appears to be involved in the non-inflammatory clearance of lipopolysaccharides or harmful particles, thereby contributing to a regulated immune response in the pulmonary environment.

These results suggest that further investigation into the relationship between SP-C and the proteins SP-D or SP-A would be valuable, as both collectins play crucial roles in alveolar homeostasis and immunologically modulate alveolar macrophage activity (Cañadas *et al.*, 2020; Wright, 2005).

In conclusion, this work underscores the multifaceted role of SP-C as a key component in alveolar homeostasis, from stabilizing the surfactant film at the air-water interface to its involvement in the fragmentation and internalization of lipid vesicles by different alveolar-like cells. SP-C's capacity to interact with lipid membranes, influenced by its palmitoylation state and lipid environment, is fundamental for maintaining pulmonary surfactant performance, particularly under conditions of mechanical and oxidative stress. These findings not only deepen our understanding of SP-C's molecular mechanism but also pave the way for developing more effective therapies for respiratory diseases associated with surfactant dysfunction.

7.
CONCLUSIONS

7. Conclusions

This Thesis provides a comprehensive investigation into the multifaceted roles of surfactant protein C (SP-C) in membrane dynamics, vesicle uptake, and intracellular trafficking within the pulmonary surfactant system. By employing advanced biophysical, biochemical, and cellular techniques, these studies have elucidated how SP-C's structural features, post-translational modifications, and lipid interactions govern its functionality. The results emphasize SP-C's dual role in both surfactant recycling and immune regulation, underscoring its critical contribution to pulmonary homeostasis. The key conclusions drawn from this work are:

1. SP-C could form dimers under specific conditions, as demonstrated by BiFC and fluorescence spectroscopy assays. Dimerization of SP-C seems to be influenced by lipid phase separation and local protein concentration. Palmitoylation plays a key role in preventing interactions between monomers and stabilizing SP-C's structure. Non-palmitoylated SP-C (rSP-C) exhibits an increased propensity for dimerization, suggesting that palmitoylation regulates its behavior. The functional significance of these dimers and the precise dimerization motifs remains unresolved.

2. SP-C may induce fragmentation of large unilamellar vesicles (LUVs) when its concentration reaches at least 7.5% by mass with respect to lipids in membranes composed by DPPC/POPC/POPG (50/25/15, w/w). The efficiency of fragmentation would be influenced by phospholipid composition, cholesterol content, and electrostatic interactions. Non-charged lipid systems (e.g., DPPC/POPC) exhibit higher fragmentation efficiency due to the absence of stabilizing electrostatic interactions. In contrast, charged systems containing POPG enhance membrane stability, requiring higher SP-C concentrations to induce fragmentation. Cholesterol increases SP-C's ability to induce membrane curvature and promotes the clustering of unsaturated lipids, contributing to vesicle remodeling. Palmitoylation seems to enhance SP-C-mediated.

3. Both the N- and C-terminal regions of SP-C appears to be critical for membrane fragmentation, althought neither is sufficient on its own. Synthetic peptide experiments suggest that these regions act synergistically.

4. SP-C enhances vesicle uptake by alveolar macrophages (AMϕ) and alveolar epithelial cells (AEC) possibly through distinct mechanisms. In AMϕ, vesicle uptake might be primarily driven by SP-C-induced membrane

fragmentation, which generates small vesicles that are more suitable for engulfment. This process is potentially influenced by both SP-C concentration and lipid composition. In AEC, vesicle uptake seems to be receptor-mediated, directly proportional to SP-C concentration, and independent of lipid composition.

5. Palmitoylation appears to be essential for SP-C-mediated vesicle uptake. Vesicles containing non-palmitoylated SP-C (rSP-C) exhibit significantly reduced uptake, underscoring the importance of palmitoyl groups in facilitating membrane interactions and receptor recognition in both AMϕ and AEC.

6. Lipid composition could be a key determinant of SP-C-mediated vesicle uptake by AMϕ. Vesicles lacking POPG (non-charged lipid models) exhibit enhanced uptake, likely due to increased SP-C-induced fragmentation. In AEC, uptake appears independent of lipid composition, suggesting a reliance on receptor-mediated pathways rather than the biophysical properties of the vesicles.

7. SP-B could play a complementary but less significant role compared to SP-C in vesicle uptake. When combined, SP-C and SP-B did not exhibit synergistic effects in either AMϕ or AEC. SP-C's interaction with lipopolysaccharide (LPS) revealed cell-type-specific effects, enhancing vesicle uptake by AMϕ whereas in AEC the effect was different in each lipid system studied. These effects vary depending on lipid composition, suggesting a complex interplay between SP-C, LPS, and the cellular environment.

8. Once internalized, SP-C predominantly localizes in acidic organelles, such as lysosomes in AMϕ and lamellar bodies in AEC cells. This localization underscores SP-C’s dual role in surfactant recycling and secretion. The protein’s intracellular trafficking is influenced by lipid composition and the presence of LPS, suggesting that SP-C contributes to the maintenance of surfactant homeostasis.

8.
BIBLIOGRAPHY

Agassandian, M., & Mallampalli, R. K. (2013). Surfactant phospholipid metabolism. *Biochim Biophys Acta*, *1831*(3), 612-625. https://doi.org/10.1016/j.bbalip.2012.09.010

Akinbi, H. T., Breslin, J. S., Ikegami, M., Iwamoto, H. S., Clark, J. C., Whitsett, J. A., Jobe, A. H., & Weaver, T. E. (1997). Function of the C-Terminal Propeptide of Surfactant Protein B (SP-B). • 224. *Pediatric Research*, *41*(4), 40-40. https://doi.org/10.1203/00006450-199704001-00244

Amrein, M., von Nahmen, A., & Sieber, M. (1997). A scanning force- and fluorescence light microscopy study of the structure and function of a model pulmonary surfactant. *Eur Biophys J*, *26*(5), 349-357. https://doi.org/10.1007/s002490050089

Andersson, M., Curstedt, T., Jörnvall, H., & Johansson, J. (1995). An amphipathic helical motif common to tumourolytic polypeptide NK-lysin and pulmonary surfactant polypeptide SP-B. *FEBS Lett*, *362*(3), 328-332. https://doi.org/10.1016/0014-5793(95)00268-e

Arroyo, R., Echaide, M., Moreno-Herrero, F., Perez-Gil, J., & Kingma, P. S. (2020). Functional characterization of the different oligomeric forms of human surfactant protein SP-D. *Biochim Biophys Acta Proteins Proteom*, *1868*(8), 140436. https://doi.org/10.1016/j.bbapap.2020.140436

Augusto, L., Le Blay, K., Auger, G., Blanot, D., & Chaby, R. (2001). Interaction of bacterial lipopolysaccharide with mouse surfactant protein C inserted into lipid vesicles. *Am J Physiol Lung Cell Mol Physiol*, *281*(4), L776-785. https://doi.org/10.1152/ajplung.2001.281.4.L776

Augusto, L. A., Li, J., Synguelakis, M., Johansson, J., & Chaby, R. (2002). Structural basis for interactions between lung surfactant protein C and bacterial lipopolysaccharide. *J Biol Chem*, *277*(26), 23484-23492. https://doi.org/10.1074/jbc.M111925200

Augusto, L. A., Synguelakis, M., Espinassous, Q., Lepoivre, M., Johansson, J., & Chaby, R. (2003). Cellular antiendotoxin activities of lung surfactant protein C in lipid vesicles. *Am J Respir Crit Care Med*, *168*(3), 335-341. https://doi.org/10.1164/rccm.200212-1440OC

Augusto, L. A., Synguelakis, M., Johansson, J., Pedron, T., Girard, R., & Chaby, R. (2003). Interaction of pulmonary surfactant protein C with CD14 and lipopolysaccharide. *Infect Immun*, *71*(1), 61-67. https://doi.org/10.1128/iai.71.1.61-67.2003

Baatz, J. E., Elledge, B., & Whitsett, J. A. (1990). Surfactant protein SP-B induces ordering at the surface of model membrane bilayers. *Biochemistry*, *29*(28), 6714-6720. https://doi.org/10.1021/bi00480a022

Baatz, J. E., Smyth, K. L., Whitsett, J. A., Baxter, C., & Absolom, D. R. (1992). Structure and functions of a dimeric form of surfactant protein SP-C: a Fourier transform infrared and surfactometry study. *Chem Phys Lipids*, *63*(1-2), 91-104. https://doi.org/10.1016/0009-3084(92)90026-l

Bals, R. (2005). Lipopolysaccharide and the lung: a story of love and hate. *Eur Respir J*, *25*(5), 776-777. https://doi.org/10.1183/09031936.05.00025405

Ban, N., Matsumura, Y., Sakai, H., Takanezawa, Y., Sasaki, M., Arai, H., & Inagaki, N. (2007). ABCA3 as a lipid transporter in pulmonary surfactant biogenesis. *J Biol Chem*, *282*(13), 9628-9634. https://doi.org/10.1074/jbc.M611767200

8. Bibliography

Baoukina, S., & Tieleman, D. P. (2010). Direct simulation of protein-mediated vesicle fusion: lung surfactant protein B. *Biophys J*, *99*(7), 2134-2142. https://doi.org/10.1016/j.bpj.2010.07.049

Bates, S. R. (2010). P63 (CKAP4) as an SP-A receptor: implications for surfactant turnover. *Cell Physiol Biochem*, *25*(1), 41-54. https://doi.org/10.1159/000272062

Bates, S. R., Dodia, C., Tao, J. Q., & Fisher, A. B. (2008). Surfactant protein-A plays an important role in lung surfactant clearance: evidence using the surfactant protein-A gene-targeted mouse. *Am J Physiol Lung Cell Mol Physiol*, *294*(2), L325-333. https://doi.org/10.1152/ajplung.00341.2007

Baumgart, F., Loura, L. s., Prieto, M., & Gil, J. s. P. r. (2009). Pulmonary Surfactant Protein C Reduces the Size of Liquid Ordered Domains in a Ternary Membrane Model System. *Biophysical Journal*, *96*(3), 608a-609a. https://doi.org/10.1016/j.bpj.2008.12.3219

Baumgart, F., Ospina, O. L., Mingarro, I., Rodríguez-Crespo, I., & Pérez-Gil, J. (2010). Palmitoylation of pulmonary surfactant protein SP-C is critical for its functional cooperation with SP-B to sustain compression/expansion dynamics in cholesterol-containing surfactant films. *Biophys J*, *99*(10), 3234-3243. https://doi.org/10.1016/j.bpj.2010.08.070

Beers, M. F., Kim, C. Y., Dodia, C., & Fisher, A. B. (1994). Localization, synthesis, and processing of surfactant protein SP-C in rat lung analyzed by epitope-specific antipeptide antibodies. *Journal of Biological Chemistry*, *269*(32), 20318-20328. https://doi.org/https://doi.org/10.1016/S0021-9258(17)31994-4

Beers, M. F., & Lomax, C. (1995). Synthesis and processing of hydrophobic surfactant protein C by isolated rat type II cells. *Am J Physiol*, *269*(6 Pt 1), L744-753. https://doi.org/10.1152/ajplung.1995.269.6.L744

Beers, M. F., & Mulugeta, S. (2005). Surfactant protein C biosynthesis and its emerging role in conformational lung disease. *Annu Rev Physiol*, *67*, 663-696. https://doi.org/10.1146/annurev.physiol.67.040403.101937

Bernardino de la Serna, J., Perez-Gil, J., Simonsen, A. C., & Bagatolli, L. A. (2004). Cholesterol Rules: DIRECT OBSERVATION OF THE COEXISTENCE OF TWO FLUID PHASES IN NATIVE PULMONARY SURFACTANT MEMBRANES AT PHYSIOLOGICAL TEMPERATURES*. *Journal of Biological Chemistry*, *279*(39), 40715-40722. https://doi.org/https://doi.org/10.1074/jbc.M404648200

Bernhard, W. (2016). Lung surfactant: Function and composition in the context of development and respiratory physiology. *Annals of Anatomy - Anatomischer Anzeiger*, *208*, 146-150. https://doi.org/https://doi.org/10.1016/j.aanat.2016.08.003

Bi, X., Flach, C. R., Pérez-Gil, J., Plasencia, I., Andreu, D., Oliveira, E., & Mendelsohn, R. (2002). Secondary structure and lipid interactions of the N-terminal segment of pulmonary surfactant SP-C in Langmuir films: IR reflection-absorption spectroscopy and surface pressure studies. *Biochemistry*, *41*(26), 8385-8395. https://doi.org/10.1021/bi020129g

Blanco, O., & Pérez-Gil, J. (2007). Biochemical and pharmacological differences between preparations of exogenous natural surfactant used to treat

Respiratory Distress Syndrome: Role of the different components in an efficient pulmonary surfactant. *European Journal of Pharmacology*, *568*(1), 1-15. https://doi.org/https://doi.org/10.1016/j.ejphar.2007.04.035

Bligh, E. G., & Dyer, W. J. (1959). A rapid method of total lipid extraction and purification. *Can J Biochem Physiol*, *37*(8), 911-917. https://doi.org/10.1139/o59-099

Bortnick, A. E., Favari, E., Tao, J. Q., Francone, O. L., Reilly, M., Zhang, Y., Rothblat, G. H., & Bates, S. R. (2003). Identification and characterization of rodent ABCA1 in isolated type II pneumocytes. *Am J Physiol Lung Cell Mol Physiol*, *285*(4), L869-878. https://doi.org/10.1152/ajplung.00077.2003

Brasch, F., Birzele, J., Ochs, M., Guttentag, S. H., Schoch, O. D., Boehler, A., Beers, M. F., Muller, K. M., Hawgood, S., & Johnen, G. (2004). Surfactant proteins in pulmonary alveolar proteinosis in adults. *Eur Respir J*, *24*(3), 426-435. https://doi.org/10.1183/09031936.04.00076403

Brasch, F., Johnen, G., Winn-Brasch, A., Guttentag, S. H., Schmiedl, A., Kapp, N., Suzuki, Y., Müller, K. M., Richter, J., Hawgood, S., & Ochs, M. (2004). Surfactant protein B in type II pneumocytes and intra-alveolar surfactant forms of human lungs. *Am J Respir Cell Mol Biol*, *30*(4), 449-458. https://doi.org/10.1165/rcmb.2003-0262OC

Brasch, F., Ten Brinke, A., Johnen, G., Ochs, M., Kapp, N., Müller, K. M., Beers, M. F., Fehrenbach, H., Richter, J., Batenburg, J. J., & Bühling, F. (2002). Involvement of cathepsin H in the processing of the hydrophobic surfactant-associated protein C in type II pneumocytes. *Am J Respir Cell Mol Biol*, *26*(6), 659-670. https://doi.org/10.1165/ajrcmb.26.6.4744

Bridges, J. P., Ikegami, M., Brilli, L. L., Chen, X., Mason, R. J., & Shannon, J. M. (2010). LPCAT1 regulates surfactant phospholipid synthesis and is required for transitioning to air breathing in mice. *J Clin Invest*, *120*(5), 1736-1748. https://doi.org/10.1172/jci38061

Butler, P. L., & Mallampalli, R. K. (2010). Cross-talk between remodeling and de novo pathways maintains phospholipid balance through ubiquitination. *J Biol Chem*, *285*(9), 6246-6258. https://doi.org/10.1074/jbc.M109.017350

Cabré, E. J., Loura, L. M., Fedorov, A., Perez-Gil, J., & Prieto, M. (2012). Topology and lipid selectivity of pulmonary surfactant protein SP-B in membranes: Answers from fluorescence. *Biochim Biophys Acta*, *1818*(7), 1717-1725. https://doi.org/10.1016/j.bbamem.2012.03.008

Cabré, E. J., Martínez-Calle, M., Prieto, M., Fedorov, A., Olmeda, B., Loura, L. M. S., & Pérez-Gil, J. (2018). Homo- and hetero-oligomerization of hydrophobic pulmonary surfactant proteins SP-B and SP-C in surfactant phospholipid membranes. *J Biol Chem*, *293*(24), 9399-9411. https://doi.org/10.1074/jbc.RA117.000222

Cannon, W. B. (1932). *The wisdom of the body*. W W Norton & Co.

Cañadas, O., Olmeda, B., Alonso, A., & Pérez-Gil, J. (2020). Lipid-Protein and Protein-Protein Interactions in the Pulmonary Surfactant System and Their Role in Lung Homeostasis. *Int J Mol Sci*, *21*(10). https://doi.org/10.3390/ijms21103708

Carreto-Binaghi, L. E., Aliouat, E. M., & Taylor, M. L. (2016). Surfactant proteins, SP-A and SP-D, in respiratory fungal infections: their role in the inflammatory

response. *Respiratory Research*, *17*(1), 66. https://doi.org/10.1186/s12931-016-0385-9

Casals, C., & Cañadas, O. (2012). Role of lipid ordered/disordered phase coexistence in pulmonary surfactant function. *Biochimica et Biophysica Acta (BBA) - Biomembranes*, *1818*(11), 2550-2562. https://doi.org/https://doi.org/10.1016/j.bbamem.2012.05.024

Castillo-Sánchez, J. C., Roldán, N., García-Álvarez, B., Batllori, E., Galindo, A., Cruz, A., & Pérez-Gil, J. (2022). The highly packed and dehydrated structure of preformed unexposed human pulmonary surfactant isolated from amniotic fluid. *Am J Physiol Lung Cell Mol Physiol*, *322*(2), L191-l203. https://doi.org/10.1152/ajplung.00230.2021

Cerrada, A., Haller, T., Cruz, A., & Pérez-Gil, J. (2015). Pneumocytes Assemble Lung Surfactant as Highly Packed/Dehydrated States with Optimal Surface Activity. *Biophys J*, *109*(11), 2295-2306. https://doi.org/10.1016/j.bpj.2015.10.022

Chaby, R., Garcia-Verdugo, I., Espinassous, Q., & Augusto, L. A. (2005). Interactions between LPS and lung surfactant proteins. *J Endotoxin Res*, *11*(3), 181-185. https://doi.org/10.1179/096805105x37358

Chang, R., Nir, S., & Poulain, F. R. (1998). Analysis of binding and membrane destabilization of phospholipid membranes by surfactant apoprotein B. *Biochim Biophys Acta*, *1371*(2), 254-264. https://doi.org/10.1016/s0005-2736(98)00031-5

Chary, A., Groff, K., Stucki, A. O., Contal, S., Stoffels, C., Cambier, S., Sharma, M., Gutleb, A. C., & Clippinger, A. J. (2022). Maximizing the relevance and reproducibility of A549 cell culture using FBS-free media. *Toxicol In Vitro*, *83*, 105423. https://doi.org/10.1016/j.tiv.2022.105423

Chavarha, M., Khoojinian, H., Schulwitz, L. E., Jr., Biswas, S. C., Rananavare, S. B., & Hall, S. B. (2010). Hydrophobic surfactant proteins induce a phosphatidylethanolamine to form cubic phases. *Biophys J*, *98*(8), 1549-1557. https://doi.org/10.1016/j.bpj.2009.12.4302

Chavarha, M., Loney, R. W., Rananavare, S. B., & Hall, S. B. (2013). An anionic phospholipid enables the hydrophobic surfactant proteins to alter spontaneous curvature. *Biophys J*, *104*(3), 594-603. https://doi.org/10.1016/j.bpj.2012.12.041

Chen, S., Saeed, A., Liu, Q., Jiang, Q., Xu, H., Xiao, G. G., Rao, L., & Duo, Y. (2023). Macrophages in immunoregulation and therapeutics. *Signal Transduct Target Ther*, *8*(1), 207. https://doi.org/10.1038/s41392-023-01452-1

Chen, X., Hyatt, B. A., Mucenski, M. L., Mason, R. J., & Shannon, J. M. (2006). Identification and characterization of a lysophosphatidylcholine acyltransferase in alveolar type II cells. *Proc Natl Acad Sci U S A*, *103*(31), 11724-11729. https://doi.org/10.1073/pnas.0604946103

Cheong, N., Zhang, H., Madesh, M., Zhao, M., Yu, K., Dodia, C., Fisher, A. B., Savani, R. C., & Shuman, H. (2007). ABCA3 is critical for lamellar body biogenesis in vivo. *J Biol Chem*, *282*(33), 23811-23817. https://doi.org/10.1074/jbc.M703927200

Chevallet, M., Luche, S., & Rabilloud, T. (2006). Silver staining of proteins in polyacrylamide gels. *Nat Protoc*, *1*(4), 1852-1858. https://doi.org/10.1038/nprot.2006.288

Clark, J. C., Wert, S. E., Bachurski, C. J., Stahlman, M. T., Stripp, B. R., Weaver, T. E., & Whitsett, J. A. (1995). Targeted disruption of the surfactant protein B gene disrupts surfactant homeostasis, causing respiratory failure in newborn mice. *Proc Natl Acad Sci U S A*, *92*(17), 7794-7798. https://doi.org/10.1073/pnas.92.17.7794

Clements, J. A. (1977). Functions of the alveolar lining. *Am Rev Respir Dis*, *115*(6 Pt 2), 67-71. https://doi.org/10.1164/arrd.1977.115.S.67

Crapo, J. D., Barry, B. E., Gehr, P., Bachofen, M., & Weibel, E. R. (1982). Cell number and cell characteristics of the normal human lung. *Am Rev Respir Dis*, *126*(2), 332-337. https://doi.org/10.1164/arrd.1982.126.2.332

Creuwels, L. A., Demel, R. A., van Golde, L. M., Benson, B. J., & Haagsman, H. P. (1993). Effect of acylation on structure and function of surfactant protein C at the air-liquid interface. *J Biol Chem*, *268*(35), 26752-26758.

Creuwels, L. A., Demel, R. A., van Golde, L. M., & Haagsman, H. P. (1995). Characterization of a dimeric canine form of surfactant protein C (SP-C). *Biochim Biophys Acta*, *1254*(3), 326-332. https://doi.org/10.1016/0005-2760(94)00195-5

Crouch, E., Persson, A., Chang, D., & Heuser, J. (1994). Molecular structure of pulmonary surfactant protein D (SP-D). *Journal of Biological Chemistry*, *269*(25), 17311-17319. https://doi.org/https://doi.org/10.1016/S0021-9258(17)32556-5

Crouch, E., & Wright, J. R. (2001). Surfactant Proteins A and D and Pulmonary Host Defense. *Annual Review of Physiology*, *63*(Volume 63, 2001), 521-554. https://doi.org/https://doi.org/10.1146/annurev.physiol.63.1.521

Crouch, E. C. (1998). Structure, biologic properties, and expression of surfactant protein D (SP-D). *Biochim Biophys Acta*, *1408*(2-3), 278-289. https://doi.org/10.1016/s0925-4439(98)00073-8

Cruz, A., Casals, C., & Perez-Gil, J. (1995). Conformational flexibility of pulmonary surfactant proteins SP-B and SP-C, studied in aqueous organic solvents. *Biochim Biophys Acta*, *1255*(1), 68-76. https://doi.org/10.1016/0005-2760(94)00210-p

Cruz, A., Casals, C., Plasencia, I., Marsh, D., & Pérez-Gil, J. (1998). Depth profiles of pulmonary surfactant protein B in phosphatidylcholine bilayers, studied by fluorescence and electron spin resonance spectroscopy. *Biochemistry*, *37*(26), 9488-9496. https://doi.org/10.1021/bi971558v

Davenport, L., Dale, R. E., Bisby, R. H., & Cundall, R. B. (1985). Transverse location of the fluorescent probe 1,6-diphenyl-1,3,5-hexatriene in model lipid bilayer membrane systems by resonance excitation energy transfer. *Biochemistry*, *24*(15), 4097-4108. https://doi.org/10.1021/bi00336a044

de Almeida, R. F. M., Loura, L. M. S., Fedorov, A., & Prieto, M. (2005). Lipid Rafts have Different Sizes Depending on Membrane Composition: A Time-resolved Fluorescence Resonance Energy Transfer Study. *Journal of Molecular Biology*, *346*(4), 1109-1120. https://doi.org/https://doi.org/10.1016/j.jmb.2004.12.026

8. Bibliography

Dico, A. S., Taneva, S., Morrow, M. R., & Keough, K. M. (1997). Effect of calcium on phospholipid interaction with pulmonary surfactant protein C. *Biophys J*, *73*(5), 2595-2602. https://doi.org/10.1016/s0006-3495(97)78289-4

Dietl, P., Haller, T., & Frick, M. (2012). Spatio-temporal aspects, pathways and actions of Ca(2+) in surfactant secreting pulmonary alveolar type II pneumocytes. *Cell Calcium*, *52*(3-4), 296-302. https://doi.org/10.1016/j.ceca.2012.04.010

Dluhy, R. A., Shanmukh, S., Leapard, J. B., Krüger, P., & Baatz, J. E. (2003). Deacylated pulmonary surfactant protein SP-C transforms from alpha-helical to amyloid fibril structure via a pH-dependent mechanism: an infrared structural investigation. *Biophys J*, *85*(4), 2417-2429. https://doi.org/10.1016/s0006-3495(03)74665-7

Doole, F. T., Kumarage, T., Ashkar, R., & Brown, M. F. (2022). Cholesterol Stiffening of Lipid Membranes. *J Membr Biol*, *255*(4-5), 385-405. https://doi.org/10.1007/s00232-022-00263-9

Doyle, I. R., Jones, M. E., Barr, H. A., Orgeig, S., Crockett, A. J., McDonald, C. F., & Nicholas, T. E. (1994). Composition of human pulmonary surfactant varies with exercise and level of fitness. *Am J Respir Crit Care Med*, *149*(6), 1619-1627. https://doi.org/10.1164/ajrccm.149.6.8004321

Ertunc, M. E., & Hotamisligil, G. S. (2016). Lipid signaling and lipotoxicity in metaflammation: indications for metabolic disease pathogenesis and treatment. *J Lipid Res*, *57*(12), 2099-2114. https://doi.org/10.1194/jlr.R066514

Escriba, P. (2018). 2014 BBA 3 Nacholeate 2-hydroxyoleic acid and sphingomyelin synthase in cancer.

Farmer, C. G. (2015). The Evolution of Unidirectional Pulmonary Airflow. *Physiology*, *30*(4), 260-272. https://doi.org/10.1152/physiol.00056.2014

Fehrenbach, H. (2001). Alveolar epithelial type II cell: defender of the alveolus revisited. *Respiratory Research*, *2*(1), 33. https://doi.org/10.1186/rr36

Fernandes, F., Loura, L. M., Prieto, M., Koehorst, R., Spruijt, R. B., & Hemminga, M. A. (2003). Dependence of M13 major coat protein oligomerization and lateral segregation on bilayer composition. *Biophys J*, *85*(4), 2430-2441. https://doi.org/10.1016/s0006-3495(03)74666-9

Filipe, H. A., Santos, L. S., Prates Ramalho, J. P., Moreno, M. J., & Loura, L. M. (2015). Behaviour of NBD-head group labelled phosphatidylethanolamines in POPC bilayers: a molecular dynamics study. *Phys Chem Chem Phys*, *17*(31), 20066-20079. https://doi.org/10.1039/c5cp01596k

Filippov, A., Orädd, G., & Lindblom, G. (2003). Influence of Cholesterol and Water Content on Phospholipid Lateral Diffusion in Bilayers. *Langmuir*, *19*(16), 6397-6400. https://doi.org/10.1021/la034222x

Filippov, A., Orädd, G., & Lindblom, G. (2004). Lipid Lateral Diffusion in Ordered and Disordered Phases in Raft Mixtures. *Biophysical Journal*, *86*(2), 891-896. https://doi.org/https://doi.org/10.1016/S0006-3495(04)74164-8

Fisher, A. B., & Dodia, C. (1996). Role of phospholipase A2 enzymes in degradation of dipalmitoylphosphatidylcholine by granular pneumocytes. *J Lipid Res*, *37*(5), 1057-1064.

Fisher, A. B., & Dodia, C. (2001). Lysosomal-type PLA2 and turnover of alveolar DPPC. *American Journal of Physiology-Lung Cellular and Molecular Physiology*, *280*(4), L748-L754. https://doi.org/10.1152/ajplung.2001.280.4.L748

Fisher, A. B., Dodia, C., & Chander, A. (1994). Inhibition of lung calcium-independent phospholipase A2 by surfactant protein A. *Am J Physiol*, *267*(3 Pt 1), L335-341. https://doi.org/10.1152/ajplung.1994.267.3.L335

Foster, K. A., Oster, C. G., Mayer, M. M., Avery, M. L., & Audus, K. L. (1998). Characterization of the A549 Cell Line as a Type II Pulmonary Epithelial Cell Model for Drug Metabolism. *Experimental Cell Research*, *243*(2), 359-366. https://doi.org/https://doi.org/10.1006/excr.1998.4172

Frick, M., Bertocchi, C., Jennings, P., Haller, T., Mair, N., Singer, W., Pfaller, W., Ritsch-Marte, M., & Dietl, P. (2004). Ca2+ entry is essential for cell strain-induced lamellar body fusion in isolated rat type II pneumocytes. *Am J Physiol Lung Cell Mol Physiol*, *286*(1), L210-220. https://doi.org/10.1152/ajplung.00332.2003

García-Álvarez, B., Alonso, A., & Pérez-Gil, J. (2019). Structure and Function of Pulmonary Surfactant Proteins. In *eLS* (pp. 1-15). https://doi.org/https://doi.org/10.1002/9780470015902.a0027639

Garcia-Mouton, C., Hidalgo, A., Cruz, A., & Pérez-Gil, J. (2019). The Lord of the Lungs: The essential role of pulmonary surfactant upon inhalation of nanoparticles. *European Journal of Pharmaceutics and Biopharmaceutics*, *144*, 230-243. https://doi.org/https://doi.org/10.1016/j.ejpb.2019.09.020

García-Murria, M. J., Expósito-Domínguez, N., Duart, G., Mingarro, I., & Martinez-Gil, L. (2019). A Bimolecular Multicellular Complementation System for the Detection of Syncytium Formation: A New Methodology for the Identification of Nipah Virus Entry Inhibitors. *Viruses*, *11*(3). https://doi.org/10.3390/v11030229

Garcia-Verdugo, I., Garcia de Paco, E., Espinassous, Q., Gonzalez-Horta, A., Synguelakis, M., Kanellopoulos, J., Rivas, L., Chaby, R., & Perez-Gil, J. (2009). Synthetic peptides representing the N-terminal segment of surfactant protein C modulate LPS-stimulated TNF-alpha production by macrophages. *Innate Immun*, *15*(1), 53-62. https://doi.org/10.1177/1753425908100500

Gerson, K. D., Foster, C. D., Zhang, P., Zhang, Z., Rosenblatt, M. M., & Guttentag, S. H. (2008). Pepsinogen C proteolytic processing of surfactant protein B. *J Biol Chem*, *283*(16), 10330-10338. https://doi.org/10.1074/jbc.M707516200

Glasser, S. W., Detmer, E. A., Ikegami, M., Na, C. L., Stahlman, M. T., & Whitsett, J. A. (2003). Pneumonitis and emphysema in sp-C gene targeted mice. *J Biol Chem*, *278*(16), 14291-14298. https://doi.org/10.1074/jbc.M210909200

Glasser, S. W., Maxfield, M. D., Ruetschilling, T. L., Akinbi, H. T., Baatz, J. E., Kitzmiller, J. A., Page, K., Xu, Y., Bao, E. L., & Korfhagen, T. R. (2013). Persistence of LPS-induced lung inflammation in surfactant protein-C-deficient mice. *Am J Respir Cell Mol Biol*, *49*(5), 845-854. https://doi.org/10.1165/rcmb.2012-0374OC

Glasser, S. W., Senft, A. P., Whitsett, J. A., Maxfield, M. D., Ross, G. F., Richardson, T. R., Prows, D. R., Xu, Y., & Korfhagen, T. R. (2008). Macrophage dysfunction

and susceptibility to pulmonary Pseudomonas aeruginosa infection in surfactant protein C-deficient mice. *J Immunol*, *181*(1), 621-628. https://doi.org/10.4049/jimmunol.181.1.621

Glasser, S. W., Witt, T. L., Senft, A. P., Baatz, J. E., Folger, D., Maxfield, M. D., Akinbi, H. T., Newton, D. A., Prows, D. R., & Korfhagen, T. R. (2009). Surfactant protein C-deficient mice are susceptible to respiratory syncytial virus infection. *Am J Physiol Lung Cell Mol Physiol*, *297*(1), L64-72. https://doi.org/10.1152/ajplung.90640.2008

Goerke, J. (1998). Pulmonary surfactant: functions and molecular composition. *Biochim Biophys Acta*, *1408*(2-3), 79-89. https://doi.org/10.1016/s0925-4439(98)00060-x

Goldstein, J. L., Anderson, R. G., & Brown, M. S. (1979). Coated pits, coated vesicles, and receptor-mediated endocytosis. *Nature*, *279*(5715), 679-685. https://doi.org/10.1038/279679a0

Gómez-Gil, L., Pérez-Gil, J., & Goormaghtigh, E. (2009). Cholesterol modulates the exposure and orientation of pulmonary surfactant protein SP-C in model surfactant membranes. *Biochim Biophys Acta*, *1788*(9), 1907-1915. https://doi.org/10.1016/j.bbamem.2009.05.011

Gómez-Gil, L., Schürch, D., Goormaghtigh, E., & Pérez-Gil, J. (2009). Pulmonary surfactant protein SP-C counteracts the deleterious effects of cholesterol on the activity of surfactant films under physiologically relevant compression-expansion dynamics. *Biophys J*, *97*(10), 2736-2745. https://doi.org/10.1016/j.bpj.2009.08.045

Gonzalez-Horta, A., Andreu, D., Morrow, M. R., & Perez-Gil, J. (2008). Effects of palmitoylation on dynamics and phospholipid-bilayer-perturbing properties of the N-terminal segment of pulmonary surfactant protein SP-C as shown by 2H-NMR. *Biophys J*, *95*(5), 2308-2317. https://doi.org/10.1529/biophysj.108.132845

González-Horta, A. D. C. (2006). *Propiedades membrano-activas e inmunomoduladoras de la proteína SP-C del surfactante pulmonar: papel del segmento N-terminal* Universidad Complutense de Madrid]. Faculty of Biological Sciences. https://produccioncientifica.ucm.es/documentos/5d1df64629995204f7666daa

Gordon, L. M., Horvath, S., Longo, M. L., Zasadzinski, J. A. N., Taeusch, H. W., Faull, K., Leung, C., & Waring, A. J. (1996). Conformation and molecular topography of the N-terminal segment of surfactant protein B in structure-promoting environments. *Protein Science*, *5*(8), 1662-1675. https://doi.org/https://doi.org/10.1002/pro.5560050820

Grau, B., Javanainen, M., García-Murria, M. J., Kulig, W., Vattulainen, I., Mingarro, I., & Martínez-Gil, L. (2017). The role of hydrophobic matching on transmembrane helix packing in cells. *Cell Stress*, *1*(2), 90-106. https://doi.org/10.15698/cst2017.11.111

Guillot, L., Nathan, N., Tabary, O., Thouvenin, G., Le Rouzic, P., Corvol, H., Amselem, S., & Clement, A. (2013). Alveolar epithelial cells: master regulators of lung homeostasis. *Int J Biochem Cell Biol*, *45*(11), 2568-2573. https://doi.org/10.1016/j.biocel.2013.08.009

Gunasekara, L., Schürch, S., Schoel, W. M., Nag, K., Leonenko, Z., Haufs, M., & Amrein, M. (2005). Pulmonary surfactant function is abolished by an elevated proportion of cholesterol. *Biochim Biophys Acta*, *1737*(1), 27-35. https://doi.org/10.1016/j.bbalip.2005.09.002

Günther, A., Schmidt, R., Feustel, A., Meier, U., Pucker, C., Ermert, M., & Seeger, W. (1999). Surfactant subtype conversion is related to loss of surfactant apoprotein B and surface activity in large surfactant aggregates. Experimental and clinical studies. *Am J Respir Crit Care Med*, *159*(1), 244-251. https://doi.org/10.1164/ajrccm.159.1.9612005

Gustafsson, M., Griffiths, W. J., Furusjö, E., & Johansson, J. (2001). The palmitoyl groups of lung surfactant protein C reduce unfolding into a fibrillogenic intermediate. *J Mol Biol*, *310*(4), 937-950. https://doi.org/10.1006/jmbi.2001.4810

Guttentag, S., Robinson, L., Zhang, P., Brasch, F., Bühling, F., & Beers, M. (2003). Cysteine protease activity is required for surfactant protein B processing and lamellar body genesis. *Am J Respir Cell Mol Biol*, *28*(1), 69-79. https://doi.org/10.1165/rcmb.2002-0111OC

Guttentag, S. H., Beers, M. F., Bieler, B. M., & Ballard, P. L. (1998). Surfactant protein B processing in human fetal lung. *American Journal of Physiology-Lung Cellular and Molecular Physiology*, *275*(3), L559-L566. https://doi.org/10.1152/ajplung.1998.275.3.L559

Haagsman, H. P., & Van Golde, L. M. G. (1991). Synthesis and Assembly of Lung Surfactant. *Annual Review of Physiology*, *53*(Volume 53), 441-464. https://doi.org/https://doi.org/10.1146/annurev.ph.53.030191.002301

Halliday, H. L. (2017). The fascinating story of surfactant. *J Paediatr Child Health*, *53*(4), 327-332. https://doi.org/10.1111/jpc.13500

Hamvas, A., Nogee, L. M., White, F. V., Schuler, P., Hackett, B. P., Huddleston, C. B., Mendeloff, E. N., Hsu, F. F., Wert, S. E., Gonzales, L. W., Beers, M. F., & Ballard, P. L. (2004). Progressive lung disease and surfactant dysfunction with a deletion in surfactant protein C gene. *Am J Respir Cell Mol Biol*, *30*(6), 771-776. https://doi.org/10.1165/rcmb.2003-0323OC

Hashimoto, M., Asai, Y., & Ogawa, T. (2003). Treponemal phospholipids inhibit innate immune responses induced by pathogen-associated molecular patterns. *J Biol Chem*, *278*(45), 44205-44213. https://doi.org/10.1074/jbc.M306735200

Haugland, R. P. (2002). *Handbook of fluorescent probes and research products*. Molecular probes.

Hawgood, S., & Poulain, F. R. (2001). The pulmonary collectins and surfactant metabolism. *Annu Rev Physiol*, *63*, 495-519. https://doi.org/10.1146/annurev.physiol.63.1.495

Hidalgo, A., Garcia-Mouton, C., Autilio, C., Carravilla, P., Orellana, G., Islam, M. N., Bhattacharya, J., Bhattacharya, S., Cruz, A., & Pérez-Gil, J. (2021). Pulmonary surfactant and drug delivery: Vehiculization, release and targeting of surfactant/tacrolimus formulations. *J Control Release*, *329*, 205-222. https://doi.org/10.1016/j.jconrel.2020.11.042

8. Bibliography

Hills, B. A. (1999). An alternative view of the role(s) of surfactant and the alveolar model. *J Appl Physiol (1985)*, *87*(5), 1567-1583. https://doi.org/10.1152/jappl.1999.87.5.1567

Hobi, N., Giolai, M., Olmeda, B., Miklavc, P., Felder, E., Walther, P., Dietl, P., Frick, M., Pérez-Gil, J., & Haller, T. (2016). A small key unlocks a heavy door: The essential function of the small hydrophobic proteins SP-B and SP-C to trigger adsorption of pulmonary surfactant lamellar bodies. *Biochimica et Biophysica Acta (BBA) - Molecular Cell Research*, *1863*(8), 2124-2134. https://doi.org/https://doi.org/10.1016/j.bbamcr.2016.04.028

Hogan, J., Smith, P., Heath, D., & Harris, P. (1986). The thickness of the alveolar capillary wall in the human lung at high and low altitude. *Br J Dis Chest*, *80*(1), 13-18. https://doi.org/10.1016/0007-0971(86)90004-5

Horowitz, A. D., Baatz, J. E., & Whitsett, J. A. (1993). Lipid effects on aggregation of pulmonary surfactant protein SP-C studied by fluorescence energy transfer. *Biochemistry*, *32*(37), 9513-9523. https://doi.org/10.1021/bi00088a001

Horowitz, A. D., Moussavian, B., Han, E. D., Baatz, J. E., & Whitsett, J. A. (1997). Distinct effects of SP-A and SP-B on endocytosis of SP-C by pulmonary epithelial cells. *Am J Physiol*, *273*(1 Pt 1), L159-171. https://doi.org/10.1152/ajplung.1997.273.1.L159

Hsia, C. C., Hyde, D. M., & Weibel, E. R. (2016). Lung Structure and the Intrinsic Challenges of Gas Exchange. *Compr Physiol*, *6*(2), 827-895. https://doi.org/10.1002/cphy.c150028

Hsia, C. C., Schmitz, A., Lambertz, M., Perry, S. F., & Maina, J. N. (2013). Evolution of air breathing: oxygen homeostasis and the transitions from water to land and sky. *Compr Physiol*, *3*(2), 849-915. https://doi.org/10.1002/cphy.c120003

Hussell, T., & Bell, T. J. (2014). Alveolar macrophages: plasticity in a tissue-specific context. *Nature Reviews Immunology*, *14*(2), 81-93. https://doi.org/10.1038/nri3600

Ikegami, M. (2000). Surfactant metabolism in SP-D deficient mice. *9*, 251-253.

Ikegami, M., Grant, S., Korfhagen, T., Scheule, R. K., & Whitsett, J. A. (2009). Surfactant protein-D regulates the postnatal maturation of pulmonary surfactant lipid pool sizes. *J Appl Physiol (1985)*, *106*(5), 1545-1552. https://doi.org/10.1152/japplphysiol.91567.2008

Ikegami, M., Horowitz, A. D., Whitsett, J. A., & Jobe, A. H. (1998). Clearance of SP-C and recombinant SP-C in vivo and in vitro. *Am J Physiol*, *274*(6), L933-939. https://doi.org/10.1152/ajplung.1998.274.6.L933

Ikegami, M., Korfhagen, T. R., Whitsett, J. A., Bruno, M. D., Wert, S. E., Wada, K., & Jobe, A. H. (1998). Characteristics of surfactant from SP-A-deficient mice. *Am J Physiol*, *275*(2), L247-254. https://doi.org/10.1152/ajplung.1998.275.2.L247

Iriondo, M. N., Etxaniz, A., Varela, Y. R., Ballesteros, U., Hervás, J. H., Montes, L. R., Goñi, F. M., & Alonso, A. (2022). LC3 subfamily in cardiolipin-mediated mitophagy: a comparison of the LC3A, LC3B and LC3C homologs. *Autophagy*, *18*(12), 2985-3003. https://doi.org/10.1080/15548627.2022.2062111

Ishiyama, J., Taguchi, R., Akasaka, Y., Shibata, S., Ito, M., Nagasawa, M., & Murakami, K. (2011). Unsaturated FAs prevent palmitate-induced LOX-1 induction via inhibition of ER stress in macrophages. *J Lipid Res*, *52*(2), 299-307. https://doi.org/10.1194/jlr.M007104

Jain, P., Motosuke, M., & Aida, T. (2021). *Fluorescence Anisotropy Studies of Fluorescein*. https://doi.org/10.20944/preprints202105.0189.v1

Jin, H., Ciechanowicz, A. K., Kaplan, A. R., Wang, L., Zhang, P. X., Lu, Y. C., Tobin, R. E., Tobin, B. A., Cohn, L., Zeiss, C. J., Lee, P. J., Bruscia, E. M., & Krause, D. S. (2018). Surfactant protein C dampens inflammation by decreasing JAK/STAT activation during lung repair. *Am J Physiol Lung Cell Mol Physiol*, *314*(5), L882-l892. https://doi.org/10.1152/ajplung.00418.2017

Johansson, H., Eriksson, M., Nordling, K., Presto, J., & Johansson, J. (2009). The Brichos domain of prosurfactant protein C can hold and fold a transmembrane segment. *Protein Sci*, *18*(6), 1175-1182. https://doi.org/10.1002/pro.123

Johansson, J. (1998). Structure and properties of surfactant protein C. *Biochim Biophys Acta*, *1408*(2-3), 161-172. https://doi.org/10.1016/s0925-4439(98)00065-9

Johansson, J. (2001). Membrane properties and amyloid fibril formation of lung surfactant protein C. *Biochem Soc Trans*, *29*(Pt 4), 601-606. https://doi.org/10.1042/bst0290601

Johansson, J., Curstedt, T., & Jörnvall, H. (1991). Surfactant protein B: disulfide bridges, structural properties, and kringle similarities. *Biochemistry*, *30*(28), 6917-6921. https://doi.org/10.1021/bi00242a015

Johansson, J., Curstedt, T., & Robertson, B. (1994). The proteins of the surfactant system. *Eur Respir J*, *7*(2), 372-391. https://doi.org/10.1183/09031936.94.07020372

Johansson, J., Nilsson, G., Strömberg, R., Robertson, B., Jörnvall, H., & Curstedt, T. (1995). Secondary structure and biophysical activity of synthetic analogues of the pulmonary surfactant polypeptide SP-C. *Biochem J*, *307 (Pt 2)*(Pt 2), 535-541. https://doi.org/10.1042/bj3070535

Johansson, J., Szyperski, T., Curstedt, T., & Wüthrich, K. (1994). The NMR structure of the pulmonary surfactant-associated polypeptide SP-C in an apolar solvent contains a valyl-rich alpha-helix. *Biochemistry*, *33*(19), 6015-6023. https://doi.org/10.1021/bi00185a042

Johansson, J., Weaver, T. E., & Tjernberg, L. O. (2004). Proteolytic generation and aggregation of peptides from transmembrane regions: lung surfactant protein C and amyloid beta-peptide. *Cell Mol Life Sci*, *61*(3), 326-335. https://doi.org/10.1007/s00018-003-3274-6

Johnson, A. L., Braidotti, P., Pietra, G. G., Russo, S. J., Kabore, A., Wang, W. J., & Beers, M. F. (2001). Post-translational processing of surfactant protein-C proprotein: targeting motifs in the NH(2)-terminal flanking domain are cleaved in late compartments. *Am J Respir Cell Mol Biol*, *24*(3), 253-263. https://doi.org/10.1165/ajrcmb.24.3.4312

Kairys, V., Gilson, M. K., & Luy, B. (2004). Structural model for an AxxxG-mediated dimer of surfactant-associated protein C. *Eur J Biochem*, *271*(11), 2086-2092. https://doi.org/10.1111/j.1432-1033.2004.04107.x

8. Bibliography

Kandasamy, P., Zarini, S., Chan, E. D., Leslie, C. C., Murphy, R. C., & Voelker, D. R. (2011). Pulmonary surfactant phosphatidylglycerol inhibits Mycoplasma pneumoniae-stimulated eicosanoid production from human and mouse macrophages. *J Biol Chem*, *286*(10), 7841-7853. https://doi.org/10.1074/jbc.M110.170241

Kang, Y.-F., Chen, W.-K., Teng, K.-X., Wang, L.-Y., Xu, X.-C., Niu, L.-Y., Cui, G., & Yang, Q.-Z. (2022). Aggregation Turns BODIPY Fluorophores into Photosensitizers: Reversibly Switching Intersystem Crossing On and Off for Smart Photodynamic Therapy. *CCS Chemistry*, *4*(11), 3516-3528. https://doi.org/doi:10.31635/ccschem.021.202101600

Kasting, J. F., & Siefert, J. L. (2002). Life and the evolution of Earth's atmosphere. *Science*, *296*(5570), 1066-1068. https://doi.org/10.1126/science.1071184

Keating, E., Rahman, L., Francis, J., Petersen, A., Possmayer, F., Veldhuizen, R., & Petersen, N. O. (2007). Effect of cholesterol on the biophysical and physiological properties of a clinical pulmonary surfactant. *Biophys J*, *93*(4), 1391-1401. https://doi.org/10.1529/biophysj.106.099762

Keating, E., Zuo, Y. Y., Tadayyon, S. M., Petersen, N. O., Possmayer, F., & Veldhuizen, R. A. (2012). A modified squeeze-out mechanism for generating high surface pressures with pulmonary surfactant. *Biochim Biophys Acta*, *1818*(5), 1225-1234. https://doi.org/10.1016/j.bbamem.2011.12.007

Keller, A., Eistetter, H. R., Voss, T., & Schäfer, K. P. (1991). The pulmonary surfactant protein C (SP-C) precursor is a type II transmembrane protein. *Biochemical Journal*, *277*(2), 493-499. https://doi.org/10.1042/bj2770493

Kelly, C., Jefferies, C., & Cryan, S. A. (2011). Targeted liposomal drug delivery to monocytes and macrophages. *J Drug Deliv*, *2011*, 727241. https://doi.org/10.1155/2011/727241

Khan, I., Saeed, K., & Khan, I. (2019). Nanoparticles: Properties, applications and toxicities. *Arabian Journal of Chemistry*, *12*(7), 908-931. https://doi.org/https://doi.org/10.1016/j.arabjc.2017.05.011

Kirchhoff, R., Chromik, M. A., & Schebb, N. H. (2024). Phagocytosis is differentially regulated by LPS in M1- and M2-like macrophages via PGE₂ formation and EP4 signaling. *bioRxiv*, 2024.2009.2029.615656. https://doi.org/10.1101/2024.09.29.615656

Kishore, U., Greenhough, T. J., Waters, P., Shrive, A. K., Ghai, R., Kamran, M. F., Bernal, A. L., Reid, K. B., Madan, T., & Chakraborty, T. (2006). Surfactant proteins SP-A and SP-D: structure, function and receptors. *Mol Immunol*, *43*(9), 1293-1315. https://doi.org/10.1016/j.molimm.2005.08.004

Knudsen, L., & Ochs, M. (2018). The micromechanics of lung alveoli: structure and function of surfactant and tissue components. *Histochem Cell Biol*, *150*(6), 661-676. https://doi.org/10.1007/s00418-018-1747-9

Korfhagen, T. R., Glasser, S. W., Wert, S. E., Bruno, M. D., Daugherty, C. C., McNeish, J. D., Stock, J. L., Potter, S. S., & Whitsett, J. A. (1990). Cis-acting sequences from a human surfactant protein gene confer pulmonary-specific gene expression in transgenic mice. *Proceedings of the National Academy of Sciences*, *87*(16), 6122-6126. https://doi.org/doi:10.1073/pnas.87.16.6122

Korolainen, H., Lolicato, F., Enkavi, G., Pérez-Gil, J., Kulig, W., & Vattulainen, I. (2022). Dimerization of the pulmonary surfactant protein C in a membrane environment. *PLoS One*, *17*(4), e0267155. https://doi.org/10.1371/journal.pone.0267155

Krol, S., Ross, M., Sieber, M., Künneke, S., Galla, H. J., & Janshoff, A. (2000). Formation of three-dimensional protein-lipid aggregates in monolayer films induced by surfactant protein B. *Biophys J*, *79*(2), 904-918. https://doi.org/10.1016/s0006-3495(00)76346-6

Kuroki, Y., & Akino, T. (1991). Pulmonary surfactant protein A (SP-A) specifically binds dipalmitoylphosphatidylcholine. *J Biol Chem*, *266*(5), 3068-3073.

Lakowicz, J. R. (2006). Introduction to Fluorescence. In J. R. Lakowicz (Ed.), *Principles of Fluorescence Spectroscopy* (Third ed., pp. 1-26). Springer US. https://doi.org/10.1007/978-0-387-46312-4_1

Lakowicz, J. R., & Masters, B. R. (2008). Principles of fluorescence spectroscopy. *Journal of Biomedical Optics*, *13*(2), 029901.

Lawson, W. E., Grant, S. W., Ambrosini, V., Womble, K. E., Dawson, E. P., Lane, K. B., Markin, C., Renzoni, E., Lympany, P., Thomas, A. Q., Roldan, J., Scott, T. A., Blackwell, T. S., Phillips, J. A., Loyd, J. E., & du Bois, R. M. (2004). Genetic mutations in surfactant protein C are a rare cause of sporadic cases of IPF. *Thorax*, *59*(11), 977. https://doi.org/10.1136/thx.2004.026336

Lee, K., Khoshnood, B., Wall, S. N., Chang, Y., Hsieh, H. L., & Singh, J. K. (1999). Trend in mortality from respiratory distress syndrome in the United States, 1970-1995. *J Pediatr*, *134*(4), 434-440. https://doi.org/10.1016/s0022-3476(99)70200-3

Lemmon, M. A., Flanagan, J. M., Treutlein, H. R., Zhang, J., & Engelman, D. M. (1992). Sequence specificity in the dimerization of transmembrane .alpha.-helixes. *Biochemistry*, *31*(51), 12719-12725. https://doi.org/10.1021/bi00166a002

Liekkinen, J., Olżyńska, A., Cwiklik, L., Bernardino de la Serna, J., Vattulainen, I., & Javanainen, M. (2023). Surfactant Proteins SP-B and SP-C in Pulmonary Surfactant Monolayers: Physical Properties Controlled by Specific Protein-Lipid Interactions. *Langmuir*, *39*(12), 4338-4350. https://doi.org/10.1021/acs.langmuir.2c03349

Liggins, G. C. (1969). Premature delivery of foetal lambs infused with glucocorticoids. *J Endocrinol*, *45*(4), 515-523. https://doi.org/10.1677/joe.0.0450515

Lin, S., Ikegami, M., Moon, C., Naren, A. P., & Shannon, J. M. (2015). Lysophosphatidylcholine Acyltransferase 1 (LPCAT1) Specifically Interacts with Phospholipid Transfer Protein StarD10 to Facilitate Surfactant Phospholipid Trafficking in Alveolar Type II Cells. *J Biol Chem*, *290*(30), 18559-18574. https://doi.org/10.1074/jbc.M115.666701

Lipowsky, R. (2023). Remodeling of Biomembranes and Vesicles by Adhesion of Condensate Droplets. *Membranes*, *13*, 223. https://doi.org/10.3390/membranes13020223

Liu, Z., Jiang, Z., Yan, M., & Wang, X. (2019). Recent Progress of BODIPY Dyes With Aggregation-Induced Emission. *Front Chem*, *7*, 712. https://doi.org/10.3389/fchem.2019.00712

8. Bibliography

Lopez-Rodriguez, E., & Pérez-Gil, J. (2014). Structure-function relationships in pulmonary surfactant membranes: from biophysics to therapy. *Biochim Biophys Acta*, *1838*(6), 1568-1585. https://doi.org/10.1016/j.bbamem.2014.01.028

Loura, L. M., Fedorov, A., & Prieto, M. (1996a). Resonance energy transfer in a model system of membranes: application to gel and liquid crystalline phases. *Biophys J*, *71*(4), 1823-1836. https://doi.org/10.1016/s0006-3495(96)79383-9

Loura, L. M., Fedorov, A., & Prieto, M. (1996b). Resonance energy transfer in a model system of membranes: application to gel and liquid crystalline phases. *Biophysical Journal*, *71*(4), 1823-1836. https://doi.org/https://doi.org/10.1016/S0006-3495(96)79383-9

Loura, L. M. S., Fedorov, A., & Prieto, M. (2000). Membrane Probe Distribution Heterogeneity: A Resonance Energy Transfer Study. *The Journal of Physical Chemistry B*, *104*(29), 6920-6931. https://doi.org/10.1021/jp000246q

Loura, L. M. S., & Prieto, M. (2000). Resonance Energy Transfer in Heterogeneous Planar and Bilayer Systems: Theory and Simulation. *The Journal of Physical Chemistry B*, *104*(29), 6911-6919. https://doi.org/10.1021/jp000245y

Lovelock, J. (2003). Gaia: the living Earth. *Nature*, *426*(6968), 769-770. https://doi.org/10.1038/426769a

Lukovic, D., Cruz, A., Gonzalez-Horta, A., Almlen, A., Curstedt, T., Mingarro, I., & Pérez-Gil, J. (2012). Interfacial behavior of recombinant forms of human pulmonary surfactant protein SP-C. *Langmuir*, *28*(20), 7811-7825. https://doi.org/10.1021/la301134v

Lukovic, D., Plasencia, I., Taberner, F. J., Salgado, J., Calvete, J. J., Pérez-Gil, J., & Mingarro, I. (2006). Production and characterisation of recombinant forms of human pulmonary surfactant protein C (SP-C): Structure and surface activity. *Biochim Biophys Acta*, *1758*(4), 509-518. https://doi.org/10.1016/j.bbamem.2006.03.005

Luy, B., Diener, A., Hummel, R. P., Sturm, E., Ulrich, W. R., & Griesinger, C. (2004). Structure and potential C-terminal dimerization of a recombinant mutant of surfactant-associated protein C in chloroform/methanol. *Eur J Biochem*, *271*(11), 2076-2085. https://doi.org/10.1111/j.1432-1033.2004.04106.x

Maina, J. N. (2000). Comparative respiratory morphology: themes and principles in the design and construction of the gas exchangers. *Anat Rec*, *261*(1), 25-44. https://doi.org/10.1002/(sici)1097-0185(20000215)261:1<25::Aid-ar6>3.0.Co;2-7

Maina, J. N. (2002). Structure, function and evolution of the gas exchangers: comparative perspectives. *Journal of Anatomy*, *201*(4), 281-304. https://doi.org/https://doi.org/10.1046/j.1469-7580.2002.00099.x

Maina, J. N., & West, J. B. (2005). Thin and strong! The bioengineering dilemma in the structural and functional design of the blood-gas barrier. *Physiol Rev*, *85*(3), 811-844. https://doi.org/10.1152/physrev.00022.2004

Malacrida, L., Astrada, S., Briva, A., Bollati-Fogolín, M., Gratton, E., & Bagatolli, L. A. (2016). Spectral phasor analysis of LAURDAN fluorescence in live A549 lung cells to study the hydration and time evolution of intracellular lamellar

body-like structures. *Biochim Biophys Acta*, *1858*(11), 2625-2635. https://doi.org/10.1016/j.bbamem.2016.07.017

Maloney, J. E., Darian-Smith, C., Russell, B., Varghese, M., Cooper, J., & Limpus, C. J. (1989). An evolutionary link for developing mammalian lungs. *J Dev Physiol*, *12*(3), 153-155.

Marquardt, D. W. (1963). An Algorithm for Least-Squares Estimation of Nonlinear Parameters. *Journal of the Society for Industrial and Applied Mathematics*, *11*(2), 431-441. https://doi.org/10.1137/0111030

Martínez-Calle, M., Olmeda, B., Dietl, P., Frick, M., & Pérez-Gil, J. (2018). Pulmonary surfactant protein SP-B promotes exocytosis of lamellar bodies in alveolar type II cells. *Faseb j*, *32*(8), 4600-4611. https://doi.org/10.1096/fj.201701462RR

Martínez-Calle, M., Parra-Ortiz, E., Cruz, A., Olmeda, B., & Pérez-Gil, J. (2021). Towards the Molecular Mechanism of Pulmonary Surfactant Protein SP-B: At the Crossroad of Membrane Permeability and Interfacial Lipid Transfer. *J Mol Biol*, *433*(3), 166749. https://doi.org/10.1016/j.jmb.2020.166749

Mason, R. J. (2006). Biology of alveolar type II cells. *Respirology*, *11*(s1), S12-S15. https://doi.org/https://doi.org/10.1111/j.1440-1843.2006.00800.x

Mathivet, L., Cribier, S., & Devaux, P. F. (1996). Shape change and physical properties of giant phospholipid vesicles prepared in the presence of an AC electric field. *Biophys J*, *70*(3), 1112-1121. https://doi.org/10.1016/s0006-3495(96)79693-5

Mayor, S., & Pagano, R. E. (2007). Pathways of clathrin-independent endocytosis. *Nat Rev Mol Cell Biol*, *8*(8), 603-612. https://doi.org/10.1038/nrm2216

McDonald, D. R., & Levy, O. (2013). 3 - Innate immunity. In R. R. Rich, T. A. Fleisher, W. T. Shearer, H. W. Schroeder, A. J. Frew, & C. M. Weyand (Eds.), *Clinical Immunology (Fourth Edition)* (pp. 35-46). Elsevier. https://doi.org/https://doi.org/10.1016/B978-0-7234-3691-1.00027-1

Merckx, P., De Backer, L., Van Hoecke, L., Guagliardo, R., Echaide, M., Baatsen, P., Olmeda, B., Saelens, X., Pérez-Gil, J., De Smedt, S. C., & Raemdonck, K. (2018). Surfactant protein B (SP-B) enhances the cellular siRNA delivery of proteolipid coated nanogels for inhalation therapy. *Acta Biomaterialia*, *78*, 236-246. https://doi.org/https://doi.org/10.1016/j.actbio.2018.08.012

Minutti, C. M., García-Fojeda, B., Sáenz, A., de Las Casas-Engel, M., Guillamat-Prats, R., de Lorenzo, A., Serrano-Mollar, A., Corbí Á, L., & Casals, C. (2016). Surfactant Protein A Prevents IFN-γ/IFN-γ Receptor Interaction and Attenuates Classical Activation of Human Alveolar Macrophages. *J Immunol*, *197*(2), 590-598. https://doi.org/10.4049/jimmunol.1501032

Morrow, M. R., Perez-Gil, J., Simatos, G., Boland, C., Stewart, J., Absolom, D., Sarin, V., & Keough, K. M. W. (1993). Pulmonary surfactant-associated protein SP-B has little effect on acyl chains in dipalmitoylphosphatidylcholine dispersions. *Biochemistry*, *32*(16), 4397-4402. https://doi.org/10.1021/bi00067a032

Morrow, M. R., Taneva, S., Simatos, G. A., Allwood, L. A., & Keough, K. M. (1993). 2H NMR studies of the effect of pulmonary surfactant SP-C on the 1,2-dipalmitoyl-sn-glycero-3-phosphocholine headgroup: a model for

transbilayer peptides in surfactant and biological membranes. *Biochemistry*, *32*(42), 11338-11344. https://doi.org/10.1021/bi00093a010

Mulugeta, S., & Beers, M. F. (2003). Processing of surfactant protein C requires a type II transmembrane topology directed by juxtamembrane positively charged residues. *J Biol Chem*, *278*(48), 47979-47986. https://doi.org/10.1074/jbc.M308210200

Mulugeta, S., Nureki, S., & Beers, M. F. (2015). Lost after translation: insights from pulmonary surfactant for understanding the role of alveolar epithelial dysfunction and cellular quality control in fibrotic lung disease. *Am J Physiol Lung Cell Mol Physiol*, *309*(6), L507-525. https://doi.org/10.1152/ajplung.00139.2015

Nag, K., Taneva, S. G., Perez-Gil, J., Cruz, A., & Keough, K. M. (1997). Combinations of fluorescently labeled pulmonary surfactant proteins SP-B and SP-C in phospholipid films. *Biophysical Journal*, *72*(6), 2638-2650. https://doi.org/https://doi.org/10.1016/S0006-3495(97)78907-0

Nakanishi, H., Shindou, H., Hishikawa, D., Harayama, T., Ogasawara, R., Suwabe, A., Taguchi, R., & Shimizu, T. (2006). Cloning and characterization of mouse lung-type acyl-CoA:lysophosphatidylcholine acyltransferase 1 (LPCAT1). Expression in alveolar type II cells and possible involvement in surfactant production. *J Biol Chem*, *281*(29), 20140-20147. https://doi.org/10.1074/jbc.M600225200

Nicholas, T. E., Power, J. H., & Barr, H. A. (1982). The pulmonary consequences of a deep breath. *Respir Physiol*, *49*(3), 315-324. https://doi.org/10.1016/0034-5687(82)90119-0

Nogee, L. M. (2004). Alterations in SP-B and SP-C expression in neonatal lung disease. *Annu Rev Physiol*, *66*, 601-623. https://doi.org/10.1146/annurev.physiol.66.032102.134711

Nolte, S. (1989). [Evolutionary biological aspects of the physiology of extracorporeal CO2 removal]. *Anaesthesist*, *38*(11), 622-625. (Evolutionsbiologische Aspekte zur Physiologie der extrakorporalen CO2-Entfernung.)

Numata, M., Chu, H. W., Dakhama, A., & Voelker, D. R. (2010). Pulmonary surfactant phosphatidylglycerol inhibits respiratory syncytial virus-induced inflammation and infection. *Proc Natl Acad Sci U S A*, *107*(1), 320-325. https://doi.org/10.1073/pnas.0909361107

Numata, M., Kandasamy, P., & Voelker, D. R. (2012). Anionic pulmonary surfactant lipid regulation of innate immunity. *Expert Rev Respir Med*, *6*(3), 243-246. https://doi.org/10.1586/ers.12.21

Ochs, M., Johnen, G., Müller, K. M., Wahlers, T., Hawgood, S., Richter, J., & Brasch, F. (2002). Intracellular and intraalveolar localization of surfactant protein A (SP-A) in the parenchymal region of the human lung. *Am J Respir Cell Mol Biol*, *26*(1), 91-98. https://doi.org/10.1165/ajrcmb.26.1.4570

Ochs, M., Nyengaard, J. R., Jung, A., Knudsen, L., Voigt, M., Wahlers, T., Richter, J., & Gundersen, H. J. (2004). The number of alveoli in the human lung. *Am J Respir Crit Care Med*, *169*(1), 120-124. https://doi.org/10.1164/rccm.200308-1107OC

Ogasawara, Y., Kuroki, Y., & Akino, T. (1992). Pulmonary surfactant protein D specifically binds to phosphatidylinositol. *J Biol Chem*, *267*(29), 21244-21249.

Olmeda, B., García-Álvarez, B., Gómez, M. J., Martínez-Calle, M., Cruz, A., & Pérez-Gil, J. (2015). A model for the structure and mechanism of action of pulmonary surfactant protein B. *Faseb j*, *29*(10), 4236-4247. https://doi.org/10.1096/fj.15-273458

Olmeda, B., García-Álvarez, B., & Pérez-Gil, J. (2013). Structure-function correlations of pulmonary surfactant protein SP-B and the saposin-like family of proteins. *Eur Biophys J*, *42*(2-3), 209-222. https://doi.org/10.1007/s00249-012-0858-9

Olmeda, B., Martínez-Calle, M., & Pérez-Gil, J. (2017). Pulmonary surfactant metabolism in the alveolar airspace: Biogenesis, extracellular conversions, recycling. *Ann Anat*, *209*, 78-92. https://doi.org/10.1016/j.aanat.2016.09.008

Olmeda, B., Villén, L., Cruz, A., Orellana, G., & Perez-Gil, J. (2010). Pulmonary surfactant layers accelerate O(2) diffusion through the air-water interface. *Biochim Biophys Acta*, *1798*(6), 1281-1284. https://doi.org/10.1016/j.bbamem.2010.03.008

Orgeig, S., Bernhard, W., Biswas, S. C., Daniels, C. B., Hall, S. B., Hetz, S. K., Lang, C. J., Maina, J. N., Panda, A. K., Perez-Gil, J., Possmayer, F., Veldhuizen, R. A., & Yan, W. (2007). The anatomy, physics, and physiology of gas exchange surfaces: is there a universal function for pulmonary surfactant in animal respiratory structures? *Integrative and Comparative Biology*, *47*(4), 610-627. https://doi.org/10.1093/icb/icm079

Orgeig, S., Daniels, C. B., Johnston, S. D., & Sullivan, L. C. (2003). The pattern of surfactant cholesterol during vertebrate evolution and development: Does ontogeny recapitulate phylogeny? [Review]. *Reproduction, Fertility and Development*, *15*(1-2), 55-73. https://doi.org/10.1071/RD02087

Osanai, K., Mason, R. J., & Voelker, D. R. (1998). Trafficking of newly synthesized surfactant protein A in isolated rat alveolar type II cells. *Am J Respir Cell Mol Biol*, *19*(6), 929-935. https://doi.org/10.1165/ajrcmb.19.6.3292

Pakhomov, A. A., Deyev, I. E., Ratnikova, N. M., Chumakov, S. P., Mironiuk, V. B., Kononevich, Y. N., Muzafarov, A. M., & Martynov, V. I. (2017). BODIPY-based dye for no-wash live-cell staining and imaging. *Biotechniques*, *63*(2), 77-80. https://doi.org/10.2144/000114577

Palaniyar, N., Ridsdale, R. A., Hearn, S. A., Possmayer, F., & Harauz, G. (1999). Formation of membrane lattice structures and their specific interactions with surfactant protein A. *American Journal of Physiology-Lung Cellular and Molecular Physiology*, *276*(4), L642-L649. https://doi.org/10.1152/ajplung.1999.276.4.L642

Parra, E., Alcaraz, A., Cruz, A., Aguilella, V. M., & Pérez-Gil, J. (2013). Hydrophobic pulmonary surfactant proteins SP-B and SP-C induce pore formation in planar lipid membranes: evidence for proteolipid pores. *Biophys J*, *104*(1), 146-155. https://doi.org/10.1016/j.bpj.2012.11.014

Parra, E., Moleiro, Lara H., López-Montero, I., Cruz, A., Monroy, F., & Pérez-Gil, J. (2011). A combined action of pulmonary surfactant proteins SP-B and SP-C

modulates permeability and dynamics of phospholipid membranes. *Biochemical Journal*, *438*(3), 555-564. https://doi.org/10.1042/bj20110681

Parra, E., & Pérez-Gil, J. (2015). Composition, structure and mechanical properties define performance of pulmonary surfactant membranes and films. *Chem Phys Lipids*, *185*, 153-175. https://doi.org/10.1016/j.chemphyslip.2014.09.002

Pastrana-Rios, B., Flach, C. R., Brauner, J. W., Mautone, A. J., & Mendelsohn, R. (1994). A direct test of the "squeeze-out" hypothesis of lung surfactant function. External reflection FT-IR at the air/water interface. *Biochemistry*, *33*(17), 5121-5127. https://doi.org/10.1021/bi00183a016

Pérez-Gil, J. (2008). Structure of pulmonary surfactant membranes and films: the role of proteins and lipid-protein interactions. *Biochim Biophys Acta*, *1778*(7-8), 1676-1695. https://doi.org/10.1016/j.bbamem.2008.05.003

Pérez-Gil, J. (2022). A recipe for a good clinical pulmonary surfactant. *Biomedical Journal*, *45*(4), 615-628. https://doi.org/https://doi.org/10.1016/j.bj.2022.03.001

Pérez-Gil, J., Casals, C., & Marsh, D. (1995). Interactions of hydrophobic lung surfactant proteins SP-B and SP-C with dipalmitoylphosphatidylcholine and dipalmitoylphosphatidylglycerol bilayers studied by electron spin resonance spectroscopy. *Biochemistry*, *34*(12), 3964-3971. https://doi.org/10.1021/bi00012a014

Pérez-Gil, J., Cruz, A., & Casals, C. (1993). Solubility of hydrophobic surfactant proteins in organic solvent/water mixtures. Structural studies on SP-B and SP-C in aqueous organic solvents and lipids. *Biochim Biophys Acta*, *1168*(3), 261-270. https://doi.org/10.1016/0005-2760(93)90181-8

Pérez-Gil, J., & Frick, M. (2024). Acidic Enough for a Healthy Breath. *Am J Respir Cell Mol Biol*, *71*(4), 383-385. https://doi.org/10.1165/rcmb.2024-0237ED

Pérez-Gil, J., Nag, K., Taneva, S., & Keough, K. M. (1992). Pulmonary surfactant protein SP-C causes packing rearrangements of dipalmitoylphosphatidylcholine in spread monolayers. *Biophys J*, *63*(1), 197-204. https://doi.org/10.1016/s0006-3495(92)81582-5

Perez-Gil, J., & Weaver, T. E. (2010). Pulmonary surfactant pathophysiology: current models and open questions. *Physiology (Bethesda)*, *25*(3), 132-141. https://doi.org/10.1152/physiol.00006.2010

Perkins, W. R., Dause, R. B., Parente, R. A., Minchey, S. R., Neuman, K. C., Gruner, S. M., Taraschi, T. F., & Janoff, A. S. (1996). Role of lipid polymorphism in pulmonary surfactant. *Science*, *273*(5273), 330-332. https://doi.org/10.1126/science.273.5273.330

Plasencia, I., Baumgart, F., Andreu, D., Marsh, D., & Pérez-Gil, J. (2008). Effect of acylation on the interaction of the N-Terminal segment of pulmonary surfactant protein SP-C with phospholipid membranes. *Biochim Biophys Acta*, *1778*(5), 1274-1282. https://doi.org/10.1016/j.bbamem.2008.02.004

Plasencia, I., Cruz, A., Casals, C., & Pérez-Gil, J. (2001). Superficial disposition of the N-terminal region of the surfactant protein SP-C and the absence of specific SP-B-SP-C interactions in phospholipid bilayers. *Biochem J*, *359*(Pt 3), 651-659. https://doi.org/10.1042/0264-6021:3590651

Plasencia, I., Keough, K. M., & Perez-Gil, J. (2005). Interaction of the N-terminal segment of pulmonary surfactant protein SP-C with interfacial phospholipid films. *Biochim Biophys Acta*, *1713*(2), 118-128. https://doi.org/10.1016/j.bbamem.2005.06.002

Plasencia, I., Rivas, L., Keough, K. M., Marsh, D., & Pérez-Gil, J. (2004). The N-terminal segment of pulmonary surfactant lipopeptide SP-C has intrinsic propensity to interact with and perturb phospholipid bilayers. *Biochem J*, *377*(Pt 1), 183-193. https://doi.org/10.1042/bj20030815

Poelma, D. L., Zimmermann, L. J., van Cappellen, W. A., Haitsma, J. J., Lachmann, B., & van Iwaarden, J. F. (2004). Distinct effects of SP-B and SP-C on the uptake of surfactant-like liposomes by alveolar cells in vivo and in vitro. *Am J Physiol Lung Cell Mol Physiol*, *287*(5), L1056-1065. https://doi.org/10.1152/ajplung.00054.2004

Possmayer, F., Nag, K., Rodriguez, K., Qanbar, R., & Schürch, S. (2001). Surface activity in vitro: role of surfactant proteins. *Comp Biochem Physiol A Mol Integr Physiol*, *129*(1), 209-220. https://doi.org/10.1016/s1095-6433(01)00317-8

Possmayer, F., Zuo, Y. Y., Veldhuizen, R. A. W., & Petersen, N. O. (2023). Pulmonary Surfactant: A Mighty Thin Film. *Chem Rev*, *123*(23), 13209-13290. https://doi.org/10.1021/acs.chemrev.3c00146

Potter, S., Orgeig, S., Donnellan, S., & Daniels, C. B. (2007). Purifying selection drives the evolution of surfactant protein C (SP-C) independently of body temperature regulation in mammals. *Comp Biochem Physiol Part D Genomics Proteomics*, *2*(2), 165-176. https://doi.org/10.1016/j.cbd.2007.02.003

Poulain, F. R., Allen, L., Williams, M. C., Hamilton, R. L., & Hawgood, S. (1992). Effects of surfactant apolipoproteins on liposome structure: implications for tubular myelin formation. *Am J Physiol*, *262*(6 Pt 1), L730-739. https://doi.org/10.1152/ajplung.1992.262.6.L730

Qanbar, R., Cheng, S., Possmayer, F., & Schürch, S. (1996). Role of the palmitoylation of surfactant-associated protein C in surfactant film formation and stability. *Am J Physiol*, *271*(4 Pt 1), L572-580. https://doi.org/10.1152/ajplung.1996.271.4.L572

Ravasio, A., Olmeda, B., Bertocchi, C., Haller, T., & Pérez-Gil, J. (2010). Lamellar Bodies Form Solid Three-dimensional Films at the Respiratory Air-Liquid Interface*. *Journal of Biological Chemistry*, *285*(36), 28174-28182. https://doi.org/https://doi.org/10.1074/jbc.M110.106518

Rebello, C. M., Proença, R. S., Troster, E. J., & Jobe, A. H. (2002). [Exogenous surfactant therapy--what is established and what still needs to be determined]. *J Pediatr (Rio J)*, *78 Suppl 2*, S215-226. https://doi.org/10.2223/jped.900 (Terapia com surfactante pulmonar exógeno--o que é estabelecido e o que necessitamos determinar.)

Rice, W. R., Sarin, V. K., Fox, J. L., Baatz, J., Wert, S., & Whitsett, J. A. (1989). Surfactant peptides stimulate uptake of phosphatidylcholine by isolated cells. *Biochim Biophys Acta*, *1006*(2), 237-245. https://doi.org/10.1016/0005-2760(89)90202-6

8. Bibliography

Rider, E. D., Ikegami, M., & Jobe, A. H. (1992). Localization of alveolar surfactant clearance in rabbit lung cells. *Am J Physiol*, *263*(2 Pt 1), L201-209. https://doi.org/10.1152/ajplung.1992.263.2.L201

Rodriguez-Capote, K., Nag, K., Schürch, S., & Possmayer, F. (2001). Surfactant protein interactions with neutral and acidic phospholipid films. *Am J Physiol Lung Cell Mol Physiol*, *281*(1), L231-242. https://doi.org/10.1152/ajplung.2001.281.1.L231

Roldan, N., Goormaghtigh, E., Pérez-Gil, J., & Garcia-Alvarez, B. (2015). Palmitoylation as a key factor to modulate SP-C-lipid interactions in lung surfactant membrane multilayers. *Biochim Biophys Acta*, *1848*(1 Pt A), 184-191. https://doi.org/10.1016/j.bbamem.2014.10.009

Roldan, N., Nyholm, T. K. M., Slotte, J. P., Pérez-Gil, J., & García-Álvarez, B. (2016). Effect of Lung Surfactant Protein SP-C and SP-C-Promoted Membrane Fragmentation on Cholesterol Dynamics. *Biophys J*, *111*(8), 1703-1713. https://doi.org/10.1016/j.bpj.2016.09.016

Roldan, N., Pérez-Gil, J., Morrow, M. R., & García-Álvarez, B. (2017). Divide & Conquer: Surfactant Protein SP-C and Cholesterol Modulate Phase Segregation in Lung Surfactant. *Biophys J*, *113*(4), 847-859. https://doi.org/10.1016/j.bpj.2017.06.059

Rooney, S. A. (2001). Regulation of surfactant secretion. *Comp Biochem Physiol A Mol Integr Physiol*, *129*(1), 233-243. https://doi.org/10.1016/s1095-6433(01)00320-8

Roszell, B. R., Tao, J. Q., Yu, K. J., Huang, S., & Bates, S. R. (2012). Characterization of the Niemann-Pick C pathway in alveolar type II cells and lamellar bodies of the lung. *Am J Physiol Lung Cell Mol Physiol*, *302*(9), L919-932. https://doi.org/10.1152/ajplung.00383.2011

Rouser, G., Siakotos, A. N., & Fleischer, S. (1966). Quantitative analysis of phospholipids by thin-layer chromatography and phosphorus analysis of spots. *Lipids*, *1*(1), 85-86. https://doi.org/10.1007/bf02668129

Roux, E. (2002). [Origin and evolution of the respiratory tract in vertebrates]. *Rev Mal Respir*, *19*(5 Pt 1), 601-615. (Origine et évolution de l'appareil respiratoire aérien des Vertébrés.)

Rowland, R. R. R., & Brandariz-Nuñez, A. (2024). Role of CD163 in PRRSV infection. *Virology*, *600*, 110262. https://doi.org/10.1016/j.virol.2024.110262

Rugonyi, S., Biswas, S. C., & Hall, S. B. (2008). The biophysical function of pulmonary surfactant. *Respir Physiol Neurobiol*, *163*(1-3), 244-255. https://doi.org/10.1016/j.resp.2008.05.018

Ruwisch, J., Sehlmeyer, K., Roldan, N., Garcia-Alvarez, B., Perez-Gil, J., Weaver, T. E., Ochs, M., Knudsen, L., & Lopez-Rodriguez, E. (2020). Air Space Distension Precedes Spontaneous Fibrotic Remodeling and Impaired Cholesterol Metabolism in the Absence of Surfactant Protein C. *Am J Respir Cell Mol Biol*, *62*(4), 466-478. https://doi.org/10.1165/rcmb.2019-0358OC

Ryan, M. A., Qi, X., Serrano, A. G., Ikegami, M., Perez-Gil, J., Johansson, J., & Weaver, T. E. (2005). Mapping and analysis of the lytic and fusogenic domains of surfactant protein B. *Biochemistry*, *44*(3), 861-872. https://doi.org/10.1021/bi0485575

Sachan, A. K., & Galla, H. J. (2013). Bidirectional surface analysis of monomolecular membrane harboring nanoscale reversible collapse structures. *Nano Lett*, *13*(3), 961-966. https://doi.org/10.1021/nl303928m

Salerno, T., Peca, D., Menchini, L., Schiavino, A., Boldrini, R., Esposito, F., Danhaive, O., & Cutrera, R. (2016). Surfactant Protein C-associated interstitial lung disease; three different phenotypes of the same SFTPC mutation. *Italian Journal of Pediatrics*, *42*(1), 23. https://doi.org/10.1186/s13052-016-0235-x

Sánchez-Pulido, L., Devos, D., & Valencia, A. (2002). BRICHOS: a conserved domain in proteins associated with dementia, respiratory distress and cancer. *Trends Biochem Sci*, *27*(7), 329-332. https://doi.org/10.1016/s0968-0004(02)02134-5

Sane, A. C., & Young, S. L. (1994). The stimulation of cellular phospholipid uptake by surfactant apoproteins. *Biochim Biophys Acta*, *1213*(1), 107-112. https://doi.org/10.1016/0005-2760(94)90228-3

Sankaram, M. B., & Thompson, T. E. (1991). Cholesterol-induced fluid-phase immiscibility in membranes. *Proceedings of the National Academy of Sciences*, *88*(19), 8686-8690. https://doi.org/doi:10.1073/pnas.88.19.8686

Sato, S., & Kishikawa, T. (2001). Ultrastructural study of the alveolar lining and the bronchial mucus layer by block staining with oolong tea extract: the role of various surfactant materials. *Med Electron Microsc*, *34*(2), 142-151. https://doi.org/10.1007/s007950170008

Schmid, E. M., Richmond, D. L., & Fletcher, D. A. (2015). Reconstitution of proteins on electroformed giant unilamellar vesicles. *Methods in cell biology*, *128*, 319-338. https://doi.org/10.1016/bs.mcb.2015.02.004

Schmid, K. F., Zeinali, S., Moser, S. K., Dubey, C., Schneider, S., Deng, H., Haefliger, S., Marti, T. M., & Guenat, O. T. (2024). Assessing the metastatic potential of circulating tumor cells using an organ-on-chip model. *Front Bioeng Biotechnol*, *12*, 1457884. https://doi.org/10.3389/fbioe.2024.1457884

Schmiedl, A., Ochs, M., Mühlfeld, C., Johnen, G., & Brasch, F. (2005). Distribution of surfactant proteins in type II pneumocytes of newborn, 14-day old, and adult rats: an immunoelectron microscopic and stereological study. *Histochem Cell Biol*, *124*(6), 465-476. https://doi.org/10.1007/s00418-005-0066-0

Schürch, D., Ospina, O. L., Cruz, A., & Pérez-Gil, J. (2010). Combined and independent action of proteins SP-B and SP-C in the surface behavior and mechanical stability of pulmonary surfactant films. *Biophys J*, *99*(10), 3290-3299. https://doi.org/10.1016/j.bpj.2010.09.039

Schürch, S., Bachofen, H., Goerke, J., & Green, F. (1992). Surface properties of rat pulmonary surfactant studied with the captive bubble method: adsorption, hysteresis, stability. *Biochimica et Biophysica Acta (BBA) - Biomembranes*, *1103*(1), 127-136. https://doi.org/https://doi.org/10.1016/0005-2736(92)90066-U

Schweizer, T., Kubach, H., & Koch, T. (2021). Investigations to characterize the interactions of light radiation, engine operating media and fluorescence tracers for the use of qualitative light-induced fluorescence in engine

systems. *Automotive and Engine Technology*, *6*(3), 275-287. https://doi.org/10.1007/s41104-021-00092-3

Schwendener, R. A., Lagocki, P. A., & Rahman, Y. E. (1984). The effects of charge and size on the interaction of unilamellar liposomes with macrophages. *Biochim Biophys Acta*, *772*(1), 93-101. https://doi.org/10.1016/0005-2736(84)90521-2

Sehlmeyer, K., Ruwisch, J., Roldan, N., & Lopez-Rodriguez, E. (2020). Alveolar Dynamics and Beyond - The Importance of Surfactant Protein C and Cholesterol in Lung Homeostasis and Fibrosis. *Front Physiol*, *11*, 386. https://doi.org/10.3389/fphys.2020.00386

Serrano, A. G., Cabré, E. J., & Pérez-Gil, J. (2007). Identification of a segment in the precursor of pulmonary surfactant protein SP-B, potentially involved in pH-dependent membrane assembly of the protein. *Biochimica et Biophysica Acta (BBA) - Biomembranes*, *1768*(5), 1059-1069. https://doi.org/https://doi.org/10.1016/j.bbamem.2007.01.010

Serrano, A. G., Cruz, A., Rodríguez-Capote, K., Possmayer, F., & Pérez-Gil, J. (2005). Intrinsic structural and functional determinants within the amino acid sequence of mature pulmonary surfactant protein SP-B. *Biochemistry*, *44*(1), 417-430. https://doi.org/10.1021/bi048781u

Serrano, A. G., & Pérez-Gil, J. (2006). Protein-lipid interactions and surface activity in the pulmonary surfactant system. *Chem Phys Lipids*, *141*(1-2), 105-118. https://doi.org/10.1016/j.chemphyslip.2006.02.017

Soncini, R., & Klein, W. (2023). Surface tension in biological systems - a common problem with a variety of solutions. *Comparative Biochemistry and Physiology Part A: Molecular & Integrative Physiology*, *284*, 111475. https://doi.org/https://doi.org/10.1016/j.cbpa.2023.111475

Sorkin, A., & von Zastrow, M. (2009). Endocytosis and signalling: intertwining molecular networks. *Nat Rev Mol Cell Biol*, *10*(9), 609-622. https://doi.org/10.1038/nrm2748

Stahlman, M. T., Gray, M. P., Falconieri, M. W., Whitsett, J. A., & Weaver, T. E. (2000). Lamellar body formation in normal and surfactant protein B-deficient fetal mice. *Lab Invest*, *80*(3), 395-403. https://doi.org/10.1038/labinvest.3780044

Suri, L. N., McCaig, L., Picardi, M. V., Ospina, O. L., Veldhuizen, R. A., Staples, J. F., Possmayer, F., Yao, L. J., Perez-Gil, J., & Orgeig, S. (2012). Adaptation to low body temperature influences pulmonary surfactant composition thereby increasing fluidity while maintaining appropriately ordered membrane structure and surface activity. *Biochim Biophys Acta*, *1818*(7), 1581-1589. https://doi.org/10.1016/j.bbamem.2012.02.021

Suri, L. N. M., Cruz, A., Veldhuizen, R. A. W., Staples, J. F., Possmayer, F., Orgeig, S., & Perez-Gil, J. (2013). Adaptations to hibernation in lung surfactant composition of 13-lined ground squirrels influence surfactant lipid phase segregation properties. *Biochimica et Biophysica Acta (BBA) - Biomembranes*, *1828*(8), 1707-1714. https://doi.org/https://doi.org/10.1016/j.bbamem.2013.03.005

Suzuki, Y., Fujita, Y., & Kogishi, K. (1989). Reconstitution of tubular myelin from synthetic lipids and proteins associated with pig pulmonary surfactant. *Am Rev Respir Dis*, *140*(1), 75-81. https://doi.org/10.1164/ajrccm/140.1.75

Szyperski, T., Vandenbussche, G., Curstedt, T., Ruysschaert, J. M., Wüthrich, K., & Johansson, J. (1998). Pulmonary surfactant-associated polypeptide C in a mixed organic solvent transforms from a monomeric alpha-helical state into insoluble beta-sheet aggregates. *Protein Sci*, *7*(12), 2533-2540. https://doi.org/10.1002/pro.5560071206

Taeusch, H. W., Bernardino de la Serna, J., Perez-Gil, J., Alonso, C., & Zasadzinski, J. A. (2005). Inactivation of pulmonary surfactant due to serum-inhibited adsorption and reversal by hydrophilic polymers: experimental. *Biophys J*, *89*(3), 1769-1779. https://doi.org/10.1529/biophysj.105.062620

Takamoto, D. Y., Lipp, M. M., von Nahmen, A., Lee, K. Y., Waring, A. J., & Zasadzinski, J. A. (2001). Interaction of lung surfactant proteins with anionic phospholipids. *Biophys J*, *81*(1), 153-169. https://doi.org/10.1016/s0006-3495(01)75688-3

Tan, E., Chin, C. S. H., Lim, Z. F. S., & Ng, S. K. (2021). HEK293 Cell Line as a Platform to Produce Recombinant Proteins and Viral Vectors. *Front Bioeng Biotechnol*, *9*, 796991. https://doi.org/10.3389/fbioe.2021.796991

Taneva, S., & Keough, K. M. (1994). Pulmonary surfactant proteins SP-B and SP-C in spread monolayers at the air-water interface: II. Monolayers of pulmonary surfactant protein SP-C and phospholipids. *Biophys J*, *66*(4), 1149-1157. https://doi.org/10.1016/s0006-3495(94)80896-3

Tareste, D., Shen, J., Melia, T., & Rothman, J. (2008). SNAREpin/Munc18 promotes adhesion and fusion of large vesicles to giant membranes. *Proceedings of the National Academy of Sciences of the United States of America*, *105*, 2380-2385. https://doi.org/10.1073/pnas.0712125105

ten Brinke, A., Batenburg, J. J., Gadella, B. M., Haagsman, H. P., Vaandrager, A. B., & van Golde, L. M. (2001). The juxtamembrane lysine and arginine residues of surfactant protein C precursor influence palmitoylation via effects on trafficking. *Am J Respir Cell Mol Biol*, *25*(2), 156-163. https://doi.org/10.1165/ajrcmb.25.2.4423

Thomas, A. Q., Lane, K., Phillips, J., 3rd, Prince, M., Markin, C., Speer, M., Schwartz, D. A., Gaddipati, R., Marney, A., Johnson, J., Roberts, R., Haines, J., Stahlman, M., & Loyd, J. E. (2002). Heterozygosity for a surfactant protein C gene mutation associated with usual interstitial pneumonitis and cellular nonspecific interstitial pneumonitis in one kindred. *Am J Respir Crit Care Med*, *165*(9), 1322-1328. https://doi.org/10.1164/rccm.200112-123OC

Tian, Y., Zhou, R., Rehg, J. E., & Jackowski, S. (2007). Role of phosphocholine cytidylyltransferase alpha in lung development. *Mol Cell Biol*, *27*(3), 975-982. https://doi.org/10.1128/mcb.01512-06

Tièche, C. C., Gao, Y., Bührer, E. D., Hobi, N., Berezowska, S. A., Wyler, K., Froment, L., Weis, S., Peng, R. W., Bruggmann, R., Schär, P., Amrein, M. A., Hall, S. R. R., Dorn, P., Kocher, G., Riether, C., Ochsenbein, A., Schmid, R. A., & Marti, T. M. (2019). Tumor Initiation Capacity and Therapy Resistance Are Differential Features of EMT-Related Subpopulations in the NSCLC Cell Line A549. *Neoplasia*, *21*(2), 185-196. https://doi.org/10.1016/j.neo.2018.09.008

Trapnell, B. C., & Whitsett, J. A. (2002). Gm-CSF regulates pulmonary surfactant homeostasis and alveolar macrophage-mediated innate host defense.

Annu Rev Physiol, *64*, 775-802. https://doi.org/10.1146/annurev.physiol.64.090601.113847

Trapnell, B. C., Whitsett, J. A., & Nakata, K. (2003). Pulmonary alveolar proteinosis. *N Engl J Med*, *349*(26), 2527-2539. https://doi.org/10.1056/NEJMra023226

Umberger, J. Q., & LaMer, V. K. (1945). The Kinetics of Diffusion Controlled Molecular and Ionic Reactions in Solution as Determined by Measurements of the Quenching of Fluorescence1,2. *Journal of the American Chemical Society*, *67*(7), 1099-1109. https://doi.org/10.1021/ja01223a023

van Golde, L. M. (1995). Potential role of surfactant proteins A and D in innate lung defense against pathogens. *Biol Neonate*, *67 Suppl 1*, 2-17. https://doi.org/10.1159/000244202

Vandenbussche, G., Clercx, A., Clercx, M., Curstedt, T., Johansson, J., Jörnvall, H., & Ruysschaert, J. M. (1992). Secondary structure and orientation of the surfactant protein SP-B in a lipid environment. A Fourier transform infrared spectroscopy study. *Biochemistry*, *31*(38), 9169-9176. https://doi.org/10.1021/bi00153a008

Vandenbussche, G., Clercx, A., Curstedt, T., Johansson, J., Jörnvall, H., & Ruysschaert, J. M. (1992). Structure and orientation of the surfactant-associated protein C in a lipid bilayer. *Eur J Biochem*, *203*(1-2), 201-209. https://doi.org/10.1111/j.1432-1033.1992.tb19848.x

Väyrynen, O., Glumoff, V., & Hallman, M. (2002). Regulation of surfactant proteins by LPS and proinflammatory cytokines in fetal and newborn lung. *Am J Physiol Lung Cell Mol Physiol*, *282*(4), L803-810. https://doi.org/10.1152/ajplung.00274.2001

Veatch, S. L., & Keller, S. L. (2002). Organization in lipid membranes containing cholesterol. *Phys Rev Lett*, *89*(26), 268101. https://doi.org/10.1103/PhysRevLett.89.268101

Veldhuizen, R., Nag, K., Orgeig, S., & Possmayer, F. (1998). The role of lipids in pulmonary surfactant [Review]. *Biochimica et Biophysica Acta - Molecular Basis of Disease*, *1408*(2-3), 90-108. https://doi.org/10.1016/S0925-4439(98)00061-1

Vockeroth, D., Gunasekara, L., Amrein, M., Possmayer, F., Lewis, J. F., & Veldhuizen, R. A. (2010). Role of cholesterol in the biophysical dysfunction of surfactant in ventilator-induced lung injury. *Am J Physiol Lung Cell Mol Physiol*, *298*(1), L117-125. https://doi.org/10.1152/ajplung.00218.2009

von Nahmen, A., Schenk, M., Sieber, M., & Amrein, M. (1997). The structure of a model pulmonary surfactant as revealed by scanning force microscopy. *Biophys J*, *72*(1), 463-469. https://doi.org/10.1016/s0006-3495(97)78687-9

Voorhout, W. F., Veenendaal, T., Kuroki, Y., Ogasawara, Y., van Golde, L. M., & Geuze, H. J. (1992). Immunocytochemical localization of surfactant protein D (SP-D) in type II cells, Clara cells, and alveolar macrophages of rat lung. *J Histochem Cytochem*, *40*(10), 1589-1597. https://doi.org/10.1177/40.10.1527377

Vorbroker, D. K., Dey, C., Weaver, T. E., & Whitsett, J. A. (1992). Surfactant protein C precursor is palmitoylated and associates with subcellular membranes. *Biochimica et Biophysica Acta (BBA) - Biomembranes*, *1105*(1), 161-169. https://doi.org/https://doi.org/10.1016/0005-2736(92)90175-L

Vorbroker, D. K., Profitt, S. A., Nogee, L. M., & Whitsett, J. A. (1995). Aberrant processing of surfactant protein C in hereditary SP-B deficiency. *American Journal of Physiology-Lung Cellular and Molecular Physiology*, *268*(4), L647-L656. https://doi.org/10.1152/ajplung.1995.268.4.L647

Voss, T., Schäfer, K. P., Nielsen, P. F., Schäfer, A., Maier, C., Hannappel, E., Maaßen, J., Landis, B., Klemm, K., & Przybylski, M. (1992). Primary structure differences of human surfactant-associated proteins isolated from normal and proteinosis lung. *Biochimica et Biophysica Acta (BBA) - Molecular Basis of Disease*, *1138*(4), 261-267. https://doi.org/https://doi.org/10.1016/0925-4439(92)90002-5

Wade, K. C., Guttentag, S. H., Gonzales, L. W., Maschhoff, K. L., Gonzales, J., Kolla, V., Singhal, S., & Ballard, P. L. (2006). Gene induction during differentiation of human pulmonary type II cells in vitro. *Am J Respir Cell Mol Biol*, *34*(6), 727-737. https://doi.org/10.1165/rcmb.2004-0389OC

Wang, J., Souza, P., Kuliszewski, M., Tanswell, A. K., & Post, M. (1994). Expression of surfactant proteins in embryonic rat lung. *Am J Respir Cell Mol Biol*, *10*(2), 222-229. https://doi.org/10.1165/ajrcmb.10.2.7509164

Wang, L., Magdaleno, S., Tabas, I., & Jackowski, S. (2005). Early embryonic lethality in mice with targeted deletion of the CTP:phosphocholine cytidylyltransferase alpha gene (Pcyt1a). *Mol Cell Biol*, *25*(8), 3357-3363. https://doi.org/10.1128/mcb.25.8.3357-3363.2005

Wang, N., Liang, H., & Zen, K. (2014). Molecular mechanisms that influence the macrophage m1-m2 polarization balance. *Front Immunol*, *5*, 614. https://doi.org/10.3389/fimmu.2014.00614

Wang, W. J., Russo, S. J., Mulugeta, S., & Beers, M. F. (2002). Biosynthesis of surfactant protein C (SP-C). Sorting of SP-C proprotein involves homomeric association via a signal anchor domain. *J Biol Chem*, *277*(22), 19929-19937. https://doi.org/10.1074/jbc.M201537200

Wang, Z., Gurel, O., Baatz, J. E., & Notter, R. H. (1996). Acylation of pulmonary surfactant protein-C is required for its optimal surface active interactions with phospholipids. *J Biol Chem*, *271*(32), 19104-19109. https://doi.org/10.1074/jbc.271.32.19104

Ware, L. B., & Matthay, M. A. (2000). The acute respiratory distress syndrome. *N Engl J Med*, *342*(18), 1334-1349. https://doi.org/10.1056/nejm200005043421806

Weaver, T. E., & Conkright, J. J. (2001). Function of Surfactant Proteins B and C. *Annual Review of Physiology*, *63*(Volume 63, 2001), 555-578. https://doi.org/https://doi.org/10.1146/annurev.physiol.63.1.555

Weaver, T. E., & Whitsett, J. A. (1991). Function and regulation of expression of pulmonary surfactant-associated proteins. *Biochem J*, *273(Pt 2)*(Pt 2), 249-264. https://doi.org/10.1042/bj2730249

West, J. B. (2003). Thoughts on the pulmonary blood-gas barrier. *Am J Physiol Lung Cell Mol Physiol*, *285*(3), L501-513. https://doi.org/10.1152/ajplung.00117.2003

Whitsett, J. A., Wert, S. E., & Weaver, T. E. (2010). Alveolar Surfactant Homeostasis and the Pathogenesis of Pulmonary Disease. *Annual Review of Medicine*,

61(Volume 61, 2010), 105-119. https://doi.org/https://doi.org/10.1146/annurev.med.60.041807.123500

Wissel, H., Lehfeldt, A., Klein, P., Müller, T., & Stevens, P. A. (2001). Endocytosed SP-A and surfactant lipids are sorted to different organelles in rat type II pneumocytes. *Am J Physiol Lung Cell Mol Physiol*, *281*(2), L345-360. https://doi.org/10.1152/ajplung.2001.281.2.L345

Wright, J. R. (2005). Immunoregulatory functions of surfactant proteins. *Nat Rev Immunol*, *5*(1), 58-68. https://doi.org/10.1038/nri1528

Wright, J. R., & Clements, J. A. (1987). Metabolism and turnover of lung surfactant. *Am Rev Respir Dis*, *136*(2), 426-444. https://doi.org/10.1164/ajrccm/136.2.426

Yang, L., Johansson, J., Ridsdale, R., Willander, H., Fitzen, M., Akinbi, H. T., & Weaver, T. E. (2010). Surfactant protein B propeptide contains a saposin-like protein domain with antimicrobial activity at low pH. *J Immunol*, *184*(2), 975-983. https://doi.org/10.4049/jimmunol.0900650

Yasmin, H., & Kishore, U. (2021). Biological Activities of SP-A and SP-D Against Extracellular and Intracellular Pathogens. In U. Kishore, T. Madan, & R. B. Sim (Eds.), *The Collectin Protein Family and Its Multiple Biological Activities* (pp. 103-133). Springer International Publishing. https://doi.org/10.1007/978-3-030-67048-1_5

Zhou, J., You, Y., Ryan, A. J., & Mallampalli, R. K. (2004). Upregulation of surfactant synthesis triggers ABCA1-mediated basolateral phospholipid efflux. *J Lipid Res*, *45*(9), 1758-1767. https://doi.org/10.1194/jlr.M400179-JLR200

Zuo, Y. Y., Veldhuizen, R. A. W., Neumann, A. W., Petersen, N. O., & Possmayer, F. (2008). Current perspectives in pulmonary surfactant — Inhibition, enhancement and evaluation. *Biochimica et Biophysica Acta (BBA) - Biomembranes*, *1778*(10), 1947-1977. https://doi.org/https://doi.org/10.1016/j.bbamem.2008.03.021